Energy Research and Development Division
FINAL PROJECT REPORT

AUTOMOTIVE THERMOELECTRIC HVAC DEVELOPMENT AND DEMONSTRATION PROJECT

Prepared for: California Energy Commission
Prepared by: National Energy Technology Laboratory
United States Department of Energy

MAY 2016
CEC-500-2016-017

Prepared by:

Primary Author(s):

Carl Maronde
U.S. Department of Energy
National Energy Technology Laboratory
P.O. Box 10940
Pittsburgh, PA, 15326
Phone: 412-386-6402 | Fax: 412-386-5835
http://www.netl.doe.gov

Clay Maranville
Ford Motor Company
MD3182 / P.O. Box 2053
Dearborn, MI 48121
Phone: 313-594-0276
http://www.corporate.ford.com

Edward Gundlach
General Motors LLC
30500 Mound Road
Warren, MI 48090
Phone: 313-556-5000 | Fax: 586-947-1495
http://www.gm.com

Contract Number: 500-08-047

Prepared for:

California Energy Commission

Rhetta DeMesa
Contract Manager

Aleecia Gutierrez
Office Manager
Energy Efficiency Research Office

Laurie ten Hope
Deputy Director
RESEARCH AND DEVELOPMENT DIVISION

Robert P. Oglesby
Executive Director

ACKNOWLEDGEMENTS

The material contained in this report is based upon work supported by the U.S. Department of Energy and the California Energy Commission under U.S. Department of Energy Award Numbers DE-EE00000014 and DE-EE0000020.

PREFACE

The California Energy Commission Energy Research and Development Division supports public interest energy research and development that will help improve the quality of life in California by bringing environmentally safe, affordable, and reliable energy services and products to the marketplace.

The Energy Research and Development Division conducts public interest research, development, and demonstration (RD&D) projects to benefit California.

The Energy Research and Development Division strives to conduct the most promising public interest energy research by partnering with RD&D entities, including individuals, businesses, utilities, and public or private research institutions.

Energy Research and Development Division funding efforts are focused on the following RD&D program areas:

- Buildings End-Use Energy Efficiency
- Energy Innovations Small Grants
- Energy-Related Environmental Research
- Energy Systems Integration
- Environmentally Preferred Advanced Generation
- Industrial/Agricultural/Water End-Use Energy Efficiency
- Renewable Energy Technologies
- Transportation

Automotive Thermoelectric HVAC Development and Demonstration Project is the final report for the Automotive Thermoelectric HVAC Development and Demonstration Project (contract number 500-08-047) conducted by the United States Department of Energy, National Energy Technology Laboratory. The information from this project contributes to Energy Research and Development Division's Transportation Program.

For more information about the Energy Research and Development Division, please visit the Energy Commission's website at www.energy.ca.gov/research/ or contact the Energy Commission at 916-327-1551.

ABSTRACT

This project is a joint effort between the California Energy Commission and the U.S. Department of Energy to co-fund projects with Ford and General Motors todevelop and demonstrate light-duty automotive thermoelectric heating, ventilating, and air conditioning (HVAC) technology. The project successfully reduced energy use for a distributed, localized (zonal) thermoelectric-based supplemental heating and cooling system for passenger vehicles.

Ford and General Motors independently completed work in the following areas: system requirements, comfort modeling with mannequin and human subject testing, vehicle climatic wind tunnel testing, system component development, thermoelectric materials development, and component integration engineering.

Both projects met and exceeded the performance for heating and cooling and achieved sufficient passenger comfort at energy savings in the target range. Both projects are on target to integrate the zonal thermoelectric HVAC systems and demonstrate them in light duty passenger vehicles by June 2014.

Researchers concluded that zonal thermoelectric HVAC is an effective method to provide passenger comfort at reduced energy consumption; however, at this time, the economic feasibility of thermoelectric HVAC systems is not sufficient for commercialization. Continued work is necessary to further improve thermoelectric material performance and cost.

Keywords: thermoelectrics, HVAC, automotive, zonal, heating, cooling, distributed, localized, comfort modeling, solid-state energy conversion

Please use the following citation for this report:

Maronde, Carl, (U.S. Department of Energy, National Energy Technology Laboratory), Edward Gundlach (General Motors), and Clay Maranville (Ford Motor Company). 2016. ***Automotive Thermoelectric HVAC Development and Demonstration Project.*** California Energy Commission. Publication number: CEC-500-2016-017.

TABLE OF CONTENTS

LIST OF FIGURES

LIST OF TABLES

EXECUTIVE SUMMARY

Introduction

Current air conditioner technology for vehicles is designed to heat and cool occupants including the surrounding structures such as the vehicle headliner, windows, flooring, and seat backs. A centralized heating, ventilation, and air conditioning (HVAC) unit distributes conditioned air to vent locations throughout the vehicle for passenger comfort. These systems require 3,500-4,500 watts of cooled air, while preliminary analysis indicates that less than 700 watts of cooling or heating per person and less than 3,000 watts for a vehicle with five occupants would be adequate for occupant comfort.

A substantial portion of this energy used by HVAC systems conditions various elements of the vehicle's interior structures and does not directly provide the occupants comfort. As the vehicle’s powertrain efficiency is increased, the energy available to provide occupant thermal comfort is becoming a more significant part of the total energy budget.

A revolutionary technology for automobiles is thermoelectric HVAC systems which uses distributed cooling/heating units to cool/heat the individual occupants rather than the entire cabin and its components. The automotive industry has been reluntant to accept this technology because of it is in the early stages of technological development, there is a lack of information on thermoelectric device and module manufacturing capability, and the costs are unknown. These devices, however, offer clear benefits to current vehicles, and a unique set of advantages for hybrid vehicles, plug-in hybrids, electric propulsion, and fuel cell power trains. Thermoelectric HVAC can provide occupant comfort when the internal combustion engine is not operating or when the battery and/or fuel cell propulsion is in use.

In addition to decreasing engine load and increasing vehicle efficiency, thermoelectric HVAC will reduce or eliminate the need for conventional air conditioning working fluids, further reducing greenhouse gas emissions.

Project Background

The U.S. Department of Energy (U.S. DOE) and the California Energy Commission (Energy Commission) partnered to advance vehicular HVAC systems and reduce energy consumption and greenhouse gas emissions. The projects were advantageous to accelerate this technology by leaveraging funds from both organizations to provide increased early financial support as well as increase the number of projects to be selected.

As a result of this partnership, the U.S. DOE, National Energy Technology Laboratory released a funding opportunity notice for *Solid State Energy Conversion for Vehicular HVAC and Waste Heat Recovery* to help address HVAC system efficiency. The intent of research was to develop and demonstrate a distributed, localized thermoelectric -based supplemental heating and cooling system for passenger vehicles to improve fuel economy and reduce greenhouse gas emissions. In 2009, the US DOE National Energy Technology Laboratory awarded funds to Ford Motor Company and General Motors for two projects. The Energy Commission also entered into a formal agreement with the National Energy Technology Laboratory to provide $2 million in funding to support the administration and funding of the Ford and General Motors projects.

Ford Motor Company

Purpose and Objectives

Thermoelectric devices were identified by U.S. DOE as one method to potentially reduce HVAC-related energy consumption in vehicles. The Ford Motor Company was funded to identify a technical and business approach to accelerate research and development of light-duty automotive thermoelectric HVAC technology. Ford developed a zonal HVAC providing thermal comfort to each occupant and reduced the overall power consumed by the HVAC system by 33 percent compared with a baseline system. Ford was also tasked to:

- Demonstrate thermoelectric devices that achieve a performance coefficients in cooling better than 1.3 and in heating of better than 2.3.
- Demonstrate the technical feasibility of a thermoelectric HVAC system for light-duty vehicles.
- Develop a commercialization pathway for a thermoelectric HVAC system.
- Integrate, test, and deliver a 5-passenger thermoelectric HVAC demonstration vehicle.

Methodology

The project was conducted in four phases with interim technical milestones and a go / no-go decision point at the end of each phase. Each phase of the project contained four major technical tasks. The four phases were:

- Phase 1: Applied Research involved identification of potential HVAC architectures, development of thermal comfort-based test criteria, and initiation of advanced thermoelectric materials and device research.
- Phase 2: Exploratory Development involved detailed modeling and analysis of the vehicle environment, packaging and design studies to assess architecture trade-offs, and a thermal-chamber trade-study of proposed thermoelectric HVAC elements. In addition, advanced thermoelectric devices and materials were further refined.
- Phase 3: Advanced Development included the developing, fabricating, and bench testing of thermoelectric HVAC hardware, power supplies, and a preliminary control system. A cost analysis of production architecture was conducted. Advanced thermoelectric subassemblies were designed, built, and tested. Strategies for reducing overall cabin thermal loads were also explored.
- Phase 4: Engineering Development is currently underway and scheduled to be completed by September 2013. This phase focuses on integrating and testing the thermoelectric HVAC hardware in a prototype vehicle to determine the system's ability to decrease HVAC system energy use, while providing equivalent occupant thermal comfort. Potential commercialization of the system is also being explored. A study of

advanced thermoelectric materials and design concepts will be completed by the end of the phase.

Results

Ford has successfully completed much of the project objectives and the final tasks will be assessed at the end of Phase 4.

- *Measured thermoelectric HVAC device efficiency meets program objectives.* The thermoelectric HVAC device efficiency targets required a minimum coefficient of performance of 1.3 in cooling mode and 2.3 in heating mode. The target coefficient of performance were achieved during calorimetric testing of the thermoelectric modules in Phase 3, with a temperature drop of 13.6°C measured in cooling mode and a temperature rise of 18°C measured in heating mode.
- *Cost study and commercialization analysis show thermoelectric system potential.* Trade studies were used to assess the component and investment cost impact of implementing zonal thermoelectric HVAC systems in a vehicle, and also established steps required for commercialization of the technology. Results obtained in Phase 3 showed significant on-cost to incorporate a full zonal thermoelectric system. The commercialization assessment completed in Phase 4 suggested that thermoelectric heated/cooled seats and zonal climate system remain viable technologies to pursue in commercial application, however there are significant issues regarding device performance capabilities and thermoelectric material costs.
- *Thermoelectric HVAC system meets comfort targets specified performance criteria.* The thermal comfort criteria were to achieve equivalent thermal comfort compared to the results obtained in a baseline vehicle. Baseline testing was completed in Phase 1. Assessment of this criterion has not yet been completed, but is on-track. Preliminary thermal chamber and modeling studies indicated that achieving equivalent comfort, as constrained by the energy-based metrics, is feasible.
- *Thermoelectric HVAC system reduces energy consumption compared with baseline vehicle.*Vehicle energy use test methods were established to assess the energy consumption from the zonal thermoelectric HVAC system, as well as to determine reducing the energy consumption of the air conditioning compressor. Baseline energy consumption analysis was completed in Phase 1. Assessing this criterion has not yet been completed. Energy modeling studies and thermal chamber testing in Phase 2 indicated that energy reduction was possible.

Conclusions

This project advanced thermoelectric technology to help reduce energy use of the vehicle climate system through a zonal thermoelectric climate control system and is on-track to meet the U.S. DOE project objectives.

General Motors

Project and Objectives

General Motors was also awarded funds to pursue develop a distributed automotive HVAC system that provides thermal comfort equivalent to current state-of-the-art centralized systems while using significantly less energy. The General Motors team proposed a substantial project scope revision to perform additional activities that would specifically benefit electrified vehicles such as the Chevrolet Volt. U.S. DOE approved an increase in funding, which included delivering a Volt demonstration vehicle initially planned for July 31, 2013. Project delays resulted in a no-cost time extension with the Buick LaCrosse demonstration vehicle available by September 30, 2013, and the Chevrolet Volt demonstration vehicle available by March 31, 2014.

General Motors was tasked to:

- Reduce the energy used in cooling mode by 30 percent while maintaining occupant comfort through the localized use of thermoelectric technology while maintaining occupant comfort and safety.
- Develop thermoelectric HVAC components with a coefficient of performance greater than 1.3 for cooling and greater than 2.3 for heating, then integrate and test these components as part of a reliable distributed HVAC system in a conventional vehicle (an eAssist Buick LaCrosse) and an extended range electric vehicle (a Chevrolet Volt).
- Update the University of California Berekley Thermal Comfort model to predict the response of vehicle occupants to localized heating and cooling based on human subject testing, and develop associated computer-aided engineering tools to support the integrating distributed HVAC components into future vehicle designs.
- Improve the efficiency of thermoelectric generators for converting engine waste heat into electricity.

Methodology

General Motors' reduced the energy consumption of the vehicle's central HVAC system (producing a warmer than desired passenger cabin temperature for a cooling situation) while maintaining occupant comfort by using distributed HVAC components to deliver local spot cooling to each occupant. While cooling individual occupant(s) instead of the entire passenger cabin is a basic method for producing energy savings, General Motors' human physiology and psychology facts that recognize cooling of the body that significantly affects perceived comfort.

The project team used humans to develop a math-based thermal comfort model that characterized the sensation and comfort responses to the localized body areas for cooling and heating in a vehicle. The model identified optimal locations and operating parameters for energy-efficient distributed HVAC components that would deliver local spot cooling and heating. The team then selected an optimal combination of locations for distributed HVAC components and developed an initial set of prototype HVAC components that featured thermoelectric modules for energy-efficient distributed cooling and heating. These functional components and the associated control strategies were integrated into a vehicle for testing and evaluation.The team also considered other production-intent requirements, such as noise and packaging. These final prototype distributed cooling and heating components and their associated control strategies will be integrated into demonstration vehicles for final testing and evaluation.

The project was conducted in four phases plus a fifth phase focused on improving engine waste heat recovery concurrent with these first four phases.

Phase 1 –Developed a Thermal Comfort model of human responses to potential locations for distributed heating and cooling and identified optimal locations.

Phase 2 – The team developed the initial prototype distributed HVAC components and evaluated them on a test bench and vehicle.

Phase 3 – Advanced the final prototype distributed HVAC components while considering production-intent requirements such as noise and packaging.

Phase 4 – Engineering integrated the final prototype distributed HVAC components with the production central HVAC system and optimized the performance of the demonstration vehicles. A final analysis will be made to compare the expected efficiency and fuel economy improvements to the program targets.

Phase 5 – Developed improvements in the thermoelectric materials for thermoelectric generators that could be used to produce electrical power for thermoelectric HVAC system loads.

Major Findings with Results

The team successfully developed a distributed automotive HVAC system that provides thermal comfort equal to current state-of-the-art systems while using significantly less energy. In achieving this primary objective, the team met the following specific goals:

- *Fuel consumption used to maintain occupant comfort. Fuel consumption* in cooling mode was reduced by at least 30 percent using thermoelectric technology for localized spot cooling and heating.
- *Measured thermoelectric HVAC device efficiency meets program objectives.* Developed thermoelectric-based components with a coefficient of performance greater than 1.3 for cooling and greater than 2.3 for heating. These prototype components were integrated and tested in an eAssist Buick LaCrosse and an extended range electric Chevrolet Volt
- *Updated the University of California Berekley Thermal Comfort model*. Information was updated for localized heating and cooling, and developed computer-aided engineering tools to integrate distributed HVAC components into future vehicles

Conclusions

Currently, activities are still in-process for Phases 3 – 5. After the project has been completed in 2014, the overall Conclusions and Recommendations will provided to this final report. Based on the interim results and analysis from Phase 2, the team expects to achieve the primary objective and the associated goals for the project.

Project Benefits

Current automotive refrigerant-based vehicle HVAC technologies represent a large mechanical load cool causing the engine to consume more fuel to meet the occupant comfort needs. Incorporating thermoelectric technology to the HVAC system enables localized (zonal) distribution and uses up to 33 percent less energy than the current conventional HVAC system that heats and cools the complete cabin beyond comfort to the occupants. Thermoelectric HVAC also allows for more design options for varying cabin configurations. Using thermoelectric HVAC technology over the conventional HVAC powered by engine combustion, results in a 30 percent reduction in greenhouse gases emitted due to less fuel consumption and refrigerant leakage.

CHAPTER F1: Ford Introduction

F1.1 Project Rationale

Current light-duty vehicles provide passenger thermal comfort primarily through the use of a centralized heating, ventilation, and air conditioning (HVAC) unit that distributes conditioned air to vent locations throughout the vehicle. A substantial portion of the energy content is spent conditioning various elements of the vehicle's interior structures and is not directly used to provide occupant thermal comfort. This is not an overwhelming issue in today's vehicles, but as pressure builds to improve powertrain efficiency, the energy to provide occupant comfort is expected to become a larger part of the total vehicle energy budget.

In February 2008 the U.S. Department of Energy (U.S. DOE) National Energy Technology Laboratory released a Funding Opportunity Announcement (FOA) DE-PS26-08NT01045-01 on behalf of the Office of Energy Efficiency and Renewable Energy Vehicle Technologies Program seeking applications for cost-shared projects in the area of Solid State Energy Conversion for Vehicular HVAC and Waste Heat Recovery to help in addressing the issue of HVAC system efficiency. Ford Motor Company and its partners responded to this FOA and were subsequently awarded a cooperative agreement that began in October 2009. In addition to funding from U.S. DOE, this project is supported by funding from the California Energy Commission (Energy Commission).

Thermoelectric (TE) devices were identified by the U.S. DOE as one potential method of reducing HVAC-related energy consumption in vehicles. In its FOA, the U.S. DOE stated the rationale for research in this area as follows: "*Current air conditioner technology is designed to heat and cool occupants according to their thermal loads in addition to the thermal loads of the surrounding structures such as the headliner, windows, flooring, and seat backs. These systems require 3,500-4,500 watts of cooled air at steady state, while preliminary analysis indicates that <700 watts of cooling or heating per person and <3000 watts for a vehicle with five occupants would be adequate for occupant comfort.*"

The U.S. DOE went on to state the program objectives as follows: "*The overall objective of this area of interest is to solicit applications to accelerate development of recently emerging high-efficiency TE modules that pump heat in either direction to provide the HVAC function in vehicles. These TE HVAC systems should reduce petroleum consumption, toxic emissions and greenhouse gases in autos, light trucks and heavy-duty trucks. The primary objective of this area of interest is to develop vehicular TE HVAC systems to augment or replace currently available air-conditioners that use compressed R-134a refrigerant gas. The TE HVAC system should incorporate appropriate design features afforded by thermoelectrics. The TE HVAC systems should have a coefficient of performance (COP) of >1.3 for cooling and > 2.3 for the heating mode. The TE HVAC system should be optimized to provide occupant comfort while reducing fuel consumption and associated regulated emissions, and eliminate the release of greenhouse gases to the atmosphere associated with HVAC. The TE HVAC system should reduce the energy required by current compressed gas air conditioners by 1/3. TE HVAC systems developed under* *this area of interest should be targeted for introduction into production vehicles in the 2012 to 2015 timeframe."*

F1.2 Ford TE HVAC Project Objectives and Goals

In the context of the U.S. DOE requirements, the overall objective of the *Ford Thermoelectric HVAC Project* was to identify a technical and business approach to accelerate research and development of light-duty automotive thermoelectric HVAC technology. In order to accomplish this objective, a zonal HVAC system was to be developed in order to provide thermal comfort to each occupant, with the goal of reducing the overall power consumption of the HVAC system, compared to a baseline system. This new thermoelectric HVAC system was to be designed to provide: (i) the basis for a down-sized central HVAC unit, (ii) equivalent thermal comfort to occupants, and (iii) reduced energy consumption. Project success was to be evaluated in a vehicle equipped with a prototype zonal thermoelectric HVAC system. The U.S. DOE further refined the global objectives to the following engineering goals:

- *Develop a TE HVAC system to optimize occupant comfort and reduce fuel consumption*
- *Reduce energy required to operate the AC compressor by 1/3*
- *Demonstrate TE devices that achieve COPcooling > 1.3 and COPheating > 2.3*
- *Demonstrate the technical feasibility of a TE HVAC system for light-duty vehicles*
- *Develop a commercialization pathway for a thermoelectric HVAC system*
- *Integrate, test, and deliver a 5-passenger thermoelectric HVAC demonstration vehicle*

The identification and demonstration of the technical and commercial approaches needed to accelerate deployment of zonal thermoelectric HVAC systems in light-duty vehicles was to be a key component of the overall project plan. To accomplish the project goals, Ford Motor Company established partnerships with stakeholders whose expertise was vital to the success of the program. Halla Visteon Climate Control Corporation is a leading integrator of HVAC systems in automobiles and provided expertise in HVAC system modeling, design, testing and commercialization. Gentherm Corporation provided expertise in thermoelectric device implementation in the automotive industry, as well as a wealth of expertise in advanced thermoelectric materials and technology. The National Renewable Energy Laboratory provided expertise in the area of vehicle occupant thermal comfort and HVAC load reduction technologies. The Ohio State University provided expertise into the development of advanced thermoelectric materials.

F1.3 Ford TE HVAC Project Plan

The project was conducted in four phases with interim technical milestones and a go / no-go decision point at the end of each phase. Each phase of the project contained four major technical tasks. The approach was to develop a supplemental zonal thermoelectric HVAC system for light-duty vehicle applications that worked in conjunction with a reduced-capacity conventional compressor-based HVAC system. The overall timeline for the project is shown in

Figure F1. Phase 1: Applied Research involved vehicle platform selection, requirement and performance specification development, an architecture trade-off study, and initial modeling analysis. The results of the architecture study were used to develop a formalized conceptual design that considered necessary modifications to the electrical system architecture, powertrain and power management strategies. The conceptual design included detailed modeling and analyses of the TE/central HVAC subsystems, and the vehicle power budget. Human comfort modeling was investigated and integrated with computational fluid dynamics (CFD) and thermal computer aided-engineering (CAE) analysis. The baseline vehicle system performance and architecture were benchmarked and advanced materials development effort was initiated. Phase 2: Exploratory Development involved detailed modeling and analysis of the vehicle environment, packaging and design studies to assess architecture trade-offs, and a thermal-chamber trade-study of proposed thermoelectric HVAC elements. In addition, further refinement of advanced thermoelectric devices and materials was pursued. Phase 3: Advanced Development included the development, fabrication, and bench testing of thermoelectric HVAC hardware, power supplies, and a preliminary control system. A cost analysis of production architecture was conducted. Advanced thermoelectric subassemblies were designed, built, and tested. Strategies for reducing overall cabin thermal loads were also explored. Phase 4: Engineering Development is currently underway and scheduled to be completed by September 2013. This phase focuses on integrating and testing the TE HVAC hardware in a prototype vehicle to determine the system's ability to decrease HVAC system energy use while providing equivalent occupant thermal comfort. System commercialization is also being explored. A study of advanced thermoelectric materials and design concepts will also be completed.

Figure F1: Timeline for the Ford TE HVAC Project

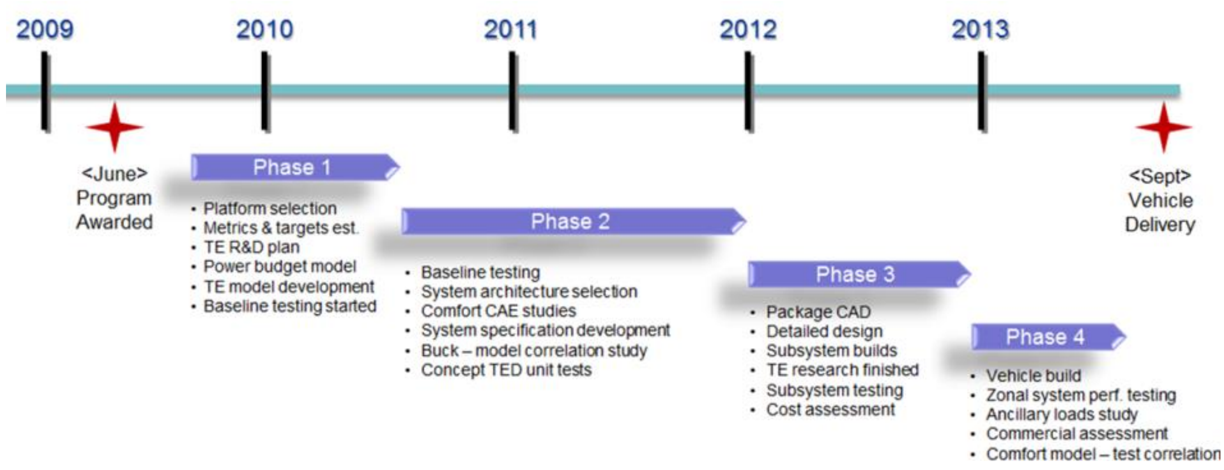

Source: Ford Motor Company

CHAPTER F2:
Ford Phase 1 – Applied Research

Phase 1, Applied Research, was started October 1, 2009 and completed September 30, 2010. Proposed HVAC architectures were studied, thermal comfort-based test criteria were developed, and advanced thermoelectric materials and devices were researched.

F2.1 Task Description and Milestones for Phase 1

The purpose of Task 1 was to develop test conditions, operating criteria, and metrics for evaluating system performance, as well as to perform an assessment of the occupant comfort CAE methods and perform baseline vehicle system modeling using the assessment criteria. The purpose of Task 2 was to begin advanced materials research, to develop thermoelectric device models, to develop new thermoelectric device designs, and to validate the performance of these new devices using the models. The purpose of Task 3 was to study and analyze potential vehicle climate system architectures in a mock vehicle environment and to use this information, along with modeling studies, to develop a proposed architecture to build and test in a vehicle. The purpose of Task 4 was to conduct a systems trade study. The proposed architectures were evaluated for their commercial feasibility, and their potential efficiency improvements were analyzed in the context of full-vehicle integration.

F2.2 Selection of Test Conditions and Performance Metrics

In order to determine the environmental test conditions to be used to assess system performance, it was necessary to study three primary contributing factors. First, geographic distribution of the U.S. population, based on data from the United States Census Bureau, was used to determine where most vehicle occupants live and drive. Second, weather conditions, derived from National Weather Service, were analyzed for U.S. locations representative of population distribution in order to determine the ambient conditions in which vehicles in the continental U.S. operate. Third, aggregate drive patterns were analyzed to determine trip start time, length, and duration. The analysis used data contained within the National Highway Transportation Survey, conducted by the U.S. Department of Transportation.

The pattern of vehicle operation was crucial to determining statistical distribution of key factors influencing the operation of vehicle climate control systems. Some of the key considerations included distance and length of a typical vehicle trip, time a vehicle was parked between trips, occupancy of the vehicle for specific trip types, average vehicle speeds, and time of day a vehicle was operated.

It was crucial to limit the number of physical test cases due to the time and cost of testing and analysis. Data needed to complete vehicle architecture trade-off studies necessitated that a minimal number of test configurations represent significant real-world conditions. To accomplish this goal, six test conditions were developed to show the benefit of improving efficiency of a vehicle climate control system on a U.S. light duty fleet aggregate basis. These conditions focused on three heating-mode tests and three cooling-mode tests. Two of the tests represented system capacity tests, and were critical for climate system sizing, but had limited weighting impact due to infrequent occurrence of these conditions in major U.S. markets. The relevant ambient temperature conditions, shown in Table F1, were population-averaged for each region and represent the average condition for each region for hot and cold months.

Table F1: Ambient Temperature Conditions in Regions of Significant Population

	Pct. Population %	Max. Jan °C	Min. Jan °C	Max Aug °C	Min Aug °C
Northeast / Midwest States	36%	0	-4.7	27	19.3
Gulf States and California	34%	16.0	7.5	31.0	21.2
Fairbanks, Alaska	-	-17	-18.2	19.1	9.4
Phoenix, Arizona	-	18.8	8.2	39.2	28

Source: Ford Motor Company

It was important to understand frequency of vehicle warm-up and cool-down events in the U.S. It was assumed that a temperature below 15°C (60°F) would require operation of the vehicle's cabin heating system to maintain occupant comfort. Likewise, vehicle operation above 25°C (78°F) would require some vehicle cabin cooling to maintain comfort. Temperature conditions in the major metropolitan areas were analyzed and are summarized in Figure F2.

Figure F2: Distribution of Annual Ambient Temperature Conditions in Primary Regions

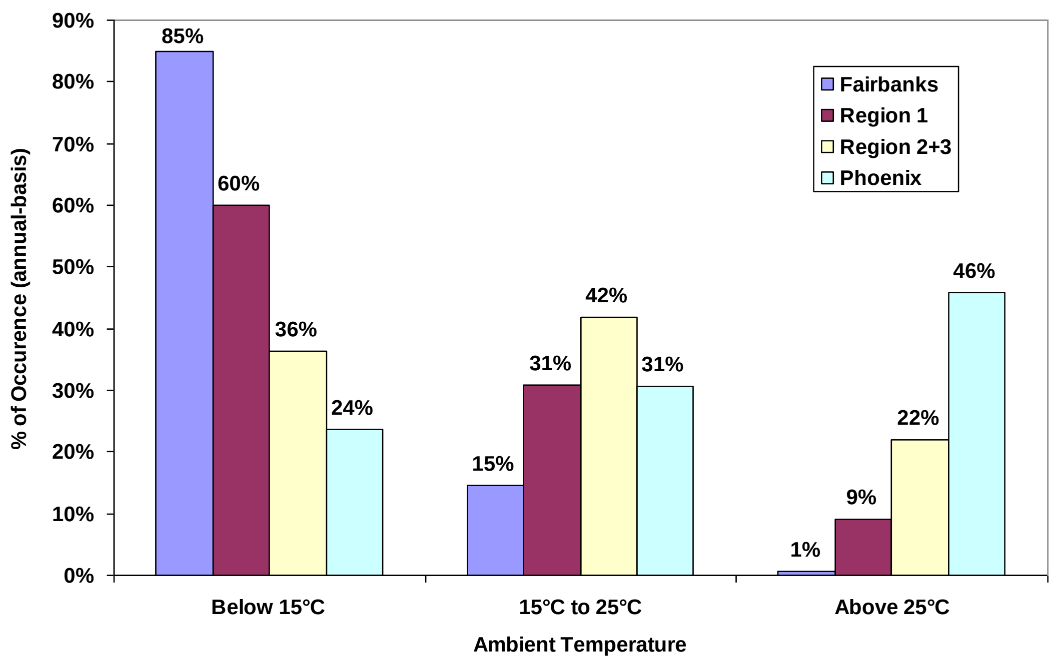

Region 1 in the graph represents the population in the upper Midwest and Northeast states. Region 2 represents populations in the Gulf Coast. Region 3 represents the major population centers in California.

Source: Ford Motor Company

Table F2: Ambient Conditions Weighting Factors for Vehicle Energy Assessment

Test Name	Ambient Conditions (°C), (% RH)	Solar (W/m^2)	Total Occupanc y	Temperatur e Weighting	Occupancy Weighting	Calculated Weighting *	Final Weighting
Cold 1	-18°C	0	2	5%	25%	6%	**6%**
Cold 2	-5°C	0	4	15%	10%	11%	**11%**
Cold 3	5°C	0	1	30%	67%	33%	**33%**
Hot 3	28°C / 70%	750	1	30%	67%	27%	**31%**
Hot 2	32°C / 70%	850	2	15%	25%	13%	**13%**
Hot 1	43°C / 40%	1000	1	5%	67%	10%	**6%**

* Overall weighting = [75% x Temperature Weighting + 25% x Occupancy Weighting] / Σ [Cold or Hot Weighting]

Source: Ford Motor Company

The weighting for energy efficiency for each test condition was determined by integrating the energy consumption of the climate control system over five periods of time representing typical driving durations. The weighting factors are listed in Table F2 and were derived from analysis of the environmental and drive-based weighting factors. Results of the overall weighting for the testing are shown in Figure F3.

Figure F3: Overall Weighting Factors for Determining HVAC System Efficiency

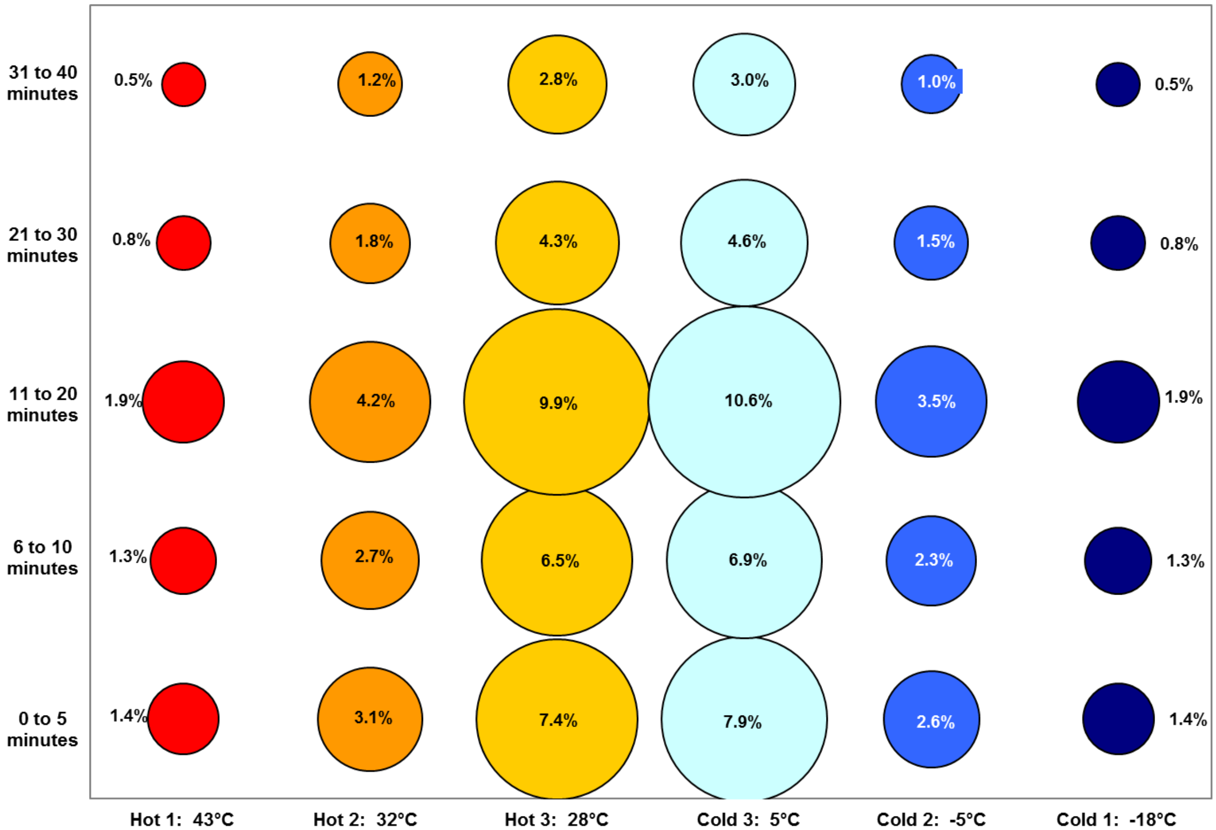

Source: Ford Motor Company

F2.3 Baseline Vehicle Climate System Test Results & Analysis

F2.3.1 Hot Condition Baseline Test Results

Vehicle tests were conducted at the three specified hot weather conditions in order to characterize performance of the vehicle HVAC system. Three tests were conducted at each temperature condition: a baseline performance test with no vehicle occupants, a subjective test where front panel vents were directed at the breath level of the front-row evaluators; and a subjective test where one front panel vent was directed at the breath, and one front panel vent was directed at the chest of each front-row evaluator. The two test evaluators were the same for the subjective tests. Their clothing ensembles were also coordinated and kept the same for each test. Results of selected vehicle temperature profiles for the three hot- test conditions are shown for the average vehicle interior air temperature, Figure F4, and average front register discharge temperature, Figure F5. Baseline hot weather thermal comfort and sensation ratings were measured by the subject raters and are reported in Figures F6 and F7. For a full discussion of the thermal sensation and comfort scales used for this project, refer to Hui Zhang's 2003 PhD thesis: "Human Thermal Sensation and Comfort in Transient and Non-Uniform Thermal Environments".

http://repositories.cdlib.org/cedr/cbe/ieq/Zhang2003Thesis

Figure F4: Average Vehicle Interior Air Temperature During Hot Condition Baseline Tests

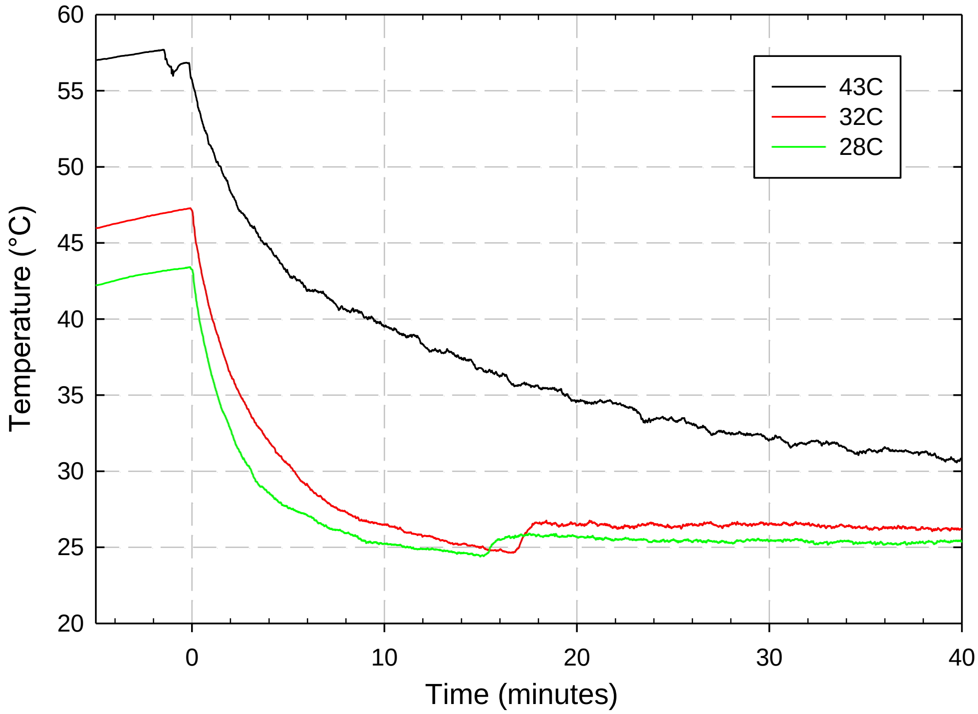

Source: Ford Motor Company

Figure F5: Average Register Discharge Temperature During Hot Condition Baseline Tests

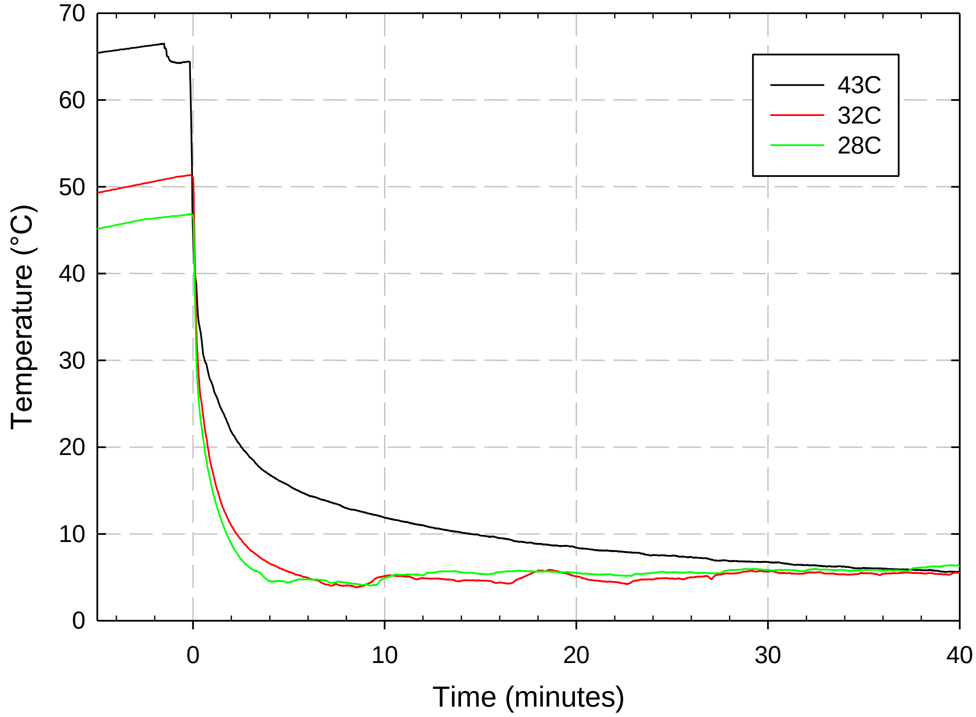

Source: Ford Motor Company

Figure F6: Thermal Comfort Ratings During Hot Condition Baseline Tests

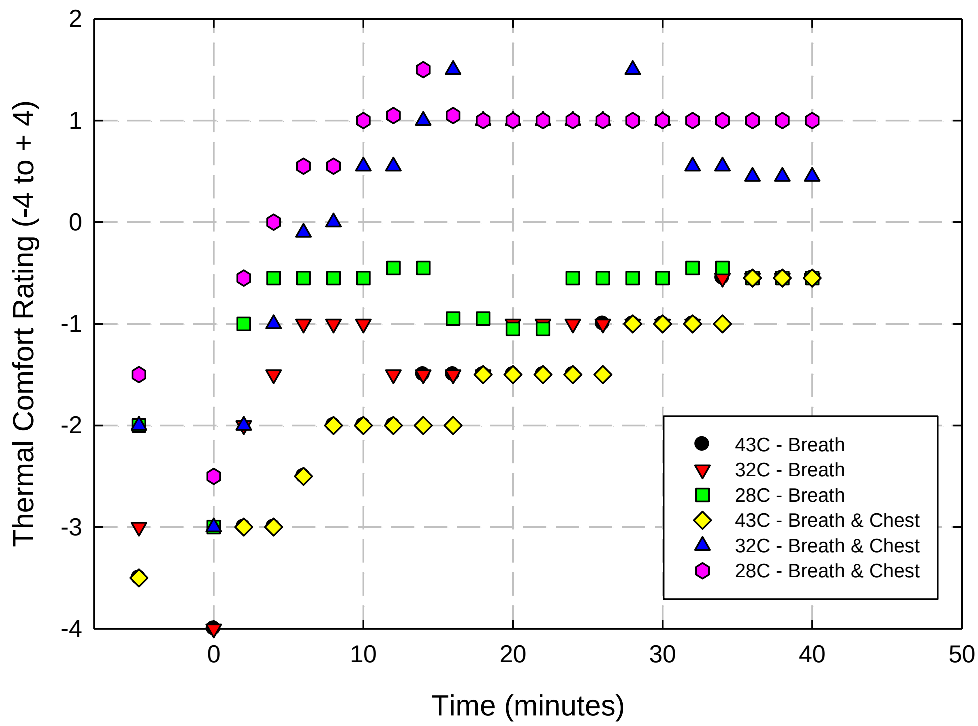

Source: Ford Motor Company

Figure F7: Thermal Sensation Ratings During Hot Condition Baseline Tests

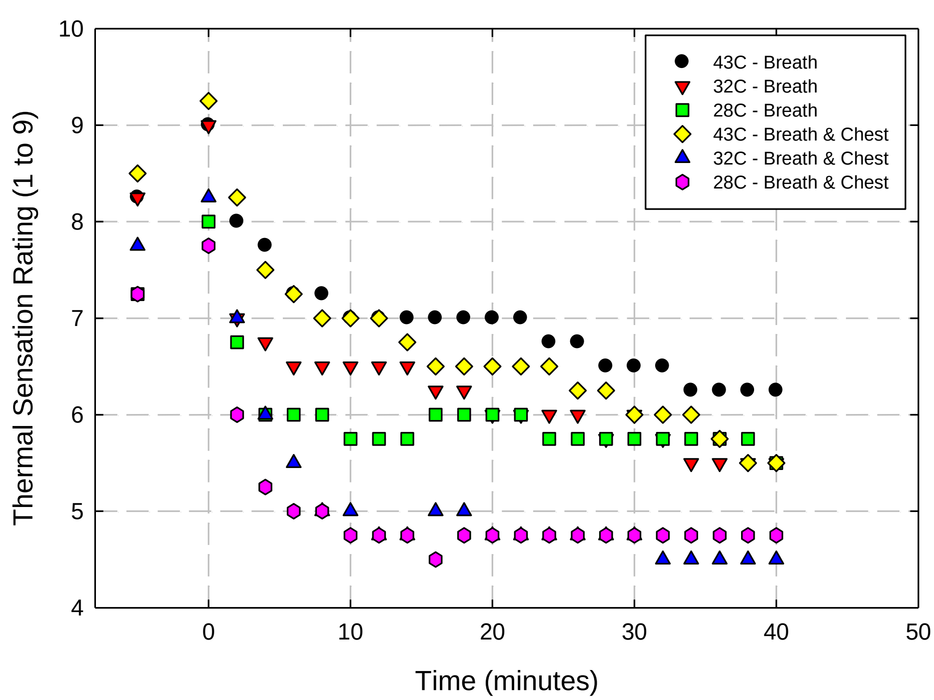

Source: Ford Motor Company

During the tests, once the air exiting the registers reached a set temperature of roughly 5°C, the compressor speed and power were gradually decreased. The weighting factor calculations to establish the baseline power draw of the air conditioning (AC) compressor were calculated based on the weighting factors listed in Figure F3. The summarized results, shown in Table F3, indicated that the modified TE HVAC system would require a weighted compressor power consumption reduction to a value less than 162.9 (arbitrary units) in order to achieve the 1/3 reduction in compressor power listed in the U.S. DOE objectives. Each value in the table was calculated by multiplying the AC compressor energy consumption (W-hr) by the hot-weather weighting factor from Figure F3.

Table F3: Summary of AC Compressor Weighting Factor Test Results

Time (min)	Hot 1: 43°C	Hot 2: 32°C	Hot 3: 28°C
0 to 5	9.39	19.32	38.05
5 to 10	9.49	13.50	16.24
10 to 20	27.64	24.09	32.28
20 to 30	11.66	8.95	13.00
30 to 40	7.10	4.80	7.55
Totals	65.28	70.66	107.13
Grand Total	243.1		

Source: Ford Motor Company

From the data presented in the previous table, a few key trends emerged. First, it was clear that in order to maintain occupant comfort under the 43°C ambient condition, it would be challenging to reduce AC compressor power, since that was known to have a significant impact on discharge air temperatures. At the more moderate ambient temperature conditions (32°C and 28°C), the data suggested that compressor power decreased significantly after cabin temperatures began to moderate. Weighting factors were applied to the data for each of the drive segments, as shown in Figure F9. Analysis of these results suggested that a 33% reduction in weighted AC compressor power demand would require compressor energy consumption to be reduced mainly during the first ten to fifteen minutes of the drive cycles.

Figure F8: Energy Consumed by the AC Compressor Under Hot Weather Conditions

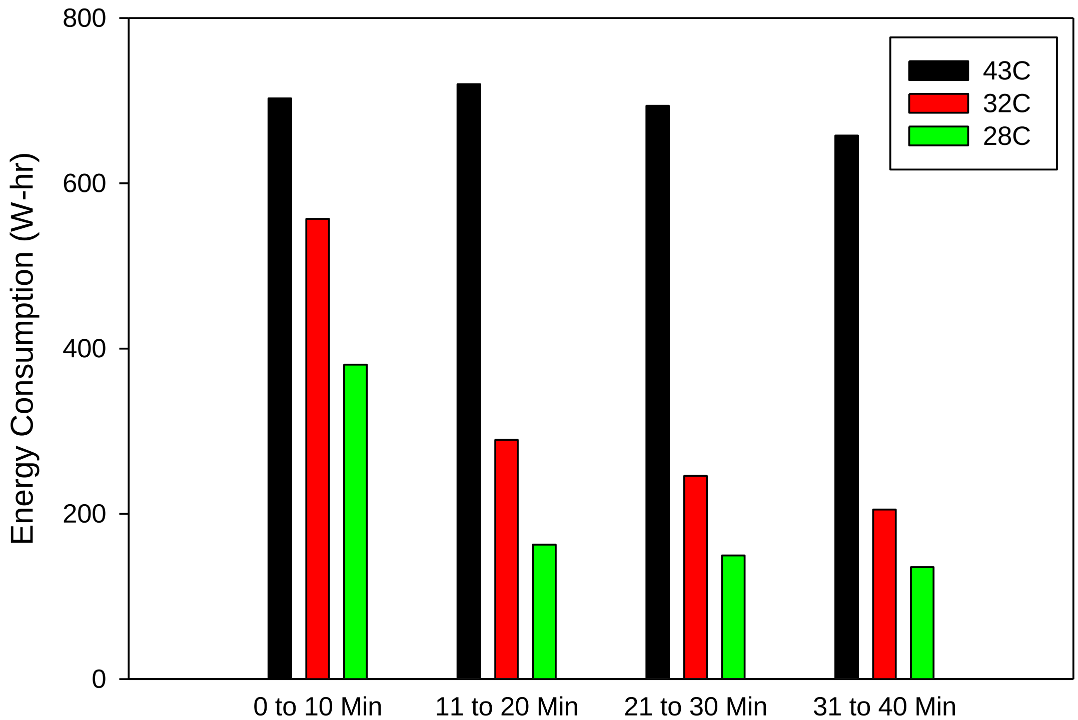

Source: Ford Motor Company

Figure F9: Weighted Energy Consumed by Compressor Under Hot Weather Conditions

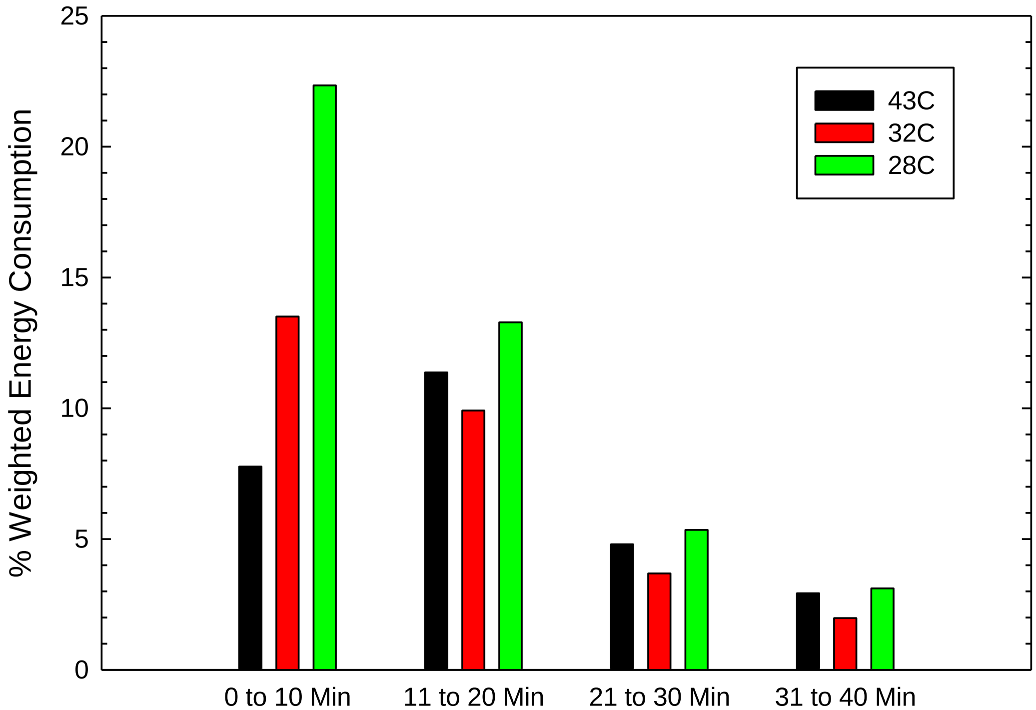

Source: Ford Motor Company

The electrical power required to cool the vehicle was a combination of the AC compressor, HVAC blower fan, and the engine cooling fan loads. All of the other electrical loads contributing to vehicle cooling were generally small or will not change between the baseline vehicle and the vehicle with the TE HVAC system. As shown in Figure F10, the HVAC blower power consumption was quite high initially, since the system operated at full blower speed, but as the cabin air temperature and the return air into the HVAC case became cooler in the milder ambient conditions, the fan power (and speed) began to decrease. In the 43°C test condition, the blower speed stayed on its maximum setting for the duration of the test. The engine fan also operated during the performance tests. As in the case of the blower, the fan speed reduced substantially over the course of the test as the cooling requirements in the cabin began to decrease. The fan ran at full speed for the duration of the test at the 43°C ambient condition due to the large demands from the refrigerant system. The overall electrical power consumption required for vehicle cooling during the three test conditions is shown in Figure F11.

Figure F10: HVAC blower power consumption for hot weather test conditions

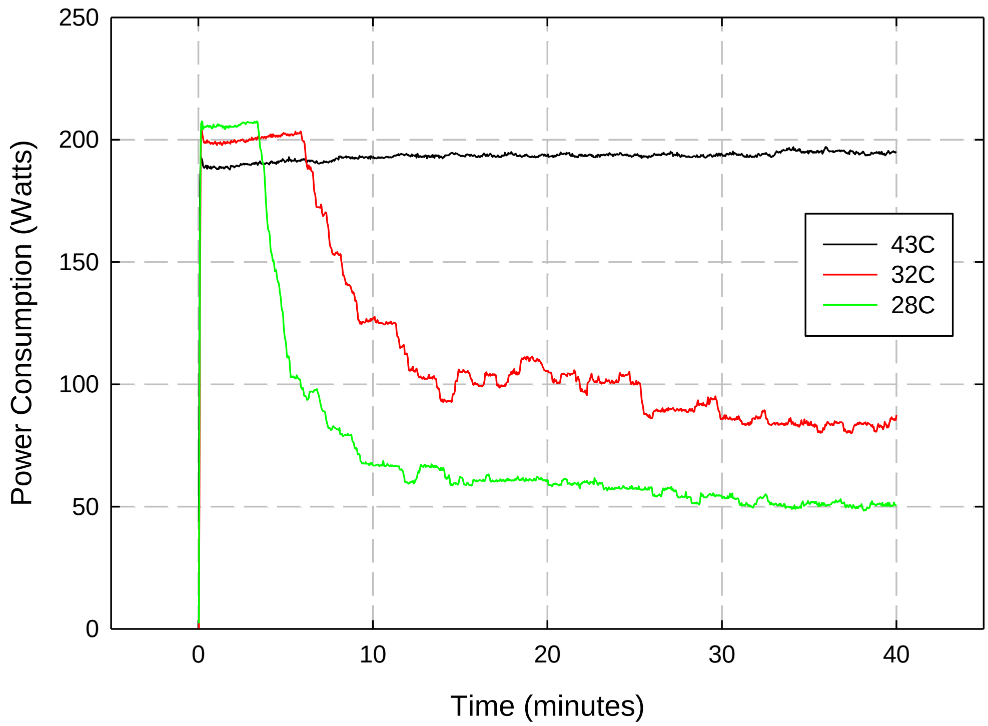

Source: Ford Motor Company

Figure F11: Total HVAC system energy consumption for hot weather test conditions

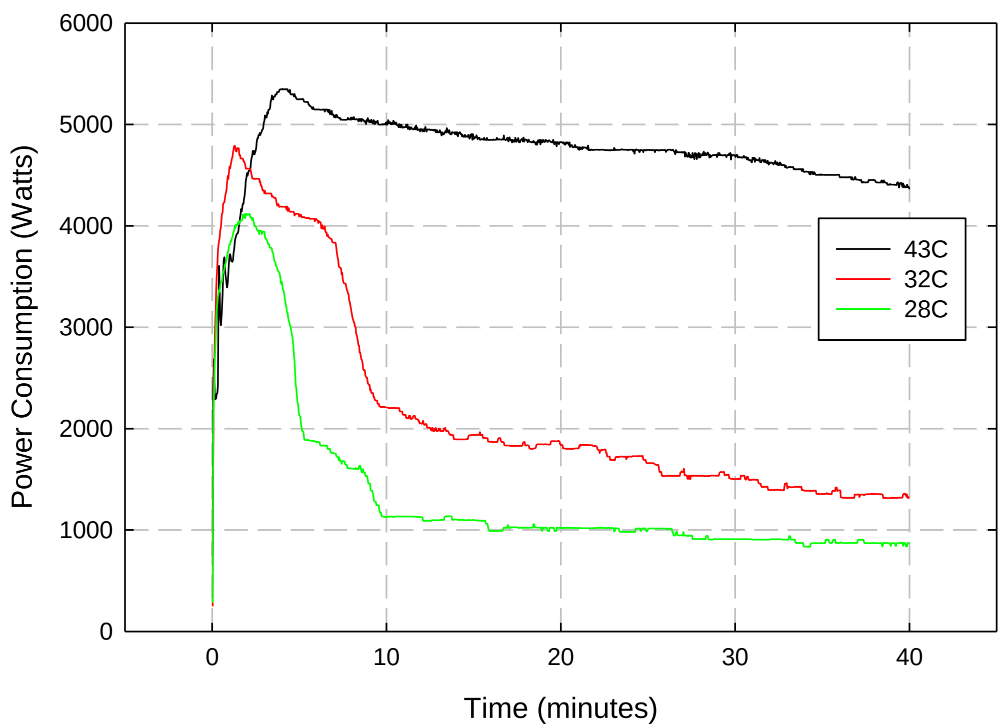

Source: Ford Motor Company

When the segment energy weighting factors were applied, impact on overall energy consumption was substantially changed, as summarized in Figure F12.

Figure F12: Hot-temperature segment weighted HVAC energy consumption

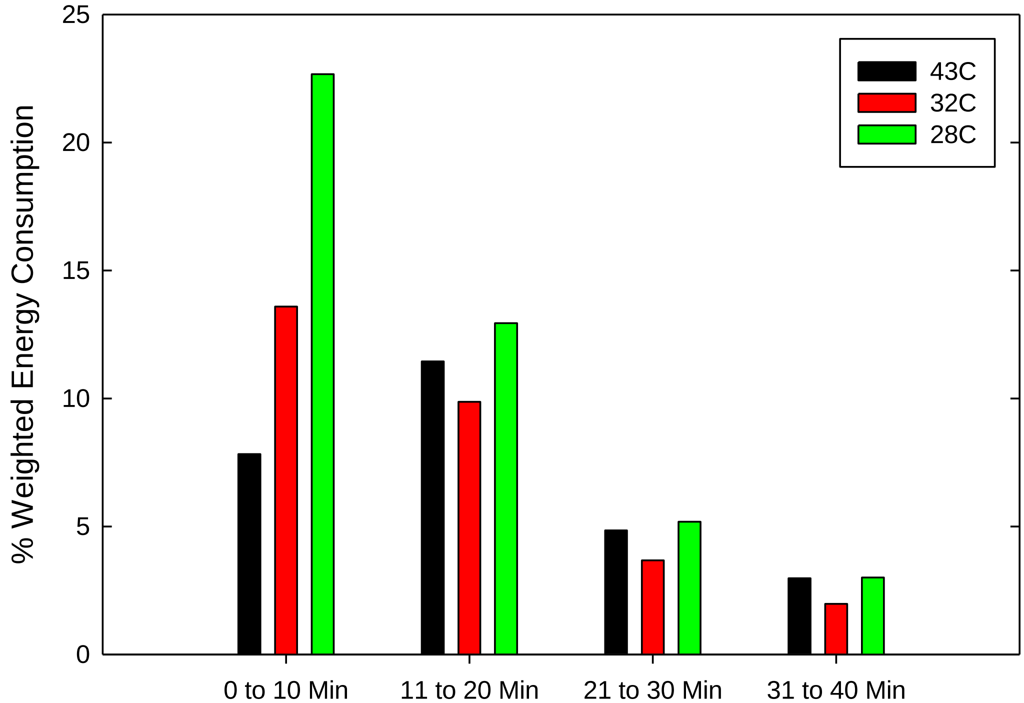

Source: Ford Motor Company

F2.3.2 Cold Condition Baseline Test Results

Vehicle tests were conducted to characterize the performance of the vehicle HVAC system under cold-weather conditions listed in Table F2. Two tests were conducted at each ambient condition: a baseline performance test with no vehicle occupants and a subjective test where the HVAC system air was directed to the vehicle floor registers. Results of vehicle average interior air temperature profiles were measured and are shown in Figure F13. Floor discharge air temperatures for the tests are shown in Figure F14. Results for occupant thermal comfort and sensation are shown in Figure F15 and F16, respectively. The testing indicated that occupant s began to approach neutral thermal comfort between 10 and 20 minutes into the test, depending on the ambient conditions.

Figure F13: Average interior air temperature during cold condition baseline tests

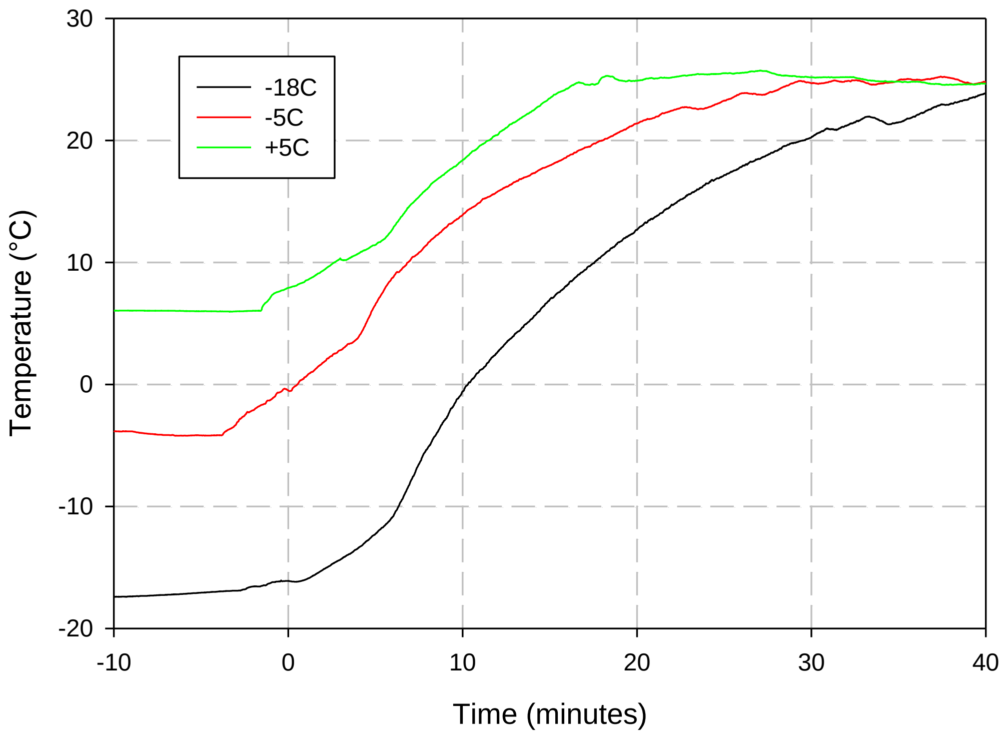

Source: Ford Motor Company

Figure F14: Average floor discharge temperature during cold condition baseline tests

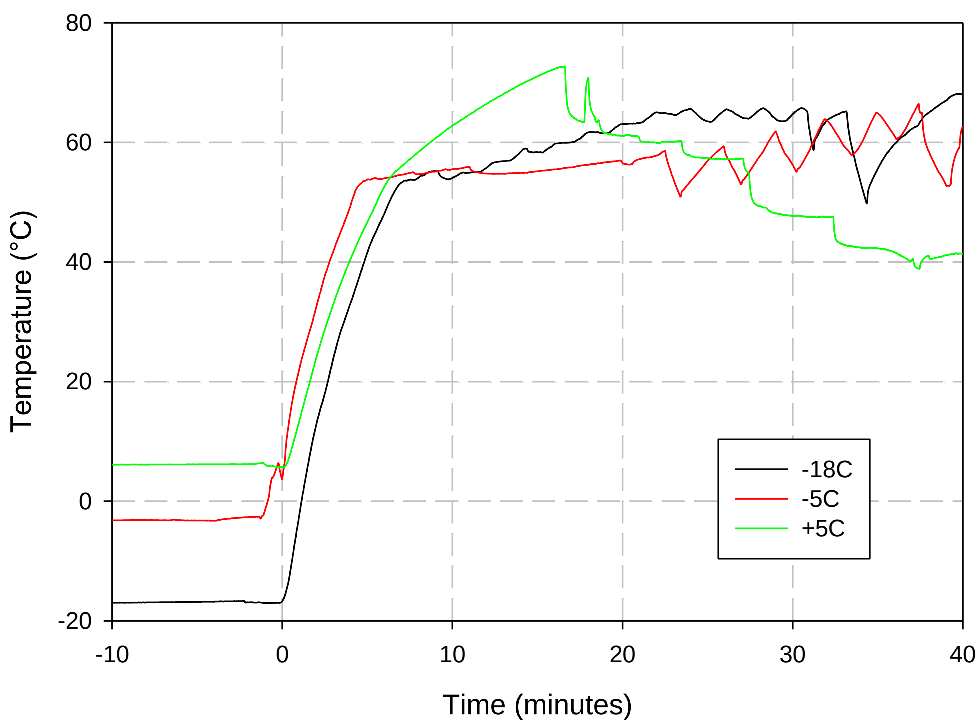

Source: Ford Motor Company

Figure F15: Average occupant thermal comfort during cold condition baseline tests

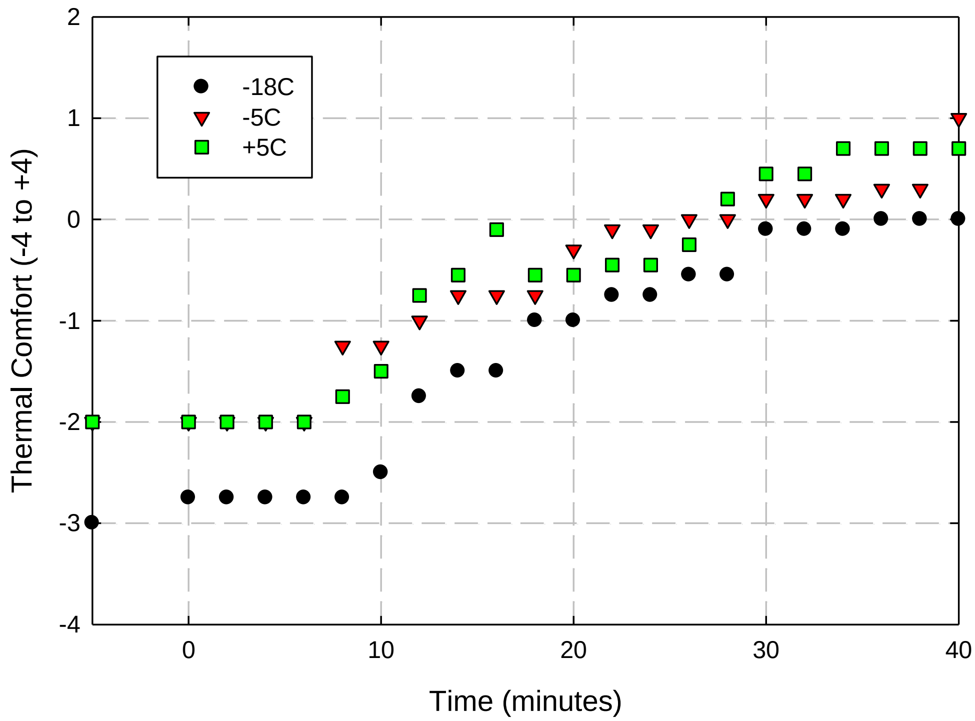

Source: Ford Motor Company

Figure F16: Average occupant thermal sensation during cold condition baseline tests

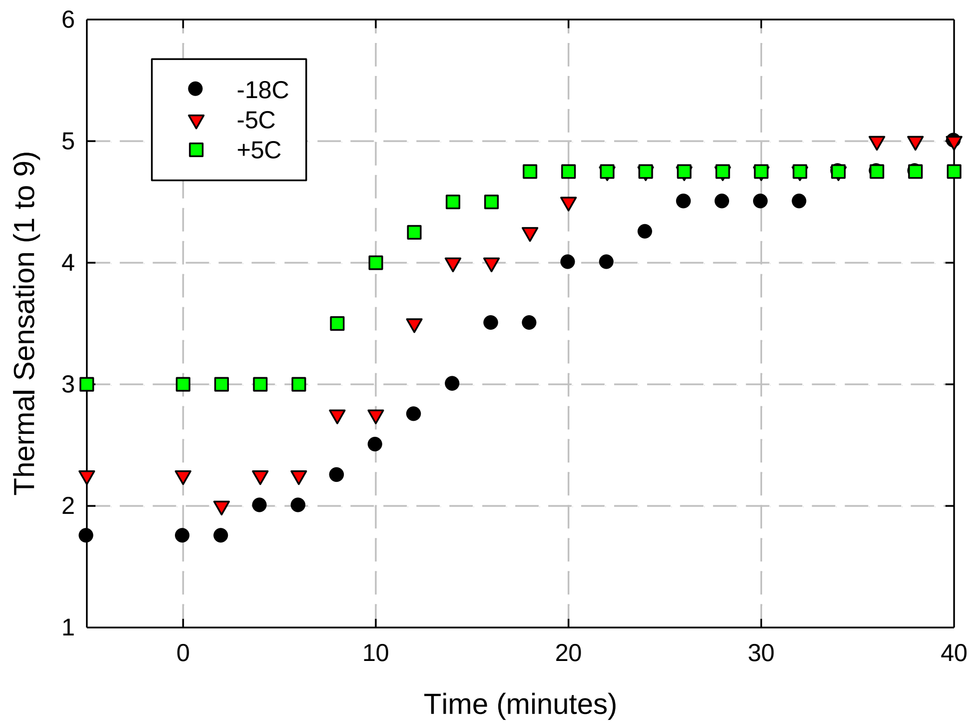

Source: Ford Motor Company

Capturing energy consumption for cabin heating in conventional hybrid electric vehicles, such as the vehicle used for this project, proved to be a challenge. It was difficult to deconvolve the uses for heat in the engine operation required to power the vehicle, warm up the powertrain lubricants, and increase the high-voltage (HV) battery temperature. Because of these challenges, there was no attempt to separate out these various functions. Instead, the electrical power consumption (i.e. the blower fan and the engine fan) and thermal energy extracted from the heater core used for cabin heating were measured in order to determine the energy required for cabin heating. The results of this analysis are shown in Figure F17, and the coolant temperature in the heater core is shown in Figure F18, along with the air and coolant flowrates. The total heating energy provided to the cabin is shown in Figure F19. The energy being directed into cabin air started out quite low, since it took the engine several minutes to warm the coolant up. The energy consumption results are summarized in Figure F20. As expected, the energy consumption peaked during the second ten-minute segment once the engine coolant was warmed up. As the cabin began to heat appreciably, the blower speed was reduced. The segmented weighted results, using the weighting factors from Figure F3, are shown in Figure F21.

Figure F17: Temperature gain between blower fan and floor outlets during warm-up tests

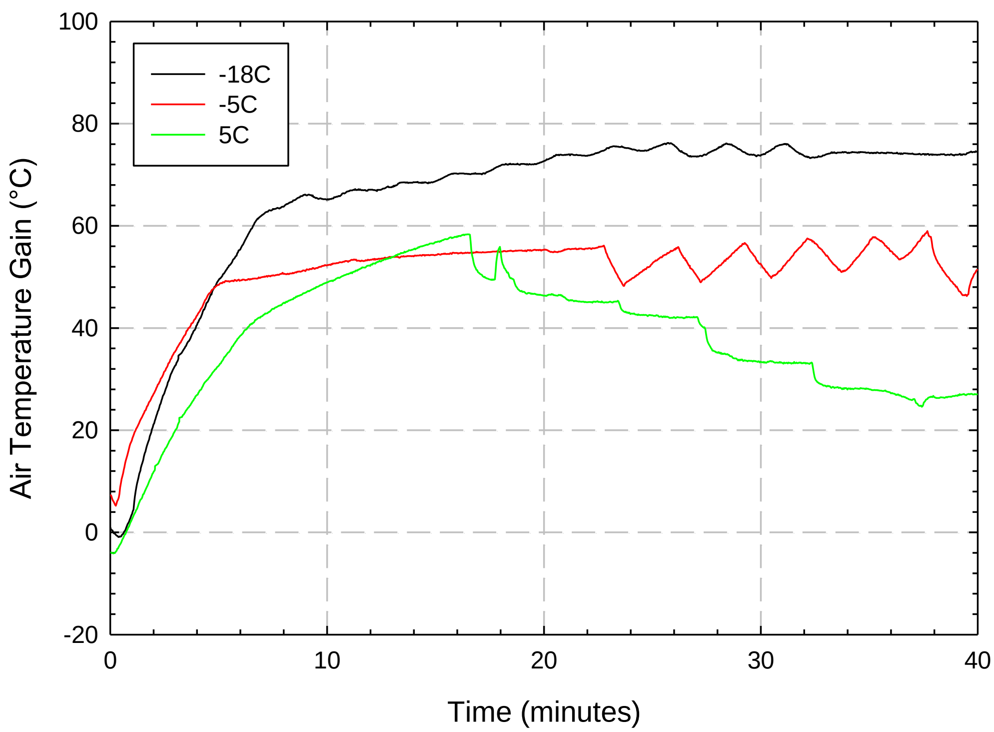

Source: Ford Motor Company

Figure F18: Measured coolant temperature into heater core during warm-up tests

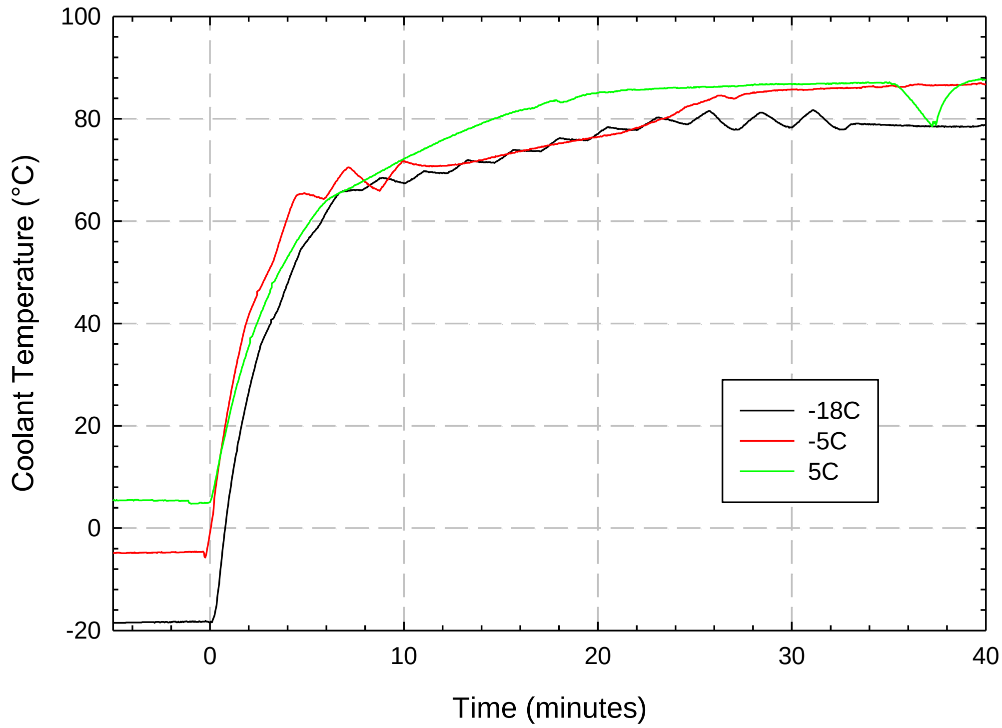

Source: Ford Motor Company

Figure F19: Calculated heat gain in air during heater tests

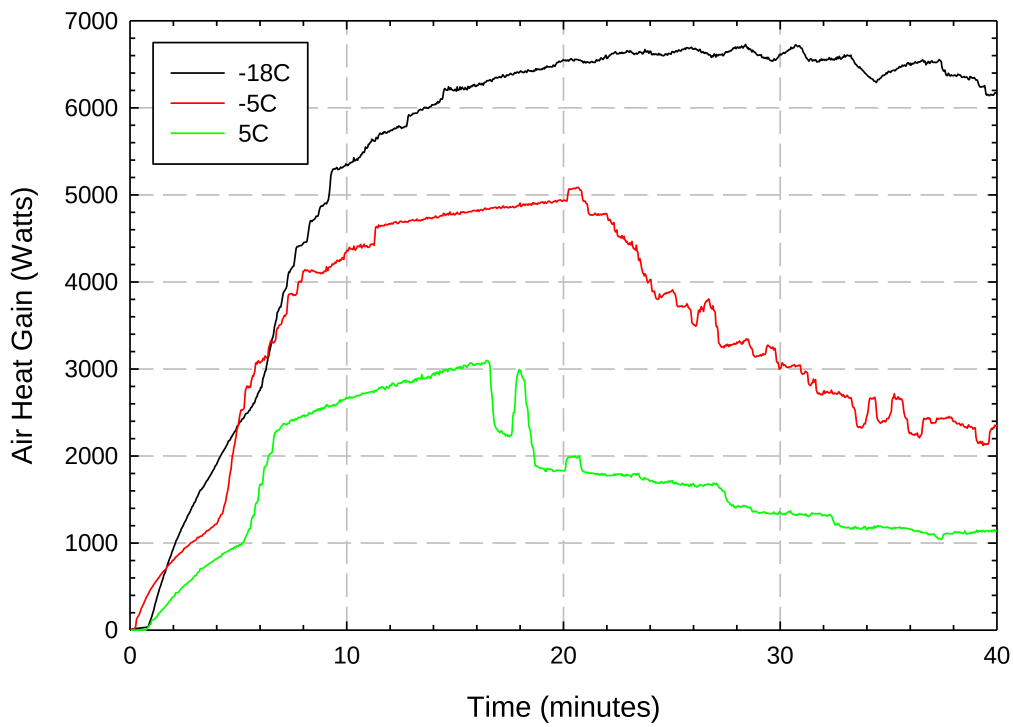

Source: Ford Motor Company

Figure F20: HVAC system energy consumption for the three cold weather conditions

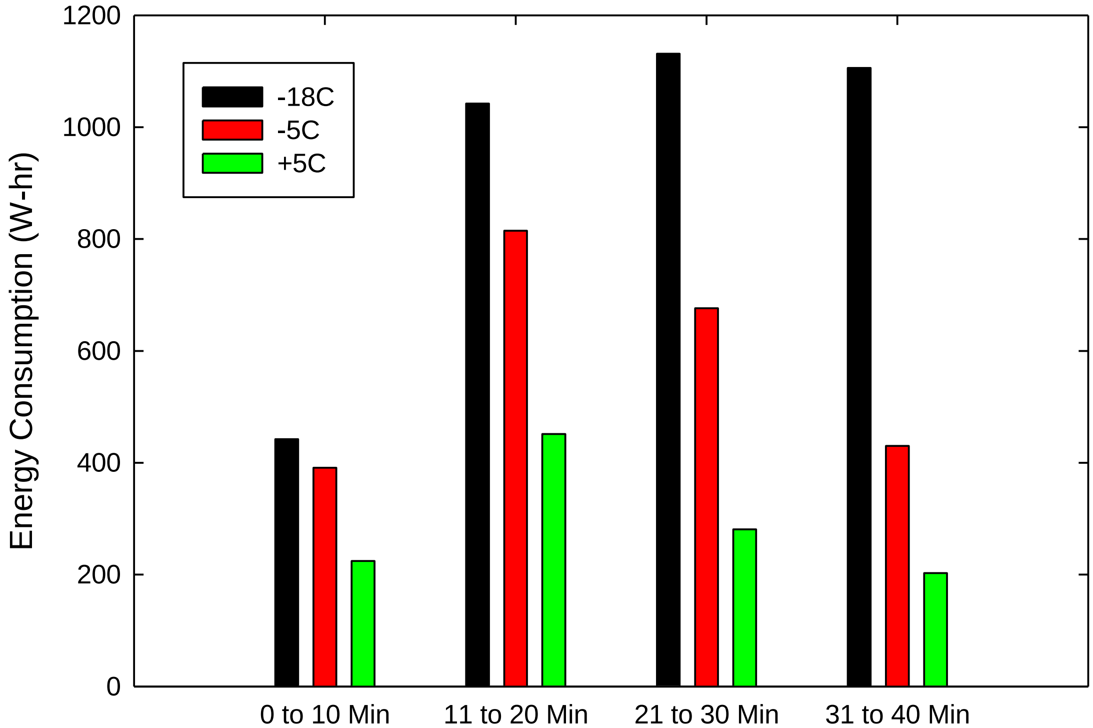

Source: Ford Motor Company

Figure F21: Segment and drive-cycle weighted HVAC baseline system energy consumption

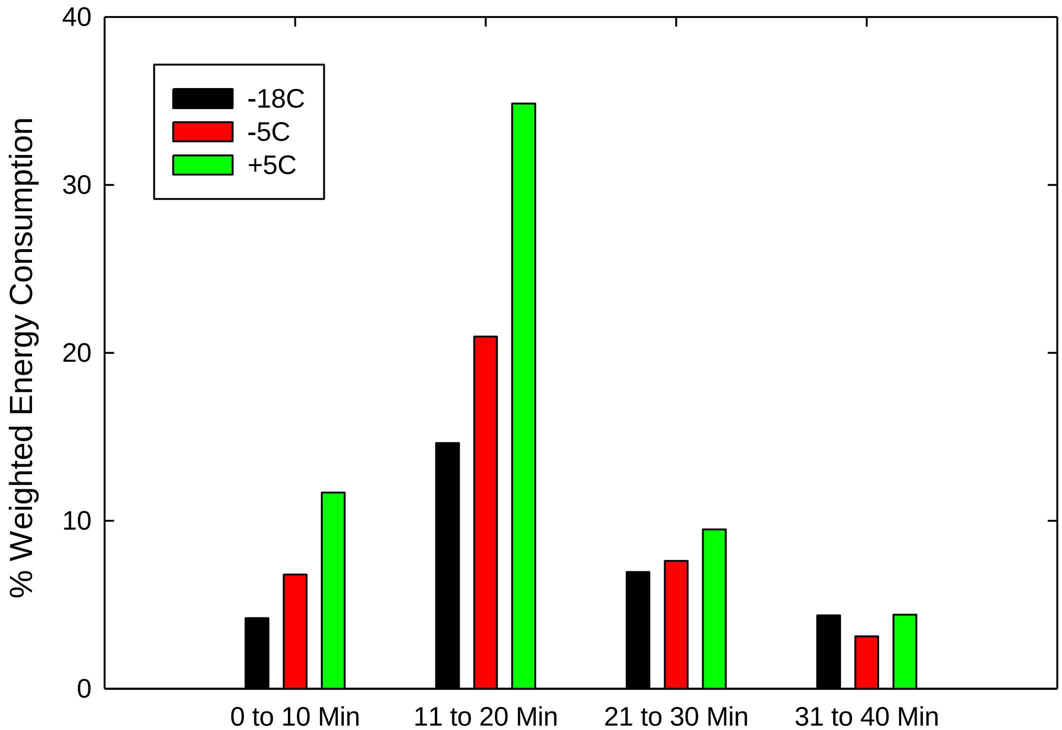

Source: Ford Motor Company

F2.3.3 Summary of Baseline Test Results

The results for the overall segment- and drive-cycle weighted energy consumption were calculated. The results, tabulated in Table F4, indicated that in order to reduce energy consumption to a value lower than 313 (arbitrary units), calculated by multiplying the total energy consumption (W-hr) by the weighting factors shown in Figure F3, significant change in system operation and control was required to maintain both cooling and heating performance, as well as to maintain occupant comfort.

Table F4: Normalized HVAC system energy consumption

Time (min)	Hot 1: 43°C	Hot 2: 32°C	Hot 3: 28°C	Cold 3: 5°C	Cold 2: -5°C	Cold 1: -18°C
0 to 5	5.37	11.06	22.08	3.25	2.08	1.45
5 to 10	5.34	7.53	8.93	12.72	7.22	4.30
10 to 20	15.66	13.50	17.71	47.67	28.69	20.01
20 to 30	6.63	5.03	7.09	12.97	10.41	9.50
30 to 40	4.07	2.70	4.11	6.02	4.26	5.97
Totals	37.07	39.83	59.92	82.64	52.65	41.23
Grand Total	313.3					

Source: Ford Motor Company

F2.4 Advanced TE Materials Research Plan

A plan was developed to investigate thermoelectric materials that could be fabricated in bulk, produced economically and which were targeted to have a figure of merit (ZT) between 1.3 and 1.7 at room temperature. The primary material used in commercial heating and cooling applications is Bi_2Te_3 based. Commercially available Bi_2Te_3 materials have ZT values ranging from 0.8 to slightly greater than 1.0 in typical heating and cooling operating temperature range. Some superlattice materials hold promise of improved performance; however, the pathway to macroscopic thicknesses, required for devices operating in heat flux conditions typical of an automotive use, is unclear and was not felt to be a viable option for this program.

The selected material needed to fit into the current manufacturing footprint for thermoelectric devices in order to be readily commercialized. In addition, the selected material could not require major developments in manufacturing techniques that would require cost-prohibitive capital investment. The major areas of manufacturability which were considered in making this assessment were ingot forming, "pellet" sizing (slicing & dicing), metallization and soldering.

Skutterudites and Bi_xSb_y were also reviewed for their economic potential, but neither family was found to be close to the performance of Bi_2Te_3 near room temperature. There were no known research paths that could potentially deliver either of these material families with a ZT of greater than 1.3 in the required working temperature range, within the time frame of the project.

The performance factors listed above, known manufacturing processes, and the broad general knowledge base surrounding Bi_2Te_3 made it the ideal candidate for this research project with the performance, timing and funding constraints provided in the scope of this program. This decision was based on recent success in improving PbTe. The primary area of research for this project was to develop stoichiometries that showed optimized levels of resonant impurities to increase the power factor (multiple of the square of Seebeck coefficient (α) and electrical conductivity) of the material and thereby increasing the ZT values. Resonant impurity levels have been shown to double the thermoelectric figure of merit of materials used in power generation. This approach was chosen to try to enhance the figure-of-merit of tetradymite semiconductors now commercially used for Peltier cooling.

F2.5 Success Criteria Assessment for Phase 1

U.S. DOE Phase 1 go / no-go criteria were evaluated and an assessment of project performance towards each goal was made per the following criteria.

Criterion 1: CAE modeling of selected TE HVAC architecture indicates that required comfort levels can be achieved.

Assessment: Initial CAE and comfort modeling results, as well as laboratory assessments on TE HVAC architectures indicated that node-based climate architectures would be able to achieve acceptable levels of occupant comfort that are equivalent to levels achieved in conventional vehicle systems.

Criterion 2: System modeling shows that the TE HVAC architecture can achieve reductions in energy usage from baseline vehicle.

Assessment: Engineering analysis of energy usage by a distributed TE HVAC system showed that based on the weighting criteria used to determine energy consumption, the system energy usage could be reduced.

Criterion 3: The research plan for TE materials and devices shows a specific path to deliver the technically and commercially viable TE system.

Assessment: TE device design analysis indicated that devices under consideration had a viable commercialization path based on early manufacturing cost estimates and engineering model performance calculations.

Outcome: Based on assessment of the major decision criteria, the team recommended that the project proceed into Phase 2. This proposal was accepted by the U.S. DOE Program Manager and the project proceeded into the second phase.

CHAPTER F3:
Ford Phase 2 – Exploratory Development

Phase 2, Exploratory Development, was started October 1, 2010 and completed December 31, 2011. This phase consisted of detailed CAE modeling, packaging/CAD studies, and initial development of a proposed TE HVAC architecture. In addition, further refinement of advanced thermoelectric devices and materials was conducted.

F3.1 Task Description and Milestones for Phase 2

The purpose of Task 1 was to use occupant comfort CAE methods to determine contribution from central HVAC system and contribution from distributed system elements; perform modeling to develop target air register parameters; and to develop recommendations for future efforts needed to provide enhanced transient thermal comfort models. The purpose of Task 2 was to continue advanced thermoelectric materials research; to improve and expand the performance of transient thermoelectric device models; to develop manufacturing and assembly methods for proof-of-concept thermoelectric device designs; and to design, build, test, and validate against models, the performance of a proof-of-principle liquid-to-air thermoelectric heat pump units on a thermal calorimeter. The purpose of Task 3 was to fully assess the performance of the selected TE HVAC architecture. This work consisted of selection of specific architecture elements; preliminary design of ducts, nozzles, and flow patterns; and preliminary controls development. Also, a physical assessment of occupant thermal comfort was completed using thermal mannequin technology. The purpose of Task 4 was to refine the proposed architectures and to develop specification for zonal HVAC system architecture.

F3.2 P-type Thermoelectric Materials Research

The scope of the advanced materials research effort in Phase 2 was to begin developing p- and n-type thermoelectric materials that could be fabricated in bulk, produced economically, and targeted a ZT between 1.3 and 1.7 at room temperature. Commercially available Bi_2Te_3 materials have ZT values ranging from 0.8 to slightly greater than 1.0 in the heating and cooling operating temperature range. The performance factors listed above, known manufacturing processes and the broad general knowledge base surrounding Bi_2Te_3 made it a good candidate material.

The process followed duringthis phase was to first use Sn as the acceptor impurity in single-crystal binary Bi_2Te_3, where the physics and the defect chemistry were simplified. The process was then transferred to thermoelectric alloys with the composition of existing commercial material, $Bi_{0.5}Sb_{1.5}Te_3$. The distortion of the density of states by a resonant impurity had been shown to double the ZT of the parent semiconductor in the case of thallium-doped PbTe. Tin is a known resonant impurity in the valence band of Bi_2Te_3 because it was previously reported to enhance the thermoelectric power S of the host material at cryogenic temperatures through resonant scattering. In this work, tin provided an excess density of states about 15 meV below the valence band edge. The experimental proof for the existence of this resonant level came from Shubnikov-de Haas measurements combined with galvanomagnetic and thermomagnetic properties measurements.

Tin-doped binary bismuth telluride Bi_2Te_3 was doped with Sn on the Bi site to yield ($Bi_{2-x}Sn_xTe_3$) with nominal concentrations in the melt of concentration x=0.0025, 0.0075, and 0.015. Single crystals were grown using a modified Bridgeman technique; these were used for both thermoelectric and Shubnikov-de Haas measurements. These single-crystal materials were solely used for the exploratory research, since their synthesis process was too slow to be suitable for commercialization.

Figure F22 shows the Seebeck coefficient vs. carrier concentration S(p) or 'Pisarenko relation. ' It formed the reference for determining if Seebeck coefficient has been improved for a given carrier concentration and scattering mechanism. The thermopower of degenerately doped Bi_2Te_3 is isotropic and S_{11} equals the scalar partial hole coefficient $S(p)$. The partial hole concentration was calculated for p-type Bi_2Te_3 , as shown in Figure F23, assuming that the relaxation time followed a power law of energy $\tau = \tau_0 E^{\lambda}$. The Seebeck coefficient was then calculated for two scattering mechanisms, optical scattering (λ =0.5) and ionized impurity scattering (λ =1) at 300 K using an integral density of states effective mass of m^*d =0.35 m_e of the upper valence band. An estimate of the influence of the lower valence band was also calculated with λ=1 and m^*_d, LVB =1 m_e. Literature data taken on p-type Bi_2Te_3 at 300 K was also included as a reference. The results showed the scattering exponent that best fit the Seebeck data changes from 0.5 to 1 with increasing carrier concentration indicated a progressive change from optical to ionized impurity scattering. Placing the data measured at 300 K in the $Bi_{2-x}Te_3Sn_x$ samples onto the Pisarenko relation, a marked departure from that of the other similarly doped samples was noted. This indicated the presence of a resonant level. The x=0.015 sample had an S double that of samples doped to similar hole concentrations without tin.

Figure F22: Pisarenko relation for Sn-doped Bi_2Te_3 showing high Seebeck coefficient

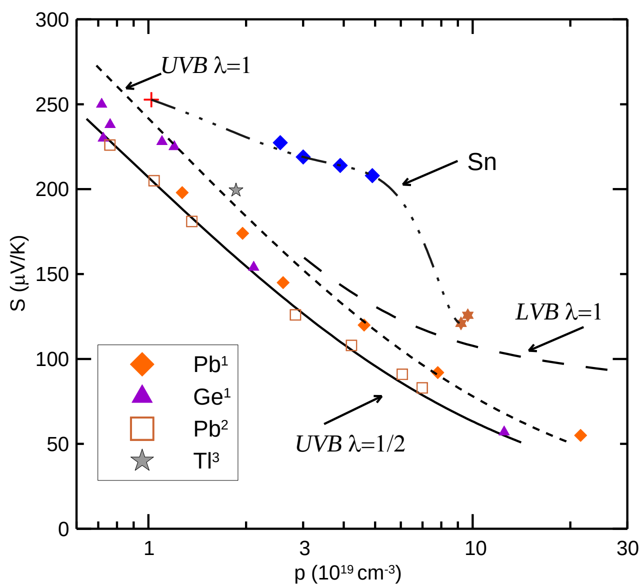

Source: Ohio State University

Figure F23: ‘Kohler’ plot for of Bi_2Te_3 showing deviation from upper valence band

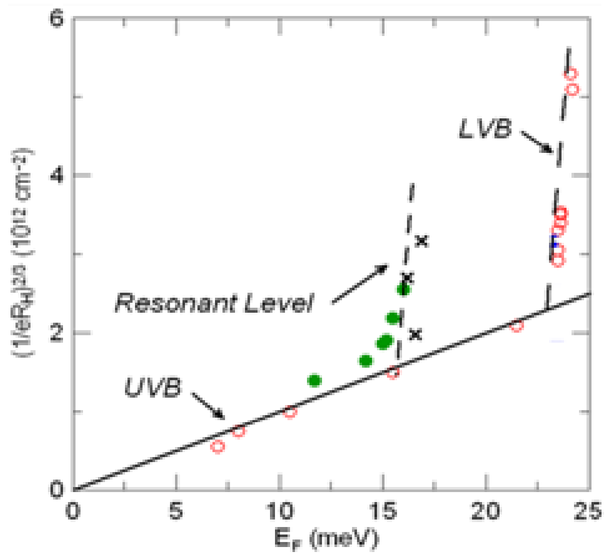

Source: Ohio State University

Figure F24 shows a summary of the galvanomagnetic and thermomagnetic measurements made on the study material. There was a sharp peak in electrical resistivity for both x=0.0075 and x=0.015 at 60 K. Below 300 K, when the samples were extrinsic, the Hall carrier density $p=(q.R_H)^{-1}$ increased with x and showed a sharp increase for 20 K<T<120 K. The thermopower showed a large increase over a simple T^1 law between 15–50 K. The Nernst coefficient N was largest for x=0.0025 and changed over temperature from negative (T≤250 K) to positive (T>350 K), with its zero point crossing the temperature where S peaked. Both S and N showed onset of the effect of thermally excited electrons at T< 300 K. At T≤250 K, the samples were extrinsic and measurements of the four galvano- and thermomagnetic properties ϱ_{11}, S_{11}, N_{21}, and R_{H21} at each temperature were used to deduce four band structure parameters: the hole density p, their mobility μ, the Fermi energy E_F and/or the integral density of states effective mass m^*_d, and the scattering exponent λ. The Fermi levels of the two higher doped samples were seen to be “pinned” at approximately 15 and 20 meV when extrapolated to 0 K, $\lim_{T\to 0}$ (E_F)=15 meV. The density of states effective mass m^*_d of the Sn doped samples was approximately double that of the integral density of states mass of the upper valence band (0.35m_e). This suggested the presence of an additional energy level distinct from the lower valence band, since the lower valence band had a much heavier mass yet (1.25m_e). This confirmed the resonant level in Figure F25 was real. Electrical mobility dropped with increasing hole concentration and followed typical temperature dependence.

Figure F24: Thermoelectric transport properties of Sn-doped samples

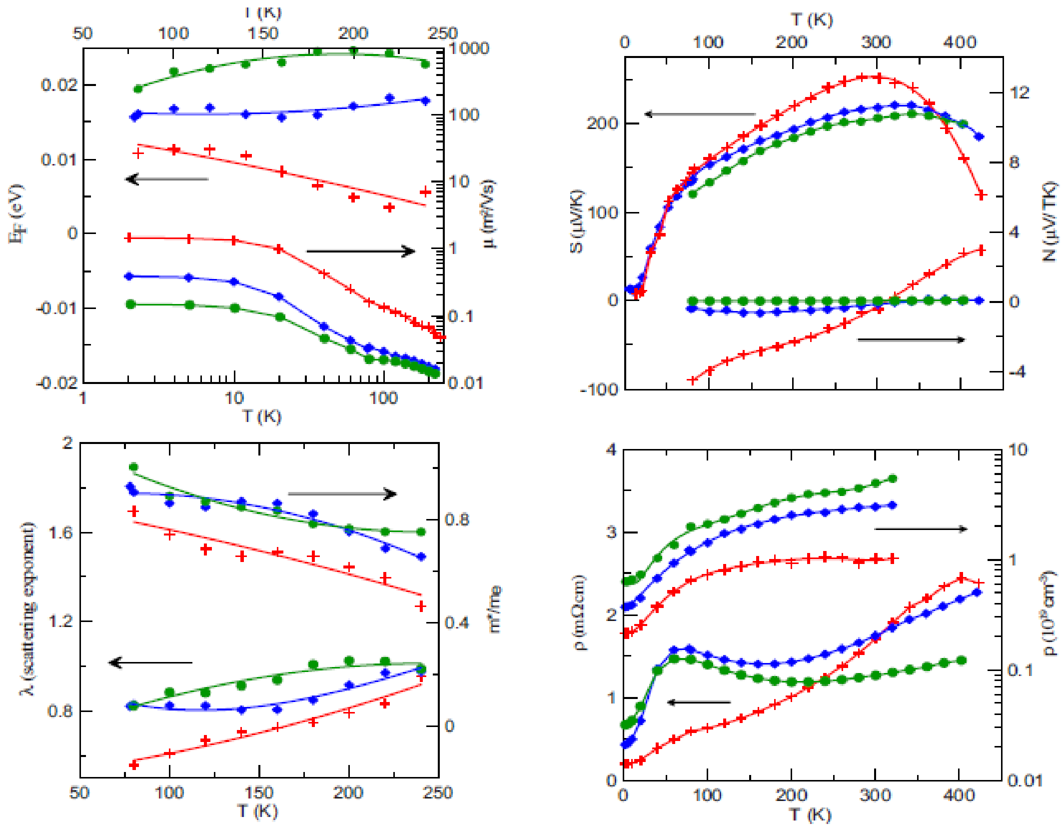

Source: Ohio State University

While Sn increased the power factor of Bi_2Te_3, its thermal conductivity was too high to be a useful thermoelectric. The commercial *p*-type thermoelectric material is based off $Bi_{0.5}Sb_{1.5}Te_3$, because it has a higher density of states, and m* (0.6 vs 0.35 m_e) is larger than the binary. The latter happened because two separate pockets of the valence band coincided at the same energy level for that alloy composition. Following these results, the next step was doping the commercial material with tin to determine if further increase m* could be obtained. Tin was added to the $Bi_{0.5}Sb_{1.5}Te_3$ composition to determine its effect on the thermoelectric properties. Thermoelectric properties from single crystal material grown by the Bridgeman method are shown in Figure F25. Results indicated that carrier density was high (>5x10^{19} cm^{-3}) due to anti-site defects of Sb on the Te site. These densities were too high for usage around 300 K because the Seebeck coefficient was too low. Attempts at lowering the carrier concentration through defect chemistry of adding excess Te to the melt were unsuccessful. Therefore, single-crystal development was stopped and synthesis moved to powder metallurgy.

Figure F25: Thermoelectric properties of Bridgeman-grown, Sn-doped samples

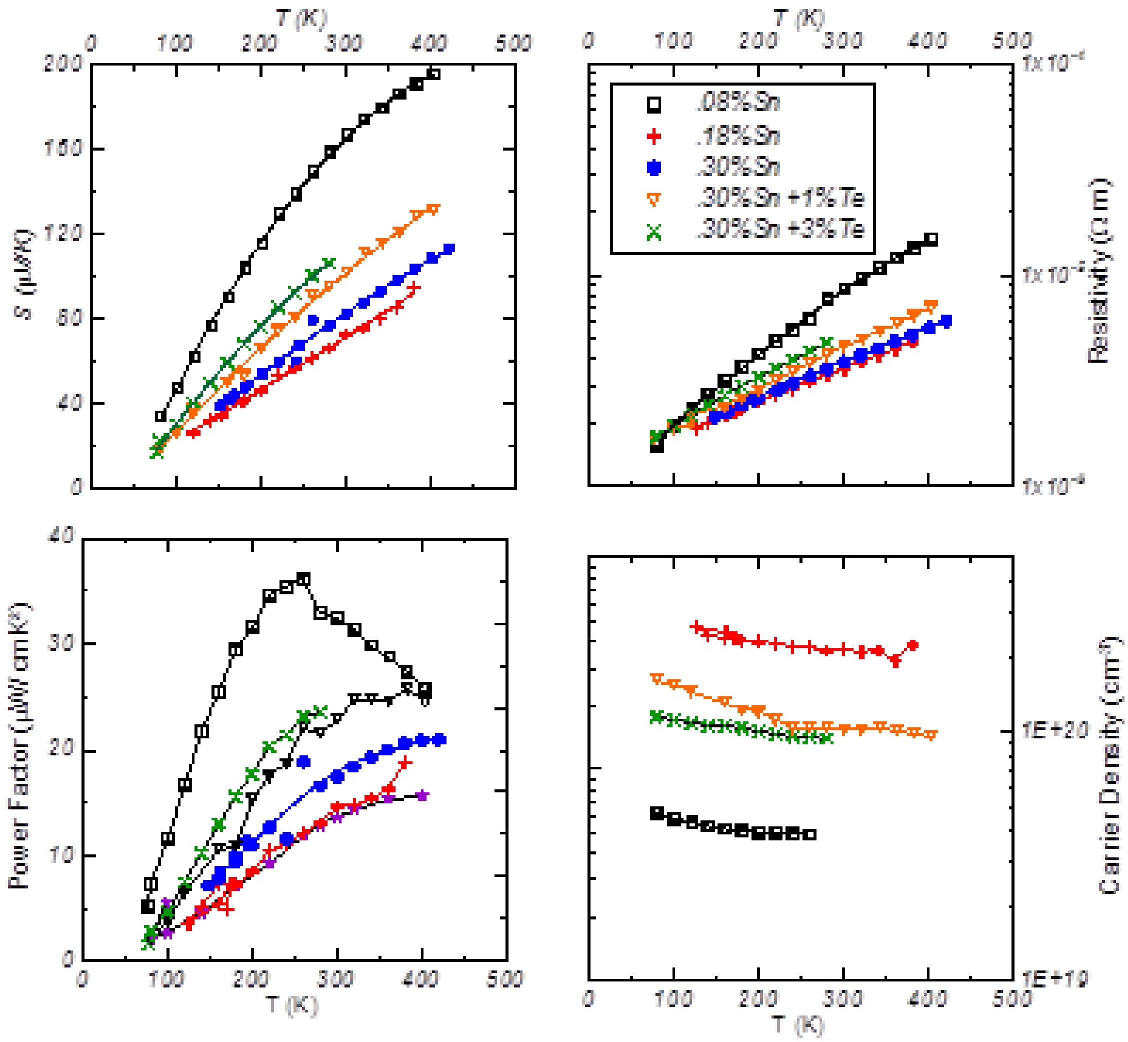

Source: Ohio State University

Due to defect chemistry issues and because any commercially relevant material based on bismuth chalcogenides was likely to be synthesized via power metallurgy, syntheses began by grinding quenched ingots of BiSbTeSe + Sn. Samples were formed via spark plasma sintering. In this technique, the material in powder form was placed in a graphite die. A uniaxial load was applied while pulsed direct electrical current was passed through the die and powder. The die and powder heated rapidly to the desired sintering temperature. The high heating rate and applied pressure helped to reduce unwanted effects such as grain growth during sintering and produced fully dense, fine grained sintered bodies. The application of uniaxial pressure led to a preferred crystallographic texture.

To produce polycrystalline bulk materials, ingots of the correct composition were cast, then ground and sieved to establish the particle size distribution. The die was placed in the sintering chamber and put under a vacuum of $1x10^{-5}$ Torr. The powder was loaded uniaxially to 60 MPa and sintered at 420°C for five to ten minutes. Resulting samples were at least 98% dense and approximately 1 cm tall. Figures F26 and F27 show the Pisarenko plot with these samples and additional curves calculated for the valence band of $Bi_{0.5}Sb_{1.5}Te_3$. The sample composition was $(Sb_{30}Bi_{9.85-x/3})$ $(Te_{58.2}Se_{1.8})$ + $Te_{1.85}$ + $(BiI_3)_{x/3}$ + 0.15 SnTe with x= 0.4, 0.2, 0.1, 0.

Figure F26: Conductivity properties of Iodine-doped samples

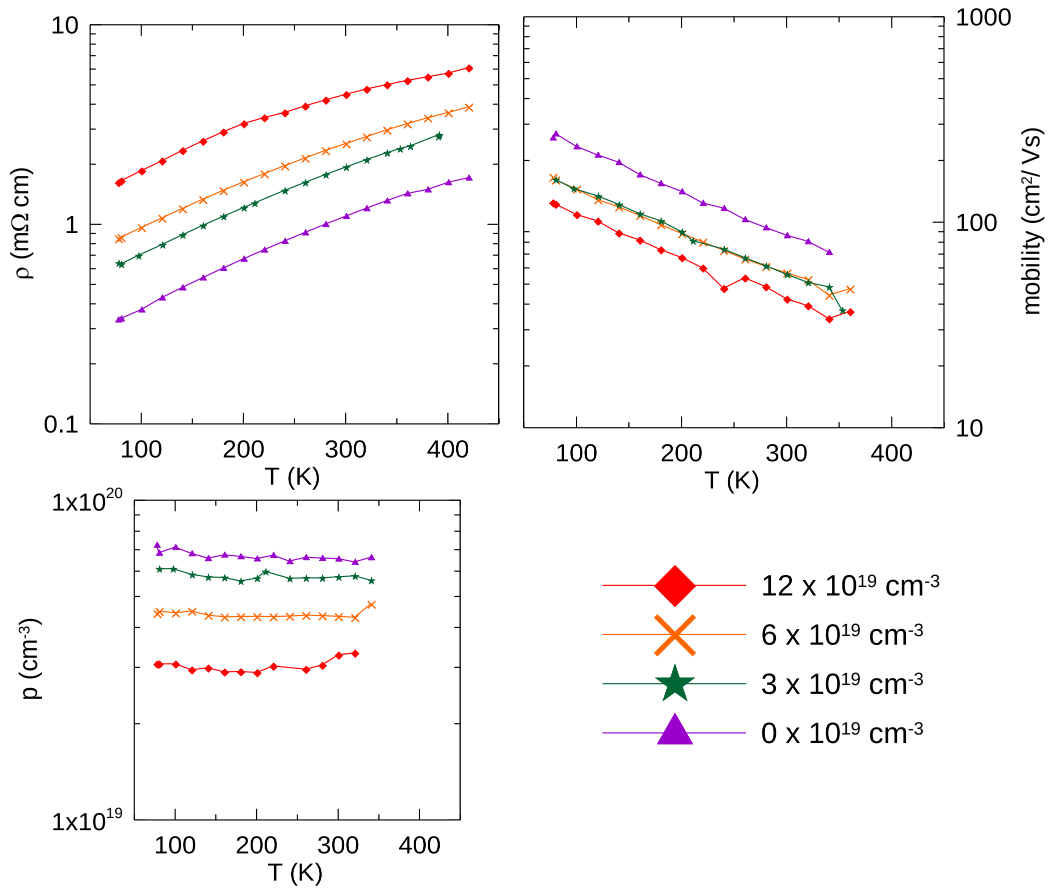

Source: Ohio State University

Figure F27: Thermal conductivity and ZT of Iodine-doped samples

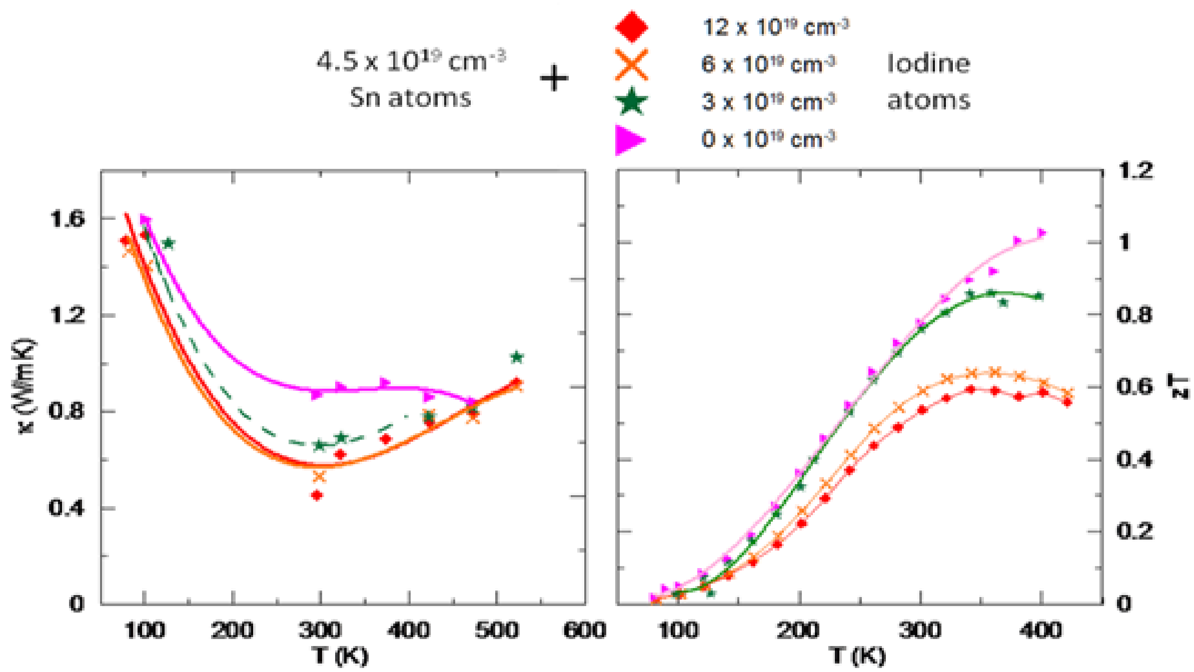

Source: Ohio State University

The hole carrier density, electrical resistivity and mobility for the samples showed that the presence of iodine diminished the electrical mobility of the samples. This was in contrast to the typical behavior of an increased mobility with a lower carrier concentration, due to fewer electron-electron interactions. Only the highest compensated sample had an increased Seebeck coefficient and the power factor dropped in all cases, as was indicated in the electrical mobility comparison. Thermal conductivity was low for all alloys and the least and undoped samples reached commercially available ZT values at 300-400 K, as shown in Figure F28. Therefore, it was concluded that introduction of ionized impurity scattering was not a successful approach in these alloys. The calculated Pisarenko relation for Bi_2Te_3 and $Bi_{0.5}Sb_{1.5}Te_3$ and experimental data points showed that the samples fell on the line calculated for the valence band of $Bi_{0.5}Sb_{1.5}Te_3$.

Figure F28: Pisarenko relation for Iodine and Tin-doped samples

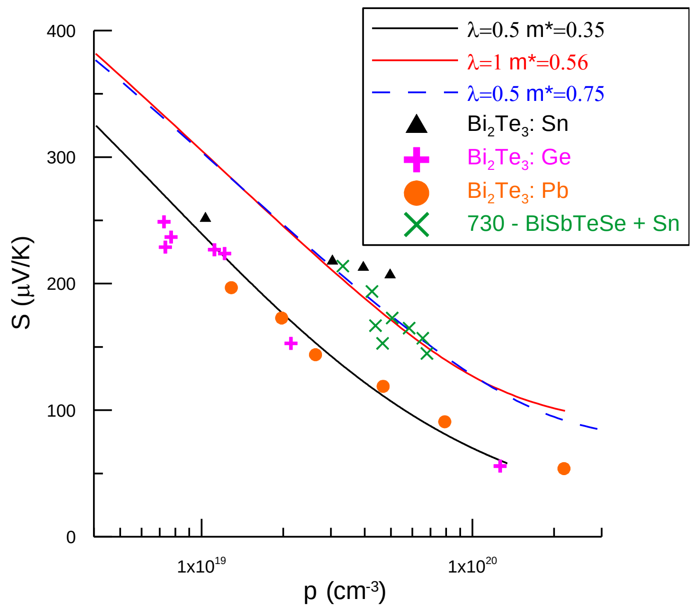

Source: Ohio State University

The work into Sn doping $Bi_{2-x}Sb_xTe_3$ alloys using porous cold compacted and sintered alloys was next investigated. There was no known published previous work on the approach applied. The hypothesis was that porosity could improve the thermoelectric figure of merit by scattering phonons more than scattering electrons. This was explored in p-type $Bi_{0.5}Sb_{1.5}Te_3$ and in n-type $Bi_{1.9}Sb_{0.1}Te_{2.85}Se_{0.15}$ alloys. The basic effect can be understood by the following equation for the thermoelectric figure of merit ZT as:

$$zT \equiv \frac{S^2\sigma}{\kappa}T = \left(S^2 n\right)\left(\frac{\mu}{\kappa}\right)qT$$

In this case, S is the thermopower, and σ and κ are the electrical and thermal conductivity, respectively, q is the electron charge, n is the concentrations of electrons, and μ is the electron mobility. Issues in optimizing thermoelectric materials included metallurgical changes that decreased κ also usually decreased μ, and those that increased n also decreased S because the latter two are related by the "Pisarenko relation." By creating porous thermoelectric materials, the thermoelectric materials showed an increase in the ratio of μ / κ, and thus increasing ZT. This concept is contrary to the accepted effective medium theory, as applied to thermoelectric composites, where consideration of one component acts as the thermoelectric alloy, and the other component as a void. From the effective medium theory, one would normally conclude that the ratio of μ / κ should be insensitive to porosity, and that the ZT would not be improved.

To synthesize porous samples, p-type alloys were doped with tin, then a matrix of samples were prepared varying compaction pressure, sintering temperature, and charge carrier density. For each sample, the optimal compositions and preparation schedule were found. Elemental Bi, Sb, Te, Se, and SnTe were loaded under argon into stainless steel vials and mechanically alloyed. The powder was densified under Ar at 300 K at pressures between 0.23-1.7 GPa, then reampouled under a vacuum. Samples were sintered for 5 days at 220°C, then five days at 500°C. Confirmation of the density of the samples at ZT::Plus indicated open-pore porosity, due to the disparity in geometrical density and pycnometric density. Percent porosity was determined from the geometrical density as a ratio of theoretical density. This set of samples had porosities between ten and twenty percent. Scanning electron microscopy analysis on samples showed open porosity in each sample. Figure F29 shows *S*, ϱ, and κ as function of temperature *T* for p-type $Bi_{0.5}Sb_{1.5}Te_3$ + Sn samples with varying hole carrier concentrations *n* and mass densities as measured by percent of theoretical density.

Figure F29: Seebeck coefficient, electrical resistivity, and thermal conductivity plots

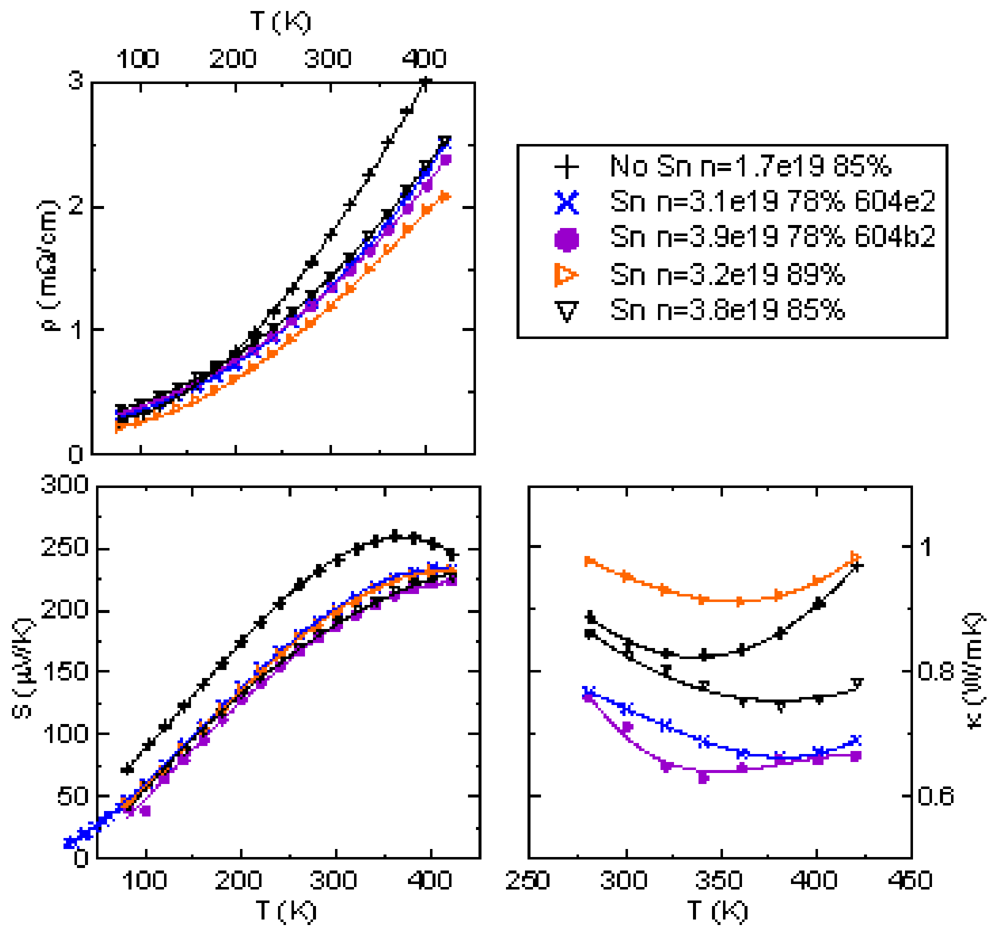

Source: Ohio State University

Figure F30 shows *zT*, S^2n, and μ/κ as function of *T* for the same samples. S^2n was higher for Sn-doped samples than the sample not doped with tin, which supported the conclusion that Sn was a resonant impurity that increased the power factor. Optimal hole doping concentration was found to be between about $1x10^{19}$ cm^{-3} to about $5x10^{19}$ cm^{-3} and optimal mass density between 76-80% of the theoretical value. *ZT* for samples with 78% dense material (i.e., with a

22% pore volume) reached about 1.35 to 1.40 at about 375 K repeatedly and reproducibly in several samples with similar mass densities.

In an n-type composition of $Bi_{1.9}Sb_{0.1}Te_{2.85}Se_{0.15}$, the thermal conductivity at 300 K was found to be about 0.6-0.7 W/m K. The value for the bulk thermal conductivity of an alloy of the same composition is about 1.1 W/m K. Therefore, the effect of introducing porosity in this n-type alloy composition was similar to the p-type alloys described previously.

Figure F30: Plots of zT, S^2n, and μ/κ as function of T

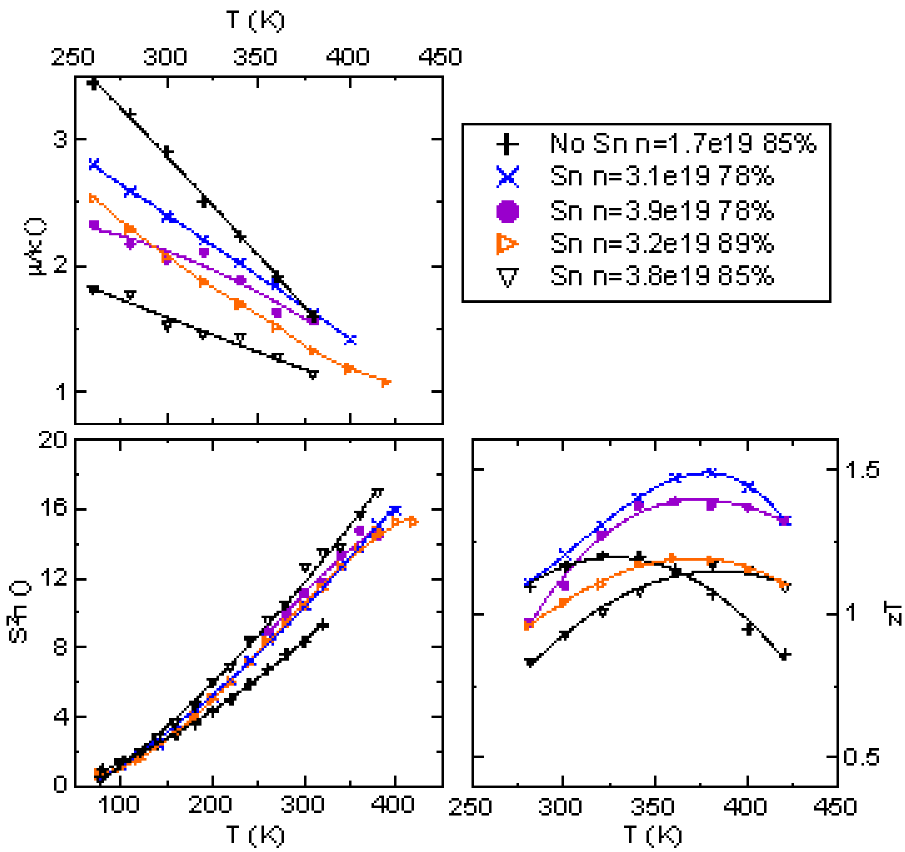

Source: Ohio State University

F3.3 Thermoelectric Device & Model Development

Thermoelectric device design continued to evolve in Phase 2 of the project. A major focus was optimization of the TE assembly and connection methodology, including a selection of components and manufacturing methods. This involved reviewing details of the air-side heat exchanger, liquid-side heat exchanger, thermoelectric pellets, connections (electrical and mechanical), and interfacial components. A proof-of-principle TE device was designed, fabricated, and tested. Its performance was measured in a calorimeter and benchmarked against a steady-state model. This comparison allowed the team to develop strategies for further refinement of both the device and the model.

At the conclusion of Phase 1, a development level thermoelectric device was falling well short of program targets of cooling COP > 1.3 and heating COP > 2.3. The Phase 1 device (not discussed in this report) nominally delivered 250 W Q_C at a cooling peak COP of 0.78 with a main side ΔT of -14.2°C and a heating peak COP of 1.84 with a main side ΔT of 14°C. The Phase 1 air-to-liquid device was primarily utilized to identify potential manufacturing techniques and assess design concepts for their impact on performance. The design team reviewed the results from the Phase 1 builds and derived a list of design and manufacturing issues to attack in this second phase of the project in order to achieve the program performance targets. The key areas of focus in Phase 2 were an improved liquid side heat exchanger, an improved dielectric system and an increase in the size of the TE device.

In addition to these planned development steps, the team also incorporated refined performance targets into the design. The new targets required the devices to provide 50 to 70 cubic feet per minute of airflow, with a main side temperature drop across the air-side heat exchange of -17°C in cooling mode with main and waste fluids both having inlet temperatures of 48°C. Input power at this condition was specified at 350 W with a target under 300 W. This new target caused the thermal cooling (Q_C) requirement to be adjusted from 250 W in Phase 1 to greater than 460 W for the Phase 2 device and forced the size of the device to be significantly increased over the original concept. At the conclusion of Phase 1 it was shown, via device models, that the liquid side heat exchanger held the most potential for improving the performance level of the device. Figure F31 demonstrates the modeled performance impact of switching from the base extruded tube heat exchanger to a customized heat exchanger with internal turbulator fin.

Once this opportunity was identified, the design team set out to optimize the liquid heat exchanger to maximize the coefficient of convective heat transfer while maintaining the internal pressure drop within acceptable limits. After reviewing the proposed range of fin densities and the targeted range of pressure drops with suppliers of extruded aluminum tubing, the team quickly realized that the extrusion process was not compatible with the design requirements and moved on to developing a custom stamped and brazed heat exchanger. Another key factor in the design of the heat exchanger was the proposed routing of the fluid transport lines. For packaging reasons it was desirable for the inlet and outlet of the liquid heat exchanger to be located on the same side of the device. This requirement drove the design of the inlet and outlet manifolds and the return tank, which impacted the total pressure drop of the device.

Figure F31: TE device performance improvement walk

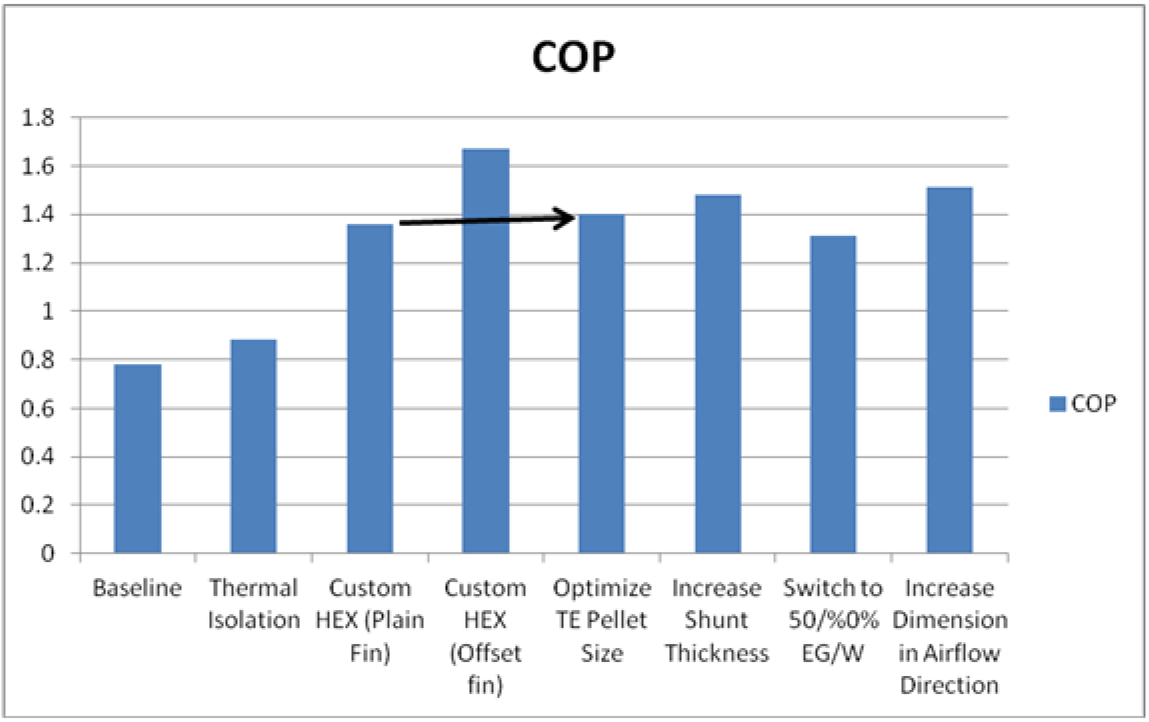

Source: Gentherm Corporation

The third consideration for the design team was manufacturing feasibility. The team was tasked with utilizing start-of-the-art processes and insuring that the designs be fully compatible with those processes. The performance of the device was developed utilizing a combination of 1-D and 3-D computer models. The initial calculations were preformed utilizing a proprietary 1-D software package, which referenced a data bank of empirical data to predict device performance. This tool was used to select fin geometries and as a secondary check against the physics based 3-D model results. The initial calculations in the 1-D study determined the fin height, thickness, type, and pitch. The key parameters evaluated were the device pressure drop and the coefficient of convective heat transfer.

After the fin geometry was selected the design team switched to 3-D analysis, performed with ANSYS Fluent, to complete the heat exchanger design. These analyses were used to optimize device pressure drop, localized velocity or flow issues and flow uniformity in the primary heat exchange zone. There were two primary studies conducted to finalize the design, the first being directed at optimizing the return tank of a 2-pass “U-flow” design and the second study compared the performance differences between the optimized U-flow design and a single-pass “S-flow” design. In the end the team found that the pressure drop of the baseline U-flow design was within acceptable limits and selected that concept for the final design. This was in order to have the inlet and outlet on the same end of the device for packaging requirements, even though the S-flow design had a significantly lower pressure drop. Figures F32 – F34 show the total pressure maps for the baseline U-flow heat exchanger, a "V" tank U-flow concept and the S-Flow heat exchanger.

Figure F32: Optimized U-Flow HEX pressure map

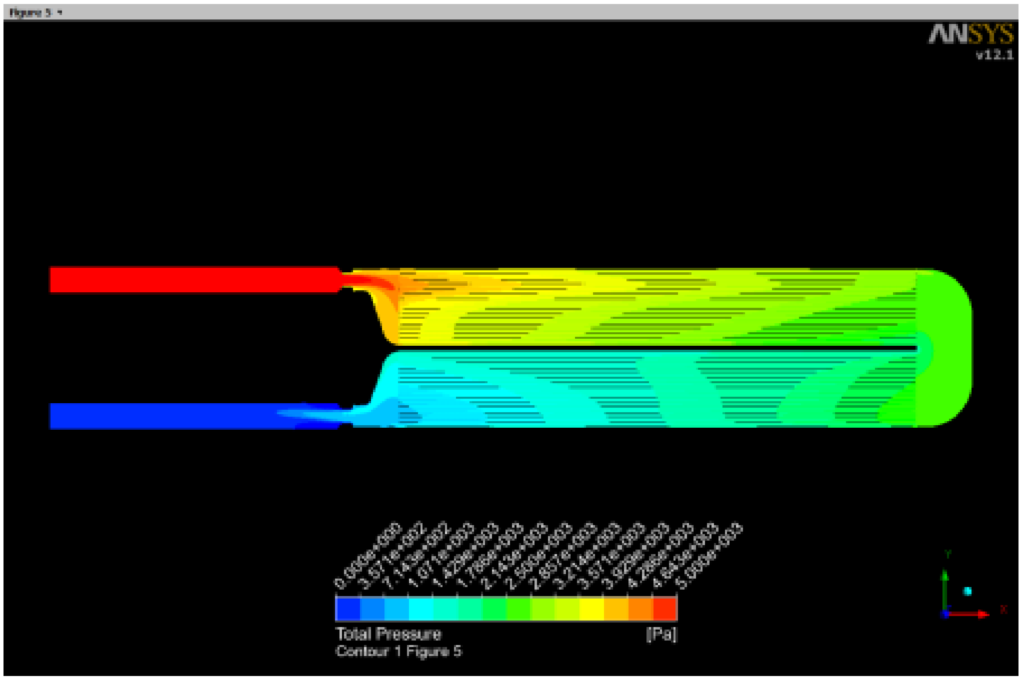

Source: Gentherm Corporation

Figure F33: "V" flow tank design concept, total pressure

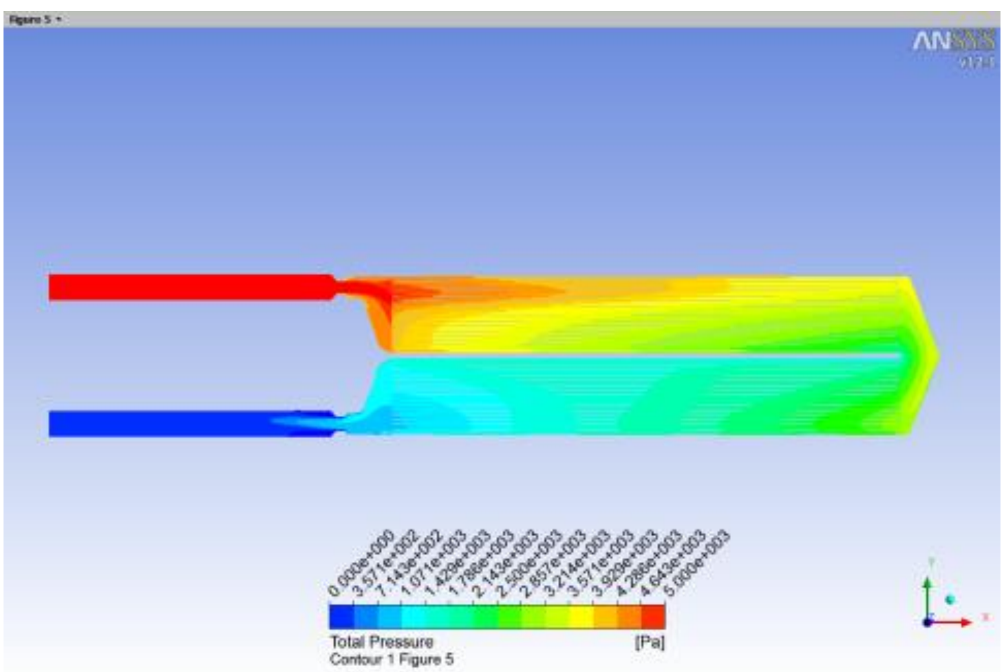

Source: Gentherm Corporation

Figure F34: "S" flow HEX concept, total pressure

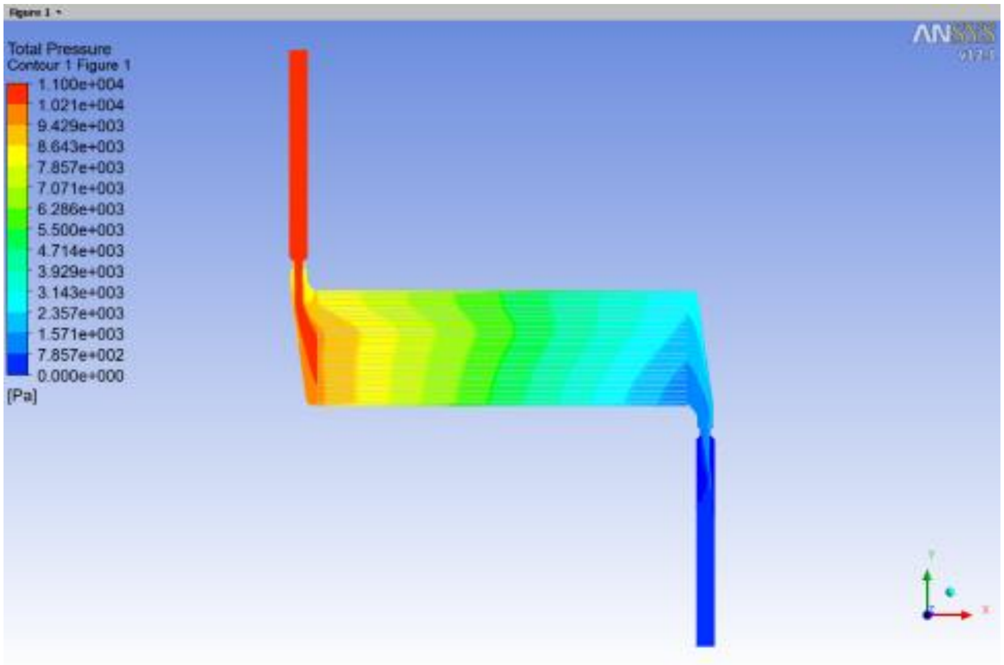

Source: Gentherm Corporation

The liquid heat exchanger consisted of four component parts: the top plate, bottom plate, turbulator fins, and the fluid fittings. The top and bottom plate were relatively simple stamped parts that were formed via a four-stage prototype die. The turbulator fins were made on a rolled fin mill. The fittings were machined parts with a female thread that allowed quick-connects to be attached for mounting hoses. The fitting design could continue to be cost reduced and simplified. For example, the machined fittings could be replaced with a stub tube with a hose bead for direct mounting the hose with a typical automotive hose-clamp.

Three air heat exchangers designs were studied in this phase: thermally isolated fins, non-thermally isolated fins, and skived fins. Each fin design was developed to evaluate various design and manufacturing approaches that could potentially be implemented for a production device. To ensure the fins were comparable, all three designs had the same nominal fin density, height, and thickness. These parameters were carried-over from Phase 1 and set to maximize the performance of the air side heat exchanger while staying within reasonable fin density limits for condensate management and air side pressure drop concerns.

The thermally isolated and non-thermally isolated fins were 12 mm wide and 38.8 mm wide respectively. The thermally isolated fins were designed to contact two out of the twelve rows of shunts, requiring that twelve fins be used per device. The non-thermally isolated fin was designed to contact six rows of shunts, requiring only four fins per device. Both types of fins were made of a rolled fin with an aluminum substrate brazed to the top and bottom of the fins.

The purpose of designing thermally isolated and non-thermally isolated fin was to better understand the advantages and disadvantages of utilizing thermal isolation in these types of thermoelectric devices. Modeling of the device predicted that the isolated fin would have a 3-5% performance advantage over the non-isolated fin. However, there were concerns that thermally isolated fin design might be less robust at preventing condensate from entering the thermoelectric engine.

The thermally isolated and non-thermally isolated fins were both fabricated using the same general approach. Both used rolled fins and went through a brazing operation to bond aluminum substrates to the top and bottom of the fin. The brazing technique used for these fins was controlled atmosphere brazing. Braze fixtures were designed for both the thermally isolated and non-thermally isolated fins. These fixtures provided alignment for the fin and substrates, constrained the fin assembly so they would braze flat, and provided a clamping force to ensure that all the fins were in contact with the substrates. The braze profile was also optimized for both fin assemblies. Chamber temperature and belt speed were adjusted until the fins reached a target braze temperature for a required length of time. Each profile was validated using fin temperature data, collected during the braze process and by evaluating the fin bond on sample parts.

The third design variant developed was the skived fin heat exchanger, shown in Figure F35. This design was based on the non-thermally isolated design; however it had a thick aluminum base that could be used to clamp the device together. The fin was made using a computer numerical control cutting operation, where the fins were cut and bent into place using knives. This process allowed the use of stiffer aluminum alloys that could be used in a brazed assembly, and it also enabled higher fin densities and taller fin heights then a machined or extruded fin.

Figure F35: Skived fin air heat exchanger design for TE devices

Photo Credit: Gentherm Corporation

Because many of the coating layers in the design were very thin, interface thermal resistance played a large role in the overall systems thermal resistance. In order to better measure the thermal resistance of the various coatings and interface materials in the device, a thermal resistance measurement apparatus was developed. This apparatus worked by inducing a heat flux through the test sample and measures the induced temperature drop. This data was used to determine the equivalent thermal resistance of test samples.

The thermoelectric materials used for this phase contained over 600 pellets and shunts. The number of pellets, shunt size, and thicknesses were initially optimized for performance at the maximum cooling condition (48°C air, 48°C coolant, 50 CFM air flow) with a target temperature drop of 17°C. Additional shunt thickness was added to increase current carrying capacity, allowing the engine to handle the 700 W needed in heating mode. The engine utilized a lead frame construction approach with reflow solder process and pick-and-place operations.

During the initial device modeling and optimization, two factors that were adjusted to optimize device performance were width and thickness of the shunt. These dimensions defined the minimum working cross-sectional area of the device. As a safety factor, a larger cross-section was used to insure adequate current carrying capacity with minimum joule heating losses. The final shunt dimensions were incorporated into the device model to check the effect of the new dimensions on device performance. This insured that the final shunt dimensions used had adequate current-carrying capacity.

Once a minimum cross-section had been established, the shunt was sized to accommodate a worst case assembly tolerance. The assembly tolerance included placement tolerances for the pick-and-place operation, minimum solder fillet, and fabrication tolerance for lead frame and assembly fixture. The same approach was applied to the shunt length.

The lead frame design approach utilized a substrate to support and connect the individual shunts during the solder process. To create these lead frames, the shunt pattern was etched from a single sheet of copper. In this etching process, a support frame was created on the perimeter of the shunt pattern to provide structure and alignment of the frame into the assembly fixtures. Additionally, small tie-bars were left in the pattern to connect the shunts with each other and to the external frame. The lead frame structure provided sufficient support to be able to screen print solder in place, mount TE pellets, and run through a reflow solder oven. After the engine has been soldered and cleaned, the lead frame and tie-bars were removed to create the intended pattern and electrical circuit.

In using this design approach, several features including shunt gap, tie-bar thickness, and material thickness had to be considered. The minimum shunt gap was defined based on the etching process and trimming operation constraints as a function of the material thickness. Since the engine footprint was fixed due to packaging constraints, increasing the shunt gap also affected the maximum length and width of the shunts. The shunt gap also affected the tie-bar thickness, since a large gap required a thicker tie-bar. It was also desirable to minimize the tie-bar thickness since a thicker tie-bar would take longer to remove and impart more stress on the engine while doing so.

Tin based solders were selected for manufacturing the thermoelectric engines for this phase. These materials were prevalent and cost effective, but their melt temperature was too high. Most Sn-based solders have melt temperatures in the 230° to 240°C range. These temperatures were significantly above the operating temperature range of the device such that after soldering, the TE elements were pre-stressed due the coefficient of thermal expansion difference between the operating temperature and the solders solidification temperature.

The thermoelectric engine assembly process utilized a solder stencil to print solder paste onto the shunt locations to mount the thermoelectric pellets. In order to maintain a consistent and uniform solder joint thickness for optimal electrical, thermal, and structural properties, the thickness of the solder paste application was controlled very carefully. Due to the thermoelectric pellet size, engine flatness, and thin solder joints specified by the design requirements, achieving a consistent application of the solder paste became a challenge. Solder paste formulation was critical to achieving the desired uniformity, repeatability, and reproducibility while stencil printing. Therefore bead size and flux chemistry were experimented with to achieve the desired outcome for a given stencil thickness and aperture.

In order to achieve consistent and uniform solder paste application, several pastes were tried with varying flux chemistry and alloy bead size. These include both no-clean and water-soluble flux chemistries. Throughout the manufacturing process development, paste thickness and uniformity were continuously measured and evaluated to assess the effectiveness of the various parameters. Standard surface mount technology equipment and processes were employed during the thermoelectric engine build, with specialized fixtures and tools which would be atypical of standard printed circuit board manufacturing. Equipment utilized was semi-automatic stencil printer, optical paste thickness measurement, a high speed pick-and-place device, a convection oven, and a parts washer.

Stencil printing became the greatest challenge, due to aperture size, stencil thickness and the paste formulation. As mentioned previously, stencil printing uniformity and consistency were critical to insure a good enough pellet to shunt electrical solder joints and desired wetting, which greatly impacted engine performance. A significant effort was made to understand the interaction of paste with stencil and printer control parameters, such as squeegee pressure and speed. Each printing trial was evaluated via optical thickness measurement. This ultimately allowed for control of final solder thickness and quality of the solder joint for both electrical and thermal performance.

After the solder stencil printing was inspected, the thermoelectric pellets were placed directly onto the lead frame via a tape and reel fed high speed pick-and-place machine. Very little effort was required to dial in the correct setup to control the placement of the pellets. Placement speed was made at approximately 25,000 pellets per hour.

The engine assembly was completed by placing the upper shunt assembly on top of the pellets prior to placing the complete stack in to the reflow fixture and securing the fixture in place. A standard convection oven was used to reflow the solder paste. Due to the mass of the thermoelectric engine and the associated solder fixturing, it took several iterations to determine the ideal reflow temperature profile. Utilization of higher melt temperature solder also compounded the balance of time and temperature with mass approaching the limitations of soldering equipment. Engines were run through a wash cycle to clean off any residual flux.

Once the engine was assembled and soldered, the lead frame was removed. This was done using a computer numerical control machining operation. In order to prevent damaging the engine, each tie bar had to be individually removed using a sophisticated cutting action, causing each engine to take four to six hours to machine. An end mill tool, cutting in the horizontal plain was used initially; however this approach applied too much load on the pellets causing some to break. EDM and laser processes were also attempted with mixed results. These options may still be viable; however they will require a significant amount of furtherdevelopment before they can be used reliably.

There were four major fixtures that were designed for the assembly of the Phase 2 devices. These fixtures included a silk-screen fixture, TE engine alignment fixture, fin placement fixture, and a final assembly fixture. Silkscreen fixtures were used to apply the interface layer to both the liquid heat exchanger and the air heat exchanger. It used a base plate to hold the part in place and a stencil to control were interface material is applied. The thickness of the stencil was varied to optimize the final interface layer thickness. The TE engine alignment fixture was used to place the TE engine on to the liquid heat exchanger, after the interface layer has been applied. The fixture used features on both the liquid heat exchanger and TE engine to align the two components, and then lowered the TE engine into place without disturbing the interface layer.

There were two devices built for this phase of the program. Device #1, shown in Figure F36, was designed to operate at up to 700 W of input power, and produced temperature differentials (ΔT) up to 24°C in cooling mode and 54°C in heating mode. It consisted of a brazed liquid heat exchanger, two lead frame thermoelectric engines, twelve thermally isolated fins, thermal grease interface layers, and two compression plates used to hold the device together. The liquid heat exchanger was designed in a U-flow configuration with a fluid channel 40mm wide and an internal turbulator fin. The device measured 350 mm x 110 mm x 52 mm and weighed 3.15 kg.

Device #2, shown in Figure F37, used the same components as Device #1 with the exception of the air fins and the compression plates. For Device #2, these components were replaced with a skived fin, which integrated the compression plate into the base of the fin. This reduced the height of the device from 52 mm to 49 mm, while maintaining the same fin density, height and wall thickness. The elimination of the steel clamp plates provides a significant weight savings, reducing the weight to 1.85 kg for the skived fin assembly.

Figure F36: TE proof-of-principal device #1

Photo Credit: Gentherm Corporation

Figure F37: TE proof-of-principal device #2

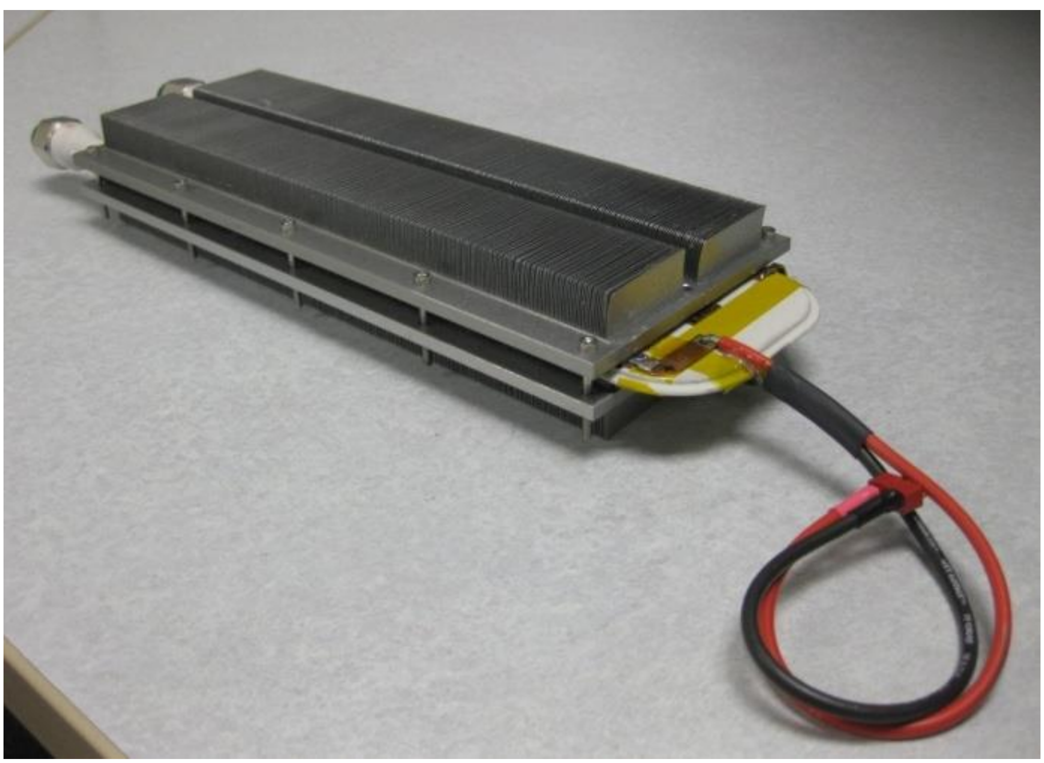

Photo Credit: Gentherm Corporation

For these devices to be commercially viable in an automotive application, techniques were developed to evaluate durability for the expected operating life. A durability test stand was developed to cycle the TE devices at on and off several hundred times in heating mode, then switch over to cooling mode to do the same thing. For each cycle the device was left on for thirty seconds then off for thirty seconds. Figure F38 shows the durability test stand.

Figure F38: Durability test stand

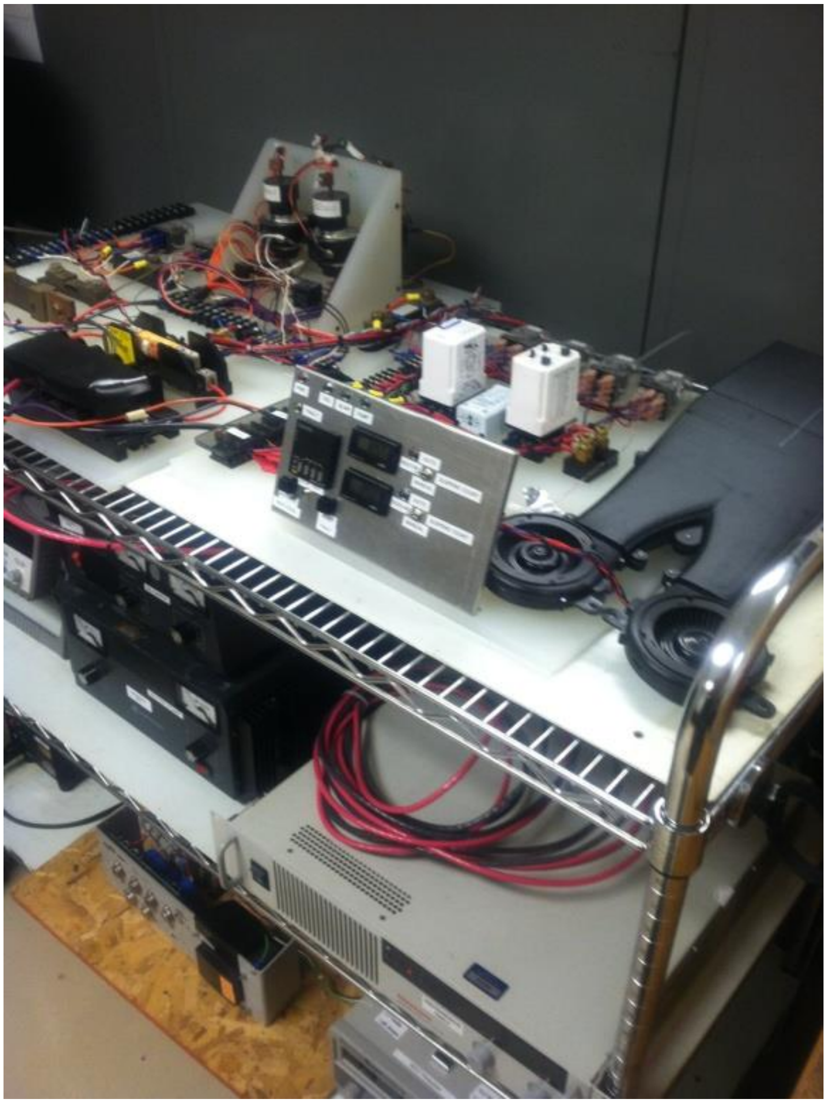

Photo Credit: Gentherm Corporation

Testing was initially performed on two of the Phase 1 devices. The first device was first cycled at 225 W of input power for both cooling and heating mode. Within the first 622 cycles the device experienced a failure at one of the corner pellets and the test ended. The second device also started at 225 W and after 1,125 cycles, it also experiences a failure at a corner pellet. However, this unit was repaired so testing could continue. This device then went on to complete 80,000 cycles at 225 W of power. The input power to the device was then increased to

475 W in cooling and 380 W in heating and testing continued. After another 80,000 cycles (160,000 in total) the device failed again, however this time the failure was internal to the device and could not be repaired. This result was much better than expected, considering that based on a 10 year life, these devices may see approximately 36,500 cycles (10 cycles/day x 365 days/yr x 10 year). However, the power input (and therefore the thermal stress) was still relatively low, and the fact that both devices experienced failures within 1000 cycles was concerning. To address this issue, the Phase 2 devices were built using the more robust design process described earlier in this section.

Following durability testing, calorimeter testing was conducted on separate TE devices. A total of twenty-two test points were chosen to characterize the performance of the TE devices, of which eleven were in cooling mode and eleven were in heating mode. Each test point was defined by and controlled to five parameters; inlet coolant temperature, inlet air temperature, coolant flow rate, air flow rate, and device input power. Combinations of these five parameters were used to simulate four different ambient conditions that the device would see in vehicle application. For heating mode the ambient conditions of -5°C and 5°C were selected, and were designated moderate heating and mild heating, respectively. For these tests, inlet coolant temperature was fixed at the ambient condition and inlet air temperature was set to either -5°C, 5°C, or -18°C depending on the test point. Device electrical input power was also varied between 100 W and 700 W. In cooling mode, the test points were chosen to simulate ambient conditions at 43°C and 28°C, designated maximum cooling and moderate cooling, respectively. For these test points, inlet coolant and air temperature was set to 5°C above the simulated ambient conditions. This was done to account for additional heating that the cabin air or coolant might see due to solar load and/or temperature rise in the coolant during the operation of the device. Device input power was varied from 100 W up to 500 W and additional test points were taken at various inlet temperatures to simulate device performance as the cabin air decreased over a drive cycle.

There were limited updates to the device model for this phase of the program. The core architecture was left unchanged from the Phase 1 model. Device geometry and the material properties were updated to match the design for the Phase 2 device. Updates such as material properties for adhesive were carried over from the Phase 1 model correlation. Additional algorithms were added to model the effect of adding thermal isolation to the air fins. The model was also updated to account for the seals used around the thermoelectric engine, which contacted both the air fin and the liquid heat exchanger. This was to account for any unwanted heat transfer between the air and liquid sides of the device.

F3.4 Thermal Chamber Assessment of Zonal Designs

This section provides a summary of the efforts carried out using the Airflow Chamber Evaluation System (ACES) chamber to replicate the performance of the specific nodes of the distributed climate system architecture in a controlled vehicle environment. The results from the ACES chamber studies were augmented through the continued use of advanced CAE tools and human thermal sensation modeling tools. In addition to studying the impact of the distributed elements in the system, the ACES chamber performance was calibrated by attempting to replicate the results from baseline vehicle wind tunnel tests. Finally, the comparative contributions of the central HVAC and distributed HVAC system were studied, both in the test chamber and in proprietary models, to determine the optimal blending of these systems.

During Phase 1, an instrument panel and seat were placed in a thermal chamber (not discussed in this report). The thermal chamber emulated the inside of a vehicle cabin. The chamber temperature was varied over six conditions that replicated wind tunnel responses. Various thermal delivery elements were introduced with varying airflows and temperatures, and the results were evaluated subjectively. The open area in the chamber was used initially to allow flexibility locating the various elements for evaluation. A total of thirteen different elements were tested individually and in combinations to determine the optimum solution.

After completing the concept stage of the study, CAE tools were used to refine the concepts to practical approaches. Performing this work allowed the team a significant amount of flexibility in assessing multiple combinations of approaches to the system configuration. The CAE studies then lead the team to experiment with various nozzle designs. These designs were fabricated and mounted in several positions in the ACES vehicle buck. The CAE tools and methods showed favorable correlations with the temperature and human thermal comfort data collected from the baseline wind tunnel tests conducted in Phase 1. This provided confidence in the CFD and human thermal sensation modeling methods and techniques.

In the Phase 1 ACES chamber tests, the flexibility of various elements location was given priority compared to improved accuracy that could be obtained in a vehicle buck. With the final elements selected, the accuracy of a vehicle buck was employed. However, fidelity of the test configuration provided a significant improvement in the ability to assess performance of the elements, both individually and in combination.

F3.4.1 ACES Chamber Testing and Modeling Results

The first part of testing was to match comfort and sensation values measured in wind tunnel tests. An attempt to replicate the average interior temperature measured in the wind tunnel tests was made in the buck and observations were recorded. After that preliminary baseline mapping task was completed, distributed heating and cooling elements were used to achieve a similar thermal comfort level. Airflow, temperature, and time of application were refined during those tests. The average front row interior temperature for this round of tests was determined through the use of CAE modeling.

To supplement the ACES testing, the baseline parametric CFD model of the thermal chamber was modified to incorporate four elements: a seat, headliner, instrument panel, and steering wheel. Of the four, only the headliner element necessitated a geometric change to the baseline model. Figure F39, shows the ProEngineer computer-aided design (CAD) model representation of the modified model that was utilized for the CAE studies. The heated/cooled seat, instrument panel, and heated steering wheel required little or no geometry changes.

Figure F39: CFD modeling of overhead register concept

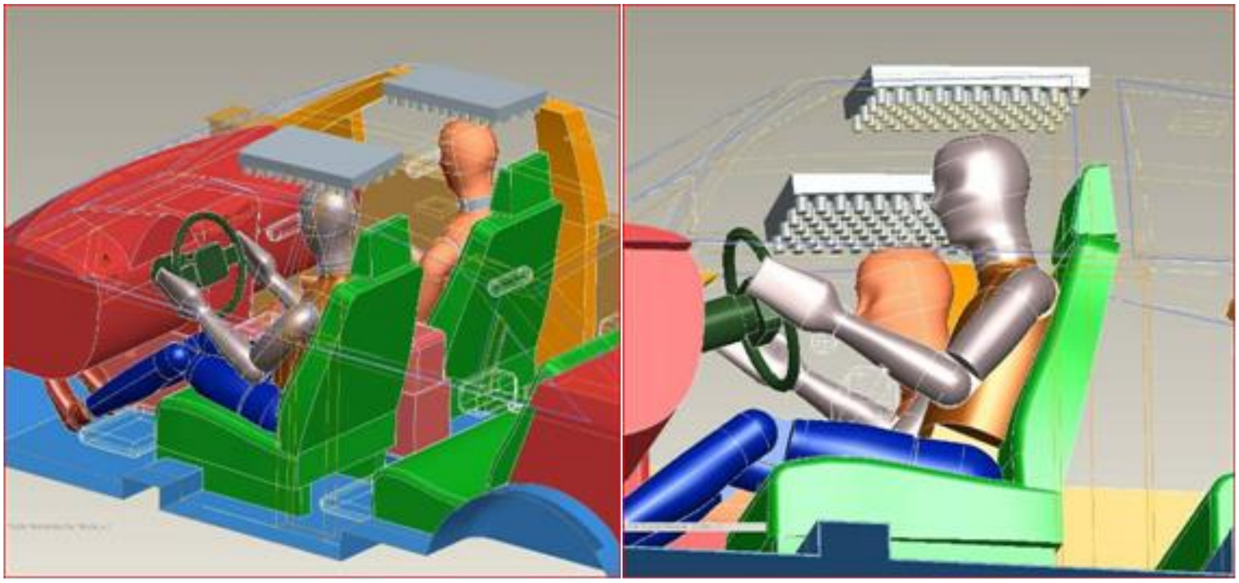

Source: Halla Visteon Climate Control Corp.

Once the baseline CFD model had been modified, the test cases were simulated at prescribed ambient conditions. The results of the simulations were translated into a thermal sensation model and a comparison of the thermal sensation data between the ACES testing and the CAE modeling was made.

Placing a half-vehicle buck in the environmental chamber added additional challenges to the climate control systems. In previous testing without the buck, there were two environmental systems and four controlled flow rate register possibilities. One environmental system controlled the main environment and a second one, through a four port manifold, controlled the flow to the experimental elements. The lack of a second row in the vehicle provided challenges in managing the airflow in the vehicle, particularly during the cold climate test conditions, where air would normally enter the vehicle through the front floor registers and leave the vehicle through openings in the vehicle package tray. Exhaust ports were added behind the front row seats to simulate this condition.

With the buck in the chamber, shown in Figure F40, two environmental systems were again used. One environmental system controlled the environment outside of the buck while the other environmental system controlled the inside environment through the conventional air handling system panel and floor registers. Three additional sets of controls were also utilized. The first set of controls adjusted the temperature and flow rate to the overhead register. The second set of controls was used to adjust the heated and cooled seat, and a final set of controls was used to control the heated steering wheel.

Figure F40: View of vehicle buck inside thermal chamber

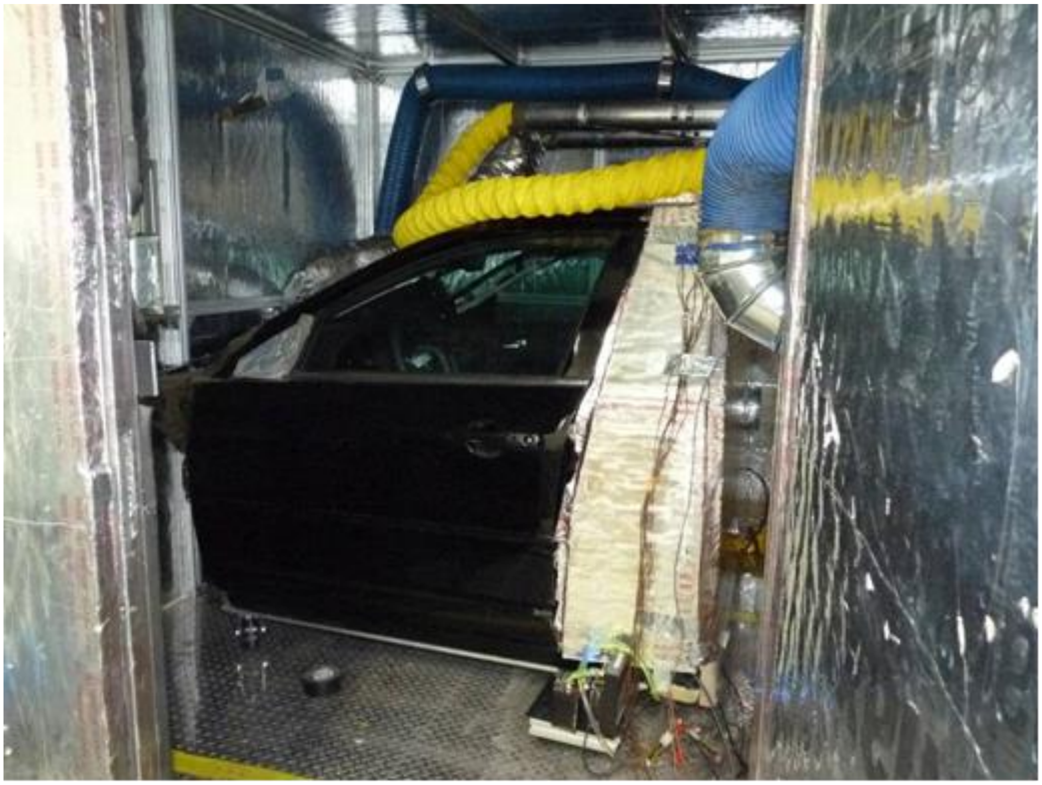

Photo Credit: Halla Visteon Climate Control Corp.

For the testing conducted in Phase 1 (without the buck), the temperature was held constant in the chamber while the different elements (and combinations) were tested. For Phase 2 testing with the buck in the chamber, specific temperature profiles were followed to duplicate the conditions in the vehicle. The goal was to have the air flowrate and discharge air temperature from the registers, and the cabin temperature all match the conditions measured during the wind tunnel tests of the vehicle. During the Phase 2 tests, the design of the test setup did not allow the control systems to achieve this level of transient control. To compensate for this limitation, one of the system parameters was selected as a 'control point', a second parameter was systematically controlled, and the third parameter was varied as needed to keep the 'control point' on target. For the buck, the cabin temperature was the control point, the register airflow was the controlled variable, and the register temperature was the process variable that would change automatically to maintain the cabin temperature. A control system within the buck adjusted the air handler modes for panel, defrost, and floor modes.

The overhead register had its own set of controls. The airflow out of the register was controlled where the 'control point' was the temperature out of that register. The concept that was explored for this node was to duplicate how a thermoelectric device would perform when connected to an overhead register. The TE device system would draw pre-conditioned air from the floor area of the vehicle, heat or cool it in the TE device, and finally vent the conditioned flow out of the overhead register. For these tests, the cabin floor temperature was measured and the output of the overhead register was controlled to a difference in temperature from that point. A blend door and blower system external to the chamber was used to control discharge temperature. The buck was outfitted with the same sensor locations as the vehicle in the wind tunnel. Additional sensors were added for the overhead register in order to measure the discharge temperature.

Figure F41: Blend controls for thermal chamber

Photo Credit: Halla Visteon Climate Corporation

F3.4.2 Assessment of Zonal HVAC Elements

There were four major design elements selected for the final distributed HVAC system architecture. The main elements remained the instrument panel, front panel and floor registers that are carried over from the original vehicle architecture. The addition of other architecture elements allowed for studying the impact of reduced airflow and temperature from the instrument panel registers.

The primary distributed element used in this architecture was the overhead register. The first version of the overhead register is shown in Figure F41. It distributed heated or cooled air around the head of the occupant. The second major element was a heated and cooled seat. The seat used thermoelectric devices to transfer heat or cooling into the air. The thermoelectric devices were connected to a liquid coolant loop to transfer the waste energy outside the vehicle.

The seat system was centrally controlled, since it was integral to the overall node-based distributed HVAC architecture and the envisioned transient control methodologies.

The final element used was a heated steering wheel. The heat to this wheel could be varied as required. There was a feedback element embedded in the wheel to maintain control of the temperature. The heated steering wheel is a standard feature on many luxury vehicles today, but is typically employed as a stand-alone feature, rather than as an element in the distributed climate system architecture. In the current project, the steering wheel becomes an important element in providing thermal comfort to the driver's hands.

The team also investigated the use of thermally conditioned touch surfaces. These perform analogously to the heated steering wheel and are critical to the current efforts. In particular, because the driver's hands are required to touch the steering wheel at all times, while the other passenger's hands may be able to compensate by minimizing exposure to thermally uncomfortable surfaces.

Only minimal geometric modification to the Phase 1 parametric CFD model was necessary to incorporate the four selected elements. The bulk of the CFD process remained similar to earlier work. Figures F42, F43, and F44 show temperature and velocity contours for the 28°C and 5°C test cases respectively.

Figure F42: Temperature contours fifteen minutes into a 28°C ambient test

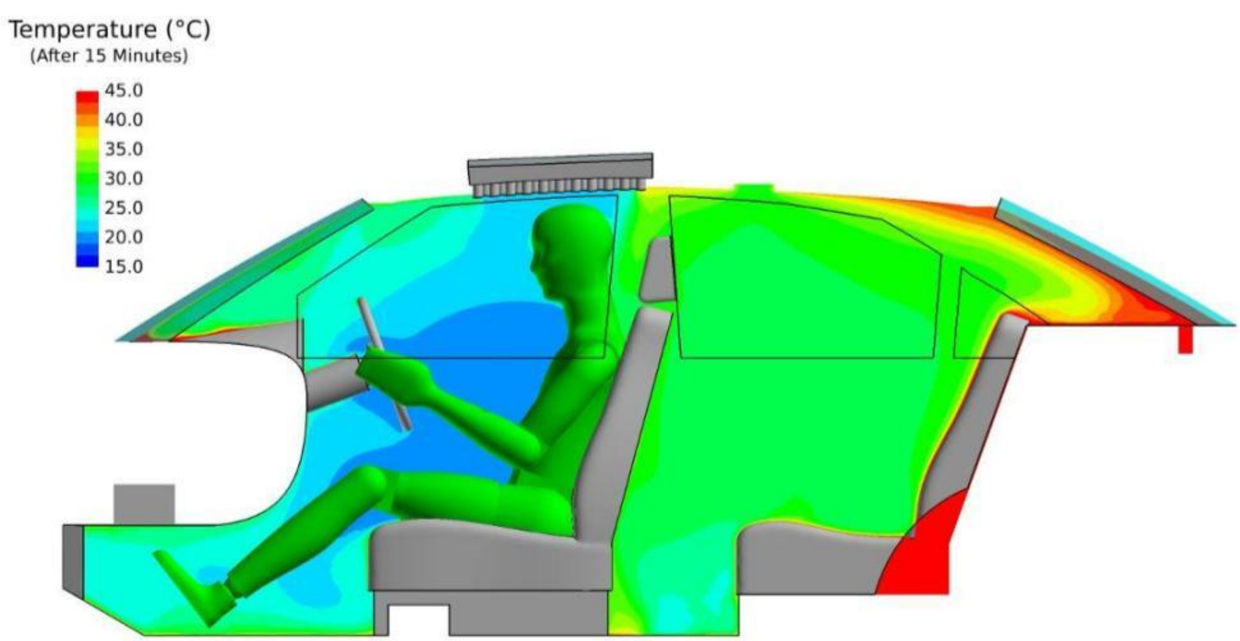

Source: Halla Visteon Climate Control Corp.

Figure F43: Temperature contours fifteen minutes into a 5°C ambient test

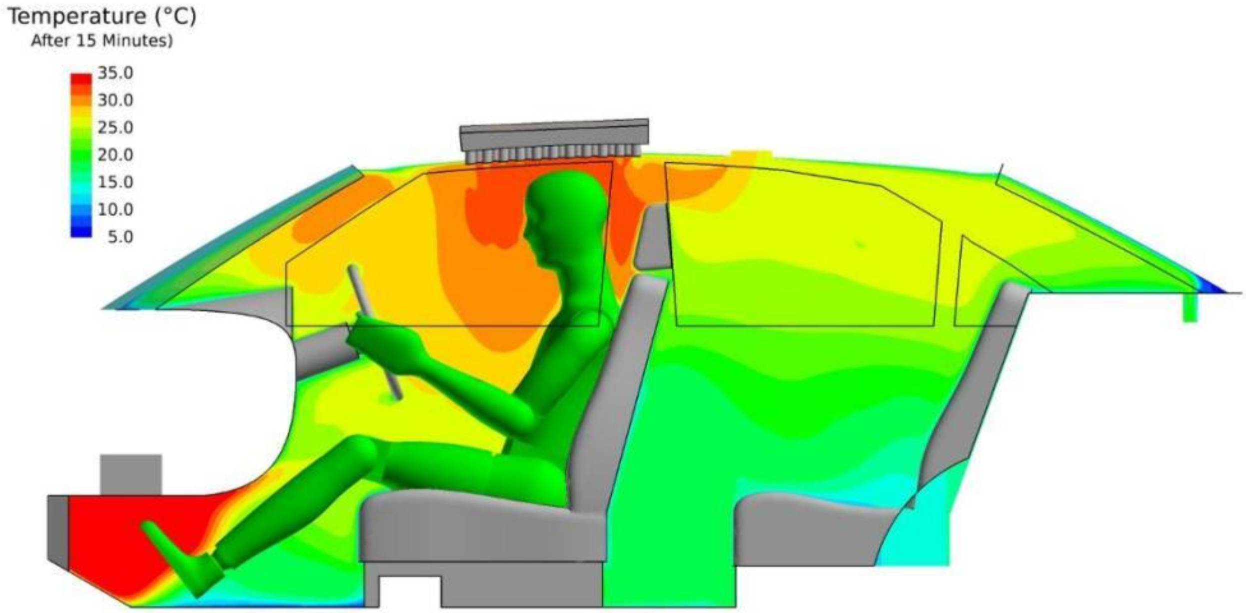

Source: Halla Visteon Climate Control Corp.

Figure F44: Representation of velocity vector field for a distributed system

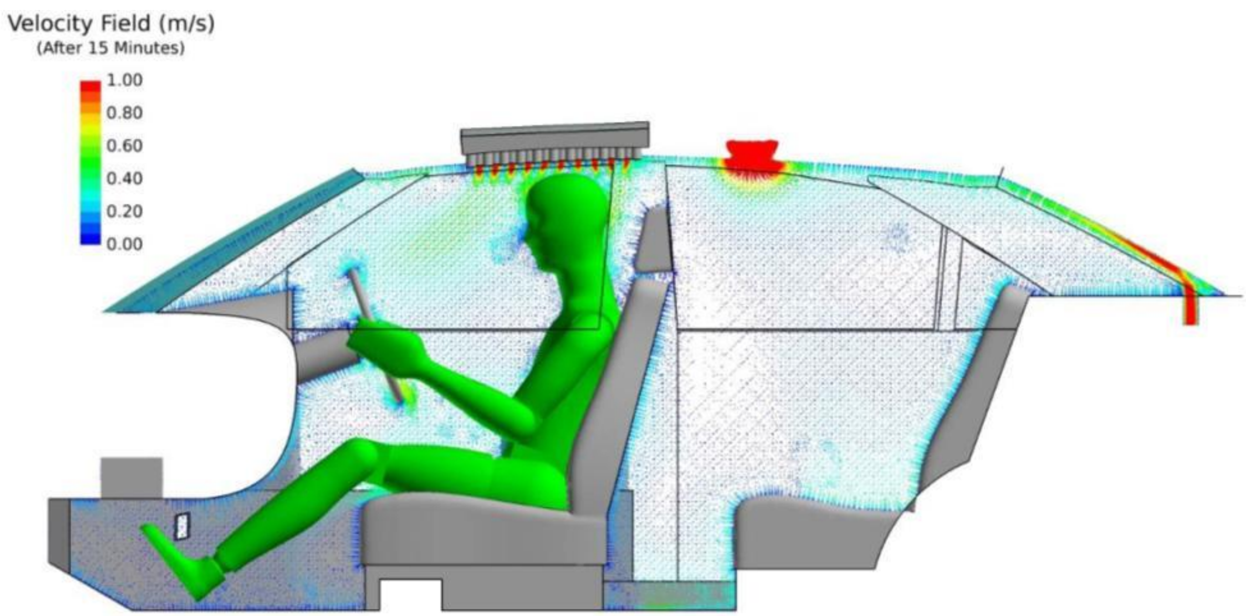

Source: Halla Visteon Climate Control Corp.

Energy savings were calculated for each of the six test scenarios and weighing factors were applied by the usage patterns. The power used in each test was calculated using proprietary tools both for heating and cooling and for the thermoelectric devices. The power usage profile of the 5°C case is shown in Figure F45 as an example. After analyzing all the profile data and applying weighting factors for all conditions, a total net energy savings with the distributed system was indicated.

Figure F45: 5°C modeled zonal system power consumption comparison with baseline

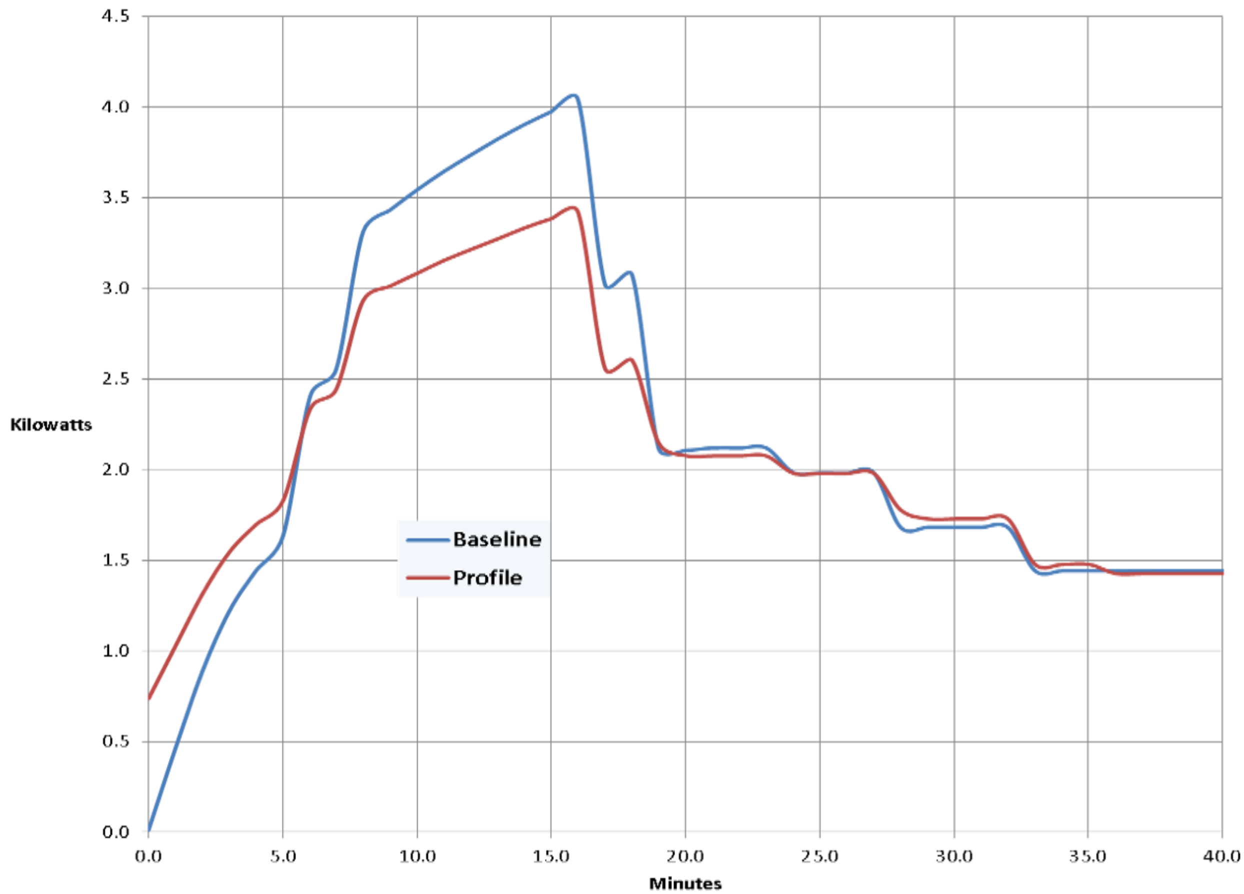

Source: Halla Visteon Climate Control Corp.

F3.5 Zonal HVAC Design Architecture Methodology

In order to establish the layout for a distributed TE HVAC system, it was necessary to detail the interfaces among and between these systems, along with their subsystems, component assemblies, and components. There were several key findings regarding the design of a distributed climate system. Results from the thermal chamber testing were also used in shaping the overall design methodology for a zonal-type system. These included five major findings.

First, asymmetrical heating and cooling of the occupant through nodes that selectively condition the left or right side of the body of the occupant are ineffectual due to the general discomfort observed with left/right temperature asymmetry. While prior studies demonstrated asymmetrical or spot heating/cooling could have positive effects on comfort, their scope did not include a left vs right bias. Rather, vertical asymmetrical heating or cooling of the feet, torso, head or other areas independently was found to have a potentially positive impact on comfort.

Second, constant heating/cooling of localized body segments with no change in airflow rate or proscribed temperature over time was found to be ineffectual. It was found that it was necessary to have a dynamic heating and cooling strategy.

Third, a heated and cooled seat was found to be influential in affecting overall comfort of the vehicle occupant. This was due in part to proximity of the source of heated or cooled air (direct contact) in close proximity to the subject's core/trunk.

Fourth, heated air blown towards the face of the subject negatively affected overall comfort, while cool air tended to positively affect overall comfort, especially during transient conditions.

Finally, the control strategy was found to be critical to overall HVAC system design. For example, transient cooling or heating could significantly increase overall comfort, but if the same temperature and volume of airflow was continued, it could quickly degrade overall comfort. A robust control strategy was critical to maximizing the positive effect of nodal heating and cooling.

Based on these rules, the engineering requirements and attributes needed to define specific implementation pathways for a distributed TE HVAC climate system were considered. This analysis work started by developing a progressively more detailed set of boundary and interface diagrams to define the key systems, subsystem, and components necessary to implement the TE solutions. The physical and informational links between each of these systems were then defined. Once this was accomplished, these diagrams were used, along with proprietary information regarding engineering specifications, system attributes, and design validation methods, to develop a set of design rules and constraints necessary for the TE system to function. Key interfaces and components needed to carry-out the specific requirements necessary to meet system requirements were developed later in Phase 3 based on this guidance.

At its simplest, the climate system interacts with a range of other vehicle systems, and required definition and input for non-vehicle details such as the occupant, the environment, and a number of manufacturer-specific details as shown in the boundary diagram of Figure F46. The key non-climate control systems that were studied included the vehicle powertrain system, which included engine, transmission, and driveline; the body and steering systems, which included interior components, exterior, seals, glass, steering wheel, seats, etc.; and the electrical and power systems, which included charging, power distribution/leveling, electrical control modules, wiring, connectors, batteries, and electric machines. All of these interactions required interface-specific development of requirements and an understanding of attribute trade-offs that impact multiple vehicle systems.

Figure F46: System-level climate system boundary diagram

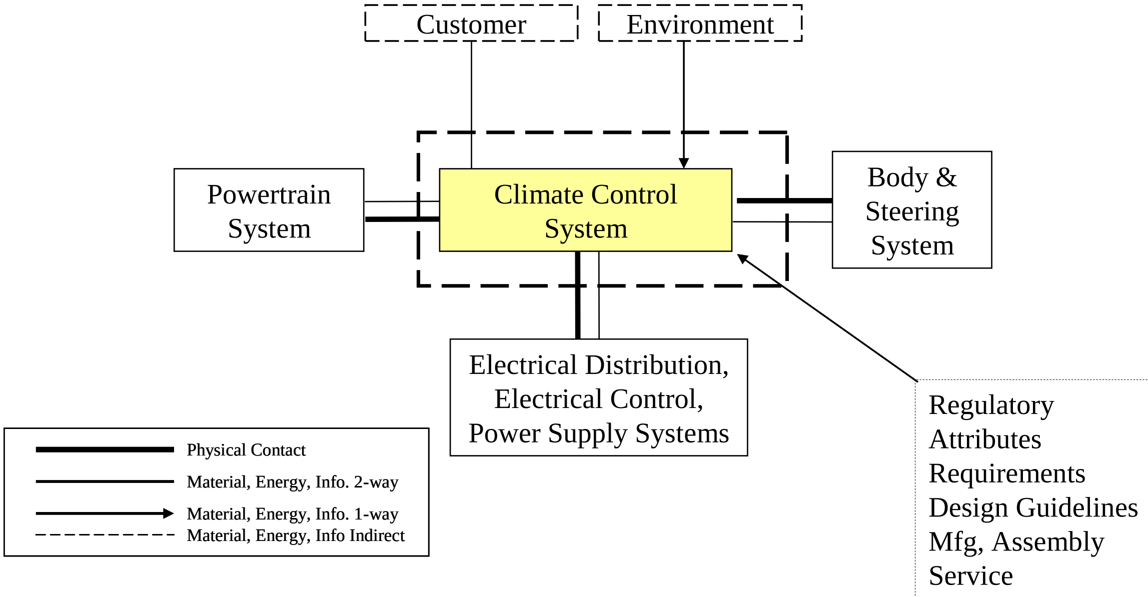

Source: Ford Motor Company

The major systems that interact with Climate are the Body System, the Electrical, Controls, Power Systems, and the Engine System. In addition, the climate system was known to interact with the environment and the customer. Finally, inputs to the climate system from engineering constraints such as regulatory and corporate requirements were considered. The identification of the four major subcomponents of the climate system allowed all of the necessary functions of the climate system to be considered in meeting vehicle-level and system-level requirements; as well as to allow the zonal system to fulfill specific attribute criteria. The details of this system-level interaction, along with specific system requirements, performance attributes, and engineering requirements were developed in detail, but are not discussed in this report.

F3.6 Success Criteria Assessment for Phase 2

Criterion 1: Thermal chamber testing validates comfort modeling predictions.

Assessment: Preliminary ACES testing using subject raters indicated that TE HVAC architectural elements operating in conjunction with the central HVAC system using a smart controls strategy could achieve required occupant comfort targets.

Criterion 2: Laboratory testing of proof-of-principle TE device validates model predictions.

Assessment: TE device modeling predictions and subscale device assessment showed a good correlation between modeling results and expected calorimeter test results.

Criterion 3: Vehicle packaging studies confirm that the TE HVAC system could be installed into the target vehicle.

Assessment: Both model-based and buck packaging studies showed that the elements of the TE HVAC architecture could be packaged into the existing test vehicle.

Criterion 4: Integrated TE CAE modeling indicates that the required thermal comfort levels can be achieved using the TE HVAC architecture.

Assessment: Preliminary modeling results showed the TE HVAC architectural elements operated in conjunction with the central system using a smart controls strategy could achieve occupant thermal comfort. TE models showed that TE devices had enough capability to meet the required airflow and temperature outlet targets in the design.

Outcome: Based on the team's assessment of the major decision criteria, the team recommended that the project proceed into Phase 3. This proposal was accepted by the U.S. DOE Program Manager and the project proceeded into the third phase.

CHAPTER F4:
Ford Phase 3 – Advanced Development

Phase 3, Advanced Development, was started January 1, 2012 and was completed November 30, 2012. This phase included the development, fabrication, and bench testing of the TE HVAC hardware, power supplies, and a basic control system. A cost analysis of production architecture was conducted. Advanced thermoelectric subassemblies were designed, built, and tested. In addition, strategies for reducing overall cabin thermal loads were explored.

F4.1 Task Description and Milestones for Phase 3

The purpose of Task 1 was to confirm the test conditions and program measureables, and to ensure development tasks were supported by appropriate model-based assessment. In addition, thermal comfort modeling tools and method development efforts were continued. The purpose of Task 2 was to design, build, and bench test vehicle-intent TE HVAC hardware. In addition, the development of advanced thermoelectric devices was continued and thermoelectric materials research work was focused on understanding manufacturability of advanced p- and n-type materials developed under this program. The purpose of Task 3 included the design, fabrication, and test of zonal HVAC items such as ducts, trim covers, manifolds, pumps, and other key components. In addition, the coordination of all TE HVAC and related component design validation was completed. The purpose of Task 4 was to conduct a cost analysis of the zonal TE HVAC system. In addition, a study into the optimization of cabin thermal loads was conducted.

F4.2 Advanced Thermoelectric Materials Research

This section describes the final efforts within the project to develop advanced p- and n-type thermoelectric materials. The goal was to develop materials that could be fabricated in bulk, be produced economically and which were targeted to have a ZT between 1.3 and 1.7 at ~300 K. As outlined in the previous chapters, the tetradymite semiconductors, i.e. the general class of quaternary $(Bi_{1-x}Sb_x)_2(Te_{1-y}Sb_y)_3$ alloys, were the object of known manufacturing processes and of a broad general knowledge base. Therefore, these materials were selected as the starting material for research in the project.

During Phase 2 of the project, tin was identified as a resonant impurity in the valence band of Bi_2Te_3. It was shown to enhance the thermoelectric power of the host material at cryogenic temperatures through resonant scattering. Those efforts showed Sn provided an excess density of states about 15 meV below the valence band edge, and it was also found that the increases in density of state resulted in an enhanced Seebeck coefficient. The experimental proof for the existence of this resonant level came from Shubnikov-de Haas measurements combined with galvanomagnetic and thermomagnetic properties measurements. Most importantly for this program, experimental analysis showed that doping with Sn could enhance the room temperature thermopower of Bi_2Te_3, leading to an enhancement of the *ZT* of the binary semiconductor that lies at the basis of commercially important materials for Peltier cooling.

While $Bi_{0.5}Sb_{1.5}Te_3$ is the best p-type composition, previous work in the open literature showed that this was not useful for *n*-type material. This was reportedly due to the degeneracy in the valence band that increased the effective mass was not present in the conduction band. Unlike the case of the p-type material, there were two spots in the $(Bi_{1-x}Sb_x)_2(Te_{1-y}Se_y)_3$ quaternary phase diagram that were known to yield useful n-type material. Previous work indicated that there was a maximum in degeneracy at low temperatures for Sb containing materials with composition $(Bi_{1-x}Sb_x)_2Te_3$ with x=0.2, y=0 and for Selenium-containing materials with the composition $Bi_2Se_{0.3}Te_{2.7}$ (x=0, y=0.1). This degeneracy increased the effective mass of the electrons in the material and also increased ZT. Due to the temperature dependence of the band structure, these exact compositions were highly unlikely to be optimal. Therefore, there was a phase space of $(Bi_{1-x}Sb_x)_2(Te_{1-y}Se_y)_3$ with 0.1 ≤x≤0.3 and 0.05≤y≤0.15 that needed to be explored to find the optimal composition to maximize degeneracy.

A literature search to identify n-type resonant levels in this system was not successful. However, there was significant literature on various methods to densify powders of BiSbTeSe alloys. These results showed that the cold press technique could increase *zT* in p-type alloys up to 50% in contrast to other cold-pressed methods. Therefore, this technique was applied to the n-type materials development efforts. Initial results indicated that successfully lowering thermal conductivity in the n-type system using the new technique was possible.

Samples were synthesized at ZT::Plus based on the Ohio State University recipe. Elemental Bi, Sb, and Te in the ratio 10:30:60 were sealed under argon into quartz ampoules, then heated to 800 to 850°C and held for 6 hours. The resulting ingots were milled to a fine powder in a planetary mill. Samples weighing 7.5 grams were then pressed and sintered in a spark plasma sintering (SPS) apparatus to form cylindrical bullets with a 10mm diameter and a 16 mm height. Sintering pressures were varied between 10 and 60 MPa, while sintering temperatures were varied between 100 and 350°C. Envelope density was measured by dividing the mass by the volume as measured with calipers. Pycnometric density was also measured in the samples using a gas pycnometer. The two methods yielded different results due to internal open porosity in the samples.

The preparation techniques used in the p-type alloys were also used for n-type compositions, similar to the commercial alloy $Bi_{1.8}Sb_{0.2}Te_{2.85}Se_{0.15}$. The samples with porosity show improved ZT compared to sample that were fully dense, as shown in Figure F47. As with the p-type material, the data shows an enhancement of the *ZT* compared to the fully dense material.

Figure F47: TE properties of n-type porous materials

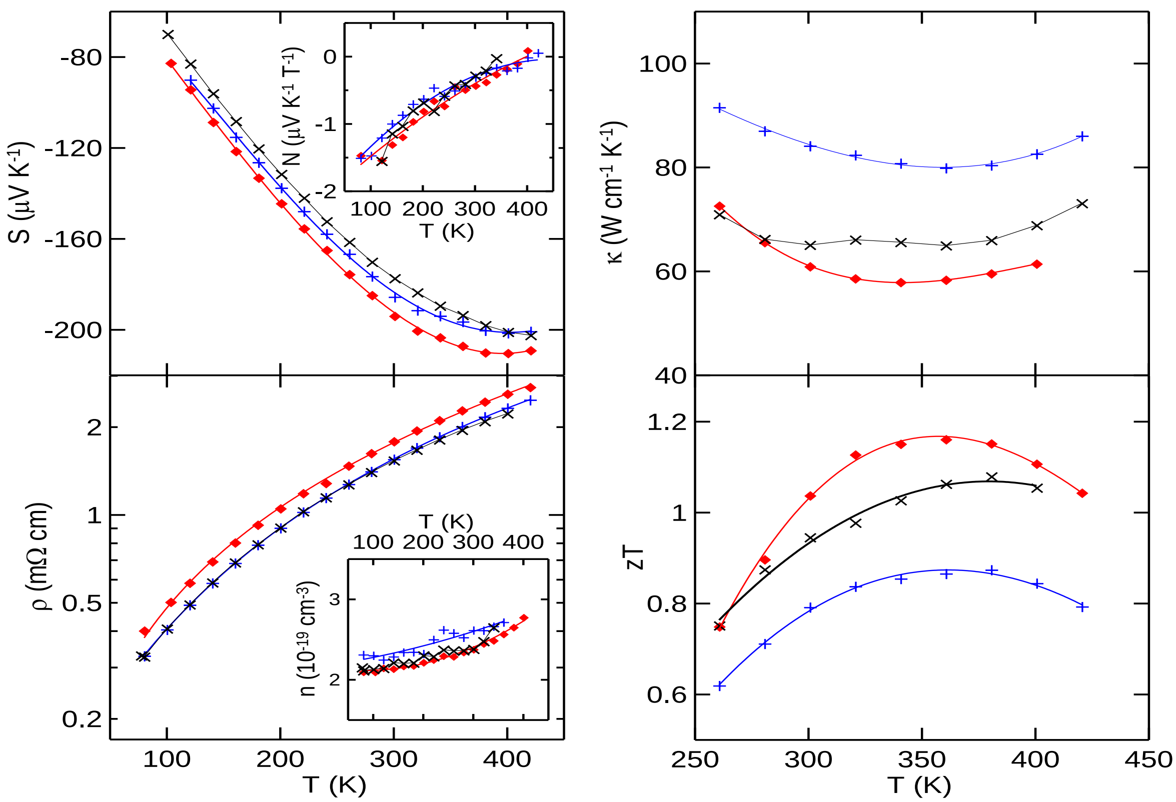

Source: Ohio State University

Material ZT such as reported in Figure F47 came from compiling the results from three transport measurements: S, σ, and κ. The device ZT is lower than the zT of the materials it is made from because of thermal and electrical contact resistances, as well as radiative and convective heat losses. With classical TE materials, the effective device ZT is typically about 30-40% belowthe average peak zT of n- and p-type materials. In order to estimate device ZT, an experiment to measure cooling performance of a Peltier couple as a function of the current (I) was developed. In the absence of an external applied heat load, the temperature gradient in cooling mode across a single-stage Peltier couple was known to be related to I^2, with a maximum value ΔT_{max} as an outcome of that measurement. Thermoelectric device equations showed that ΔT_{max} was related to the device ZT at the cold side temperature T_c. The ZT value deduced from this experiment was more directly related to the performance of the material in its intended application. Assembling a real Peltier couple proved to be a technologically difficult task because it required good contact and binding technology. Ten nanometers of Ni was deposited onto the cleaned surface, which served as both the bonding and diffusion layers. The electrical contact was made with either a BiSn solder, or S-Bond, a fluxless solder, because it seemed important to avoid penetration of the flux in the pores. In the fracture surface shown in Figure F48, the fine grain structure of the deposited nickel is visible to the right of the porous BiTe. The metallization adhered well to the BiTe matrix. The metallized elements of p- and n-type material were then assembled into the Peltier couple shown in Figure F49. Thermocouples measured the temperature of the junction between n and p-type material, and the heat sinks. These thermocouples provide a measurement relative to the known temperature of the cryostat.

In the experimental setup, the temperature drop $\Delta T(I)$ between the junction and the heat sink (a cryostat) was measured as a function of the electrical current sent though the Peltier couple. Then, for each value of the heat sink temperature, the maximum of $\Delta T(I)$ was picked out to be ΔT_{max}. This value was then plotted as function of heat sink temperature T_{HOT}. Results from a set of couples prepared from commercial material are shown in Figure F50, as a reference for the quality of the assembly.

Figure F48: Image of porous- BiTe based alloy and metallization

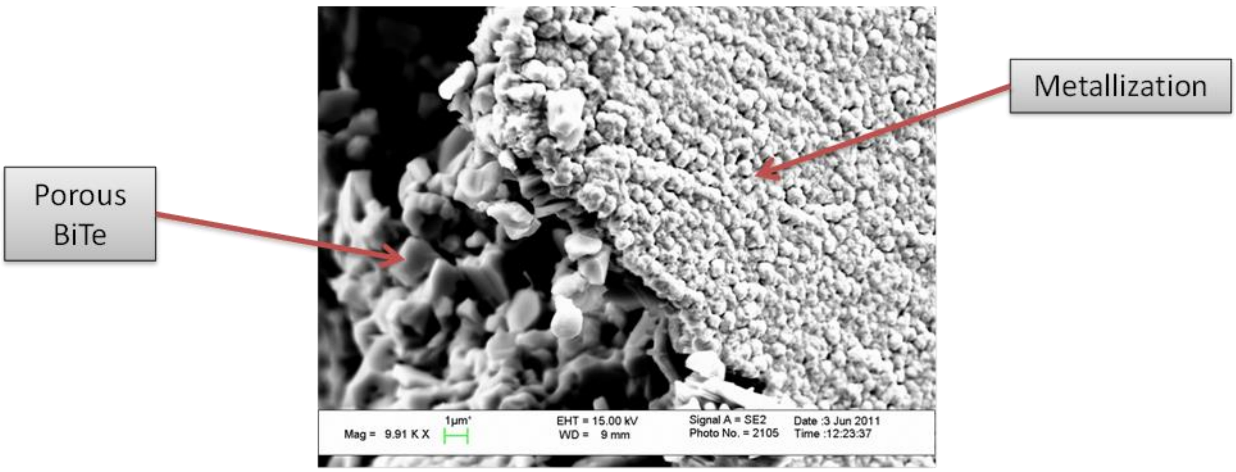

Photo Credit: Ohio State University

Figure F49: Image of assembled TE couple (top) and TE legs prior to metallization (bottom)

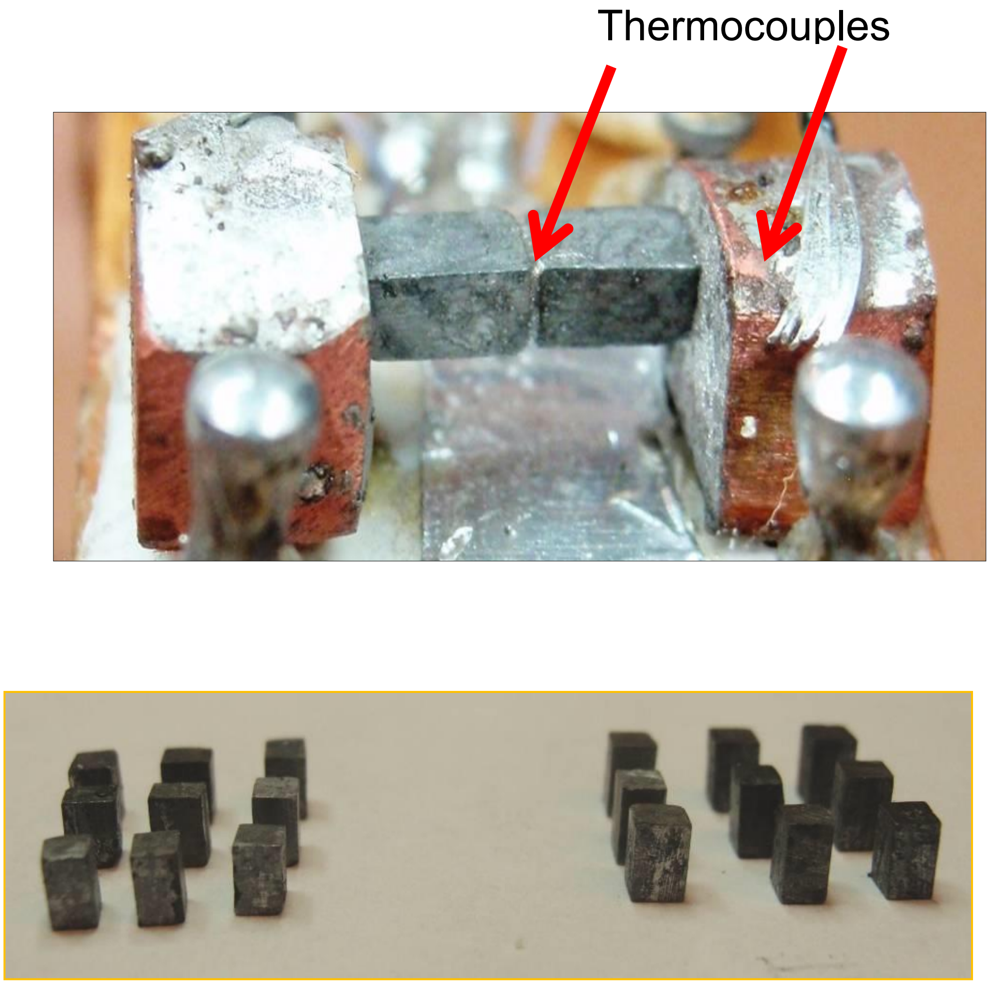

Photo Credit: Ohio State University

Figure F50: Results of ΔT_{max} Peltier testing

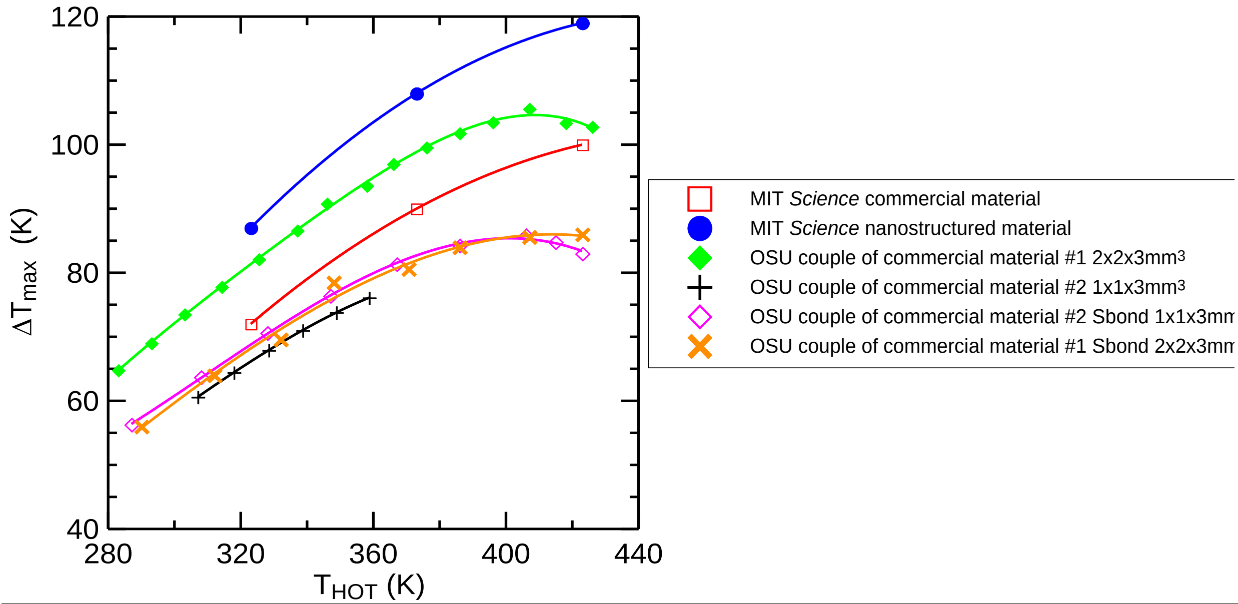

Source: Ohio State University

A couple was made from porous p-type and n-type material, of the type that gave the highest zT values. Results obtained from couple-testing indicted that the porous material which held high promise in its materials zT did not improve the performance beyond that of commercial TE materials. This was in contrast to the 3-parameter measurements of zT from thermopower, electrical and thermal conductivities. The team was not able to explain the underlying reasons for the discrepancy between the two types of measurements. The results for ΔT_{max} measurements versus T_{HOT} taken at ZT::Plus on their materials were also consistent with the OSU results. Before the use of porous material can be recommended or the idea be ultimately discarded, an explanation needs to be formulated, and verified experimentally. This effort will be the subject of future research.

Additional future work will focus on the high cost of tellurium and on its replacement by a more abundant chalcogen in thermoelectric materials for room temperature operation in Peltier cooling applications. Until now, the tetradymite semiconductors $(Bi_{1-x}Sb_x)_2(Te_{1-y}Se_y)_3$ have remained the best suited near 300 K. Only a few favorable composition ranges exist in the $(Bi_{1-x}Sb_x)_2(Te_{1-y}Se_y)_3$ phase diagram, for p-type material (x~0.75 and y=0), and for n-type material (0.1 ≤x≤0.3 and 0.05≤y≤0.15), all Te-rich. New band-structure engineering ideas are needed, on top of the nanostructuring that has already been successfully developed, in order to substitute effectively for tellurium. This is also an area open for future research efforts.

F4.3 Design of Thermoelectric HVAC System Components

The efforts to design the TE zonal system hardware involved developing designs of the zonal TE HVAC sub-systems and components identified in Phase 2 that would be necessary to integrate the concept into a vehicle in Phase 4. No design changes were made to the central

HVAC system hardware or controls in this task. The following components and sub-systems were included in the system study:

- Power supplies and power distribution for thermoelectric devices and blower fans
- Air handling units, including air distribution ducting
- Liquid loop sub-system
- Interior trim components
- Thermoelectric heat pump devices

F4.3.1 Electrical Power Control and Distribution Subsystem

The electrical subsystem consists of four major components:

- Thermoelectric device power supply
- Blower fan power supply
- Seat thermoelectric device and fan power supply
- Power distribution system

The power supply consists of:

- A high voltage input circuit containing the line filter, high voltage bias supply, inrush limiter and high voltage bus sensor
- A control and communication circuit which interfaces with the 12-V battery, fault reporting and command interface
- Two blower circuits, each ~140 W, to power the overhead blowers
- Two thermoelectric device driver circuits, each capable of regulating up to 750 W, to drive the TE devices
- One step down circuit to drop the high voltage battery down to 40 V, to be used by the low power converters. Each one of these circuits will be rated at 740 W and have similar topology to the TE device drive circuits
- Eight seat blower circuits, used to drive the seat blowers
- Eight seat TE device driver circuits

The power supply sections that provide power to the thermoelectric devices can provide positive or negative power to control the devices for both heating and cooling. Because of the nature of thermoelectric devices, the power sections incorporated unique control circuitry tailored to this special application.

F4.3.2 Air Handling Subsystem

Determination of the packaging for the air handling subsystem indicated that the optimal location for the prototype design was to mount the bulk of the air handling system in the trunk of the test vehicle in order to provide optimum position with respect to the power supply, coolant lines and blower. This allowed mounting of the major components on one power supply board along with the controller.

The location of the overhead thermoelectric devices are contained within the ductwork, as shown in Figure F51, in a manner to avoid excessive temperature heat pick-up, facilitate robust device mounting, minimize electrical and fluid system complexity, and to minimize impacts on the open package space in the vehicle cabin. For the prototype design, the system was trunk-mounted in order to optimize these design constraints in the test vehicle, Figure F52. The analysis of TE device performance indicated that it will raise or drop the temperature of the air by the same number of degrees, regardless of package location. Analysis showed that only a large temperature gradient created by a measurable difference between the air temperature going through the TE device and the coolant temperature will have an effect in bulk heat transfer. Calculations did not consider a large temperature gradient. Results from simulation of airflow in the unit indicated a balanced flow.

Figure F51: Air distribution and handling subsystem design

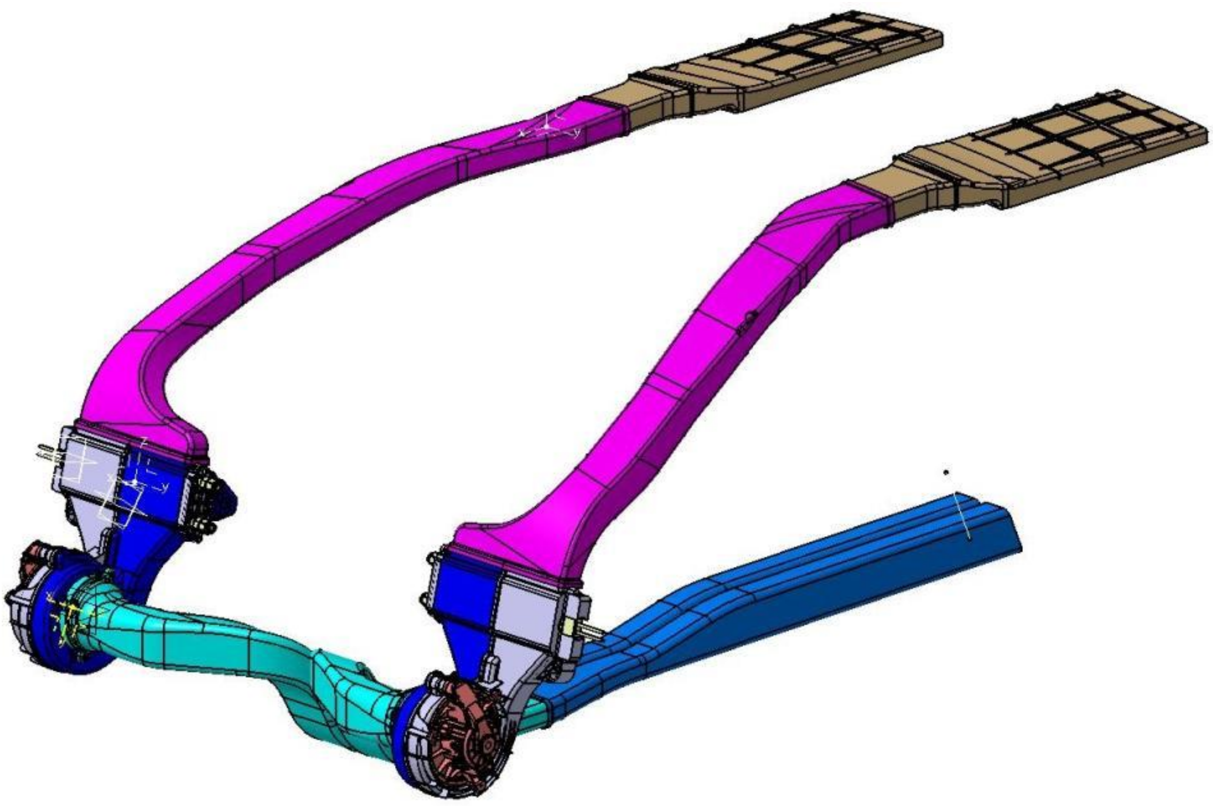

Source: Halla Visteon Climate Control Corp.

Figure F52: Air distribution and handling system packaged in vehicle CAD

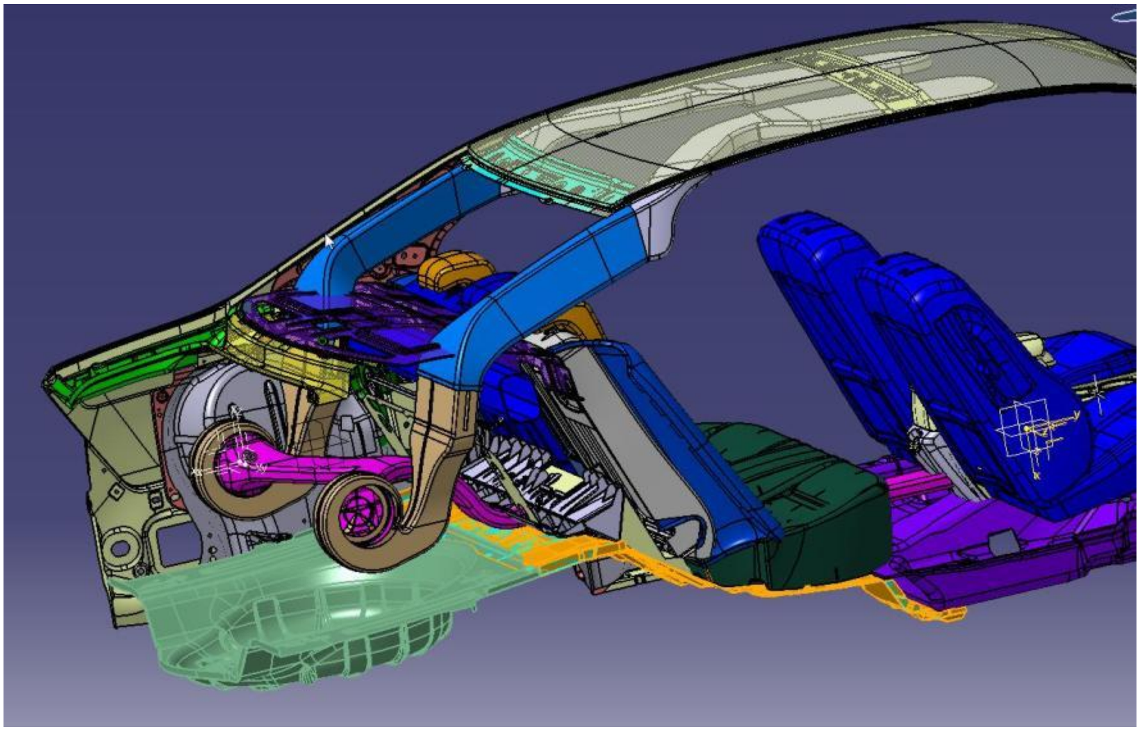

Source: Halla Visteon Climate Control Corp.

F4.3.3 Liquid Loop Sub-System

The liquid loop was designed to conduct heat gain or loss from the thermoelectric devices to an external heat exchanger. An electric water pump and a degas/overflow bottle were included in the overall design study. Manifolds and controlled orifices were employed to distribute the coolant to the various TE devices to optimize performance of each device. The heat exchanger for the liquid loop was placed so that it got first air in the lower air intake of the vehicle. Optimization of coolant flow and coolant temperature, and the influence of these parameters on the various TE systems were modeled to provide proper sizing of heat exchangers, lines, and the pump. The design of the system, shown in Figure F53, also included the analysis of the various pressure drops caused by flow in the various devices.

Figure F53: Liquid loop circuit for the zonal TE HVAC system

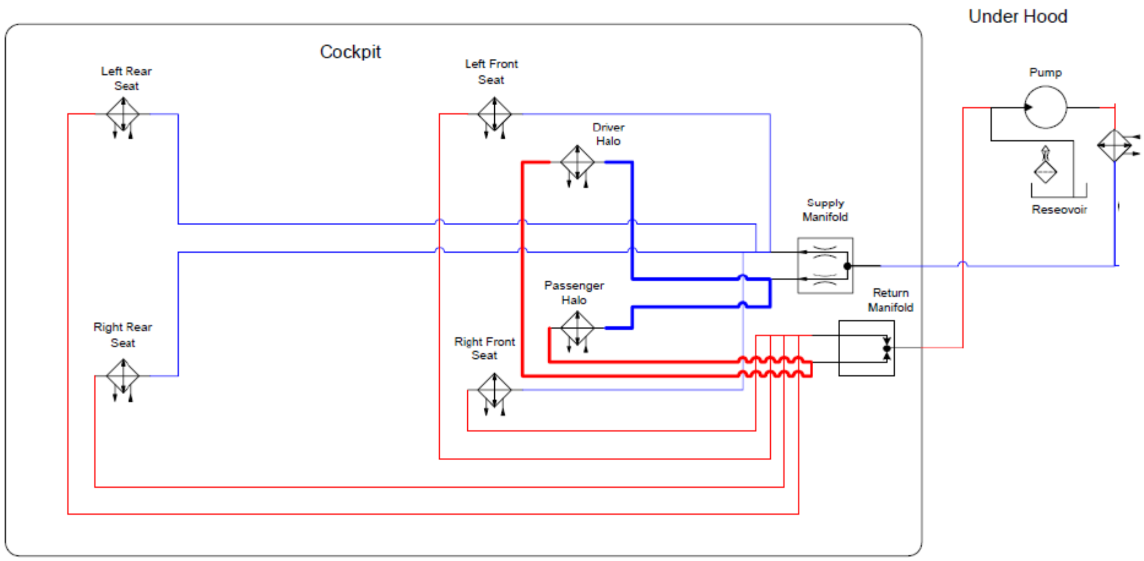

Source: Halla Visteon Climate Control Corp.

F4.3.4 Trim Design

The air inlet design (on the center console), halo facing, pillar trim and headliner were all modified to accommodate the thermoelectric systems. The halo system was superimposed on the CAD drawings of the vehicle in a 3-D visualization system. Then each element affected was modified to provide a pleasing look with the new system inserted.

F4.3.5 Seat Thermoelectric Device Development

Thermoelectric devices (TEDs) were packaged and designed to fit into all four seating positions to provide both heating and cooling function for the vehicle occupants. The designs of these systems are shown in Figure F54 and F55.

Figure F54: Seat-based liquid-air TE device design

Source: Gentherm Corporation

Figure F55: TE devices packaged into front and rear vehicle seats

Source: Gentherm Corporation

The final halo TE device design was similar to the Phase 2 devices reported in the previous chapter. The devices designed for Phase 3 were upgraded for minor performance improvements, reduced weight, and improved integration into the air handling subsystem. A CAD rendition of the final design is shown in Figure F56.

Figure F56: Final design of Halo TE device

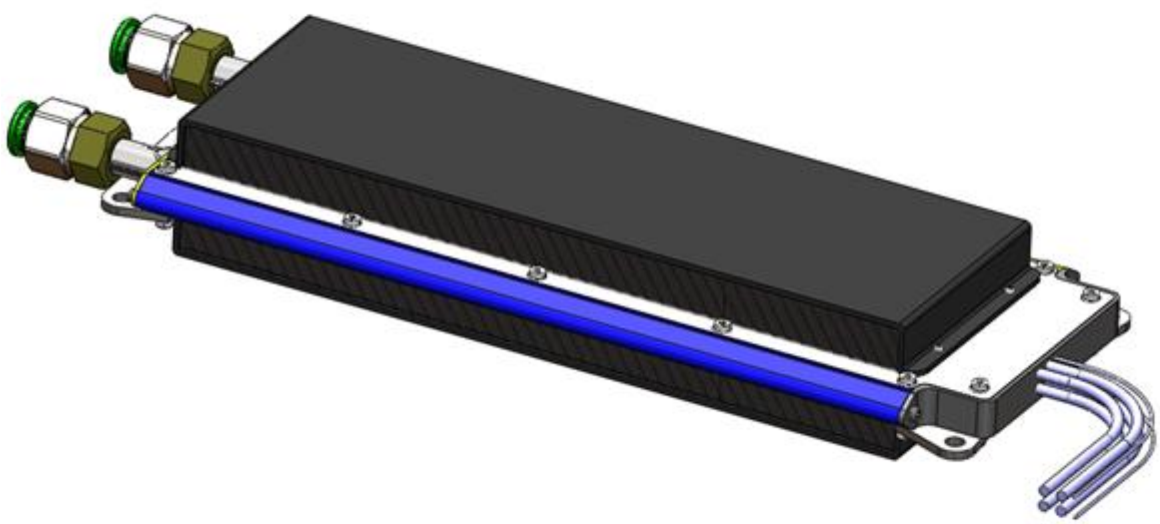

Source: Gentherm Corporation

F4.4 Vehicle-Intent TE Device Hardware & Bench Test Results

This section reports the efforts carried out to update the design of the TE assemblies for vehicle integration. Major tasks included improving the sealing strategy for the device, improving device durability, and simplifying the final assembly. Test procedures were also developed and used to verify that the devices meet performance and durability requirements. In addition, several devices were fabricated, bench-tested, and are being used in system level testing. Ultimately two of the devices built were selected for integration into the test vehicle.

At the conclusion of Phase 2, the development level thermoelectric devices had met the program targets of a cooling COP of 1.3 and a heating COP of 2.3. The Phase 2 devices nominally delivered 380 W Q_C at a peak COP of 1.5 in cooling mode with a main side ΔT of -17.5°C and a heating peak COP of 2.8 with a main side ΔT of +15.9°C. With the performance targets met, the focus for the Phase 3 devices was on improving design robustness, simplifying assembly, and preparing the device for integration into the vehicle. The design team reviewed the results of the Phase 2 testing and "Lessons Learned" from the Phase 2 builds and derived a list of changes that could be made to improve the design.

In addition to these planned development steps, new performance targets were established that increased the device input power requirements from 350 W to 750 W. The team decided not to re-optimize the TE assembly design around this new requirement. This was done for two reasons; first it would be cost prohibitive to operate efficiently at this range due to the amount of TE material that would be needed. Second, the device would only be used at these input powers at the outer limits of the vehicles operating range and therefore would not spend much of its life working at this input power.

Much of the design focus was placed on improving manufacturability and reliability of the device, while maintaining or improving the overall device performance. Testing performed during Phase 2 helped to identify several key areas that needed to be improved including: TE engine durability, liquid heat exchanger durability, sealing, general device assembly, and reducing thermal mass.

Many of the TE device system components were reused for the Phase 3 design, including the liquid heat exchanger, TE engines, skived fin, and interface materials. The skived fin design was updated slightly to improve performance and manufacturability. The device also included several new plastic parts which were designed to help with assembly and sealing. Two internal thermistors were added on the air fin side of the device to monitor TE engine temperature. The device was also set up to have four power wires, as opposed to the two wires used on the Phase 2 device. This made it possible to diagnose issues with the thermoelectric engines and allowed for the engine configuration to be switched from series to parallel without taking the device apart.

Overall weight of the device remained at 1.9 kg, but a reduction in the mass of the skived fins allowed for a reduction in thermal mass and thus, improved time to temperature performance. During durability testing, the average performance of the six devices built for this phase also met expectations, matching the performance of the device built in Phase 2 within 5%. Finally, manufacturing time was reduced by about 50%, allowing two devices to be built per day.

To ensure equal or better performance to the previous skived fin design, the design for this phase carried forward much of the geometry from its predecessor. Changes that were made were either to address shortcomings in the design that were identified in Phase 2 or in an attempt to improve the performance of the fin. A list of updated changes to fins is shown in Table F5.

Table F5: TE device geometry changes from Phase 2 to Phase 3

Feature	Phase 2 vs. Phase 3
Fin Density	Unchanged
Number of Fins	Increased by 1 fin
Fin Thickness	Unchanged
Total Fin Width	Increased by 3.5mm per fin section
Fin Height	Increased by 1.5mm
Base Plate Thickness	Decreased by 50%
Mass	Decreased by 27%
Material	Unchanged
Dielectric Coating	Unchanged

Source: Gentherm Corporation

Performance testing was done using the calorimeter stand developed during Phases 1 and 2 of this project. In total, six devices were used for performance testing. The test points used to verify the device performance reflected the outer limits of the vehicles operation range, simulating ambient environments of 43°C in cooling mode and -18°C in heating mode.

In cooling mode, the 43°C ambient condition was created by setting the inlet liquid temperature to 50°C. This assumed that the liquid loop would see a 7°C rise over the ambient environment. Two air inlet conditions were tested at this inlet liquid temperature; 60°C and 30°C. The 60°C inlet air condition was done to simulate a vehicle with an elevated cabin temperature due to solar load. For this test case, input power was set to max and airflow was varied. The 30°C inlet air condition was used to simulate a vehicle after the cabin had been cooled down. For this test condition, airflow was fixed and device input power was varied.

In heating mode, the liquid inlet temperature was set to -25°C, 7°C below the simulated ambient environment, while the inlet air temperature was tested at 10°C and -18°C. The -18°C inlet air condition simulated a cabin temperature at startup and was run at a max inlet power with varying airflow rate. The 10°C inlet air condition simulated a cabin temperature after being warmed up. For this case, the airflow was held constant and the inlet power was varied.

Performance results are tabulated in Table F6 for both cooling and heating mode tests. In addition to these test points, a TE device was also tested at a several additional test points to demonstrate compliance to the original project goal of achieving a COP of 1.3 in cooling mode and 2.3 in heating mode. In cooling mode, the device was tested at a 48°C inlet condition for both the air and liquid sides, with 3.6 lpm liquid flow and 50 cfm air flow. The input power was varied from 100 W to 700 W to show a distribution of COP over the different input powers. In heating mode, the device was tested at a 5°C inlet condition of both the air and liquid. Airflow was fixed at 60 cfm and liquid flow was set to 1.2 lpm and 3.6 lpm. Input power was adjusted slightly for each case to meet the COP requirement of 2.3 in heating mode, Figure F57, and 1.3 in cooling mode, Figure F57.

Table F6: COP and thermal performance results for Phase 3 TE devices

Description	Test #	Control Points Inlet Temp. Air (°C)	Inlet Temp. H_2O (°C)	Flow Rates Air (CFM)	Flow Rates H_2O (Ltr/mi	Device Power (W)	Δ T.air Measured (°C)	Q_m (W)	Q_w (W)	COP	Balance (W)	% Balance
Cooling Mode	DOE3a.1	48	48	50	3.6	100	-11.01	-277.7	402.2	2.7	18.8	5%
Cooling Mode	DOE3b.1	48	48	50	3.6	200	-14.19	-363.2	593.5	1.8	25.5	4%
Cooling Mode	DOE3c.1	48	48	50	3.6	300	-16.51	-421.8	754.9	1.4	27.7	4%
Cooling Mode	DOE3e.1	48	48	50	3.6	400	-18.33	-471.4	902.0	1.2	24.6	3%
Cooling Mode	DOE3f.1	48	48	50	3.6	500	-19.70	-509.4	1041.1	1.0	25.3	2%
Cooling Mode	DOE3g.1	48	48	50	3.6	600	-20.86	-541.5	1172.9	0.9	25.2	2%
Cooling Mode	DOE3h.1	48	48	50	3.6	700	-21.82	-568.3	1298.8	0.8	23.6	2%
Heating Mode	DOE2a	5	5	60	3.6	240	15.44	551.7	-349.6	2.3	-37.0	7%
Heating Mode	DOE2b	5	5	60	1.2	211	13.62	489.7	-277.8	2.3	1.5	0%

Source: Gentherm Corporation

Figure F57: TE device power sweep in cooling mode

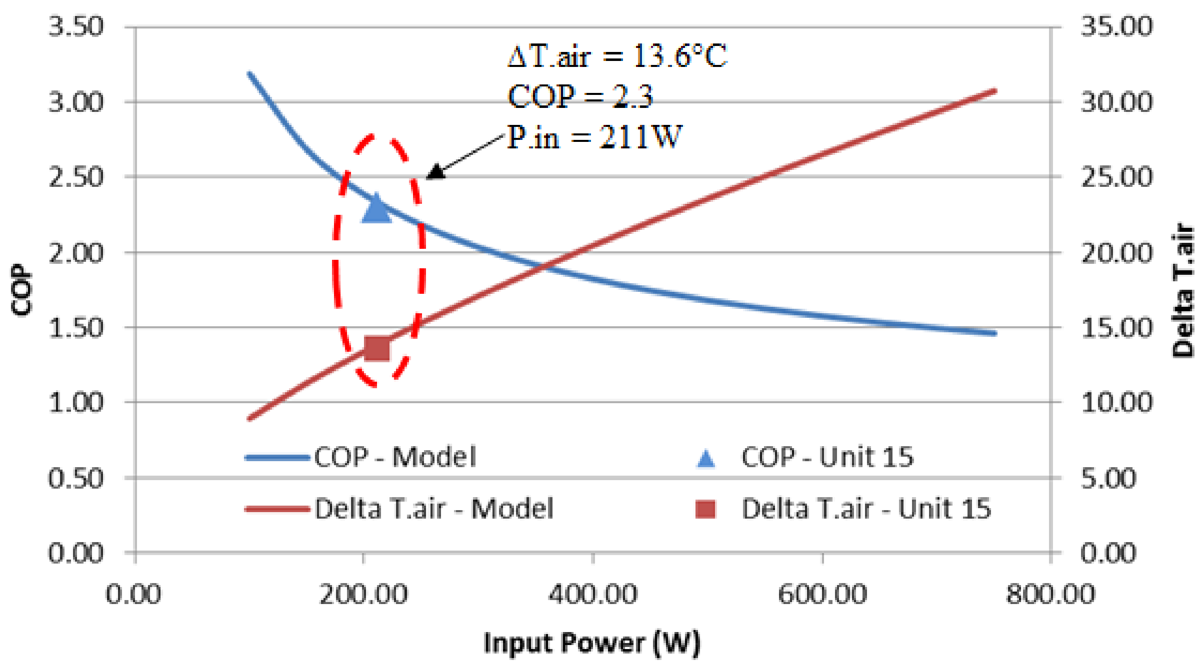

Source: Gentherm Corporation

Figure F58: TE device power sweep in heating mode

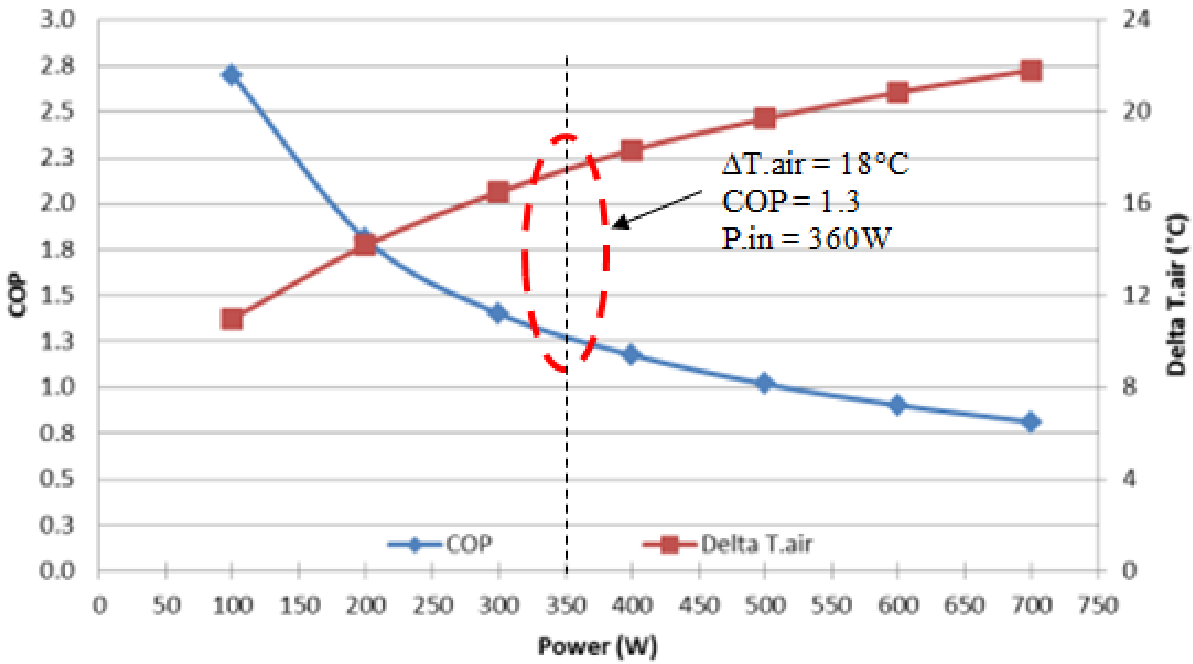

Source: Gentherm Corporation

F4.5 TE HVAC System Cost Analysis

An analysis of the system costs of a commercialized Zonal TE HVAC climate system for light duty hybrid-electric vehicles was conducted. The basic assumption for developing costing models assumed 20K and 100K per annum vehicle volumes that utilized a specific embodiment of a Zonal TE HVAC climate system. The cost analysis was intended to make allowances for cost of all affected components and systems. The study was conducted using an assumption based on two base-level current-production vehicles that were upgraded to accommodate a Zonal TE HVAC climate system. The assumption for these vehicles was that it was a ground-up design that could accommodate changes to sheet metal, interior trim & seating, and power & control system needed to implement a zonal system. The lower volume study was conducted at 20K per year volume. The higher volume study was conducted at 100K per year volume. All costs were estimated based on a baseline vehicle configured with current production level systems.

All costs were developed using proprietary and business confidential methods that were developed internally by the individual companies participating in this cost assessment. Therefore, the detailed cost-roll up information is not presented in this report. Instead, a surrogate method was developed to allow better understanding of direction in which the system costs were trending. This methodology is detailed in Table F7.

Table F7: Directional costs associated with TE HVAC system

$+++	More than 100% increase in cost (piece or ED&T) from base system
$++	More than 25% increase in cost (piece or ED&T) from base system
$+	Less than 25% increase in cost (piece or ED&T) from base system
$0	Cost neutral (piece or ED&T) compared to base system
$-	Less than 25% decrease in cost from base system
$--	More than 25% decrease in cost (piece or ED&T) from base system
$X	Component or system eliminated from new design. No associated piece or ED&T costs

Source: Ford Motor Company

For the purposes of the current analysis, the vehicle and subsystem development process were envisioned as being for a new platform development effort for a family of vehicles. The case study for the assessment focused on two design variants off of a global platform development effort. In this case, the assumption was that global engineering and production system costs applying to all platform variants were carried by the platform program and were not captured here. Other specific changes and costs incurred in the platform variant's bill-of-materials that were driven exclusively by the incorporation of a Zonal TE HVAC design were taken into account and were rolled-up to the system level.

<u>20K per annum TE HVAC vehicle content</u>

The following system design assumptions were studied in this variant:

- **Central HVAC** – No change to AC and heating capacity at 110°F and 0°F. System required to be capable of providing occupant control of temperature, mode, and blower speed. New refrigerant subsystem design was assumed for to optimize TE system cooling.
- **Row 1 Seats** – Upgrade to liquid/air climate-controlled seats. Separate control commands for back and seat units, allowing for independent temperature control of the contact surfaces. Required additional features to minimize fan noise and other noise, vibration, and harshness (NVH) sources. Optimize energy consumption, based on full climate control strategy. Controls for seat TE system were via controller connected through a controller area network (CAN) connection. Strategy assumed controlled by climate system, with manual override capability. System assumed powered by key-on +12V bus. Power provided to TE devices and blowers via stand-alone power supply and device controller.
- **Row 2 Seats** - Upgrade to liquid/air climate-controlled seats. Common control commands for back and seat units. Required additional features to minimize fan noise

and other NVH sources. Optimize energy consumption, based on full climate control strategy. Strategy assumed specified by climate control module (CCM). Controls for seat climate control system (CCS) assumed via controller connected through a CAN network connection. Strategy assumed controlled by climate system, with manual override capability. System assumed powered by key-on +12V bus. Power provided to TE and blower via stand-alone power supply and device controller.

- **Overhead Air** – Add TE overhead air distribution system with independent air handling capable of providing driver and front passenger overhead heating, cooling, and ventilation. TE device power assumed via high-voltage bus. All other systems operate on +12V bus. System assumes continuously variable heating and cooling capable of operating from a minimal maintenance level to a max performance level, as well as fully variable blower speed. Additional features added to minimize fan noise and other NVH sources. Optimize energy consumption, based on full climate control strategy. Strategy assumed specified by CCM. Controls for overhead TE device system via controller connected through a CAN network connection. Strategy assumed controlled by climate system, with manual override capability and mode disable possible.
- **Other system changes** –Incorporate control of all climate functions with central controls, allowing for manual override. Incorporate separate front HEX for TE liquid loop. Assume additional circulation pump for TE system.

<u>100K per annum TE HVAC vehicle content</u>

The following system design assumptions were studied in this variant:

- **Central HVAC** – No change to AC and heating capacity at 110°F and 0°F. System required to be capable of providing occupant control of temperature, mode, and blower speed. New refrigerant subsystem design was assumed for to optimize TE system cooling.
- **Row 1 Seats** – Upgrade to liquid/air climate-controlled seats. Separate control commands for back and seat units, allowing for independent temperature control of the contact surfaces. Required additional features to minimize fan noise and other NVH sources. Optimize energy consumption, based on full climate control strategy. Controls for seat TE system were via controller connected through a CAN network connection. Strategy assumed controlled by climate system, with manual override capability. System assumed powered by key-on +12V bus. Power provided to TE devices and blowers via stand-alone power supply and device controller.
- **Row 2 Bench** – No climate capability.
- **Overhead Air** – Add TE overhead air distribution system with independent air handling capable of providing driver and front passenger overhead heating, cooling, and ventilation. TE device power assumed via high-voltage bus. All other systems operate on +12V bus. System assumes continuously variable heating and cooling capable of operating from a minimal maintenance level to a max performance level, as well as fully

variable blower speed. Additional features added to minimize fan noise and other NVH sources. Optimize energy consumption, based on full climate control strategy. Strategy assumed specified by CCM. Controls for overhead TE device system via controller connected through a CAN network connection. Strategy assumed controlled by climate system, with manual override capability and mode disable possible.

- **Other system changes** –Incorporate central control of all climate functions with central controls, allowing for manual override. Incorporate separate front HEX for TE liquid loop.

The cost study detailed the system and subsystem interfaces, design requirements and validation methods to be used for deploying a production version of the system. In addition, the attribute requirements were also specified. These requirements were inherent to the deployment of systems specified in the previous section. A summary of key system and component changes are show in Table F8.

Table F8: Vehicle content modifications made for zonal TE HVAC system

System	Subsystem	20K	100K
Body Interior	Front Seats	Advanced CCS	Advanced CCS
	Rear Seats	Advanced CCS	-
	Interior Hard Trim	modified	modified
	Headliner & Pkg Tray	Modify to accommodate aux distribution	Modify to accommodate aux distribution
	Interior Soft Trim	Heated Door Inner, Heated Console + Control	-
HVAC Subsystem	Aux TE, Ducting, Airflow, Register	TE Unit, Power Supply, Blower, Motor, Ducting, Outlet Panel	TE Unit, Power Supply, Blower, Motor, Ducting, Outlet Panel
	Ducting + Registers	Add content	-
	AC Lines	New components	New components
	HV Cooling System	Add content	Add content
	HV cables, HV junction box + buss, connectors & fittings	HV connection to TE power supply	HV connection to TE power supply
12-V Elec.	BJB + SJB + Batt	Relays, fused junctions for CCS, wiring and fusing, CAN signal & power harness	-
Controls	Modules	New modules for TE content	New modules for TE content
Zonal TE Additions	Airside	Overhead TE unit, Blower motor + Scroll, ducting + outlet panel	Overhead TE unit, Blower motor + Scroll, ducting + outlet panel
	Liquid Loop	Liquid distribution lines, aux pump, LT Rad, degas	Liquid distribution lines, aux pump, LT Rad, degas

Source: Ford Motor Company

F4.5.1 Central HVAC System Costs

Current central HVAC systems consist of the five major subsystems.

1. HVAC unit, which has the responsibility of delivering conditioned air to the vehicle cabin and contains the evaporator core, heater core, blower and scroll, and associated doors to provide the desired temperature and mode.
2. Central air handling, distribution, and registers are the plastic plenum, ducts, and registers that deliver the conditioned air to the passenger compartment.
3. Refrigerant subsystem consists of the AC compressor, AC lines, expansion valve, condenser, receiver and drier, and the AC refrigerant.
4. The heating subsystem consists of the heater lines, aux water pump, and valves. Typically the radiator and thermostat belong to the powertrain system.
5. The central control module and control head are software that send and receive signals from sensors, actuators, and the driver interface; and command changes to actuator-door position, blower speed, compressor speed/power, and other functions.

Central HVAC Subsystem:

HVAC module with evap, heater core, dual automatic temperature (DATC) control

System cost estimate (delta from baseline HVAC):

- Cost low volume: $0 at 20K (modifications carried in base design cost assumptions)
- Cost high volume: $0 at 100K (modifications carried in base design cost assumptions)

Air Handling and Distribution:

Panel & floor ducts, panel & rear console registers, rear floor ducts (carry-over)

System cost estimate (delta from baseline Air Handling & Distribution Costs):

- Cost low volume: $0 at 20K (carry-over)
- Cost high volume: $0 at 100K (carry-over)

Refrigerant Subsystem:

AC Compressor, Condenser with IRD, TXV, Refrigerant (carry-over)
AC lines: new lines + component

System cost estimate (delta from baseline Refrigerant Subsystem Costs):

- Cost low volume: $+
- Cost high volume: $+

Heater Subsystem:

Aux pump, heater hoses and clamps (carry-over)

System cost estimate (delta from baseline Heater Subsystem Costs):

- Cost low volume: $0 at 20K
- Cost high volume: $0 at 100K

Climate Controls and Head:

User interface (added function for aux overhead control)

- Control over-ride for aux temperature
- Control over-ride for aux blower speed
- Add new Seat heating/cooling button

Controls (integrated controls for Full Auto mode)

System cost estimate (delta from baseline Heater Subsystem Costs):

- Cost low volume: $+ at 20K
- Cost high volume: $+ at 100K

F4.5.2 Seat-Based Climate System Costs

Current seats units contain air-air TE CCS assemblies, attachment hangers, air distribution manifold, and an air diffusion pad. Seat units are controlled by a central control module that provides power and signal I/O to four TE CCS assemblies. In the new system, the design assumed to be changed to an Advanced CCS unit. The system assumed capable of being manually overridden by the occupant.

Advanced CCS unit: (8 units per vehicle for 20K variant, 4 units per vehicle for 100K variant) Advanced CCS unit uses a liquid HEX on the waste side of the device to mitigate the temperature rise seen on the waste side of the device.

2 TE modules with temperature control thermistor (replace air-air TE module)
Liquid heat exchanger and liquid connector fittings (new)
Blower fan and housing (new design)
Power and signal I/O connector (carry-over)
Connectors and mounts (new design)

System cost estimate (delta from baseline CCS):

- Cost low volume: $++ front and $+++ rear at 20K (new design, all new in rear seats)
- Cost high volume: $++ at 100K (new design)

Seat Air Handling Subsystem: (8 units per vehicle for low volume, 4 units per vehicle for high volume). The system designed for the vehicles will be similar in construction to the air handling subsystems in use for current production CCS seats.

Inlet / Outlet Ducting

Air Distribution Manifold

Air Distribution Diffusion

System cost estimate (delta from baseline CCS):

- Cost low volume: $0 at 20K x 2 units (carry-over design)
- Cost high volume: $0 at 100K x 1 unit (carry-over design)

CCS control module: (2 units per vehicle for 20K variant, 1 unit per vehicle for 100K variant) The CCS control module regulates the input power to the TEs and the blower units. The module interfaces with and can be driven by the main HVAC control or it can receive manual inputs via a 3-step switch to override the HVAC systems automatic set point CCS Control Modules.

Power and control module (2x for 20K, 1x for 100K)

System cost estimate (delta from baseline CCS):

- Cost low volume: $+++ at 20K x 2 units (new design, rear unit new)
- Cost high volume: $+ at 100K x 1 unit (new design)

F4.5.3 Overhead Auxiliary System Costs

This system consists of an Air-to-Liquid thermoelectric device packaged into an auxiliary HVAC system consisting of an air inlet duct, centrifugal type blower, TE device housing, distribution duct, outlet register, power supply/regulator and control module. Systems control assumed to be integrated and communicate with the main HVAC system control.

Overheat TE Unit

TED assumed optimized for peak cooling efficiency at a moderate airflow rate. Under peak load conditions device assumed able to achieve a maximum output, to meet system load requirements. Device consists of three main components, plus wiring and sealing systems. The three main components are: air fins (2), thermoelectric engines (2) and a liquid HEX (1).

System cost estimate:

- Cost low volume: $+++ at 20K (all new)
- Cost high volume: $+++ at 100K (all new)

Overhead Unit Air Induction, Handling, Distribution, and Registers

A zonal air distribution subsystem assumed to draw recirculated cabin air and moved by an auxiliary blower through ductwork into overhead registers located in the headliner.

System cost estimate:

- Cost low volume: $+++ at 20K (all new)
- Cost high volume: $+++ at 100K (all new)

Overhead Power and Control Module

Overhead TE device auxiliary air system assumed powered from the high voltage bus, with blower powered from the 12-V bus. Controls for the TE device integrated into the power supply to provide discrete control. Assume existing control module modified to provide fully variable blower control for the overhead system.

System cost estimate:

- Cost low volume: $+++ at 20K (all new)
- Cost high volume: $+++ at 100K (all new)

Overhead Blower & Scroll

Overhead blower and scroll assumed similar to current auxiliary units available in the market. System is sized to provide up to 160 cfm. TE device to be placed upstream of diverter door.

System cost estimate:

- Cost low volume: $+ at 20K (similar to blower aux system)
- Cost high volume: $+ at 100K (similar to blower aux system)

F4.5.4 Balance of Zonal TE HVAC System Costs

The remainder of the zonal climate system consists of the liquid system loop, the modifications to powertrain and body controls modules, and the additional sensors required to provide system operational feedback.

Low temp liquid waste loop

Low-temperature loop consists of hoses, connections, valves, distribution manifold, pump, and heat exchangers. Liquid-loop system designed to provide TE devices an appropriate source or sink temperature, depending on ambient and cabin climate conditions, as well as commanded performance of the individual TE device.

System cost estimate:

- Cost low volume: $+++ at 20K (all-new systems)
- Cost high volume: $+++ at 100K (all-new systems)

Other vehicle control modules

Modifications to existing powertrain control module and body control module required to process signals for the HVAC control module and the zonal TE modules. Signal I/O occurs via

CAN message and is used to define the operational state of various systems. This is used to define strategy for various vehicle subsystems, including the allocation of power to the climate control system, based on various calibration and strategy requirements.

System cost estimate:

- Cost low volume: $0 at 20K (costs carried in base design)
- Cost high volume: $0 at 100K (costs carried in base design)

Other vehicle sensors and actuators

The only additional sensor incorporated into this design to provide diagnostic and control feedback is a thermistor placed into the distribution manifold. This sensor feeds the feedback to the TE controls.

System cost estimate:

- Cost low volume: $+ at 20K
- Cost high volume: $+ at 100K

F4.6 Success Criteria Assessment for Phase 3

Criterion 1: Newly developed, vehicle-intent TE based subsystems meet bench-level performance and reliability test targets.

Assessment: TE device performance was evaluated in both calorimetric and durability bench tests. The performance of the devices on these test stands met or exceeded minimum performance requirements established in the project.

Criterion 2: Cost analysis shows a potential business case for a TE-HVAC system in the specified timeframe.

Assessment: Assessment of the commercial viability of thermoelectric HVAC systems, based on existing CCS commercial viability, indicated a potential future business case for portions of the TE HVAC system. However, overall costs remain high.

Outcome: Based on the team's assessment of the major decision criteria, the team recommended that the project proceed into Phase 4. This proposal was accepted by the U.S. DOE Program Manager and the project proceeded into the fourth, and final, phase.

CHAPTER F5: Ford Phase 4 – Engineering Development

Phase IV, Engineering Development, was started December 1, 2012 and is expected to be completed by August 31, 2013. It focuses on integrating and testing the TE HVAC hardware in a prototype vehicle to determine the system's ability to improve HVAC system efficiency while meeting occupant thermal comfort criteria. The potential commercialization of the system will be explored in a business-case study. In addition, a study exploring advanced thermoelectric materials and design concepts will be completed.

F5.1 Task Description and Milestones for Phase 4

The purpose of Task 1 is to finalize the vehicle system and thermal comfort models, and to compare the results obtained using these models with actual test data obtained in baseline and prototype vehicle system tests. In addition, results from thermal comfort modeling will be assessed using results from system testing. This study will be used to assess the predictive capabilities of the modeling tools for a distributed, zonal system design. The purpose of Task 2 will be focused on a study assessing the current state of thermoelectric HVAC design, including its commercial and technical viability; and the technological and commercial advancements necessary to improve device operating range, efficiency, cost, and other metrics critical to the future success of the technology. The purpose of Task 3 is to install the TE HVAC system hardware into a test vehicle, and to evaluate the system's performance in a wind tunnel environment. Tasks for installing the TE HVAC system into the test vehicle include: (i) removing the existing vehicle interior and HVAC system, (ii) adding sensors and a data acquisition system into the vehicle to measure system performance, (iii) installation of all TE HVAC system components (including vehicle trim) developed and build in Phase 3; and (iv) verifying and calibrating the system prior to performance testing. The purpose of Task 4 is the completion of a commercialization assessment for a zonal TE HVAC climate control system to assess the commercialization pathways for incorporation of TE HVAC climate control systems into light-duty passenger vehicles, including needs for further development work.

F5.2 Phase 4 Timing Plan and Technical Accomplishments To-Date

The Phase 4 task list and timing plan is shown in Figure F59.

Figure F59: Phase 4 tasks and timing plan

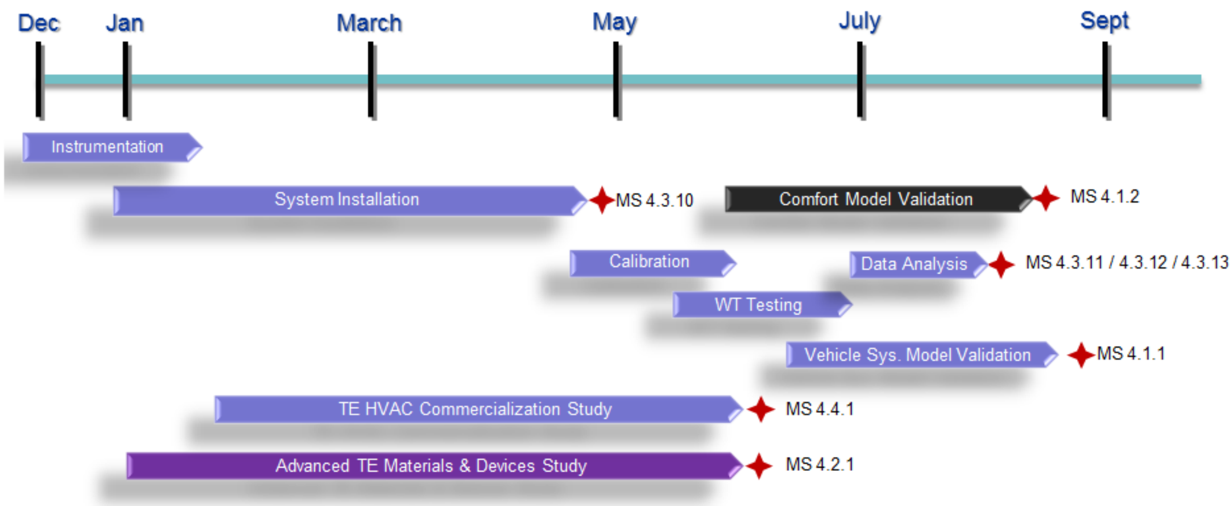

Source: Ford Motor Company

The following technical tasks are being performed in Phase 4 of the project. Several tasks are already completed. Tentative completion dates for the remaining tasks are shown below.

F5.2.1 Completed Tasks

Subtask 4.2.1: Advanced TE materials & device study (Complete)

Subtask 4.3.1: Installation of soft-mounted sensors (Complete)

Subtask 4.3.2: Validate instrumentation and sensors (Complete)

Subtask 4.3.3: Baseline vehicle testing (Complete)

Subtask 4.3.4: Baseline HVAC system removal (Complete)

Subtask 4.3.5: TE HVAC system distributed components added (Complete)

Subtask 4.3.6: Vehicle trim and interior reinstalled (Complete)

Subtask 4.3.7: Verify function of zonal HVAC system (Complete)

Subtask 4.3.8: Operation verified for all system sensor (Complete)

Subtask 4.3.9: Re-installation of soft-mounted sensors (Complete)

Subtask 4.3.10: Final integration of vehicle with TE HVAC system (Complete)

Subtask 4.4.1: Vehicle and system commercialization study (Complete)

F5.2.2 Ongoing Tasks

Subtask 4.1.1: Analysis of zonal TE system benefit to FE/energy use (August 2013)

Subtask 4.3.11: Perform vehicle performance testing (August 2013)

Subtask 4.3.12: Conduct vehicle level TE HVAC system testing (August 2013)

Subtask 4.3.13: In-vehicle jury testing of climate system (August 2013)

Subtask 4.3.14: Post-test vehicle preparation (September 2013)

Subtask 4.3.15: Vehicle demo for U.S. DOE and Energy Commission (Sept / Oct 2013)

F5.3 Zonal HVAC System Installation

As of the writing of this report, much of the initial HVAC system installation has been completed, but finalized system check-out and calibration has not yet been completed. An image of a liquid-to-air thermoelectric device similar to the two being installed in the vehicle for the overhead system is shown in Figure F60. A unit typical of the eight units installed in the vehicle seats is shown in Figure F61.

Figure F60: Liquid-air thermoelectric device for overhead system

Photo Credit: Gentherm Corporation

Figure F61: Liquid-air thermoelectric device and blower for seat system

Photo Credit: Gentherm Corporation

A typical front seat installation is shown in Figure F62 for the seat back. Installation of the TE devices in the rear seat bottom is shown in Figure F63.

Figure F62: Liquid-air thermoelectric device and blower installed in front seat back

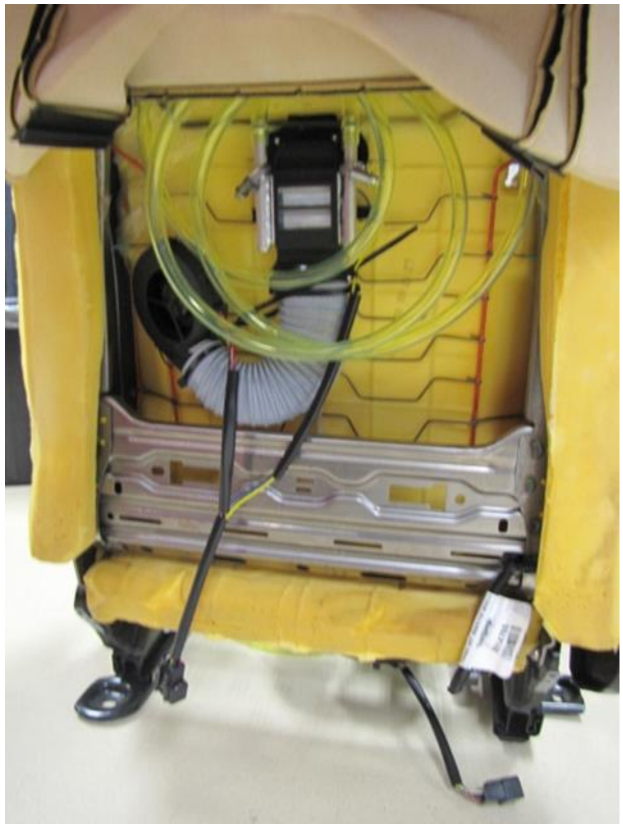

Photo Credit: Gentherm Corporation

Figure F63: Liquid-air thermoelectric devices and blowers installed in rear bench

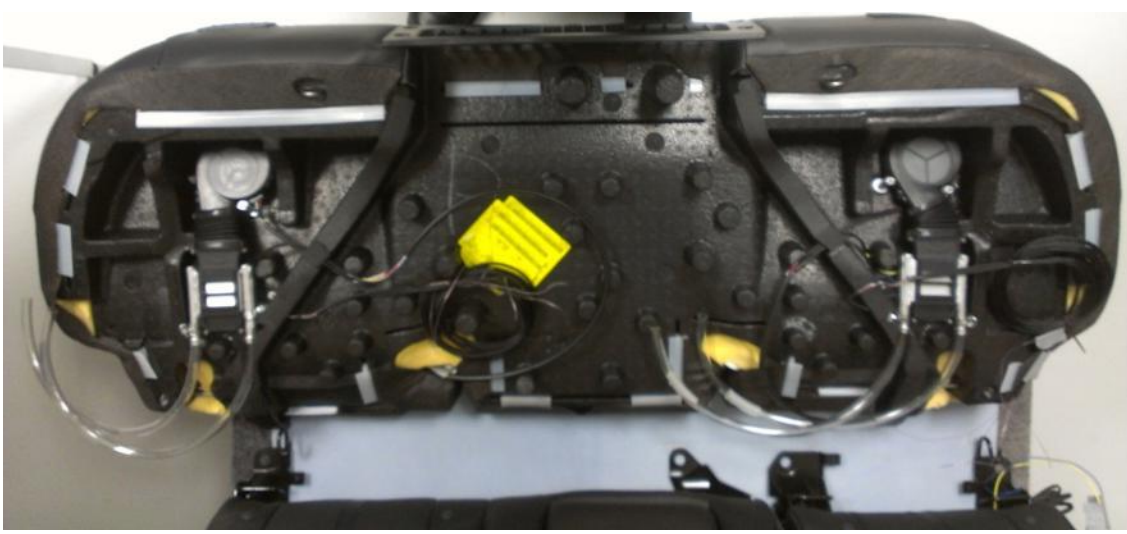

Photo Credit: Gentherm Corporation

Installation of the overhead unit ducting, inlet ducting, and blower fan installation is shown in Figure F64. The front-end heat exchanger installation and lines are shown in Figure F65. Overhead air diffusers are shown in Figure F66. Power supplies, controllers, data acquisition system, ducting, blowers, and overhead thermoelectric devices installed in trunk are shown in Figure F67.

Figure F64: Overhead unit ducting, blower, and TE device cavity installed in trunk

Photo Credit: Halla Visteon Climate Control Corp.

Figure F65: Front-end heat exchanger for TE devices

Photo Credit: Halla Visteon Climate Control Corp.

Figure F66: Overhead zonal air distribution diffusers

Photo Credit: Halla Visteon Climate Control Corp.

Figure F67: Vehicle trunk with data acquisition, power supply, and controls

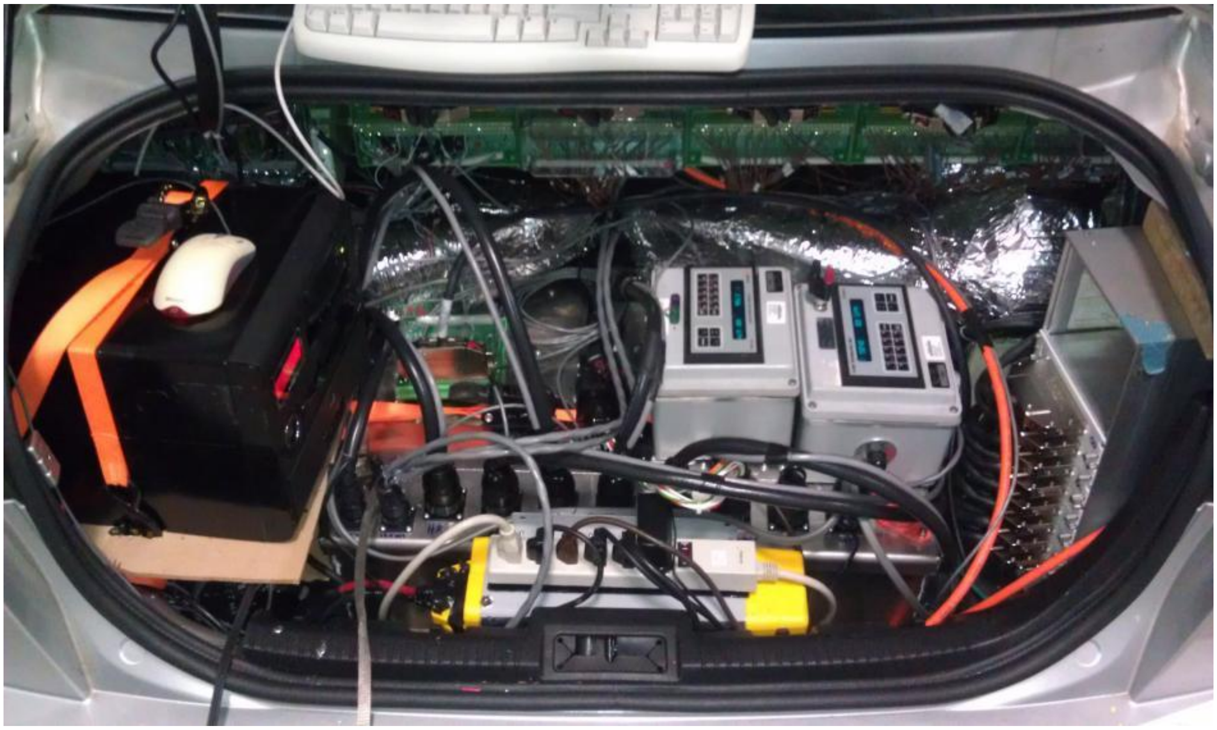

Photo Credit: Halla Visteon Climate Control Corp.

F5.4 Commercialization of Thermoelectric Technology

An assessment of the expanded use of zonal thermoelectric devices and materials was conducted to understand the potential to incorporate these devices into light-duty passenger vehicles. Two types of systems were considered in this analysis: seat-based devices and auxiliary devices embedded behind vehicle trim (e.g., headliner, pillar-trim, console trim, instrument panel, package tray, etc.). The current project explored the use of liquid-to-air thermoelectric devices to improve device performance and efficiency; as well as to reduce package size in the passenger compartment and other space-sensitive areas in the vehicle.

The study indicated that progress in TE device design should continue to evolve from existing air-air seat-based units towards more advanced seat-based system and eventually, could migrate into air-air units installed strategically in vehicles to support zonal climate architectural design. Liquid-air TE systems were found to be significantly further from production readiness due to cost, complexity, and unresolved failure modes. These issues are significant and will need to be overcome before being considered for serial production. The use of climate comfort modeling tools in production engineering development continues to be critical in the understanding of zonal TE system trade-offs.

Efficiency of thermoelectrics were not found to be competitive with large scale bulk conversion systems, including two-phase vapor compression refrigeration systems, on a COP basis. Additionally, TE device efficiency also degraded rapidly as temperature difference (ΔT) across the devices increased. For example, at typical automotive air conditioning system sizing conditions, such as 45°C, the minimum requirement for the airside ΔT was between -30 to -20°C, the difference between inlet and discharge air temperature, in order to achieve passenger comfort. The relatively high ΔT's in this range of working points caused the TE devices to operate with decreased efficiency and prevents them from being used as the primary air conditioning system in the vehicle. In heating modes, typical system sizing conditions were around -20°C, creating a 65-80°C ΔT between the ambient air and discharge air temperature. Driving thermoelectrics to achieve such large heating ΔT caused them to operate at a COP of unity or slightly above, more or less eliminating the TE device efficiency advantage over resistive heating elements. At more mild heating conditions, such as -5 to 5°C, TE devices offered more reasonable efficiency advantages; the economic value of this added efficiency has yet to be determined. Thermoelectrics also tended to have a higher cost per watt of Qc or Qh ($/W) than vapor compression systems or resistive heating technologies.

Higher cost and performance limitations at high ambient temperatures of TE devices currently prevent them from replacing the current vapor compression systems for automotive applications. In highly electrified vehicles, such as plug-in hybrid electric vehicles and battery electrice vehicles, thermoelectrics may provide an energy efficiency advantage in heating modes over resistive heating technologies, but it is questionable if the efficiency gains will be large enough over an annualized cycle to justify the higher cost of a TED. Combining these factors it appears that today's thermoelectrics will be limited to use in supplemental systems. These supplemental systems will need to offer both improved passenger thermal comfort and a reduction in the overall amount of energy being consumed to provide passenger with thermal comfort to be an interesting solution for automotive applications. As a supplemental system, there will likely be extreme pressures on cost to justify implementation, as there will be minimal climate system cost offsets and the vehicle original equipment manufacturers have many technologies to select from when chasing energy savings.

In part, cost and performance of the TEDs was found to be limited by thermoelectric materials available for these applications. Today the only appropriate thermoelectric materials for applications near room temperature are alloys derived from bismuth telluride, Bi_2Te_3. Alloys of bismuth telluride have been undergoing constant development ever since they were developed in the 1950's and 1960's with only marginal performance increases, as reflected in the ZT, which is typically between 0.8 and 1.0 for current materials. The use of tellurium in these materials was found to have a major impact on cost which limits wide scale adoption of TE devices.

To improve economic viability of thermoelectric devices for automotive applications, both the cost structure and power density of the designs need to be improved. Improvements in cost can be achieved through the traditional means of finding lower cost design options that deliver equal performance or by finding design options that may have no cost advantage per unit measure, but improve performance thereby reducing the cost per watt of thermal output ($/W). For reference, the TE devices developed for this project has a cost per watt of thermal output that is 5-10 times higher than the cost per watt of thermal output from a vapor compression AC system. The reason for the wide range in the TE device cost ratio was due to fact that thermal output variability dependence on operating point.

With today's technology, thermoelectric devices will need to be of limited capacity and utilized with highly effective delivery systems, such as the Climate Control Seat, in order to achieve a noticeable improvement in occupant comfort and HVAC system energy efficiency, while meeting automobile manufacturer's cost targets. Current bismuth telluride material systems are a major component of device cost and global tellurium supplies could constrain wide scale adoption of the technology in the future.

To make a zonal HVAC system economically viable, there must be significant effort to reduce the cost of the TE devices. In addition, the number and size of the TE devices in any climate system need to be minimized to meet the anticipated cost targets from automotive manufacturers. This cost limit on the total system capacity may require new and novel delivery systems to be developed to insure that the limited device capacity is delivered effectively to the occupant. The manufacturing techniques developed and utilized in this program demonstrated that contemporary mass production methods can be utilized for the fabrication of advanced TE devices. These methods require further development to scale-up to automotive production volumes, but the use of automation to increase throughput and reduce assembly cost are viable approaches to accomplish this. The most significant cost and performance hurdle continues to be the BiTe elements, of which there are currently no readily available replacement opportunities.

F5.5 Success Criteria Assessment for Phase 4

The following success criteria are to be assessed at the end of Phase 4 of the project. These criteria will be reported in the Final Technical Report to the U.S. Department of Energy after the project is completed. The success criteria were established as a method to assess performance of the system against the six U.S. DOE program objectives:

- *Develop a TE HVAC system to optimize occupant comfort and reduce fuel consumption*
- *Reduce energy required to operate the AC compressor by 1/3*
- *Demonstrate TE devices that achieve $COP_{cooling} > 1.3$ and $COP_{heating} > 2.3$*
- *Demonstrate the technical feasibility of a TE HVAC system for light-duty vehicles*
- *Develop a commercialization pathway for a TE HVAC system*
- *Integrate, test, and deliver a 5-passenger TE HVAC demonstration vehicle*

Criterion #1: Measured thermoelectric HVAC device efficiency meets program objectives

Status: The thermoelectric HVAC device efficiency targets required a minimum COP of 1.3 in cooling mode and 2.3 in heating mode. The target COP were achieved during calorimetric testing of the thermoelectric modules in Phase 3, with a temperature drop of 13.6°C measured in cooling mode and a temperature rise of 18°C measured in heating mode.

Criterion #2: Cost study and commercialization analysis show thermoelectric system commercialization potential

Status: Trade studies were used to assess the component and investment cost impact of implementing zonal thermoelectric HVAC systems in a vehicle, and also established steps required for commercialization of the technology. Results obtained in Phase 3 showed significant on-cost to incorporate a full zonal thermoelectric system. The commercialization assessment completed in Phase 4 suggested that thermoelectric heated/cooled seats and zonal climate system remain viable technologies to pursue in commercial application, but there continues to be significant issues around device performance capabilities and thermoelectric material costs.

Criterion #3: Thermoelectric HVAC system meets comfort targets specified performance criteria

Status: The thermal comfort criteria were to achieve equivalent thermal comfort compared to the results obtained in a baseline vehicle. Baseline testing was completed in Phase 1. Assessment of this criterion has not yet been completed, but is on-track. Preliminary thermal chamber and modeling studies indicated that achieving equivalent comfort, as constrained by the energy-based metrics, is feasible.

Criterion #4: Thermoelectric HVAC system reduces energy consumption compared with baseline vehicle

Status: Vehicle energy usage test methods were established to assess the energy consumption from the zonal thermoelectric HVAC system, as well as for determining the energy consumption reduction of the air conditioning compressor. Baseline energy consumption analysis was completed in Phase 1. Assessment of this criterion has not yet been completed. Energy modeling studies and thermal chamber testing in Phase 2 indicated that energy reduction was possible.

CHAPTER F6: Ford Conclusions

The ability to produce and market the thermoelectric devices developed in this program was assessed by a detailed business analysis, and resulted in recommendations regarding the next-steps required for thermoelectric HVAC devices to come to market. Key hardware and controls attribute requirements were identified to determine how they contribute to the commercialization potential of the technology. Final results and conclusions from this project have not been completed and will be included as a part of the final report to the U.S. Department of Energy, which will be submitted as a supplement to this report. Specific areas that will be assessed in the conclusion section of the report are:

- Assessment of the U.S. DOE Success Criteria
- Lessons-learned in this project
- Possible next-steps for TE HVAC and zonal climate system research
- Potential next-steps for TE HVAC and zonal climate system commercial applications

FORD GLOSSARY

Acronym	Definition
AC	Air Conditioning
ACES	Air Chamber Evaluation System
BJB	Battery Junction Box
CAD	Computer Aided Design
CAE	Computer Aided Engineering
CAN	Controller Area Network
CCM	Climate Control Module
CCS	Climate Controlled Seat
CFD	Computational Fluid Dynamics
CFM	Cubic Feet per Minute
COP	Coefficient of Performance
DATC	Dual Automatic Temperature Controller
U.S. DOE	United States Department of Energy
ED&T	Engineering Development & Tooling
EG	Ethylene Glycol
FOA	Funding Opportunity Announcement
HEX	Heat Exchanger
HV	High Voltage
HVAC	Heating, Ventilation, and Air Conditioning
I/O	Input-Output
IRD	Internal
LT	Low-Temperature
NVH	Noise, Vibration, Harshness
Q_C	Thermal Cooling (Watts)
Q_H	Thermal Heating (Watts)
SJB	Smart Junction Box
SLI	Starting, Lighting, Ignition
TE	Thermoelectric
TED	Thermoelectric Device
TXV	Thermostatic Expansion Valve
ZT	Thermoelectric Figure-of-Merit
ΔT	Temperature difference

CHAPTER G1: GM Introduction

G1.1 Project Overview

On November 3, 2009, General Motors (GM) accepted U.S. Department of Energy (U.S. DOE) Cooperative Agreement award number DE-EE0000014 from the National Energy Technology Laboratory. GM was selected to execute a three-year cost shared research and development project on Solid State Energy Conversion for Vehicular Heating, Ventilation & Air Conditioning (HVAC) and for Waste Heat Recovery. This area of interest from Funding Opportunity Announcement DE-PS26-08NT01045 supports the Office of Energy Efficiency and Renewable Energy's Vehicle Technologies Program. In addition to funding from U.S. DOE, this project is supported by funding from the California Energy Commission (Energy Commission).

In the summer of 2010, the GM team proposed a substantial revision to the Statement of Project Objectives to perform additional activities that would specifically benefit electrified vehicles such as the Chevrolet Volt. U.S. DOE approved a corresponding increase in government funding for the proposed change in project scope, which included the delivery of a Volt demonstration vehicle initially planned for July 31, 2013. Subsequent delays in the project have resulted in a no-cost time extension for the project with the mainstream Buick LaCrosse demonstration vehicle scheduled to be available by September 30, 2013, and the Chevrolet Volt demonstration vehicle scheduled to be available by March 31, 2014.

G1.2 Project Objectives

The primary objective of this project was to develop a distributed automotive HVAC system that provides thermal comfort equivalent to current state-of-the-art centralized systems while using significantly less energy. To satisfy this objective, the team identified the following goals:

- Reduce by at least 30% of the “billions of gallons” the fuel used in cooling mode to maintain occupant comfort through the localized use of TE technology while maintaining occupant comfort and safety
- Develop TE HVAC components with a coefficient of performance (COP) greater than 1.3 for cooling and greater than 2.3 for heating, then integrate and test these components as part of a reliable distributed HVAC system in a conventional vehicle (an eAssist Buick LaCrosse) and an extended range electric vehicle (a Chevrolet Volt)
- Update the University of California at Berkeley (UCB) Thermal Comfort model to predict the response of vehicle occupants to localized heating and cooling based on human subject testing, and develop associated computer-aided engineering (CAE) tools to support the integration of distributed HVAC components into future vehicle designs

A secondary objective of the project was to improve the efficiency of thermoelectric generators for converting engine waste heat into electricity.

G1.3 Methodology

GM's approach reduced the energy consumption of the vehicle's central HVAC system (producing a warmer than desired passenger cabin temperature for a cooling situation) while maintaining occupant comfort by using distributed HVAC components to delivering local spot cooling to each occupant. While cooling individual occupant(s) instead of the entire passenger cabin is a basic method for producing energy savings, GM's approach was further optimized by applying scientific knowledge of human physiology and psychology regarding thermal comfort that recognizes local cooling of some key body segments significantly affects perceived comfort. The team's premise was that the energy consumption of the distributed HVAC system would still result in substantial net energy savings and corresponding reductions in fuel usage for air conditioning, while providing the vehicle occupants with equivalent thermal comfort.

The project team used human subject testing to develop a math-based thermal comfort model that characterized the sensation and comfort responses to the localized cooling and heating of body segments in a vehicle environment. The model identified optimal locations and operating parameters for energy-efficient distributed HVAC components that would deliver local spot cooling and heating. Based on an analysis that comprehended vehicle constraints, the team selected an optimal combination of locations for distributed HVAC components.

The project team developed an initial set of prototype HVAC components that featured thermoelectric modules for energy-efficient distributed cooling and heating. These functional components and the associated control strategies were integrated into a mule vehicle for testing and evaluation.

Based on the performance analysis of the initial prototype components, the project team developed a final set of prototype HVAC components to further optimize performance while considering production-intent requirements such as noise and packaging. These final prototype distributed cooling and heating components and their associated control strategies will be integrated into demonstration vehicles for final testing and evaluation.

The activities to achieve the primary objective were performed in four standard research and development phases shown in the project timeline below. The activities to achieve the secondary objective for improving engine waste heat recovery were performed in a fifth phase of the project that was concurrent with these first four phases.

G1.4 Project Timeline and Milestones

The timeline of project phases, tasks, and milestones is shown in Figure G1. The detailed timing of the project milestones is documented in Table G1.

Figure G1: Project Phases, Tasks, and Milestones Timeline Chart

Budget Period 1 | BP 2 | Budget Period 3

Nov-09, Dec-09, Jan-10, Feb-10, Mar-10, Apr-10, May-10, Jun-10, Jul-10, Aug-10, Sep-10, Oct-10, Nov-10, Dec-10, Jan-11, Feb-11, Mar-11, Apr-11, May-11, Jun-11, Jul-11, Aug-11, Sep-11, Oct-11, Nov-11, Dec-11, Jan-12, Feb-12, Mar-12, Apr-12, May-12, Jun-12, Jul-12, Aug-12, Sep-12, Oct-12, Nov-12, Dec-12, Jan-13, Feb-13, Mar-13, Apr-13, May-13, Jun-13, Jul-13, Aug-13, Sep-13, Oct-13, Nov-13, Dec-13, Jan-14, Feb-14, Mar-14

Task #	Phase, Task, and Milestone Descriptions	months	
MAINSTREAM	(Cadillac SRX mule vehicle and Buick LaCrosse demo vehicle)	53	MAINSTREAM DEMO VEHICLE DEVELOPMENT
Phase 1	**Applied Research**	53	PHASE 1
1	Project Management and Planning	18	ALL
2	Expand UCB Comfort Model	53	UCB / GM / Delphi * * *
3	Perform Human Subject Testing	18	UCB / GM / Delphi
Milestone	Identify initial set of locations for distributed heating/cooling	1	*
4	Define Design of Experiments (DoE) for Target Platform	6	Delphi / GM
5	Define & Build Mule Vehicle for Thermal Comfort Evaluation	5	Delphi / GM
6	Perform Design of Experiments (DoE) for Target Platform	8	UCB / Delphi
Milestone	Identify final set of locations for distributed heating/cooling	1	*
Phase 2	**Exploratory Development**	19	PHASE 2
7	Project Management and Planning	17	ALL
8	Define New Comfort Component Specifications	5	Delphi / GM
9	Define Control Strategies and Algorithms	11	Delphi / GM
Milestone	Specify interface between GM & Delphi controllers	1	*
10	Build and Demonstrate Function-Intent Components	15	Delphi / Faurecia
11	Define Metrics for Efficiency and Comfort	11	GM / Delphi
12	Integrate Initial Components into Mule Vehicle	11	Delphi
13	Evaluate Initial Comfort Components	11	UCB / GM / Delphi
Milestone	Estimate Coefficient of Performance for Thermoelectric Devices	1	*
Phase 3	**Advanced Development**	9	PHASE 3
14	Project Management and Planning	6	ALL
15	Commercialize Design of New Comfort Components	3	Delphi
16	Produce Packaging- and Function-Intent Final Components	5	Delphi / Faurecia
17	Test and Evaluate Final Comfort Components	2	GM / Delphi
18	Estimate Efficiency Improvements	2	GM / Delphi
Phase 4	**Engineering Development**	9	PHASE 4
19	Project Management and Planning	6	ALL
20	Integrate Final Components into Demonstration Vehicle	7	GM / Delphi
21	Test and Evaluate Distributed HVAC System in Vehicle	6	GM / Delphi
22	Calculate Efficiency Improvements of Distributed HVAC System	4	GM / Delphi
Milestone	Provide mainstream demonstration vehicle to DOE	1	*
VOLT	(Chevrolet Volt demonstration vehicle lags LaCrosse by 6 months)	34	CHEVY VOLT DEMO VEHICLE DEVELOPMEN
Phase 2	**Exploratory Development**	28	PHASE 2
10	Marlow development of prototype replacement for PTC heater	28	Marlow / GM
Phase 3	**Advanced Development**	14	PHASE 3
15	Commercialize Design of New Comfort Components	12	GM
16	Produce Final Components	13	GM / Marlow / Delphi
17	Test and Evaluate Final Comfort Components	10	GM
Phase 4	**Engineering Development**	12	PHASE 4
19	Project Management and Planning	12	ALL
20	Integrate Final Components into Demonstration Vehicle	7	GM / Delphi
21	Test and Evaluate Distributed HVAC System in Vehicle	6	GM
22	Calculate Efficiency Improvements of Distributed HVAC System	4	GM
Milestone	Provide Chevrolet Volt demonstration vehicle to DOE	1	*
Phase 5	**Thermoelectric Generator Development**	49	PHASE 5
23	Develop Thermoelectric Materials / Modules for Waste Heat Recovery	49	GM / UNLV / Marlow / ORNL

Table G1: Project Milestone Timing

Completion Date	Phase	Milestone	Key Project Milestone Description
31-Mar-2010	1	1	Identify initial set of locations for distributed heating/cooling
28-May-2010	1	2	Definition of Design of Experiments (DoE) for Target Platform Completed
31-Aug-2010	1	3	Build Mule Vehicle for Thermal Comfort Evaluation Completed
26-Apr-2011	1	4	UCB Comfort Model initial update released
29-Apr-2011	1	5	Identify final set of locations for distributed heating/cooling
19-Dec-2011	2	6	Specify interface between GM & Delphi controllers completed
27-Nov-2012	2	7	Evaluate Initial Comfort Components Completed
27-Nov-2012	2	8	Estimate Final Coefficient of Performance for Thermoelectric Devices
16-Jan-2013	1	9	UCB Comfort Model second update released
30-Jun-2013	3	10	Evaluate Final Comfort Components Completed
31-Mar-2014	1	11	UCB Comfort Model third update released
30-Sep-2013	4	12	Make mainstream demonstration vehicle (Buick LaCrosse) available to DOE
30-Sep-2013	4	13	Calculate Efficiency Improvements of Distributed HVAC System Completed
31-Mar-2014	4	14	Make Chevrolet Volt demonstration vehicle available to DOE

CHAPTER G2:
GM Phase 1 – Applied Research

The focus of this phase was to develop a Thermal Comfort model of human responses to potential locations for distributed heating and cooling and to identify optimal locations. For this phase of the project, GM worked with Delphi Thermal Systems and UCB. UCB developed a vehicle mock-up in the Environmental Test Chamber for the first set of human subject testing. Delphi modified a Cadillac SRX for the second set of human subject testing that was performed in their climatic wind tunnel. Both test setups used highly configurable systems for delivering distributed spot cooling and heating.

G2.1 Task 1 – Project Management and Planning

The planning and coordination of the overall project began with the project kickoff meeting with the U.S. DOE program managers followed by the internal kickoff and initial working meeting of the project team. For this 18-month phase that was fully half of the original project timeline, the execution of the project closely followed the project plan and it was completed on schedule.

G2.2 Task 2 – Expand UCB Comfort Model

For Task 2, Expand UCB Comfort Model, the main activity was to enhance the existing UCB Thermal Comfort Model to consider the affect from the spot heating and cooling of 16 body segments on a person's overall thermal sensation and thermal comfort (see scale in Figure G24). In addition, other key parameters of the model were examined. For example, the model's existing assumptions about the impact of age and gender on perceived comfort were revisited. Another key activity was to implement CAE tools based on the enhanced version of the Thermal Comfort Model.

G2.2.1 Enhance the existing Thermal Comfort Model

G2.2.1.1 Age and gender thermal sensation analysis:

The goal of the study was to analyze the differences among different age and gender. The results allowed the team to determine whether significant differences exist and whether the composition of the test group should be adjusted for age or gender. The differences found by this analysis are fundamentally due to:

- Thermal receptors of elderly people are less sensitive, so they might be less sensitive to thermal environments.
- Blood circulation might be less effective in elderly than in young people, so they might be more sensitive to cool environments.
- The metabolic level for elderly might be lower than young people; therefore, elderly may feel cooler than young in the same environments.

- The body fat might be higher in elderly than in young people in general; that will result in higher insulation levels and higher metabolic levels if they are working (heavy weight people need carry more body mass). This would results in greater sensitivity to warm environments in elderly.
- Elderly people normally dress well corresponding to seasons and ambient air temperatures, therefore, their thermal sensations are less influenced by the environment

Due to these somewhat conflicting differences, we were uncertain whether the elderly are more or less sensitive to the environment than young people. If a difference exists, we were also uncertain whether the difference was sufficiently significant to affect our test plans. Therefore, a detailed analysis was conducted, and the proprietary results were appropriately incorporated into the team's plans for the project.

G2.2.1.2 Improvements in physiology modeling

Not many studies exist about sweat distribution coefficients because the measurements to obtain these values are difficult to conduct. Our previous sweat distribution coefficients in the physiology model were inherited from the Stolwijk's model in 1970s. Much of the information from Stolwijk's model was from an earlier study by Kuno in 1956.

These previous coefficients assigned large values to the trunk of the body, i.e., the chest, back, and pelvis (as shown by the values marked green in Figure G). This weighting resulted in flat skin temperature predictions for these body parts in warm environments due to the severe sweating predicted by the distribution coefficients (see left portion on Figure G).

Figure G2: Skin temperature predictions with old and new sweat distributions (resting nude body)

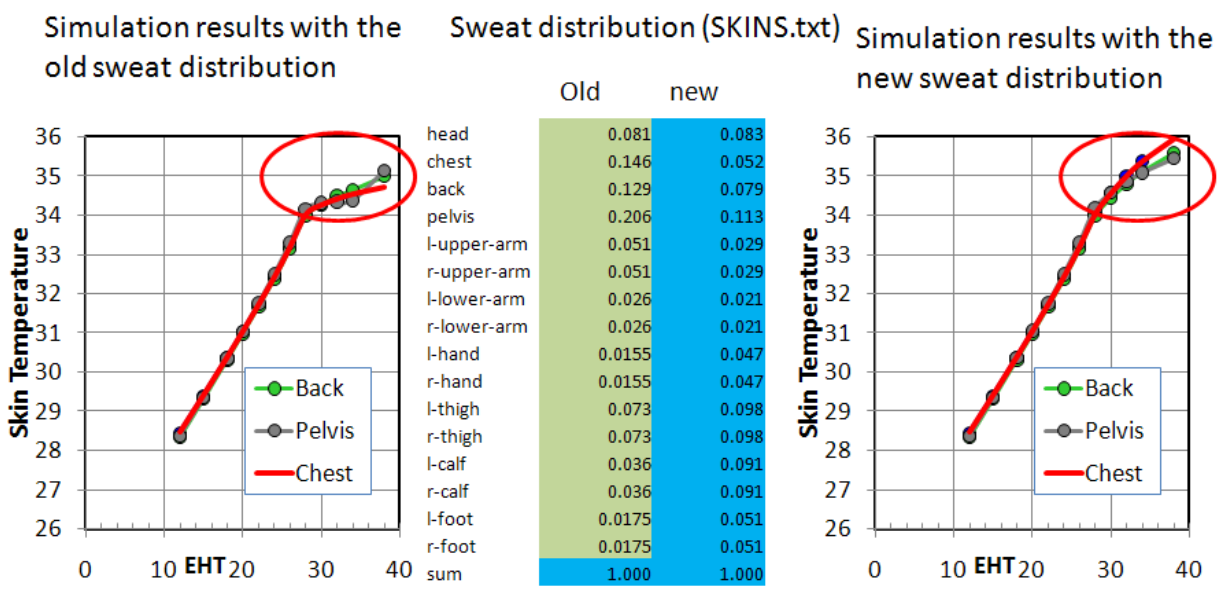

	Old	new
head	0.081	0.083
chest	0.146	0.052
back	0.129	0.079
pelvis	0.206	0.113
l-upper-arm	0.051	0.029
r-upper-arm	0.051	0.029
l-lower-arm	0.026	0.021
r-lower-arm	0.026	0.021
l-hand	0.0155	0.047
r-hand	0.0155	0.047
l-thigh	0.073	0.098
r-thigh	0.073	0.098
l-calf	0.036	0.091
r-calf	0.036	0.091
l-foot	0.0175	0.051
r-foot	0.0175	0.051
sum	1.000	1.000

Park and Tamura (1992) measured the local skin temperature distributions for resting nude people under various ambient conditions from 25 – 28ºC. The sweat distributions under ambient air temperature between 34ºC and 38ºC are similar, but they are different from the distributions at the lower ambient air temperatures. Because warm environments generally are the cause of sweat, we decided to use the distributions under warm conditions. The values in Figure G (the column marked blue) are the calculated distributions based on the measured data under a 34ºC environmental condition. The distributions for the trunk regions (chest, back, and pelvis) are much smaller than the old values, but they are much larger for the hands and feet.

The skin temperatures for the chest, back, and pelvis with the new sweat distributions from Park and Tamura are shown in the right portion of Figure G. Indeed, the flat shape of the skin temperatures in warm environments as shown for the old distribution coefficients is gone; instead, the skin temperatures for these body parts increased significantly when the ambient air temperature increased from 30ºC to 38ºC.

The skin temperatures with both the old and new sweat distributions under air temperatures below 26ºC are very similar (comparing the left and right portions of Figure G), because the sweat distributions only affect skin temperatures under warm environments when the skin actually sweats.

We compared the simulated skin temperatures using the old and the new sweat distributions with measured data. Werner (1980) measured nude subjects' skin temperatures under supine resting conditions for air temperatures between 10 – 50ºC. The skin temperature sensors were exposed to the ambient air without a layer of tape.

The comparisons were made for key body segments, including the chest, pelvis, hands, and feet, and some example results are shown for the chest in Figure G3 and for the hands in Figure G4. The solid lines are the simulated skin temperatures with both the new and the old sweat distributions, and the red dots represent the measured skin temperatures by Werner.

Figure G3: Comparison of measured and predicted skin temperatures for chest

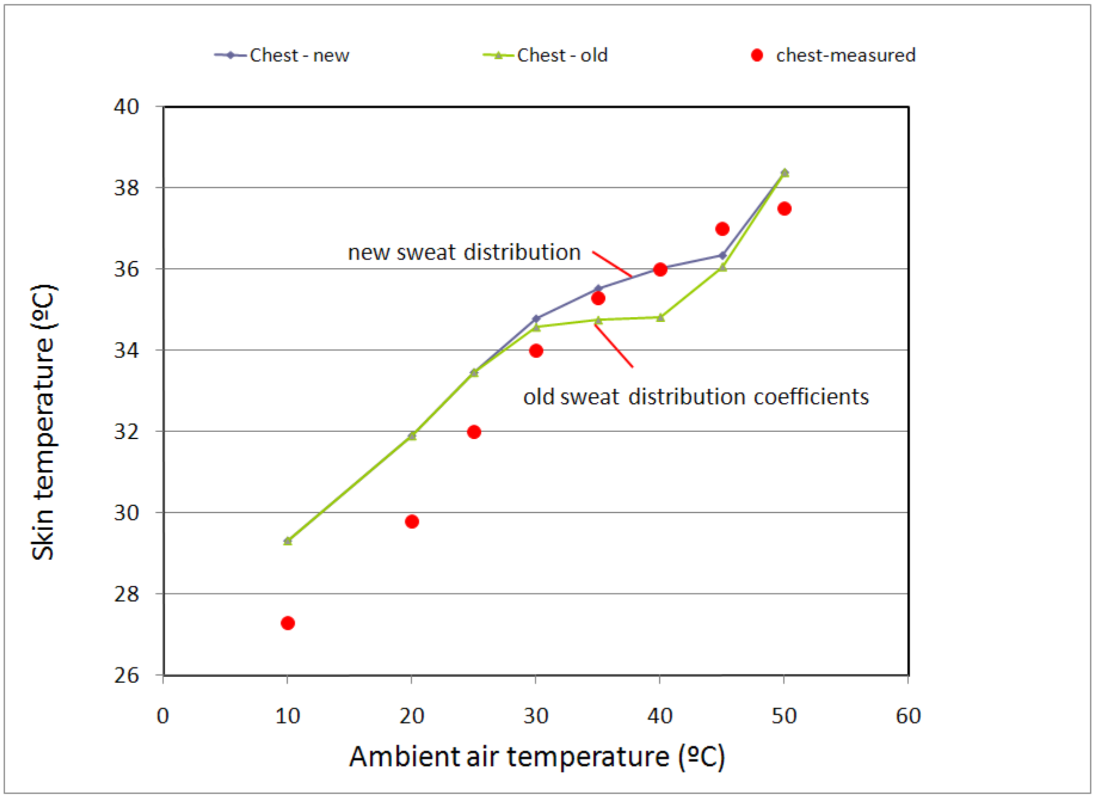

Figure G4: Comparison of measured and predicted skin temperatures for hands

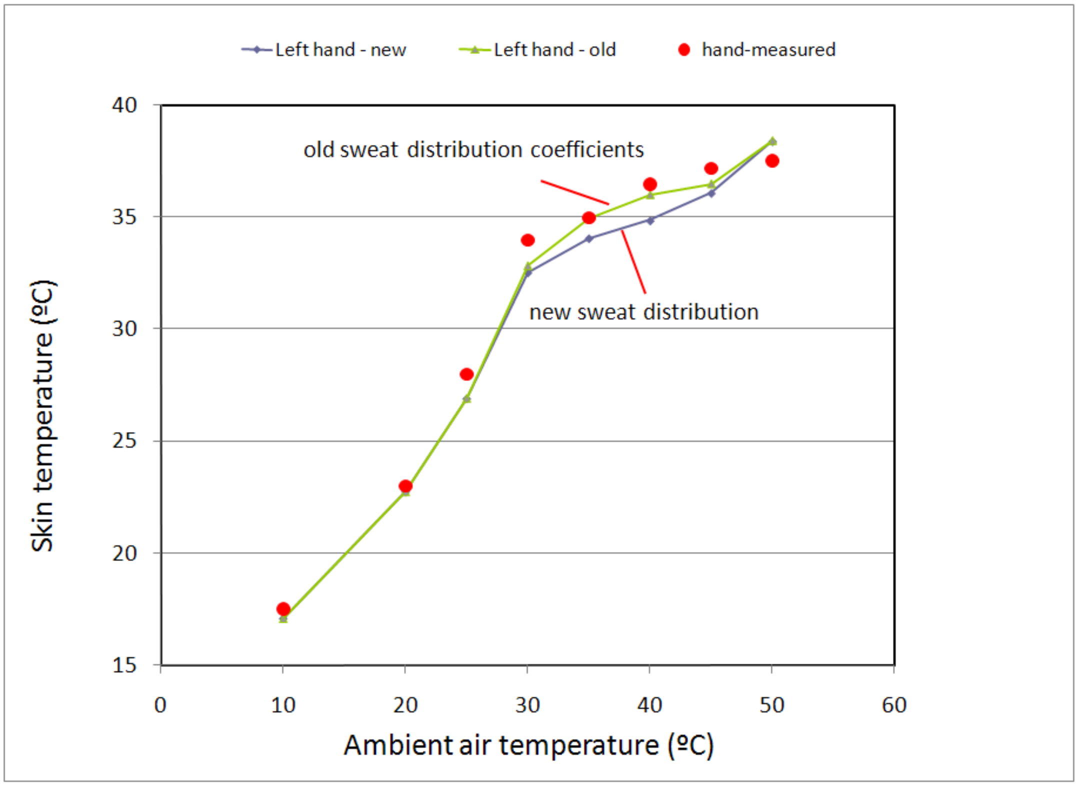

With the new sweat distributions, the simulated skin temperatures under warm conditions (between 30 – 50ºC) for the chest and pelvis are much higher than the simulated results with the old sweat distributions, and they are much closer to the measured data. As expected, under air temperatures between 30 and 50ºC, the simulated skin temperatures for hands and feet are lower with the new sweat distributions than with the old distributions. For feet, the simulated skin temperatures are closer with the new distributions than with the old distributions. For hands, however, the simulated skin temperatures with the old distributions are much closer to the measured data.

In cool environments (10 – 26ºC), the simulated skin temperatures for the chest and pelvis are significantly higher than the measured skin temperatures. This difference didn't occur for the hands and feet, which matched very well between the simulated and the measured skin temperatures. In Werner's tests, they used skin temperature sensors that were exposed to the ambient air without a layer of tape. The sensors in fact partially measured the ambient air temperature, which would cause errors. For the chest and pelvis, when the differences between the skin and the ambient air temperature were large, the influences of the ambient air were larger; therefore, the measured skin temperatures were lower than the actual skin temperatures.

Whether the sweat distributions from Park and Tamura measured under resting conditions represent the distribution during exercise needs to be further analyzed. Cotter et al. (1995) and Smith and Havenith (2010) measured sweat distributions under different levels of exercise and different environmental conditions. Our next step is to compare the sweat distributions from Park and Tamura with the results from Cotter and Smith.

G2.2.1.3 Clothing insulation testing and model updates

UCB completed clothing insulation testing for about 50 typical clothing ensembles using the thermal manikin (see Figure G). Clothing provides insulation for the 16 body segments considered by the UCB Thermal Comfort model, as well as an insulation factor for the whole body. The objective data from the manikin was used for the UCB advanced Thermal Comfort model, which can evaluate the impact of insulation values for each body part. The UCB team developed a paper on this topic that has been accepted by Clima 2013. The next step for the program is to revise the Thermal Comfort model, so it will be linked to the new clothing database when calculating comfort.

Figure G5: Measuring insulation levels for 16 body parts in typical clothing ensembles

In 2010 comfort models for body-segment-specific sensation and comfort were put forward in a three-part series in the Building and Environments journal. The models predict the subjective responses to the environment from thermo-physiological measurements or predictions of skin and core temperatures, and they apply to a range of environments, including uniform and non-uniform or transient and stable. The models are based on unique experimental data, and they are formulated in a rational (i.e., piecewise) structure that simplifies further validation and refinement. These models received significant critical attention, and this led to the identification of two issues that need improvement at the fundamental level:

- In the local sensation model, the neutral set-points for segment skin temperatures are sensitive to metabolic rate and to the distribution of clothing insulation provided by different clothing ensembles. A calculation sequence that automatically creates segment set-points for specific clothing and activity levels has been developed and programmed into the comfort model.
- In the overall sensation model, the piecewise model construction produced unrealistic jumps in output at the transitions. A smoothing technique using the model's key organizational variables was developed and incorporated into the original equations.

To resolve these issues, the team developed mathematical solutions in order to smooth the piece-wise model. A LabView program was subsequently developed to validate the smoothing functions. A paper has been drafted to describe these smoothing functions. The UCB team plans to submit the paper to the Building and Environments journal. The next step is to incorporate the smoothing functions into the existing UCB advanced comfort model.

G2.2.2 Human thermal comfort (HTC) analytical procedure

These research activities focus primarily on validating the newly developed numerical procedures for thermal comfort prediction. Continuing on from the earlier development, UCB test conditions were put into the GM-developed CFD procedure for simulation; the thermal comfort and sensation were calculated and compared to the human test subject data gathered by UCB. During the study, all airflows and temperatures were obtained for various combinations of localized spot cooling configurations. A few selected transient simulations were also conducted.

G2.2.2.1 Passenger Compartment Model

The proposed HTC analytical procedure begins with identifying and modeling all the interior surfaces that comprise the passenger compartment, including seats and appropriately segmented manikins, in the CAD system. In this study, we created both the Fluent and the Radtherm models of a Cadillac SRX passenger compartment as shown in figure 3.1. The model has all the key design parameters for thermal comfort modeling, such as the ari conditioning (AC) outlet location and size, windshield angle, body vent locations, and many other parameters that influence the performance of the HVAC system. Figure G5 shows the corresponding CFD model in Fluent with a manikin representing a 50-percentile male in the driver's seat. ANSA modeling software was used to mesh the SRX passenger compartment. In this report, only the driver-side manikin, segmented into 21 body parts, was modeled. A separate 2-D surface mesh model of the identical passenger cabin for analysis in Radtherm is also shown in Figure G5.

G2.2.2.2 Passenger Compartment CFD Air Flow Analysis in Fluent

Prior to predicting human thermal comfort and sensation levels using UCB's HTC model, it is first required to compute both the core and the skin temperatures of all body segments. These are computed in Radtherm through the solution of energy balance equations at the surface of these body segments. However, since Radtherm relies on a CFD solution for convective boundary conditions, Fluent was used in this study to provide this information. Around 3,000,000 tetrahedral elements were required to capture the geometric and the flow details of the passenger compartment with Fluent. A converged steady-state flow solution in Fluent was used to provide the convective heat transfer coefficients and film temperatures on the entire model to Radtherm. However, velocities close to the surface calculated in Fluent were used to compute the heat transfer coefficients for the manikin based on an empirical formulation available in Radtherm. The entire data transfer process between Fluent and Radtherm has been fully automated.

G2.2.2.3 Passenger Compartment Thermal Analysis in Radtherm

As mentioned in the above sub-section, the convection heat transfer coefficient and the film temperature distribution on the entire passenger compartment (including the manikin) was imported from Fluent and mapped onto the much coarser Radtherm surface mesh model.

However, the empirical formula relating velocity to heat transfer coefficients on the manikin was chosen instead of the Fluent convective coefficients. This was done primarily because of the limitation of the wall-function based formulation to provide accurate convective coefficients on the relatively low-velocity regions of the manikin. One can observe a checkerboard pattern of the heat transfer coefficient distribution on the manikin when plotted in Fluent. In this study, the standard procedure recommended by Radtherm for HTC was followed.

G2.2.2.4 Prediction of occupant skin and core temperatures

The human physiology model in Radtherm can simulate an arbitrary number of body segments. Each of these segments consists of four body layers (core, muscle, fat, and skin tissues) and a clothing layer. A blood pool node and a series of conductors provide for convective heat transfer between arterial blood and the tissue nodes as well as for the countercurrent heat exchange between the arteries and the veins. The human body thermal regulation is mainly achieved by regulating the blood flow, so a realistic blood flow model is important for any dynamic model of human thermal comfort. A vehicle occupant's body uses vasoconstriction and vasodilatation to regulate blood distribution in order to control the skin temperature through an increase or decrease of heat loss to the environment. Veins and arteries are paired, even down to very small vessels, and veins carry heat from the arteries back to the core. The model is able to predict both core and extremity skin temperatures with reasonable accuracy under a broad range of environmental conditions.

The current model includes clothing nodes to model the heat capacitance and resistance to the flow of both heat and moisture due to the clothing. The heat capacity of clothing is important when considering transient effects. Moisture resistance is important to correctly model the evaporative heat loss from the body through clothing. The human physiology varies significantly among individuals, and these differences can affect the perceptions of thermal comfort, e.g., a higher metabolic rate or increased body fat can cause people to feel warmer. The present model has a standard 50-percentile human physiology model with a metabolic rate of 2 MET (1 MET = 1 kcal/kg/hr). Clothing levels vary based on the body segment; we assumed a short sleeve shirt, trousers, socks, shoes, etc. for summer clothing during cool-down simulations.

In almost any environment, the body is in contact with solid surfaces which results in body heat gains or losses via heat conduction. In the vehicle passenger compartment, the seat contacts a considerable portion of the occupant's body; this must be considered to accurately model the thermal impact to the occupant. The current model includes a contact surface for each body segment. The thermal properties of the contact surface are used to simulate its surface temperature. Each body segment model includes the fractions of exposed skin and clothed skin that are in contact with vehicle surfaces.

G2.2.2.5 Prediction of thermal sensation and thermal comfort from the skin and core temperatures

The human sense of thermal comfort is very complex; it involves both the physiological and the psychological states of a person under specific conditions. In uniform environments, sensation and comfort correlate well: a neutral sensation corresponds to the best comfort; warmer or cooler sensations correspond to reduced comfort. In non-uniform or transient environments, however, the relationship between sensation and comfort becomes more complex. For example, the same cool face sensation could be perceived as very pleasant if the whole body is warm or uncomfortable if the whole body is cold.

Over the past few years, UCB has worked on studies of local body part thermal comfort. UCB has carried out human subject tests, developed comfort predictive models, and gained valuable knowledge regarding human responses to local cooling and heating. The human subject test results and local comfort predictive models developed from those tests provide unique information for understanding and predicting human responses to their thermal environment. In both uniform and non-uniform environments, different parts of the body feel warmth and coolness to varying levels. The differences obviously depend on many factors, such as how the body's thermoregulatory physiology responds to the body's overall thermal state, the asymmetric effect of clothing insulation and environmental conditions around the body, the rate of change in the body's skin and core temperatures, and the thermal sensitivity of the different body parts involved.

UCB proposed to develop a local sensation model of the form shown in Eq. (1). The local sensation model is a function of local skin temperature, mean skin (or core) temperature, and their rates of change. The local and mean skin temperatures represent the body's response to stable conditions; the derivatives of these skin and core temperatures represent the response to transients. The local skin temperature represents the local skin thermal conditions. Mean skin temperature represents the whole body thermal status in the static part of the model. There will be a distinct model for each body part, so that together they capture the asymmetrical features of their environments. Based on the overall whole body sensation, the local body sensations, and the comfort votes from the human subject tests, UCB performed regression analyses to arrive at the overall sensation and comfort models that are shown in Figure G6.

$$Local\ Sensation = f(T_{skin,i}, \frac{dT_{skin,i}}{dt}, \overline{T}_{skin}, \frac{dT_{core}}{dt}) \quad \text{Eq. (1)}$$

where:

$T_{skin,i}$ = local skin temperature of one body part
t = time
$\overline{T}_{skin}$ = the mean skin temperature
$dT_{skin,I}/dt$ = the derivative of local skin temperature
dT_{core}/dt = the derivative of the core temperature

The term i in the model ranges from 1 to 19, corresponding to the body parts: head, face, neck, breathing zone, chest, back, pelvis, left and right upper arms, left and right lower arms, left and right hands, left and right thighs, left and right lower legs, plus left and right feet.

Figure G6: Flow chart to show models developed and their relationships

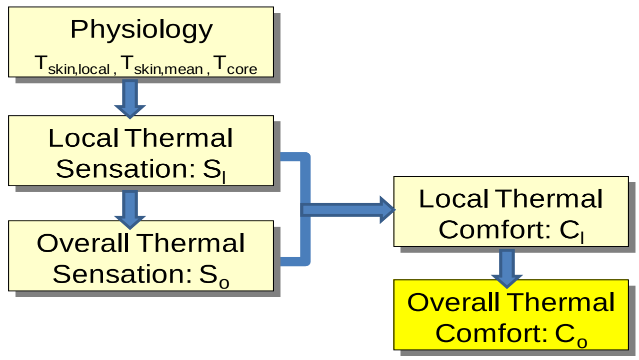

G2.2.3 Milestone 4 – UCB Comfort Model initial update released

The project's fourth major milestone, "UCB Comfort Model initial update released", was successfully completed slightly behind schedule on April 26, 2011. The project team decided to allow this delay in order to significantly increase the scope of the model update. By incorporating a PC version of the model into this first update, the resulting delay of this milestone actually had a positive effect on the overall execution of the project.

G2.2.4 Implement the enhanced Thermal Comfort Model in a CAE tool

A CAE tool called the Virtual Thermal Comfort Engineering (VTCE) tool was implemented into commercial code called Radtherm from ThermoAnalytics, Inc. GM successfully completed testing of the procedure using the Cadillac SRX baseline CFD results (calculated with Fluent software) as inputs into Radtherm to generate a thermal comfort index. To evaluate the localized cooling configuration, GM has built a CFD model with exactly the same localized cooling setup as used at UCB.

G2.2.4.1 Validation of Human Subject Testing Results from UCB

The GM developed VTCE tool implements the following procedure to obtain thermal comfort and thermal sensation:

1. Run the airflow and temperature solution from CFD tool (Fluent)
2. Export the airflow and temperature solution in the cabin and around the manikin to Radtherm
3. Evaluate the thermal comfort and thermal sensation in Radtherm

The team compared the thermal comfort and sensation for the four spot cooling configurations from the VTCE prediction and the UCB test data. The test thermal comfort and sensation values for this comparison were the average values from the 20 human subject test data at UCB. The thermal sensation index is ranging from -4 to +4 with -4 being very cold and +4 being very hot and 0 is neutral. The thermal comfort index is also ranging from -4 to +4 with -4 being very uncomfortable and +4 being very comfortable. Usually, we need thermal comfort index to be +2 and above to comfortably good.

The team also examined the standard deviation for the thermal sensation and comfort from the 20 human subject tests. Both standard deviations for the sensation and comfort are higher than 1 for the four spot cooling flow configurations. This is due to gender, body size, and metabolism variation for each individual. The VTCE predictions are comparing to the average values from the test. For the thermal sensation, which indicates whether you are feeling hot or cold during the spot cooling configuration in this hot ambient temperature condition, the VTCE predictions are correlated quite well with the test. The largest discrepancy shows a difference between test and prediction is 0.3; considering the sensation range being -4 and +4, this is still within the range for a very reasonable correlation. The other three cooling configurations are all comparing very close to the test values within 0.1. The predictions for all four configurations indicate results that are cooler than the actual test data.

The thermal comfort indexes from these analyses indicate the predictions for all four cooling configurations are in a more comfortable state than the test. The differences between predictions and test data for the comfort indexes are higher than the sensation indexes, ranging from 0.142 to 0.64. For this higher ambient temperature environment, the predictions for the higher comfort values than the test data are consistent with the predictions in cooler thermal sensation for all configurations. Again, the comparison between the prediction and the test are deemed satisfactory for the comfort range between -4 and +4.

G2.2.4.2 Further VTCE validation in a real vehicle environment

The success of the two validations for the VTCE tool with the ideal control test environment at UCB has prompted the project team to move to the next step with the test data from the Delphi wind tunnel test. In late September and early October 2010, the project team completed wind tunnel tests to evaluate various spot cooling concepts. The test data and engineering report were completed and available in December 2010. During the test, a limited number of human subjects were available to evaluate the thermal comfort and sensation for the baseline case without the localized spot cooling and with various spot cooling configurations. All test cases are with solar load. For this validation, Delphi conducted the flow simulation for the baseline case and at least two spot cooling cases. GM then applied the VTCE tool for thermal comfort and sensation validation based on Delphi's flow results.

During the test, the localized spot cooling conditions were implemented in the Cadillac SRX vehicle. For CFD VTC tool validation, the following two conditions are selected for comparison:

1. Baseline (no spot cooling): $T_{ambient}$=30°C, solar load= 500 W/m2, RH=55%
2. Baseline + high flow combination spot cooling

For the baseline case, the volumetric flow rate is equally distributed across the four main registers. For the combined spot cooling, the tested volumetric flow rate was used for each nozzle. The Fluent simulation was conducted with about 7 million volume elements. Both driver and passenger manikins were included in the model. The Fluent calculations for flow and temperature were carried out by Delphi according to the above condition. The results were transferred to GM for thermal comfort and sensation processing with the VTC tool.

Figure 6.2.A shows the flow traces originally from the four main HVAC outlet registers for the baseline case. The color indicates the flow velocity in m/s. The flow direction of the main HVAC points to the chest and neck area of the manikins.

Figure G7: Particle trace for the baseline case

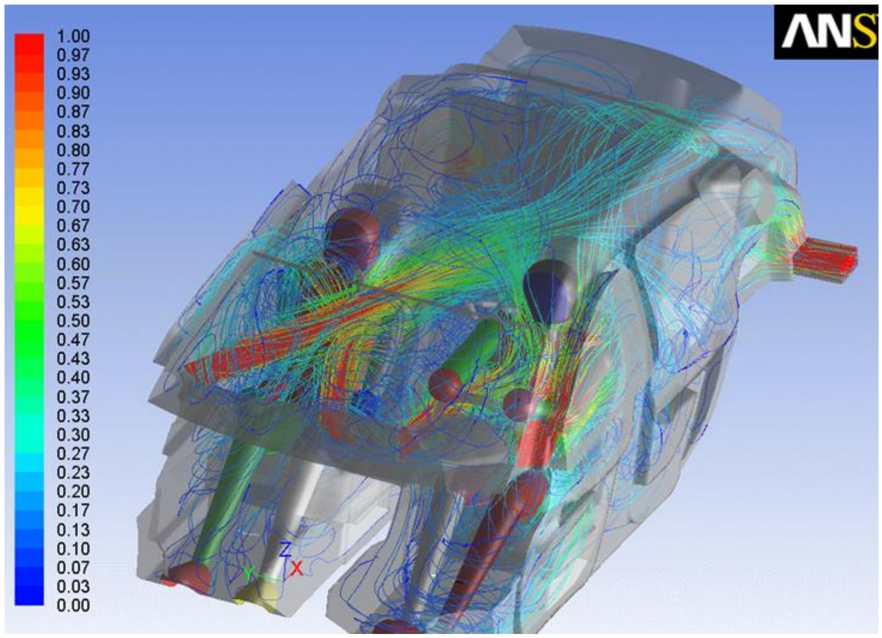

The team analyzed the flow velocity vectors and contours for both baseline and high flow spot cooling cases on the surfaces of both manikins. The convective heat transfer coefficients and film temperature for the baseline case are shown in Fig. G8.

Figure G8: CFD convective heat transfer coefficient and film temperature for baseline case on manikin surfaces

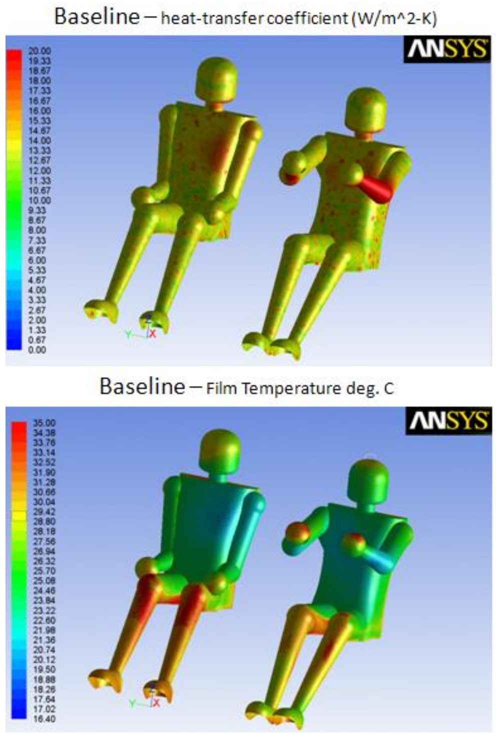

The VTC tool at GM is used to process the thermal sensation and the thermal comfort levels. During the process, the average velocity and temperature values for each body segment 5 mm away from the manikin surfaces and the convective heat transfer coefficients for the entire vehicle surface panels are extracted from the CFD results and imported into Radtherm. Radtherm uses these CFD data coupled with the specified solar load to invoke a human physiological model to calculate body skin and core temperature and sweating level with a specified clothing type. The overall and local thermal comfort and sensation levels are then predicted based on the correlations between thermal sensation and thermal comfort levels and physiological outputs. The technology involved here is evolving dynamically since it is still in its infancy, and more test data are needed to better understand the insight of this modeling technology.

The overall sensation compares quite reasonably between the test and the simulation. The local sensation levels of some spot cooling locations are in the same trend as the test data and their levels are in the reasonable agreements. However, the sensations for two locations are totally in the opposite direction from the test data. It is clear that the model did not predict the trend and absolute level. GM has been in frequent contact and worked with TAI, Inc. (vendor of the Radtherm software) and UCB to at least figure out the cause of such inconsistency and then to improve the modeling capability. The thermal comfort prediction for the same comparison is similar to the sensation level prediction and the overall comfort level is reasonably good, but the comfort levels for two locations are in the wrong trend.

With the comparison issue in mind for the baseline case, we feel that finding ways to improve the predictive capability of the VTC tool for the baseline case should be the current focus, and we have been doing that with the UCB team and TAI, Inc. So far, the predicted thermal sensation and thermal comfort levels for the spot cooling case have been obtained, but the comparison with the test data is currently on hold until the accuracy and trend issue for the baseline case has been resolved.

G2.2.4.3 Personal Computer version development of the VTC tool

The personal computer (PC) version development started in January 2011 between GM and UCB with the focus on developing a quick vehicle architecture level thermal comfort evaluation. This tool is intended to be used in GM's Advanced Vehicle Development Center. The idea is to choose some representative vehicles from a broad range of categories, such as small sedan, large sedan, compact SUV, full size SUV and pick-up truck, and so on to build a CFD flow database around each representative vehicle with various predefined HVAC operation modes, fan levels, and air velocity and temperature around the manikin. This CFD database will be implemented into a PC-based thermal comfort predictor so that an HVAC engineer can specify HVAC operation mode, fan speed, discharge temperature, solar load, and desired vehicle type from the database to understand the impact on human thermal comfort and sensation. This PC thermal comfort tool runs very quickly on a PC, since it does not require detailed CFD meshing and calculations. The flow and temperature around the manikin are purely done based on the pre-calculated CFD results for each representative vehicle. Data interpolation is needed for HVAC user input of outlet velocity and temperature that are different from the database. The solar radiation, convection, and face-to-face radiation does enter into the energy balance on the surface of the manikin when the human physiology model is used to calculate the skin and core temperature under the vehicle thermal environment.

The UCB team incorporated the SRX geometry into the comfort model. Preliminary tests were finished to check the results. Currently, the number of polygons used to represent the car is 3000, which is relatively low in order to maintain the fast speed of the model simulation.

One of the input features of the PC tool is that it provides a user interface to bring in the air velocity and temperature around the manikin and the vehicle panel temperature from an external CFD flow simulation. We are taking advantage of this feature to enable the VTC validation process. During the course of the past few months, Delphi has tested and obtained valuable thermal sensation and comfort data for various spot cooling and heating configurations, and GM has been using CFD to compute the flow and temperature according to the test conditions. Although this effort is still early in the validation stage due to the complexity and uncertainty of the specific conditions of the thermal environment on the human subject test, we have managed to obtain favorable correlations between the prediction and the test for the baseline case. We have made continued progress in validating more cases with various cooling/heating combinations. During this quarter, two more validation cases have been attempted. In summary, we believe that the tool's thermal comfort prediction for the vehicle in the real world environment is very encouraging, and that these test successfully demonstrate the capabilities of the VTC tool.

Figure G9: SRX geometry in the PC Comfort model

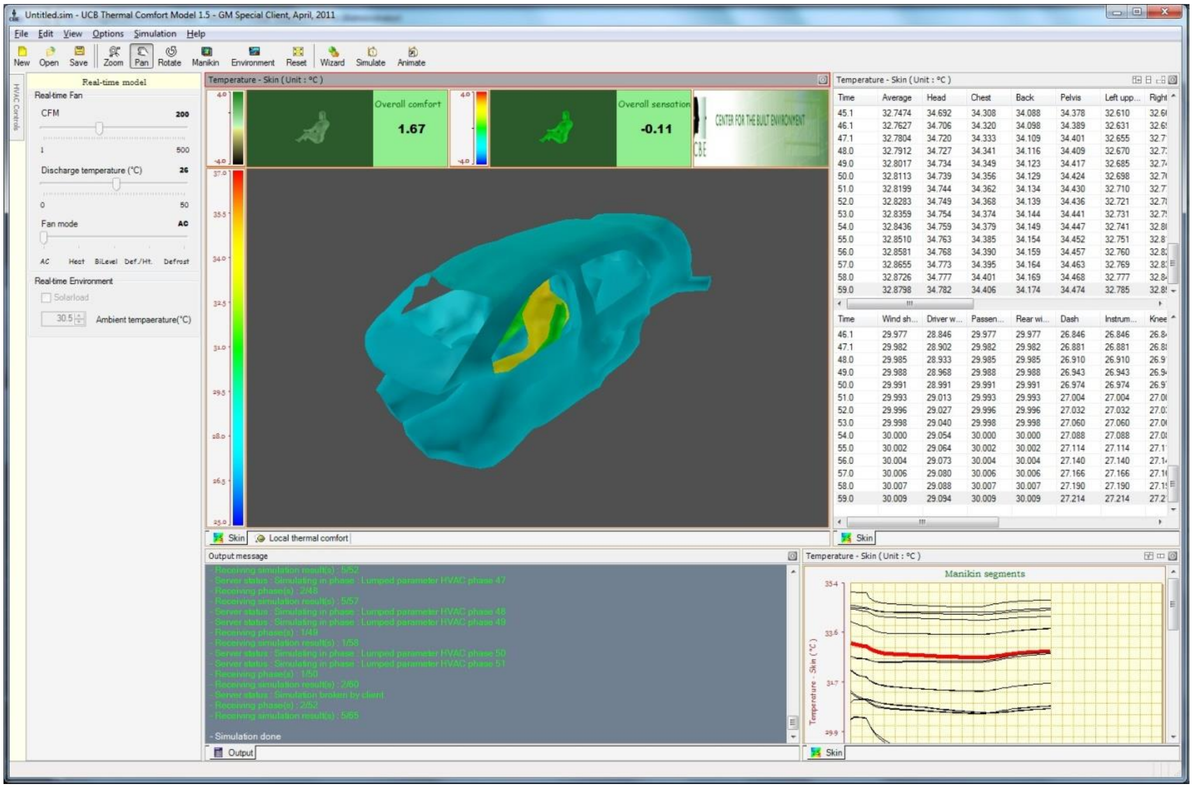

In addition to the standard Thermal Comfort model predictions of sensation and comfort, the PC tool added new features for GM engineers designing advanced HVAC systems for future vehicles. One very useful feature developed for the initial release of the PC tool was automatic set point temperature calculation for body parts. The set point temperatures for all body parts are generated and saved in a single pre-defined file before the comfort simulation based on either “summer” or “winter” condition and also manikin clothing level and metabolic rate. For various environmental and manikin’s conditions, the set point temperature file is used in the model to calculate the local sensation and comfort values. It requires a deeper understanding of the model in order to generate this file and usually this task doesn’t belong to the users. As a result, UCB made the set point temperature calculation as a dynamic process based on the simulation condition. This implementation in the final release makes the PC tool flexible and user-friendly.

G2.2.4.4 Vehicle library in the PC version

A total of six vehicles have been chosen to be included in the PC tool. The vehicles are grouped into the following three categories:

- Sedan: Chevrolet Volt (Extended-Range Electric Vehicle, mid-size), Buick Lacrosse (mid-full size), Chevrolet mini (compact size)
- Sport Utility Vehicle: Cadillac SRX (compact size), Chevrolet Tahoe (full size)

- Pick-up Truck: Chevrolet Silverado (full size)

Each vehicle represents a typical type in each category in terms of size and function. The noticeable exceptions are the Chevrolet Volt and the Buick Lacrosse. They are in a similar size category, although the Volt is an E-REV and the Lacrosse is a traditional gas-powered vehicle. Because these two were selected as demonstration vehicles, we want to have detailed data for future analysis under this project. Each vehicle chosen should have distinct features in HVAC distribution and the thermal comfort characteristics in the category it represents.

For each vehicle, we carefully model all AC outlets into the cabin. These includes four main AC panel outlets, two side window outlets, defrost outlet, heater outlets in the driver and front passenger foot well area, floor outlets under the driver and front passenger seats, and finally outlets on the center console toward the rear seat. Keeping track of airflow in all the outlets is essential to apply flow measurement data from the proving ground in order to generate CFD database for each vehicle.

The surface mesh usually built for CFD applications is in the order of hundreds of thousand elements to ensure enough resolution for the vehicle feature lines. However, in the PC tool application, no such detailed refine mesh is necessary due to the following two reasons. First, it does not solve complicated flow equations (Navier-Stokes) to obtain solution. Instead, simple discharge coefficient (to be explained later) is needed to relate HVAC discharge velocity and temperature to the air speed and temperature around the manikin. Also lumped parameter thermal analysis is used to account for the energy balance between solar load gain, heat loss/gain through cabin walls, heat from human subjects in the cabin and to speed-up the view factor calculation in thermal radiation analysis. Usually for the later reason, the total surface element numbers including the manikin and vehicle panels has to be limited to fewer than 7,000. Because of this, the fine mesh vehicle model used for CFD calculation has to be further coarsened to be included into PC tool. Figure G0 shows the six coarsened vehicle models implemented in the VTC tool.

Figure G10: The six vehicles implemented in the VTC PC tool

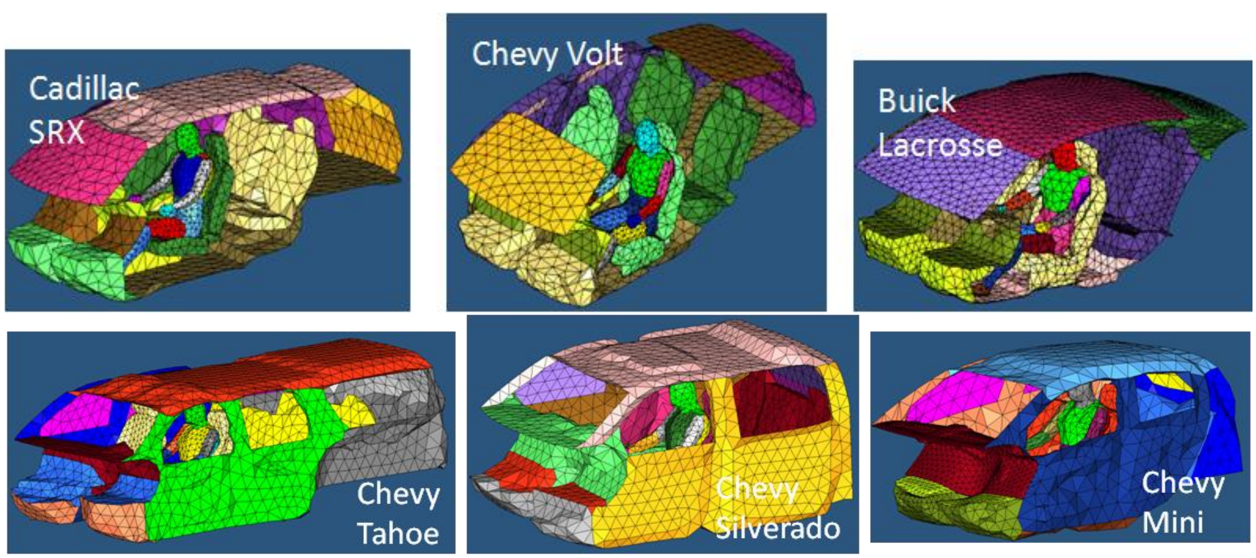

G2.2.4.5 CFD flow database corresponding to the Vehicles in the library

The routines in the PC version to evaluate the human thermal comfort for the occupant are based on the following energy balance between environmental factors and heat generation/loss controlled by the human physiology. For vehicle, the environmental factors include: (1) HVAC airflow rate and temperature around the manikin surface, (2) air relative humidity, (3) location of the HVAC outlet registers, (4) solar load, and (5) vehicle body panel temperature and ambient air temperature. For the physiology model used in PC version, the following parameters are needed: (1) occupant metabolic rate, (2) body build (there are various body builder option in the tool), and (3) clothing level. The parameters related to human physiology calculation have been implemented in the tool already. For the environmental factors, the existing PC tool from UCB has everything to calculate the energy balance on the manikin skin surface and to evaluate the thermal comfort. The only data missing to enable the thermal comfort prediction for each built-in vehicle is the airflow distribution around the surface of the manikin. The airflow around the surface of the manikin depends on the HVAC operating mode and fan blower speed. We have pre-selected 5 HVAC operating modes and 4 fan blower speeds to cover all possible cooling and heating HVAC scenarios for each vehicle. This is the task that the computational fluid dynamics (CFD) tool can be used effectively to generate a complete airflow map around the manikin. Table G2 shows the 5 HVAC operating modes for 4 fan blower speeds.

Table G2: HVAC operating mode for 4 fan blower speeds

AC mode	Non-AC mode			
	Bi-level	Heater	Defrost	Defrost/heater

To conduct the CFD simulation to map the airflow around the manikin surface, the exact air velocity (flow rate) at the exit of each HVAC register has to be specified. The airflow data at the register location can only be determined by tedious measurement in the flow measurement Lab. The following steps are required to complete the CFD HVAC flow database in the PC tool for each vehicle:

1. Flow measurement at the GM Proving Ground test facilities to obtain the air flow distribution at each HVAC outlet register at four blower speeds and five operational modes. The four blower speeds are set at 100%, 75%, 50%, and 25% and the HVAC operational modes are AC, Bi-Level, Heater, Defrost and Defog modes.

2. Based on the air flow rate distribution from measurement, CFD simulations with 20 cases (4 blower speeds x 5 operational modes) are conducted by specifying the exact discharge mass flow rate from each HVAC outlet.

3. The air velocities at 3 cm away from the manikin surface for 16 body segments are recorded.

4. The correlations between the discharge velocity and the velocity at each body segment for the manikin are calculated for all HVAC operational modes.

With this database, the tool is used to obtain thermal comfort by specifying any desired discharge velocity and temperature, HVAC operational mode, and solar load for the chosen vehicle platform. Using the relationship between the HVAC discharge air flow rate and the average discharge velocity, the user selects a discharge flow rate to run the HVAC system in the selected vehicle. The CFD calculated discharge coefficients for each individual HVAC operation mode is used to calculate the air velocity at each body segment: Based on this simulation, the PC tool can estimate the thermal sensation and comfort for each vehicle occupant.

G2.2.4.6 PC Tool Thermal Comfort validation

One of the input features of the PC tool is that it provides a user interface to bring in the air velocity and temperature around the manikin and the vehicle panel temperature from an external CFD flow simulation. We are taking advantage of this feature to the VTC (Virtual Thermal Comfort) validation process. During the course of the past few months, when Delphi has tested and obtained valuable thermal sensation and comfort data for various spot cooling and heating configurations, we have been using CFD to compute the flow and temperature according to the test condition. Although this is still early in the validation stage, due to the complexity and uncertainty of the test condition of the thermal environment on the human subject test, we have managed to obtain favorable correlations between the prediction and the test for the baseline case. We are still working hard to inch closer to both the spot cooling and heating condition. Figure 2.2 shows the baseline case for the SRX condition we are using for this validation. The baseline localized spot cooling test case specified the wind speed, ambient temperature, relative humidity (RH), and solar load as indicated in Figure G1.

Figure G11: Thermal comfort validation setup for the baseline spot cooling case

All the spot cooling nozzle flows are off, and the discharge airflow from the main front panels is 95 CFM and the discharge temperature is 18 C. The CFD simulation was set up as closely to the tunnel test environment as possible. The air velocity and temperature 3 cm away from the surface of the manikin were extracted from the results and used as input to the PC version. The body panel temperatures were also recorded and used as input. Figure G12 and Figure G13 show the comparison between predictions and tunnel test data for thermal sensation and comfort respectively. We are quite satisfied with the comparison results since this is the first validation against the real asymmetric harsh thermal environment.

Figure G12: Thermal sensation comparison between prediction and test for the baseline case for Delphi's SRX tunnel test

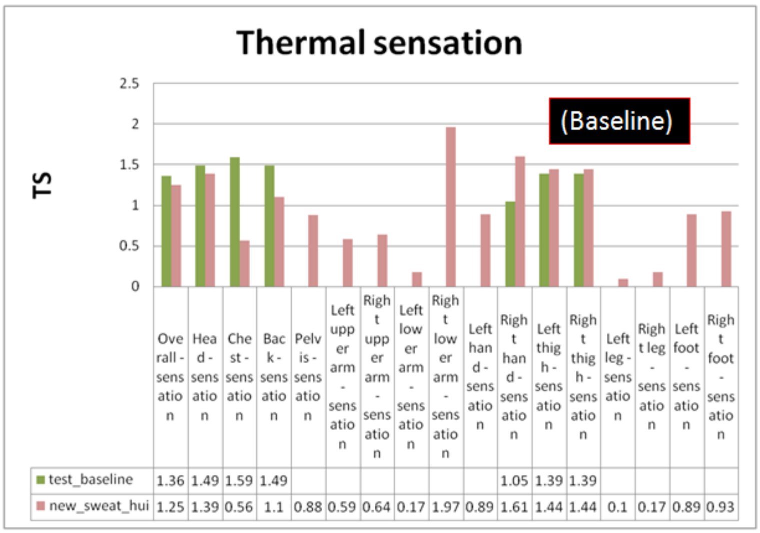

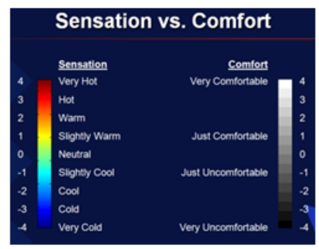

Figure G13: Thermal comfort comparison between prediction and test for the baseline case for Delphi's SRX tunnel test

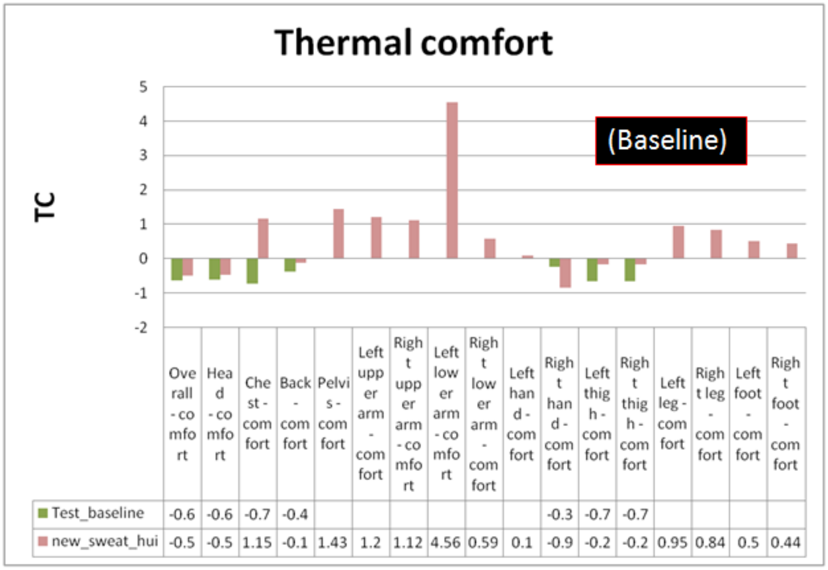

G2.2.4.7 Development updates to the PC-based VTC tool

UCB released two updated versions of the tool to GM. The latest version includes the following bug fixes and modeling enhancements: (1) calling to the correct fan data when one of the GM's built-in vehicles is used, (2) correcting the code freeze issue when the solar load is activated in the 64-bit version, (3) fixing the bug for using the winter clothing, and (4) sweat distribution enhancement. Using this new enhanced version, the previous spot-cooling configuration cases are redone to check the new version's consistency with the old version of these two cases. In addition, the validations are done with two new cases for the spot-heating configuration. These four cases are examples of the analysis performed to validate these cases. These are some of the methods employed to perform the tool validation.

Figure G14: Velocity vectors (left) and streamlines (right) for the spot-heating baseline case

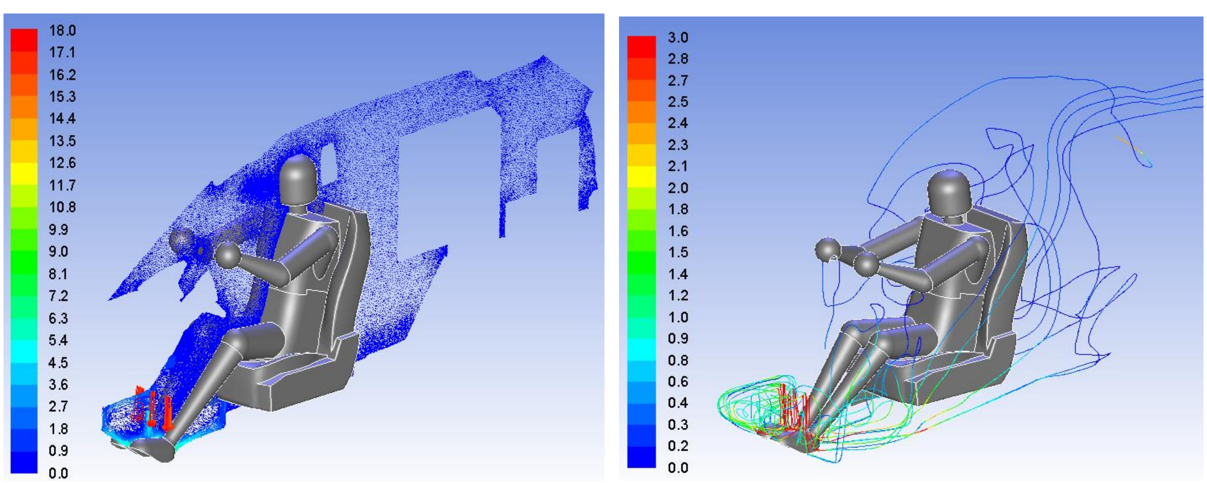

Figure G15: Manikin skin temperature (^{0}C) (left) and velocity (m/s) (right) for the spot-heating baseline case

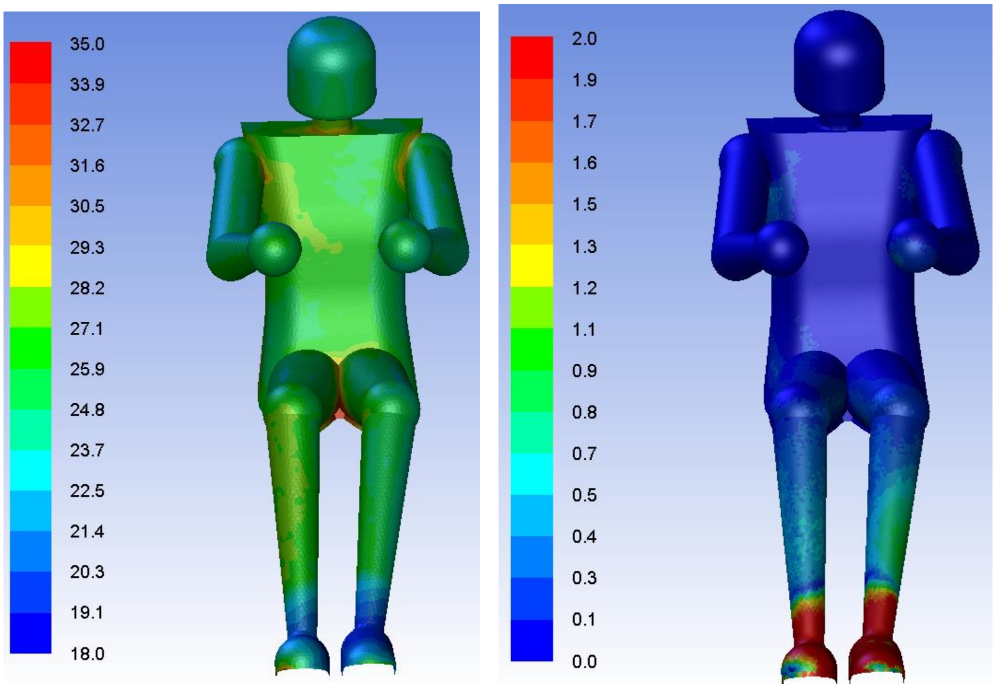

Figure G16: Air flow temperature (^{0}C) (left) and velocity (m/s), 3 cm off manikin skin surface for the spot-heating baseline case

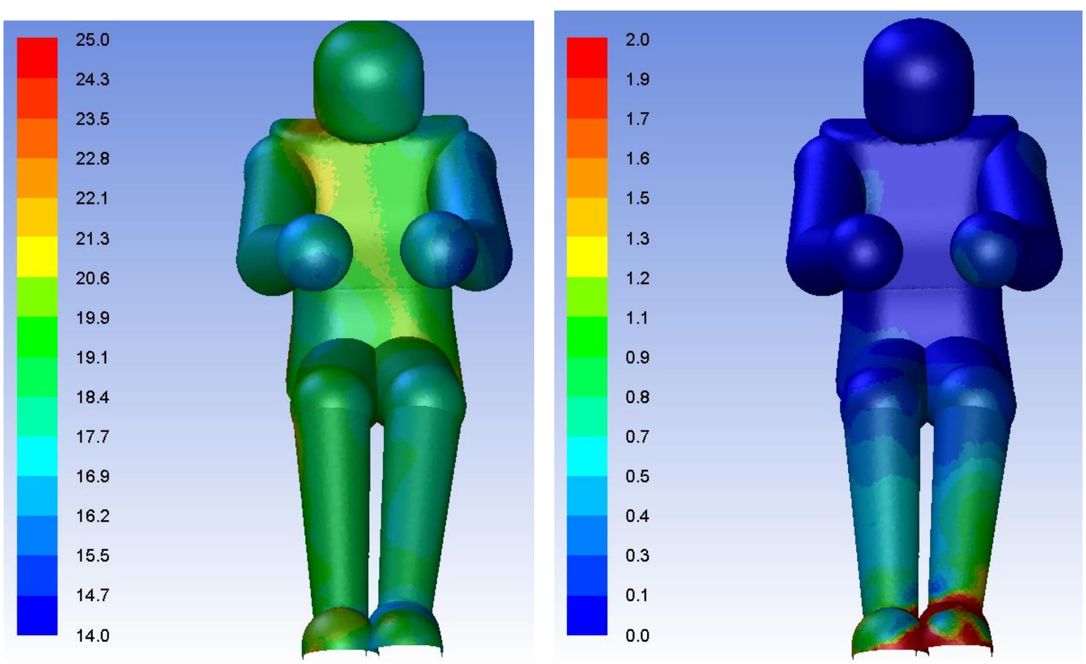

Figure G17: Vehicle body panel temperature contours.

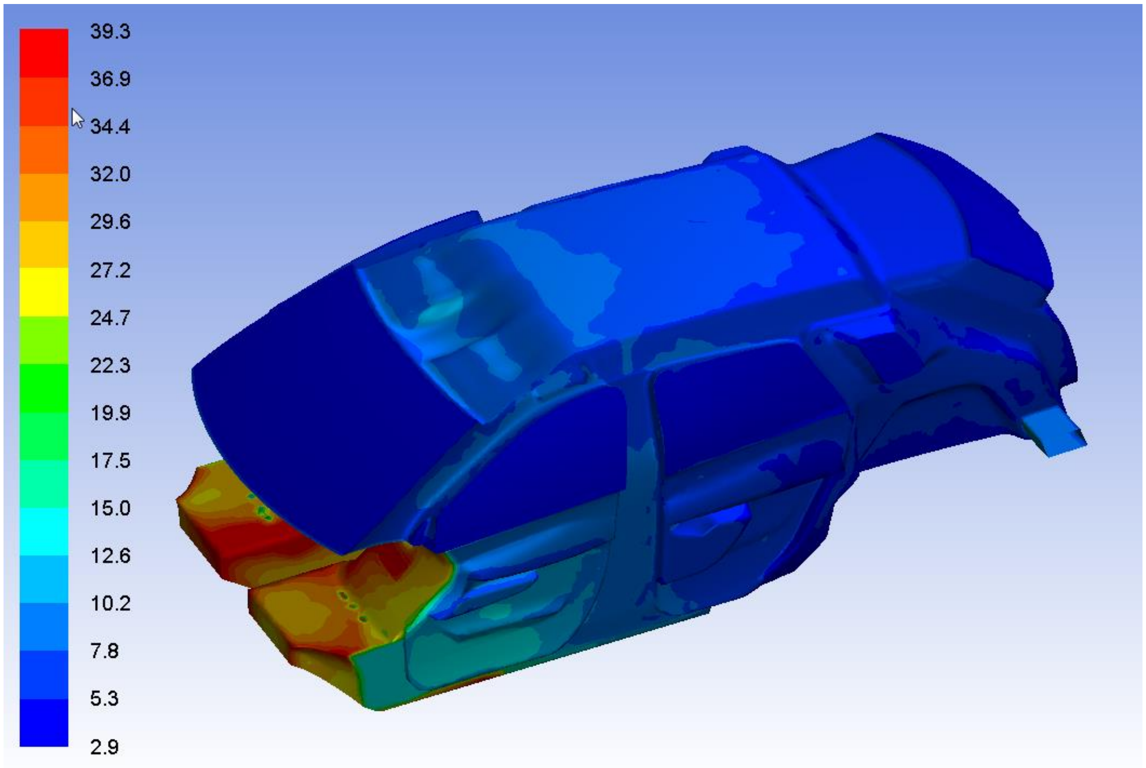

G2.2.4.8 Development of a new stand-alone Thermal Comfort Control Tool

This activity developed a "stand-alone" thermal comfort module (tool) that will interact with GM's HVAC control software such that the thermal comfort index can be used as part of the HVAC automatic climate control (ACC) strategy. Traditionally, HVAC control loop either uses the in-car breath level temperature as a feedback to adjust the air discharge flow rate and temperature to reach comfort. Or in some other cases, it completely relies on mathematical model to provide HVAC air discharge flow rate and temperature based on some other indicators such as solar load sensor, outside air temperature and humidity level. None of the above methods directly address the need from the occupant thermal comfort which indeed is the purpose of the HVAC climate control. The current project will be using the existing PC comfort tool but to modify it from the current GUI based operation to a batch tool operation. The new comfort module will maintain the core thermal comfort capability but move some of the inputs from the GUI to be part of the interface between the new comfort module and the control software SIMULINK. Figure G8 shows the conceptual operation of this control software. The SIMULINK is the control software that GM is currently using for the vehicle HVAC ACC system. This developing module is to be interacted with the SIMULINK with a new clear defined interface that facilitates the data exchange between the comfort output and the instructional inputs from the main controller – SIMULINK. The SIMULINK GUI is shown in Figure G18.

For the control operation:

- Users can provide their own routine in C into SIMULINK environment (called S function) to perform the required task.
- The comfort module will become a C code S function in Simulink.
- The data exchange between Simulink and comfort module can be done by the external ASCII files or clearly defined interface.

Figure G18: The schematic of the thermal comfort PC control tool operation

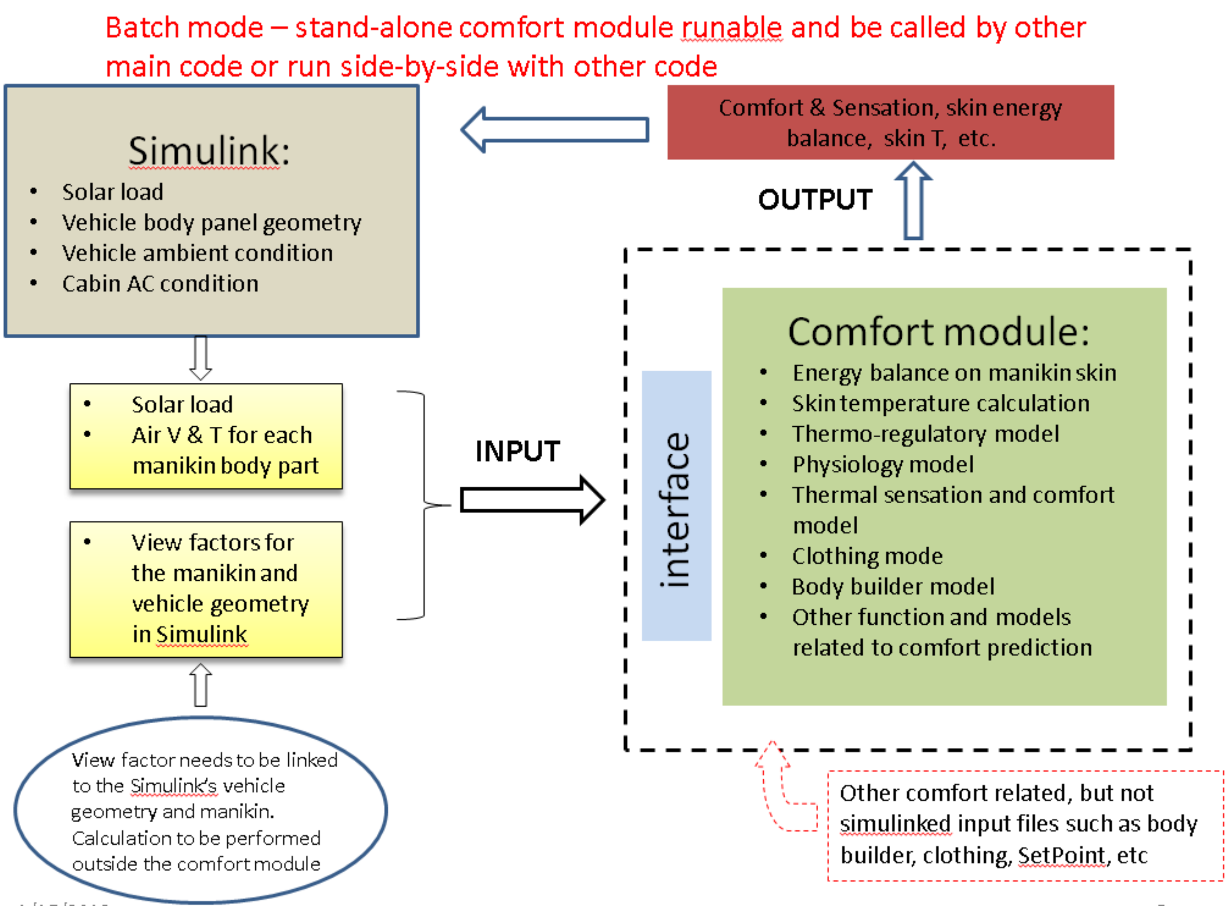

Figure G19: The SIMULINK GUI

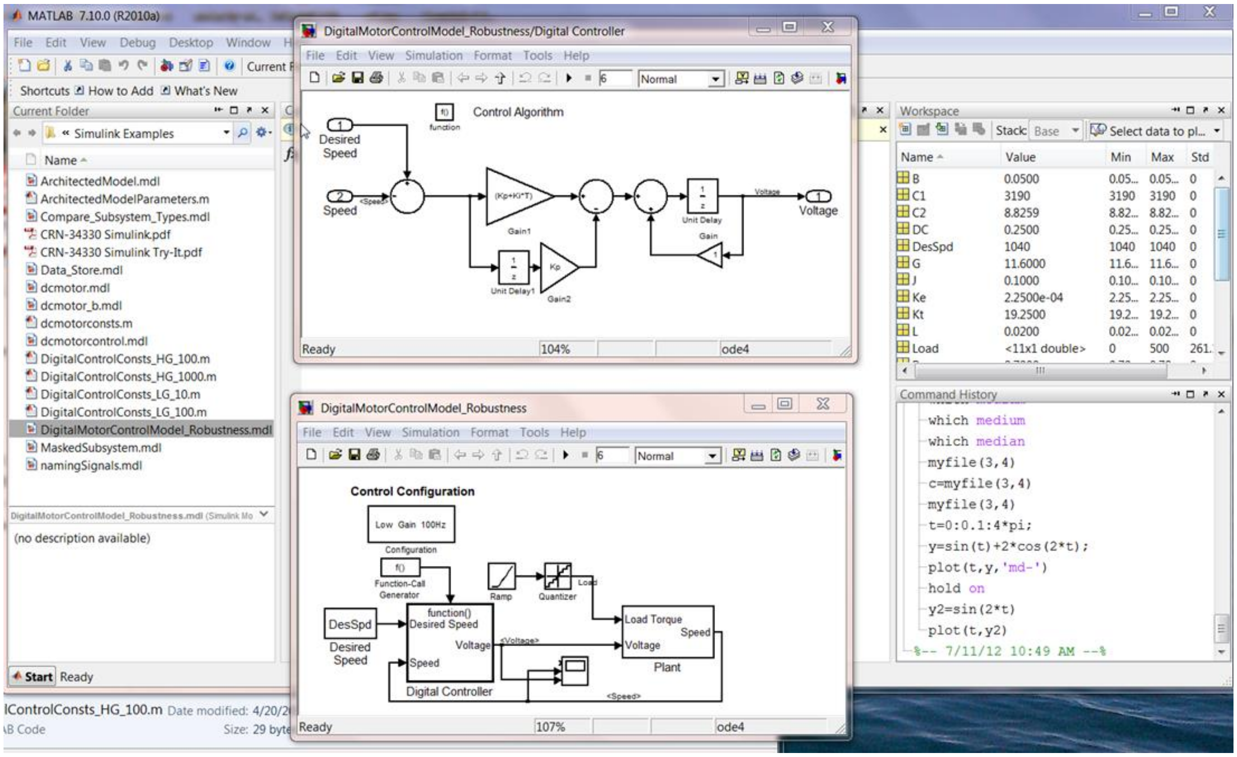

G2.2.5 Milestone 9 – UCB Comfort Model second update released

On January 16, 2013, the team released the UCB Comfort Model update to complete this project milestone, and the corresponding release of the CAE advanced comfort model supported the development and release of associated engineering tools. To integrate the UCB Comfort Model with other third-party applications and tools that provide environmental conditions, we developed the UCB Comfort C-API interface, which can be called in a tool supporting C-program extensions like Simulink. We successfully linked the CAE advanced comfort model into Simulink. The link is based on the C-mex Sfunction in Simulink, where the UCB Comfort API dynamic link library (dll) was loaded and called. The primary demo code segments have been successfully executed. All of those code segments are able to be encapsulated in a self-defined block within Simulink, and other common blocks can be further designed based on the need to support further simulation.

G2.2.6 Milestone 11 – UCB Comfort Model third update released

This milestone is planned for completion by 3/31/2014. This third update of the UCB Comfort Model will incorporate the latest testing and analysis to create the final validated release.

G2.3 Task 3 – Perform Human Subject Testing

The main activity for this task was to perform the first set of human subject testing in a vehicle mock-up in the UCB Environmental Test Chamber. Subsequent human subject testing was performed in their climatic wind tunnel under other project tasks, but those results were also correlated and incorporated into updates of the UCB Comfort Model.

G2.3.1 Testing in the automotive mockup at the UCB environmental test chamber

The automotive mockup for the UCB environmental test chamber was designed (see Figure G0) and built.

Figure G20: Automotive mockup in the UCB environmental test chamber

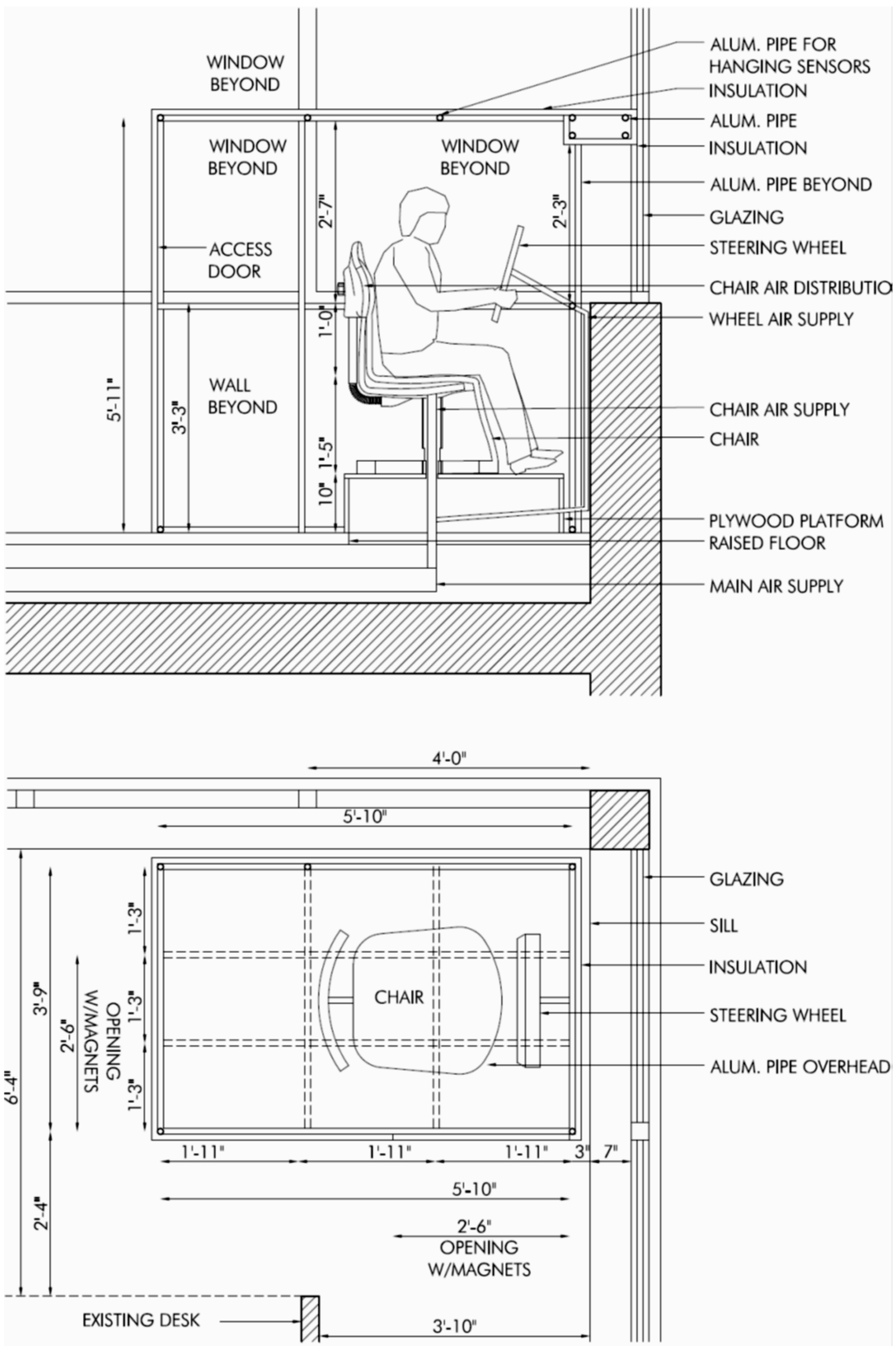

G2.3.1.1 *Experiment set up:*

The test setup for the vehicle mockup car in the UCB Environment Chamber is show in Figure G21. The chamber has two areas, a car space for human subject measurements and an ante room; the ante room is where subjects stay between test conditions and do step exercises during recovery periods. There are windows on three sides of the car space, similar to the space in an actual car. The window between the car and the ante room provides light to the ante room. There is a curved skylight installed in the ante room to provide additional light, and it also provides additional height for tall people performing the step exercises.

Figure G21: The mockup "car" in the chamber. It has two spaces, the car space, and the ante room space. A skylight is installed in the ante room

Mock up car in the chamber | Car space | Ante room | Skylight in the ante room

All the local cooling/heating strategies are mocked up and installed. They include ventilated seat, seat belt, air supplied from A-pillar, B-pillar, headliner, around neck towards the breathing zone, and behind the driving wheel towards hands. The three images in Figure G12 show the ventilated seat (seat side and the back side). The duct in the picture provides cooled air to the back of the seat. There is a radiation heater installed in front of driver's seat to simulate solar radiation.

Figure G22: Ventilated seat

The local cooling/heating control is carried out through a program in a computer. The interface controlling the local fan speeds is presented in Figure G. The fan speeds can be individually adjusted from high to low by moving the sliders up and down. The computer program also records the settings of the speed for each fan.

The manifold controlling the fans is also shown in Figure G. There are five fans installed in the manifold to provide air to the local cooling/heating devices (such as the ventilated seat). The air supply to the manifold comes from a spot cooling supply from the chamber HVAC system, which can control the supply air temperature to various levels.

Figure G23: Local fan speed control software interface and the manifold hosting fans

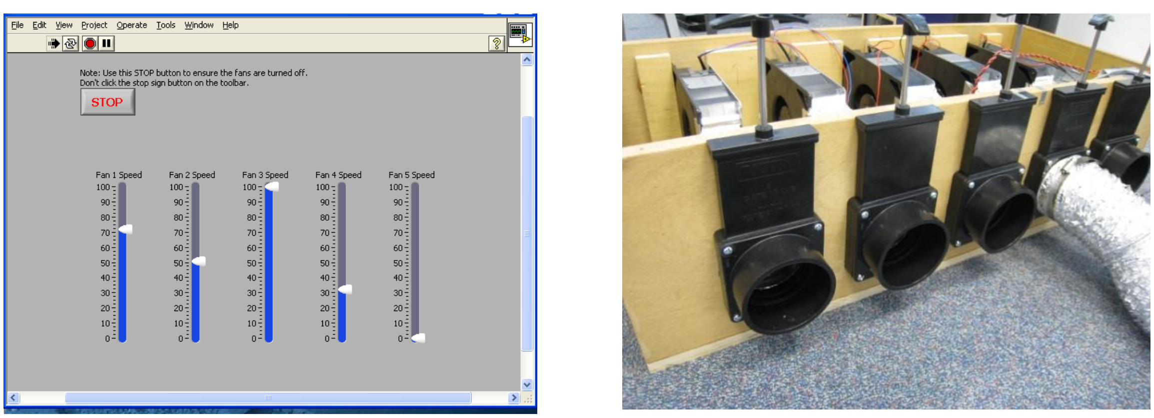

a. interface controlling local fan speed

b. manifold

G2.3.1.2 *Pilot tests:*

First, we used a thermal manikin to measure the heat loss for each of 16 body parts (see Figure 4). The manikin tests at this stage were preliminary and used to help identify the effectiveness of local cooling/heating strategies. Following the human subject tests and after the manikin had been upgraded and repaired, more complete manikin tests were conducted.

Figure G24: A thermal manikin is used to measure the heat loss of various local cooling/heating devices

We conducted pilot tests with human subjects to provide an initial evaluation of different local cooling/heating strategies (as shown in three images in Figure).

Figure G25: Pilot tests

The goal of the pilot testing was to identify the most effective local strategies. Based on pilot human subject tests and heat loss measurement from the thermal manikin, UCB provided initial recommended effective local cooling/heating strategies and their supply temperatures and flow rates to the rest of the team. After combining the pilot test results and the feedback from the project team discussion, the chamber test conditions were finalized for the UCB human subject testing.

G2.3.1.3 Conducting human subject tests:

One test procedure covered six local conditions, and each local condition continued for 15 minutes. Two subjects participated simultaneously during the 3.5-hour test period. When one subject was inside the mockup car undergoing a local test condition, the second person waited in the anteroom. They alternated positions every 15 minutes. In the anteroom, the person climbed 12-steps every 5 minutes in order to simulate the metabolic rate of walking outdoors (see Figure G6). The test procedure also specified consistent clothing insulation levels, where summer clothes were a short-sleeved shirt, pants, thin socks, and shoes while the winter clothes were a long-sleeved shirt, T-shirt, pants, thick socks, and shoes.

Figure G26: Seasonal clothing and the 12-steps exercise in the anteroom during tests

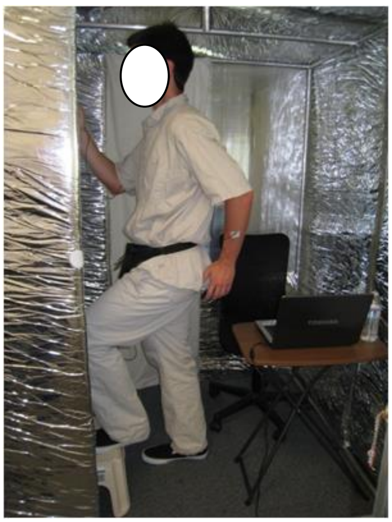

Summer clothing

Winter clothing

We measured skin temperature at 10 locations, allowing us to calculate mean skin temperature using standard procedures. The locations include key locations for our purposes of this study, e.g. gluteal region and face (see Figure G27). We used thermistors for locations where the skin temperatures do not change quickly, and thermocouples for cheek and gluteal locations where the skin temperatures changes rapidly due to impinging supply air flows.

Figure G27: Skin temperature measurement sites

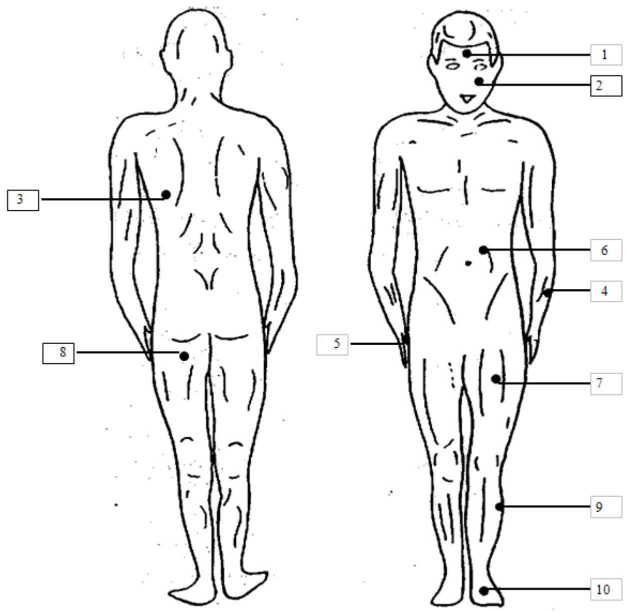

The thermal sensation and comfort scales were presented to the subjects on a computer screen. They appeared right after the subjects get into the car, then at 2, 5, and 8 minutes later during the 15 minutes of test. They apply to the different body parts (such as chest, whole body). The major questions are shown in Figure G28. We conducted four 2-hour training sessions for all 30 subjects to explain the test procedures, behavioral requirements, and survey questions, and to conduct a pilot test for each subject.

Figure G28: Thermal comfort survey questions

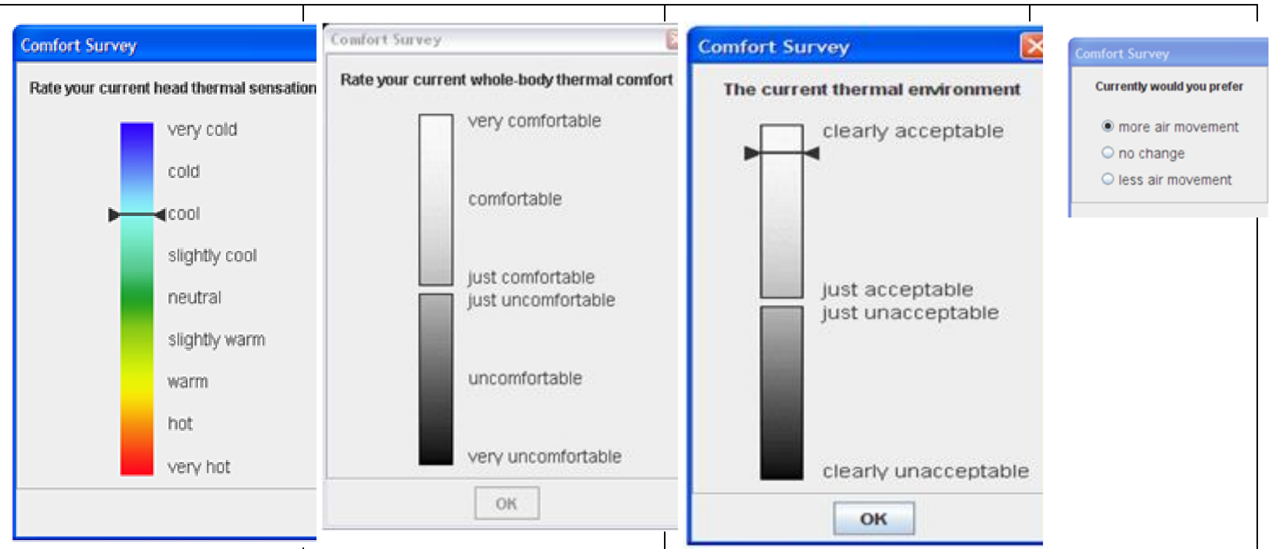

Thermal sensation scale	Comfort scale	Acceptability scale	Air movement preference

The human subject testing resulted in the following conclusions about the effectiveness of the distributed HVAC approach: 1) comfort is maintained with local cooling at the tested temperatures; and 2) with a high solar radiation load, comfort is still well maintained when all localized cooling components are applied.

G2.3.2 Milestone 1 – Identify initial set of locations for distributed heating/cooling

The project's first major milestone, identifying the initial set of locations for distributed heating and cooling, was successfully completed as scheduled on March 31, 2010. UCB was responsible for completing this initial evaluation of potential distributed HVAC components. UCB based their recommendation on their pilot human subject testing, which began in early March. UCB's findings for this milestone allowed the team to proceed with the subsequent steps of the project.

G2.4 Task 4 – Define Design of Experiments (DoE) for Target Platform

For Task 4, Define Design of Experiments for Target Platform, the team developed vehicle selection criteria to choose the target platform. The team selected the Cadillac SRX from GM's portfolio as the vehicle that best satisfied the project's requirements. This vehicle selection allowed CFD modeling and other activities to be performed as scheduled.

G2.4.1 Develop and Define the Design of Experiments

The team created a baseline CFD model for Cadillac SRX and successfully simulated the baseline thermal comfort cases as described below. The team prepared the geometry model from a CAD file for air flow and thermal analysis. The surface mesh using ANSYS's TGRID is shown in Figure G29, where the roof has been removed to show the interior meshing. The baseline model is used to check that the basic setup is correct and running without any numerical issues. This baseline SRX model is then used to analyze many AC cooling flow conditions with solar radiation. For the solar load simulation, the PPG green glass is used for all the windows. Its solar properties are listed in Table G3. The α value is the absorptivity, ϱ is the reflectivity, and τ is the transmissivity. These properties are specified for visible and infrared portions of the spectrum. The solar radiation is calculated by the solar calculator in Fluent. The location is at Phoenix, Arizona, and the time 1 p.m. on June 21. The solar load distribution on the windows into the cabin is listed in Figure G31.

Figure G29: Cadillac SRX surface mesh: shown here with one manikin and the roof removed to show the interior

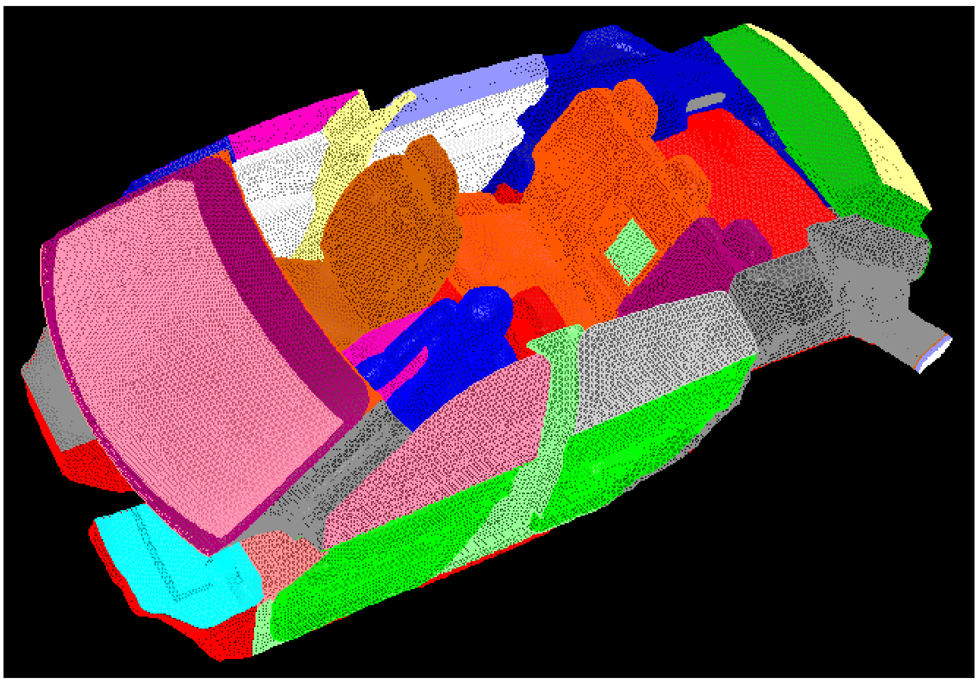

Table G3: Glass solar properties

Glass solar properties	A	ρ	τ
Direct visible	0.22	0.06	0.72
IR	0.72	0.06	0.22

Figure G30: Solar load distributions through the windows of the SRX

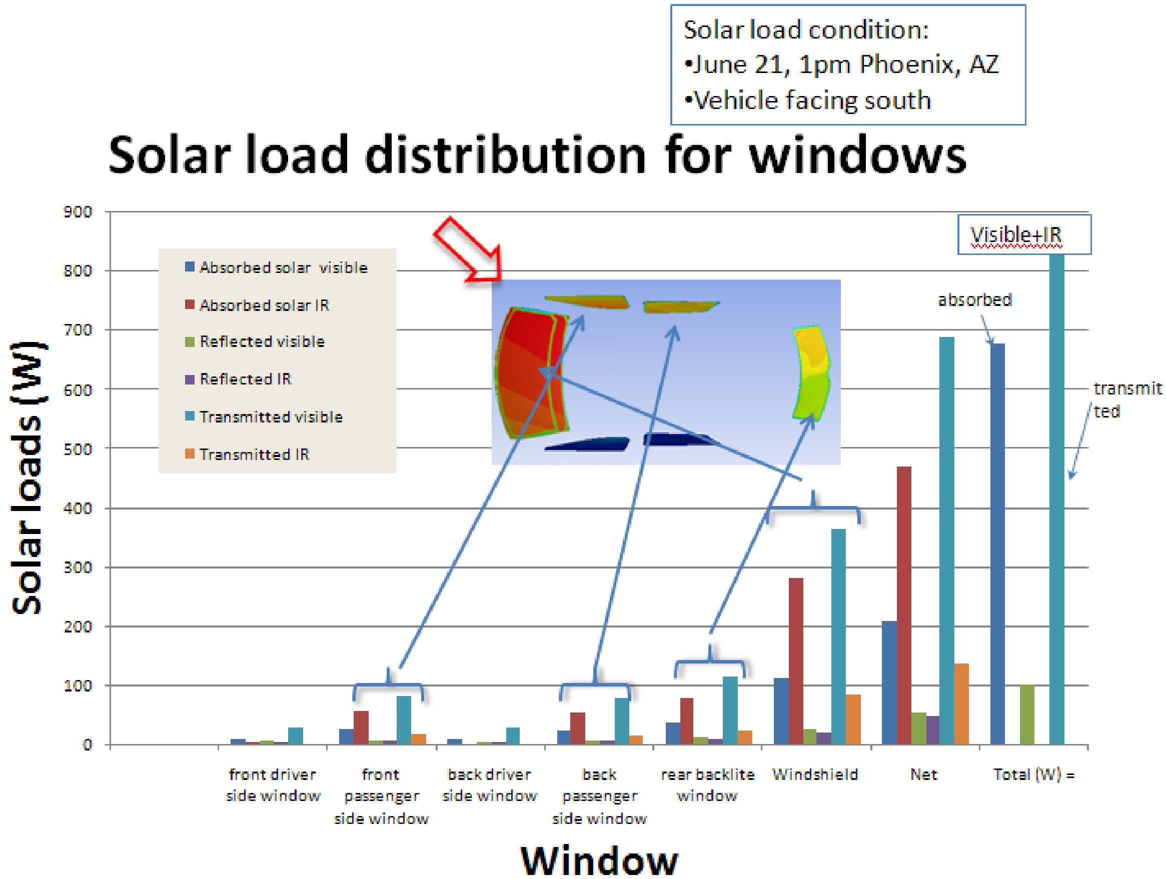

For the baseline SRX calculation, the team analyzed seven cases for various AC exit flow rates including one with no AC flow. Figure G31 shows the temperature contours for the solar soaking condition only (no AC flow). From the temperature contours on the seats, the direction of the solar load at 1 p.m. in Phoenix, Arizona, is quite clear – from the passenger side angled at above A-pillar direction.

Figure G31: Temperature contours for solar soak – no AC flow

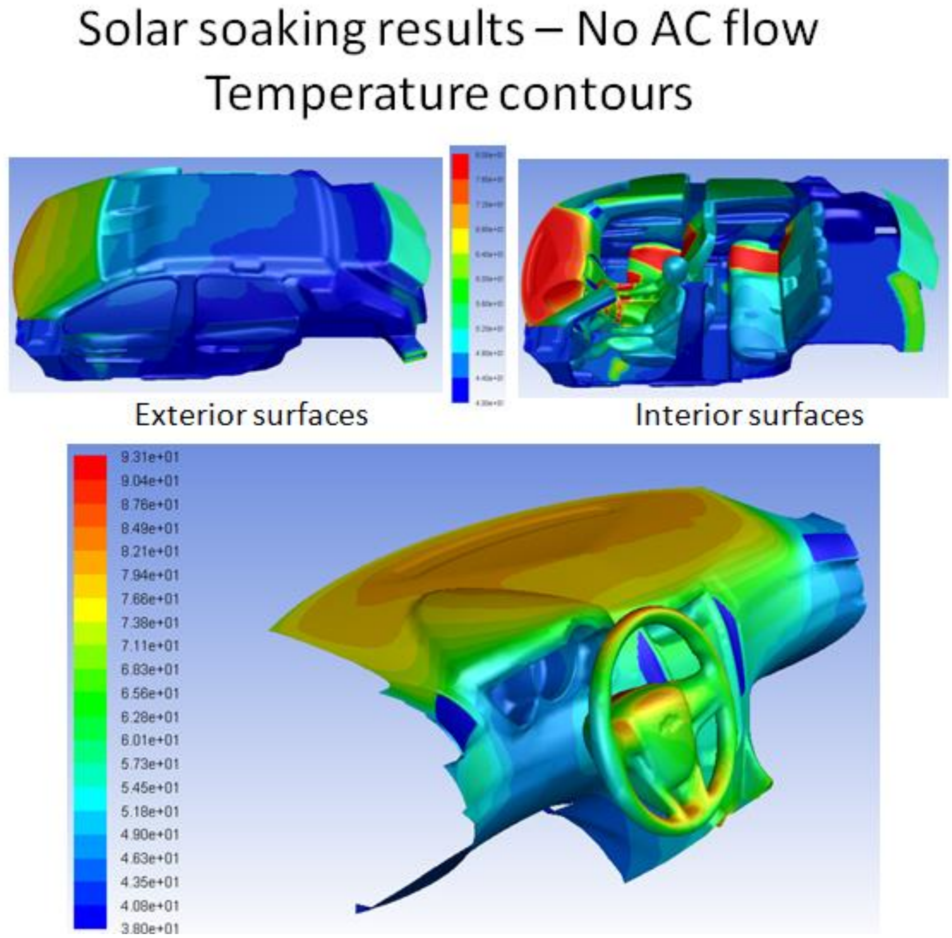

G2.4.2 Milestone 2 – Definition of Design of Experiments for Target Platform Completed

The project's second major milestone, Definition of Design of Experiments (DoE) for Target Platform, was successfully completed as scheduled on May 28, 2010. Delphi had lead responsibility for completing this activity. Delphi constructed a test matrix and conducted a DoE to study the different cooling spot locations to determine their effectiveness in providing passenger comfort. UCB and GM reviewed the initial test matrix and provided feedback to Delphi. After some final revisions, GM reviewed the developed testing parameters and approved the final DoE.

G2.5 Task 5 – Define & Build Mule Vehicle for Thermal Comfort Evaluation

For Task 5, Define & Build Mule Vehicle for Thermal Comfort Evaluation, the team ordered a 2010 Cadillac SRX with the options required to serve as the mule vehicle for the project. The SRX was airflow tested to determine the appropriate inputs for CFD modeling and correlation data for tunnel testing. The airflow data was collected using the zero body method, where air is removed by a measuring device from the vehicle interior at the same rate the HVAC system is flowing, allowing the team to determine the flow from the HVAC system into the vehicle interior. Airflow was also collected at each outlet in each mode to determine the percentage of airflow leaving each duct. This information was input into the CFD model to determine the HVAC's contribution to cooling and heating vs. the spot cooling that will be supplied by thermoelectrics. The airflow data was collected versus a pressure drop in the module, which allows one to determine instantly in the tunnel the airflow quantity through the vehicle HVAC. This allowed the team to determine what the actual airflows are during our testing process without having to install the airflow device. A Solar Load simulation was performed for Arizona at 1PM in June with ~1500 W of solar load entering the cabin and an outside ambient of 37 ºC. HVAC airflow in vent (outside air) mode was let into the cabin through all 4 front outlets. The outside ambient temperature was assumed to be 37 ºC. The basic simulation with HVAC airflow in vent (outside air) mode ran quite well with good heat balance shown in the CFD run.

For the Cadillac SRX mule vehicle, the team designed and built a method to simulate thermoelectric device (TED) cooling that uses mini-heaters, tubes, nozzles, fans, and all the necessary electronic controls needed to set temperatures and air flow rates. The design of the simulated TED required extensive CFD analysis in order to quantify the range for the control parameters properly.

G2.5.1 Computational Fluid Dynamics (CFD) Analysis of Mule Vehicle

CFD analysis was performed to locate the nozzles for cooling each targeted body part. Simple conical nozzles were used for the analysis. The nozzle diameters were dictated by air exit velocity considerations. The nozzle location (i.e., distance from the passenger) was dictated by the physics of airflow entrainment and airflow spread and impingement velocities on the targeted body part. CFD analysis was very useful in optimizing the nozzle location and evaluating the sensitivity of nozzle directivity to cooling. Nozzles for each passenger were investigated in the CFD analysis and recommendations were incorporated for cooling the targeted body parts.

Based on the airflow results of single spot cooling strategies, combination spot cooling strategies were developed. The goal of combination cooling CFD analysis was to arrive at maximum airflow coverage without substantial velocity and temperature gradients with the minimum number of nozzles. In identifying the best cooling combinations, it was important not having adverse interaction between the airflows from the different nozzles. Based on CFD analysis, the team identified the best airflow coverage at minimal overall airflow and minimum number of nozzles to implement two proprietary design strategies.

G2.5.2 Instrumentation & Final Build of Mule Vehicle

The vehicle instrumentation and final build included the refrigeration system, HVAC air handling system, and cabin temperature monitoring. The vehicle build also included the TED simulation system and controls to provide air flows to the spot cooling nozzles. Figure G32

2 shows the completed vehicle in the climatic wind tunnel for spot cooling testing.

Figure G32: Instrumented Mule Vehicle in Climatic Wind Tunnel

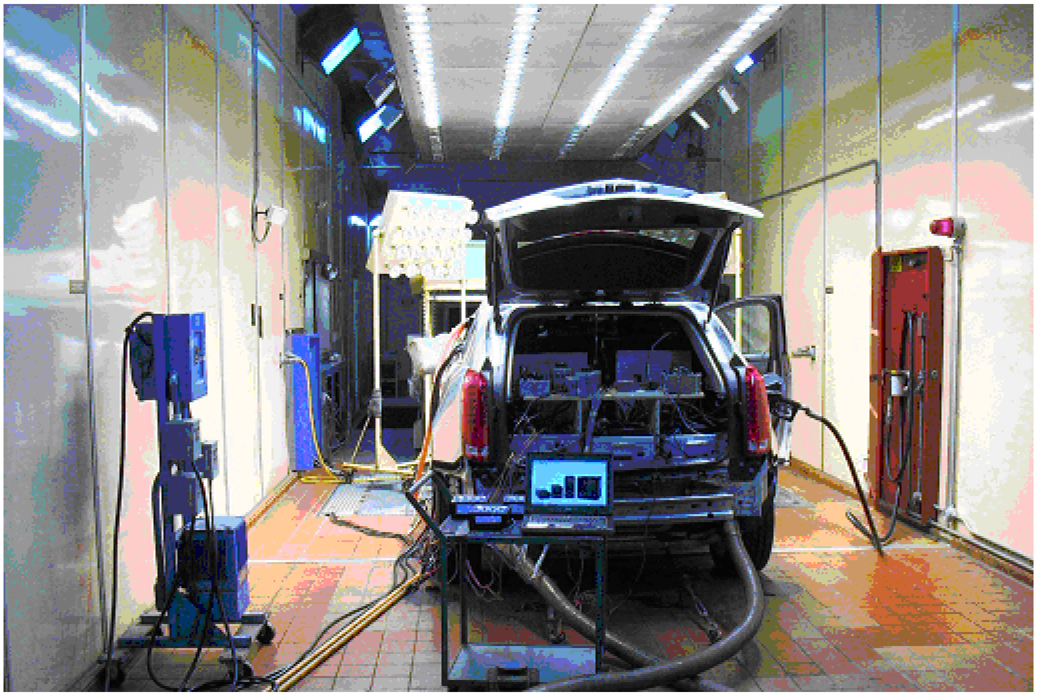

The spot cooling nozzles were fed by a thermoelectric device (TED) simulation system as illustrated in Figure G33. The TED simulation system (aka the Central Chamber System) had a built-in chiller to provide cold air that was sent through six hoses leading to the spot cooling nozzles. At the connection point for each hose, an electrical heater was installed to re-heat the air to a specified discharge temperature. The discharge temperature was controlled to a thermocouple reading at the exit of the nozzle to ensure that the desired discharge temperature was achieved. Within each hose, a small fan was installed to propel the air through the discharging nozzle. Behind the chiller, an air balance fan was installed to ensure that the air pressure downstream of the chiller was balanced to the air pressure outside the central chamber and within the car cabin. The purpose for this is to allow airflow measurement by using the spot cooling fan PWM control signal, which was correlated to an airflow rate prior to the tunnel testing in the Airflow Lab. Two of these TED simulation systems were built, one for the driver and one for the passenger.

Figure G33: TED Simulation System Design

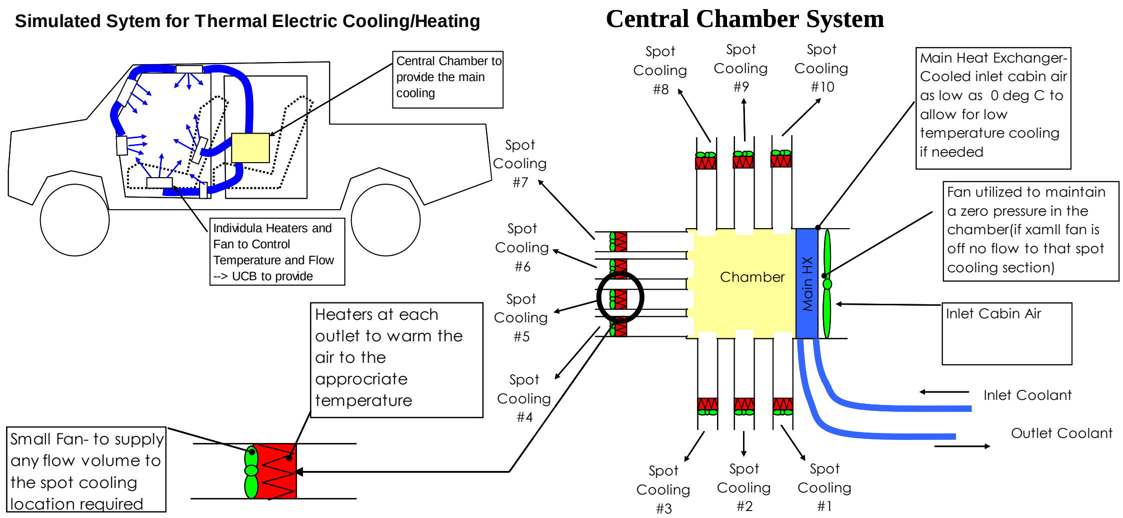

Figure G34 shows a view of the two TED simulation systems from the back of the vehicle with the trunk lift-gate open. Partially hidden behind various instruments in the foreground are the two TED simulation system units in square box shapes. The aluminum grille allows air to be drawn into the chiller to be cooled down. The semi-visible fan behind the grille provides air pressure balance needed for airflow measurement. On top of the "boxes" are low temperature coolant flow connections feeding the chiller inside of the "box".

Figure G34: The TED Simulation System Hosted in the SRX Trunk

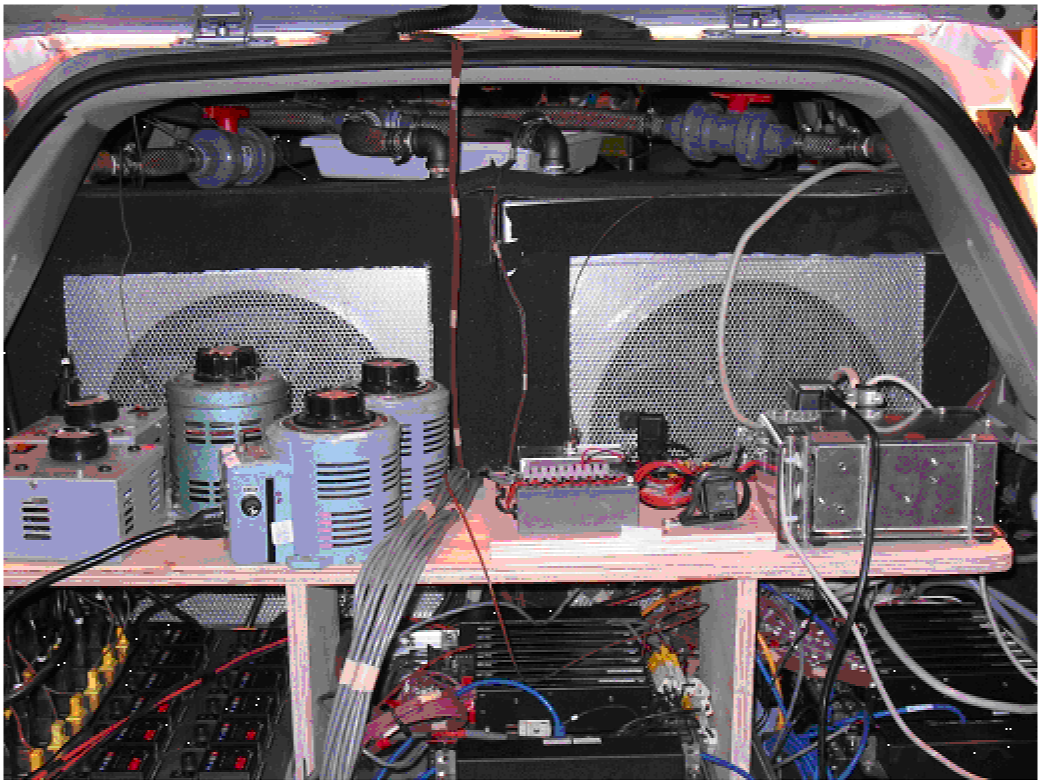

Figure G5 shows two rows of hose connections out of the TED simulation system for a total of 12 hoses connected to the two TED simulation system units. The straight portions out of the units that are wrapped in insulation tape are the electrical heaters used to control the discharge air temperature from the spot cooling nozzles. Imbedded within the hoses are small electrical PWM-controlled fans to meter airflow to each spot cooling nozzle.

Figure G35: Front Side of the TED Simulation System

Two data loggers were used to record the refrigerant temperatures and pressures and the air temperatures in various parts of the vehicle. Other signals such as the HVAC blower voltage and current, engine cooling fan voltage and current, and spot cooling nozzle temperatures were also logged. The two Campbell Scientific CR9000 data loggers are connected through an Ethernet switch to a logging/monitoring laptop computer to provide real-time feedback.

The simulated TED system was airflowed to determine the flow volume versus the PWM frequency input to the blower motors. There were six blowers each for the passenger and the driver. Each blower was operator via a PWM voltage frequency to vary the airflow rate. To determine the amount of flow delivered to the passenger, a calibrated orifice was used to deliver the same airflow that was supplied by the fan to both the passenger and the driver.

G2.5.3 Milestone 3 – Build Mule Vehicle for Thermal Comfort Evaluation Completed

The project's third major milestone, Build Mule Vehicle for Thermal Comfort Evaluation, was successfully completed as scheduled by August 31, 2010. Delphi had lead responsibility for completing this activity. Delphi designed and constructed a thermoelectric device simulation system for the mule vehicle. This simulation system and test instrumentation were installed into the mule vehicle to enable thermal comfort evaluation testing.

G2.6 Task 6 – Perform Design of Experiments (DoE) for Target Platform

The main activity for this task was to perform the second set of human subject testing in a modified mule vehicle inside Delphi's climatic wind tunnel. During the weeks of September 20 through October 7, 2010, the Cadillac SRX with spot cooling was evaluated in the climatic wind tunnel chambers at Lockport, NY. The test matrix included the following studies:

- Solar Calibration
- Automatic Climate Control (ACC) Setting and EHT Relationship Study
- Spot Cooling Steady State Evaluations
    - Individual Spot Cooling Development
    - Combination Spot Cooling Evaluation and Development
    - Spot Cooling Delivery Per Comfort Group Classification
    - Baseline Comfort Study (No Spot Cooling)
    - Automatic AC Set Point Comfort Under Three Given Ambient Conditions
- Spot Cooling Transient Evaluation
- Miscellaneous Development: Cabin Surface Temperature Distribution Measurement

The first evaluation, Solar Calibration, involved placing the vehicle in Delphi Tunnel #2 where the vehicle was calibrated with breath temperatures using the "Full Solar Simulation, Full Spectrum Lighting" to determine the appropriate lighting in Tunnel #5. The calibration included soaking the vehicle at 300 W/m^2, 500 W/m^2, and 1000 W/m^2 to determine the steady state breath temperatures. In Tunnel #5, the lights were added or subtracted to achieve the same breath temperatures as in Tunnel #2 to ensure that the correct solar radiation was being applied.

The second evaluation used the mannequin from UCB to determine the Equivalent Homogeneous Temperature (EHT) for different ambients and different set points on the automatic climate control system. The following combination of ambients, ACC set points, and vehicle conditions was run to determine the EHT for the occupant with no spot cooling.

Thirdly, the vehicle was evaluated to determine the effectiveness of spot cooling at steady-state conditions under various test conditions.

- Spot cooling flow rate based on CFD and UCB recommendations
- Each spot cooling test condition is repeated once
- Each test has passenger and driver riding to provide comfort ratings
- Each test condition is re-run with mannequin

This testing was used to determine the most effective spot cooling locations and conditions. Once these locations were identified, along with the most effective temperature and airflow, the combination cooling evaluations began. The combination cooling evaluation included the following conditions and criteria. Baseline testing was also conducted at the same conditions above to understand the comfort without spot cooling. This provided a good comparison. Lastly, the effect of spot cooling on transient comfort was evaluated for a hot soak condition.

G2.6.1 Spot Cooling Test Results and Analysis

The spot cooling development was accomplished in two stages. Stage I development studied the working of individual spot cooling nozzles to determine their effectiveness. Stage II development evaluated and optimized the combination of the selected individual cooling nozzles to ensure that they work together coherently to provide optimal passenger comfort in a passenger compartment with elevated Equivalent Homogeneous Temperature (EHT). In addition to the two major stages of studies, a set of baseline comfort rides were conducted for 29˚C EHT under the tunnel ambient of 29.4˚C x 55% RH x 500W/m2 solar load. These baseline tests were done to gauge passenger discomfort when spot cooling was not instituted.

G2.6.1.1 Baseline Comfort at 29˚C EHT

During the subjective comfort rides, the UCB comfort evaluation software was used to log the riders' evaluation of their comfort. The software employs two indices: thermal sensation and thermal comfort. The rider's thermal sensation was an indication of the environmental temperature that he or she is experiencing. The rider may feel cold if the temperature is low and he may feel hot if the temperature is high. From cold to hot, there are nine gradations from -4 through 0 to +4, with -4 being the coldest and +4 the hottest (see Figure G36).

Figure G36: Scale for Thermal Sensation and Thermal Comfort

Similar to the thermal sensation scale, the thermal comfort scale also runs from -4 to +4, with -4 being most uncomfortable and +4 most comfortable (see Figure G36). Under steady state conditions, it was expected that a thermal comfort index of +2 is the upper limit. Ratings beyond +2 can only be achieved during transient thermal process, such as when a cold-soaked passenger is exposed to a warm environment. Not fully aware of this limit for the thermal comfort index, some wind tunnel test riders occasionally rated comfort greater than +2.

Figure G37 shows the thermal sensation rating during the 29˚C EHT rides without spot cooling. There are five body parts rated during the rides: Face, Back, Gluteal, Right Hand, and Chest. Additionally, the whole body thermal sensation was also rated. The chart shows consistently warm ratings for the in-car environment among all riders. Each of the body parts registered warm to hot sensation, as did the whole body. The "whole-body" thermal sensation on average was rated at +1.4.

Figure G37: Baseline Thermal Sensation at 29˚C EHT without Spot Cooling

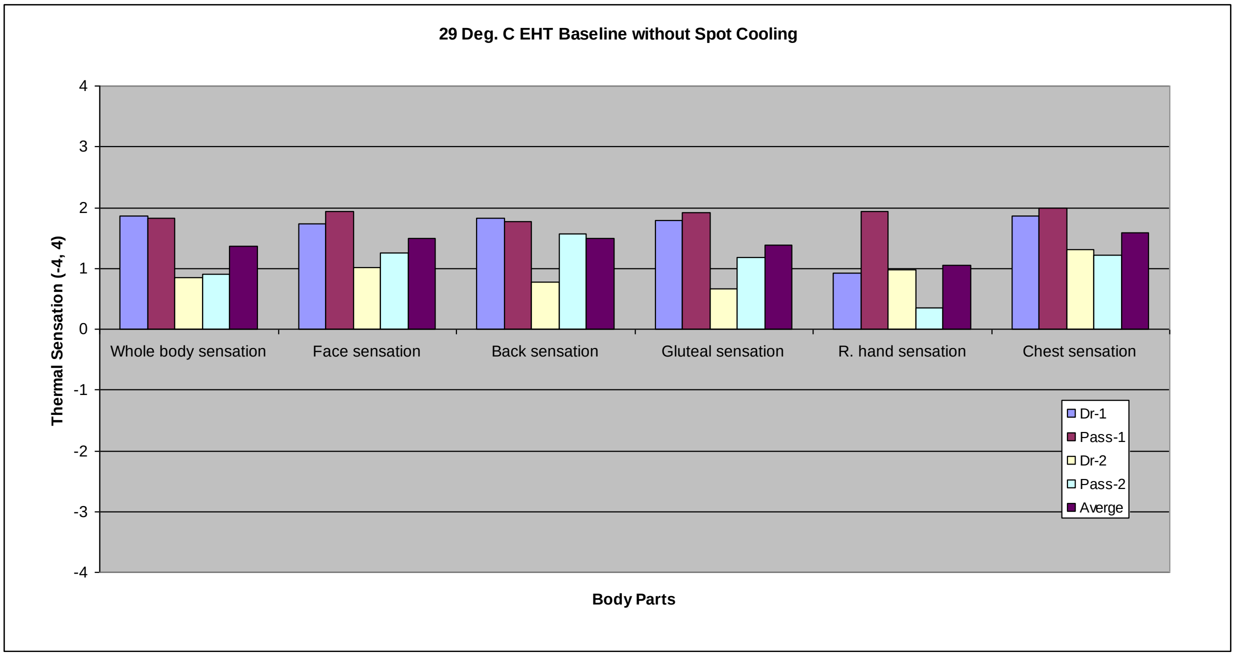

Figure G38 shows the corresponding thermal comfort rating for the 29˚C EHT rides without spot cooling. Most riders rated the riding experience uncomfortable with the average "whole-body" thermal comfort at -0.6. For steady-state comfort, a thermal comfort rating approaching +2 is desired.

Figure G38: Baseline Thermal Comfort at 29˚C EHT without Spot Cooling

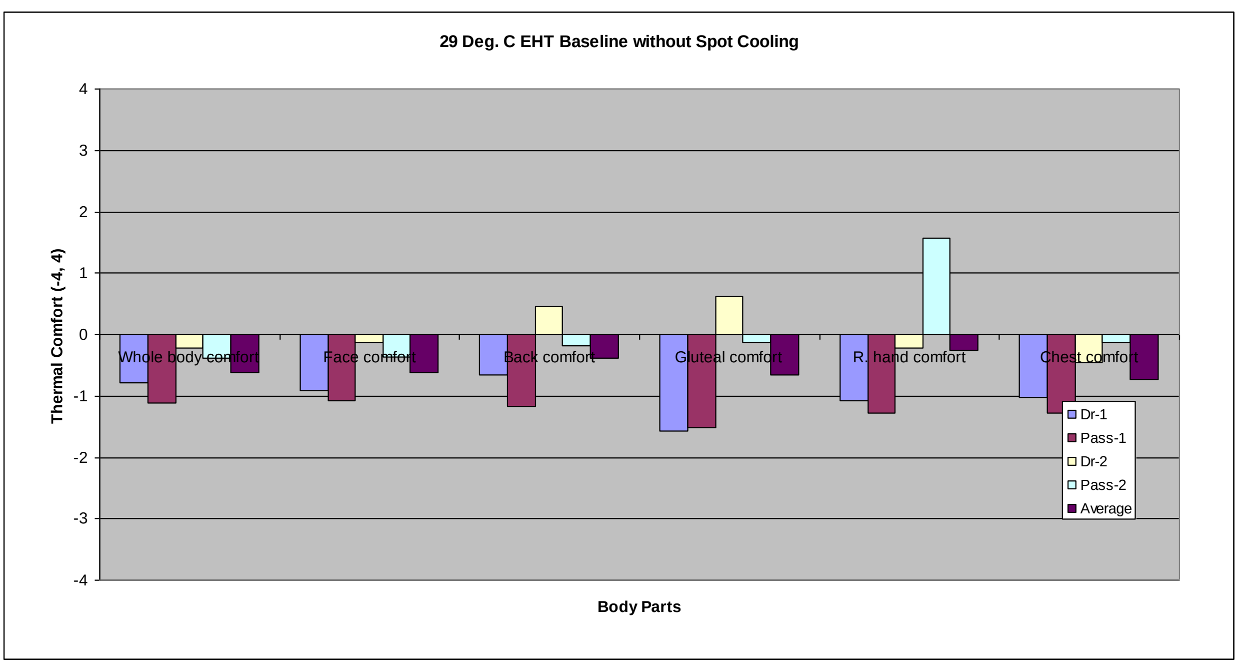

G2.6.1.2 Individual Spot Cooling Studies

For individual spot cooling strategy studies, each of the spot cooling locations was examined under two airflows and two discharge temperatures. The in-car condition was controlled by the Automatic Climate Control system to either 29˚C or 31˚C EHT. The ambient condition used for the most part was 29.4˚C x 55% RH x 500W/m2 solar load. Comfort riders and a mannequin were employed to assess the effectiveness of the spot cooling and to optimize the discharge temperature and the delivery of spot cooling airflow.

The impact on the whole body EHT by the five major cooling locations was evaluated. The EHT whole body impact was not the sole criteria used to select individual cooling locations for further development in cooling combinations; however, the rankings for whole body EHT does coincide with the final selected locations. The rankings were quantified as “recommended”, “marginal”, and “not recommended”.

G2.6.1.3 Combination Cooling Strategy Studies

Based on the individual spot cooling results of the Stage I studies, nozzle locations were selected for the Stage II studies to provide a combination strategy for comfort maintenance. The combination strategy was subjected to optimization development so the most effective comfort cooling delivery could be achieved.

The initial combination strategy was composed of the three spot cooling nozzle locations. The airflow rates used for these nozzles are the lower of the two airflow rates used during the individual spot cooling studies. In comparison with the previously shown baseline case (see Figure G) where most riders rated the in-car conditions as being too warm, the combination of the three-spot-cooling strategies at the same in-car EHT of 29˚C significantly improved the passenger comfort. As a result, the thermal sensation in general is cooler than neutral. The same initial combination strategy was re-evaluated at the in-car temperature of 31˚C EHT. The results of this test show that the degree of over-cooling is reduced by this hotter in-car environment. However, the whole body thermal comfort rating showed a similar drop to +1.4, which still indicates a reasonably comfortable environment.

After the initial combination strategy was tested and evaluated, improvement to the airflow delivery and discharge temperature was made to fine-tune the cooling. The improved delivery settings were tested with another round of vehicle rides. The thermal sensation did move toward neutral for every body part. On average, the whole body thermal sensation is exactly at neutral, but some specific and important body part complaints persisted. Interestingly, the whole body thermal comfort rating did not improve from the previous testing. The average whole body comfort rating was rated at +1.6. This may indicate that the initial combination strategy with the original airflow delivery is harsh and some spot temperatures were too cold, but the whole body thermal comfort is actually better, whereas with the improved airflow delivery and discharge temperature, the objectionable harshness and overcooling were removed, but the overall whole body thermal comfort actually declined. Thus, the improved delivery may be a compromise solution.

During the development rides, it became clear that at least one additional specific body part complaint should be addressed. It had been a consistent detractor from the overall thermal comfort. However, by providing spot cooling to address this “warmth” complaint, a new issue arose from this additional airflow. The team discovered in the quad-combination study that it requires a delicate balance to make the flow acceptable to the riders in order to eliminate the “warmth”, while not creating a new complaint. This study indicated a “whole body comfort” rating of +2.4; there also seemed to be less variation in comfort perception than with the tri-combination configuration. However, more people raised minor complaints about the secondary issue with the additional spot cooling location. Subsequently, the airflow for the additional nozzle was further reduced by using a higher resistance grid at the outlet of the nozzle. The quad combination with low face airflow was further evaluated through comfort rides at the 31ºC EHT. The overall comfort was acceptable and the higher resistance grid seemed to provide a consistent improvement over the original nozzle.

Evaluating the comfort data, the project team concluded that individuals have differing comfort requirements due to age, gender, body fat ratio, bio-cycles, day-to-day health condition variation, weather preconditioning, etc. The subjective data from the comfort rides reflect all this variations. It was further recognized at this point that a single combination strategy would not be able to provide satisfactory comfort to everyone, just as in the case of Automatic Climate Control, where a set point temperature dial is provided to address comfort requirement variations. Subsequently, a multi-tiered combination strategy was devised and tested. The new combination strategies offered four levels of cooling capacity: Extra-High, High, Medium, and Low. The four strategies provided variations in some of the nozzle discharge temperatures for the quad-combination configuration, plus the original tri-combination configuration. With these multi-tiered capacity spot cooling, most people found their comfort satisfied with one of the four discharge levels.

The project team collected the thermal sensation and thermal comfort ratings for the multi-tiered spot cooling delivery during repeat rides at the 37.8ºC x 40% RH x 1000W/m2 solar load and 29.4˚C x 55% RH x500W/m2 solar load. Even though the comfort rating was in general improved and more uniform than before, the comfort rating was not perfect. So we asked the following question, “Given the baseline Automatic Climate Control System, what kind of comfort rating should we expect to see from the riders if they are allowed to make adjustment to the ACC set temperature to satisfy their individual comfort requirement?” The answer to this question is actually quite surprising! The test data indicates that quad spot cooling with multi-tiered capacity delivery is a good system, even in comparison with the traditional Automatic Climate Control systems.

G2.6.1.4 Thermal Mannequin Objective Data Analysis for the Combination Cooling Strategies

Mannequin data were taken during the combination cooling development. The mannequin skin temperature and heat flux were converted into Equivalent Homogeneous Temperature to indicate the comfort of the body part and whole body. The comfort impact of the multi-tiered combination strategies were evaluated for two standard EHT environments. The comfort rating by the mannequin at 29ºC EHT without spot cooling was similar to the subjective thermal sensation and thermal comfort ratings of human riders who were warm and uncomfortable. The comfort level when the in-car control is set at 24ºC EHT is acceptable for most people. However, the hands, forearm, and upper arm are overcooled.

The multi-tiered spot cooling strategies were tested under the elevated in-car environment of 29ºC EHT. The ambient condition was 29.4ºC x 55% RH x 500W/m2 solar load. With the general in-car environment at 29ºC EHT and with the combination spot cooling turned on at various levels of cooling capacity, the in-car comfort was significantly improved without the side effect of hand/arm overcooling. The team also studied the impact of the ambient condition on the in-car comfort. For both of the ambient conditions (75ºF x 65% RH x 300W/m2 solar load and 85ºF x 55% RH x 500W/m2 solar load), it can be seen that the capacity level of the spot cooling made a difference in the body part comfort, but the ambient temperature change did not have any impact on the in-car comfort.

G2.6.1.5 CFD Analysis of Spot Cooling

After all the tunnel tests were completed, the CAD model of the SRX cabin was updated with all the nozzle locations built into the SRX vehicle. CFD analysis was run post-factum to understand the airflow around the occupants for the final optimized combination cooling tested in the tunnel. In general, the airflow distribution was about the same as the CFD results predicted before the tunnel, but the body surface air velocity was slightly higher. The higher body surface velocities were attributed to the nozzles being closer to the passengers than originally planned due to the large diameter tubes supplying airflow to the nozzles in the vehicle. For the quad combination spot cooling when conventional HVAC was turned off, the CFD analysis identified the velocity contour around the passengers at 7.5mm above the passenger's skin. It is clearly evident that the airflow velocities in both their magnitude and distribution were quite uniform over the entire upper body in cooling mode.

Based on the tunnel configuration, the CAD of the SRX cabin was updated to mimic the test conditions. The changes that were made to the CAD included removing the rear seat and replacing it with two large TE simulations boxes in the rear of the car along with the instrument boxes in the trunk. The nozzles locations were same as tested in the tunnel. The CAD of the dummies was a 50-percentile male in the CFD model, as opposed to varied range of individuals of both gender for tests. The more accurate, but computationally intensive, Discrete Ordinates (DO) Radiation model was applied for Solar Load simulation.

The primary objective of enhancing the CFD model after the tunnel tests was to improve the accuracy of prediction so that good correlation could be obtained with test data in terms of airflow distribution and comfort prediction. The model was run at the tunnel conditions. The inputs to the CFD model were: a) Solar load into the cabin, b) AC vent airflow, and c) AC vent temperatures were obtained from test data at specific ambient conditions. A simplified version of the Sunroof model was added to the CFD simulation to better mimic the roof's thermal condition. Mostly, the two front passenger breath temperatures were used to correlate the CFD model with test data for the baseline case when spot cooling was turned off.

Quite a few pre-runs were conducted to evaluate the sensitivity of HVAC vent directivity towards the passenger on front breath temperature. From the CFD analysis, it was found that the front breath temperatures could vary by as much as 4ºC due to different airflow directions from the AC vents towards the passengers. The AC vent airflow into the cabin was not directly measured during the tunnel tests, so the airflow at a particular in-car set point was estimated from indirect HVAC module pressure drop and fan power data. 105 CFM airflow was estimated for 88ºF / 55 RH under solar load test condition to obtain a 29ºC in-car condition. The AC vent outlet air temperatures were measured in the car.

Figure G39 shows the airflow path lines for the baseline case when spot cooling was off. From test data, 103 CFM airflow at 17ºC was forced into the cabin by the automatic climate control system at 88ºF x 55% RH x 500 w/m^2 solar load with the automatic climate control set to outside air / partial recirculation mode. These conditions were imposed as the boundary conditions for the CFD model.

Figure G40 shows the velocity vectors in the mid-plane of the driver dummy. A number of complex circulatory cells are visible from the velocity vector plot. Figure G shows how the high velocity air hits the upper body of the driver in the facial region contributing to cooler breath temperature. Even though the in-car condition was around 29-30ºC, the breath level temperature was around 25-27ºC in the front of the vehicle for baseline case when no spot cooling was employed.

Figure G39: Airflow path lines originating from front HVAC AC vents

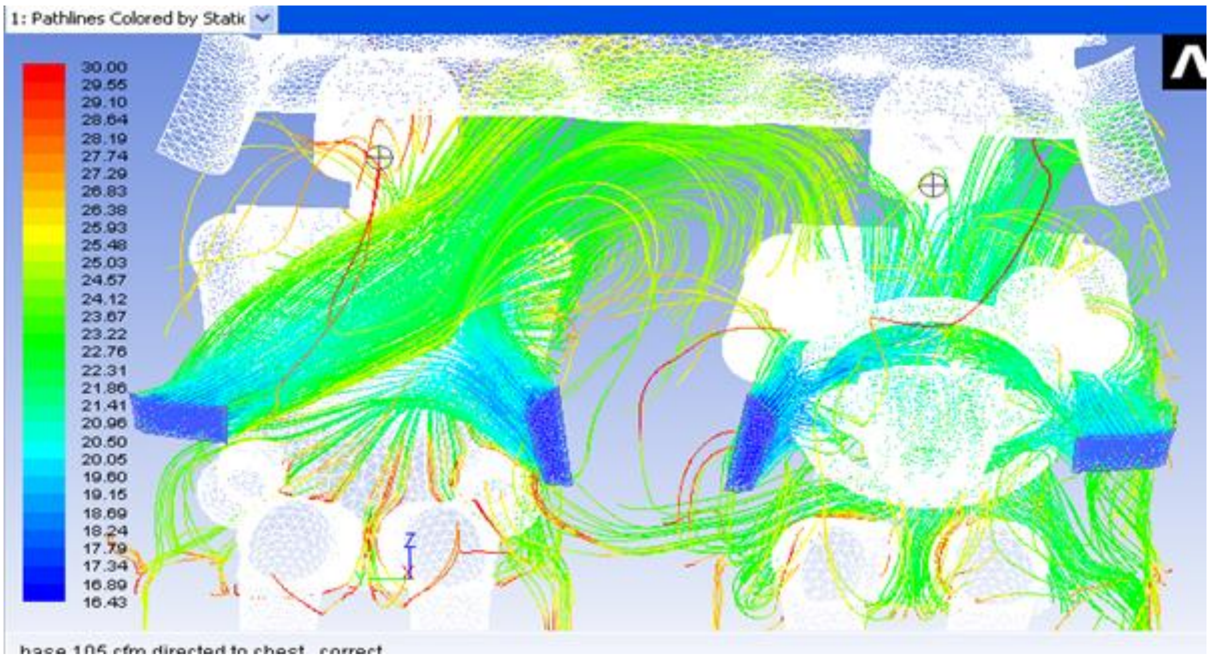

Figure G40: Air Velocity Vectors at mid-plane of the driver for Baseline case (Box model)

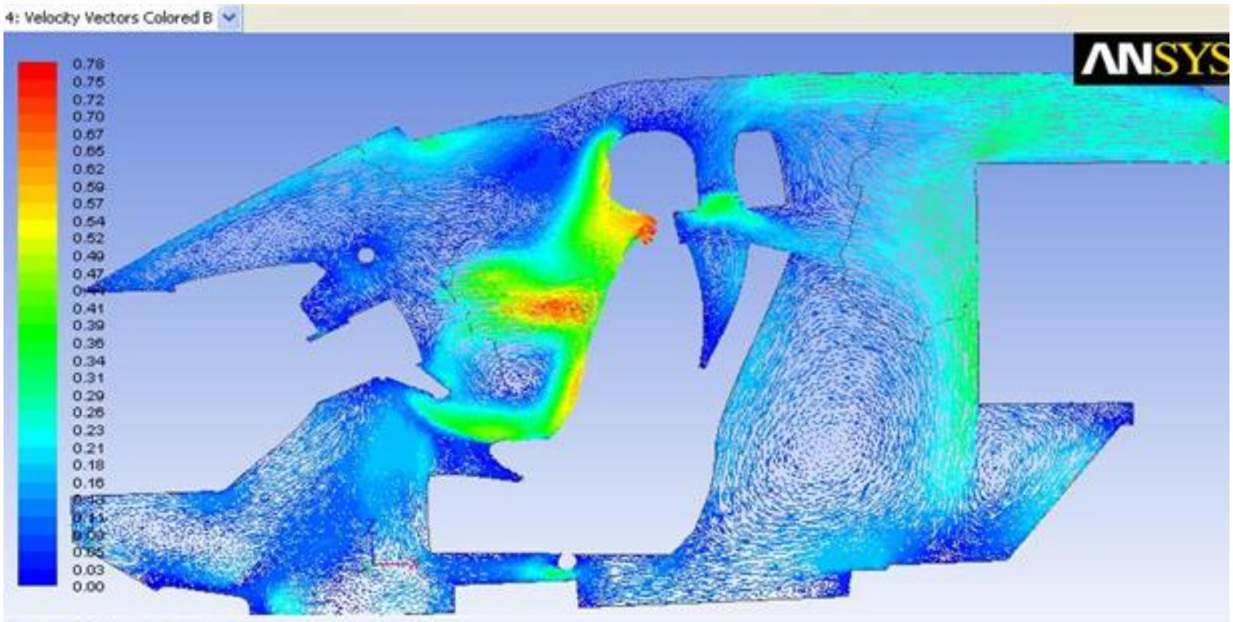

Figure G41: Velocity contours around the face due to front HVAC AC vent airflow for Baseline

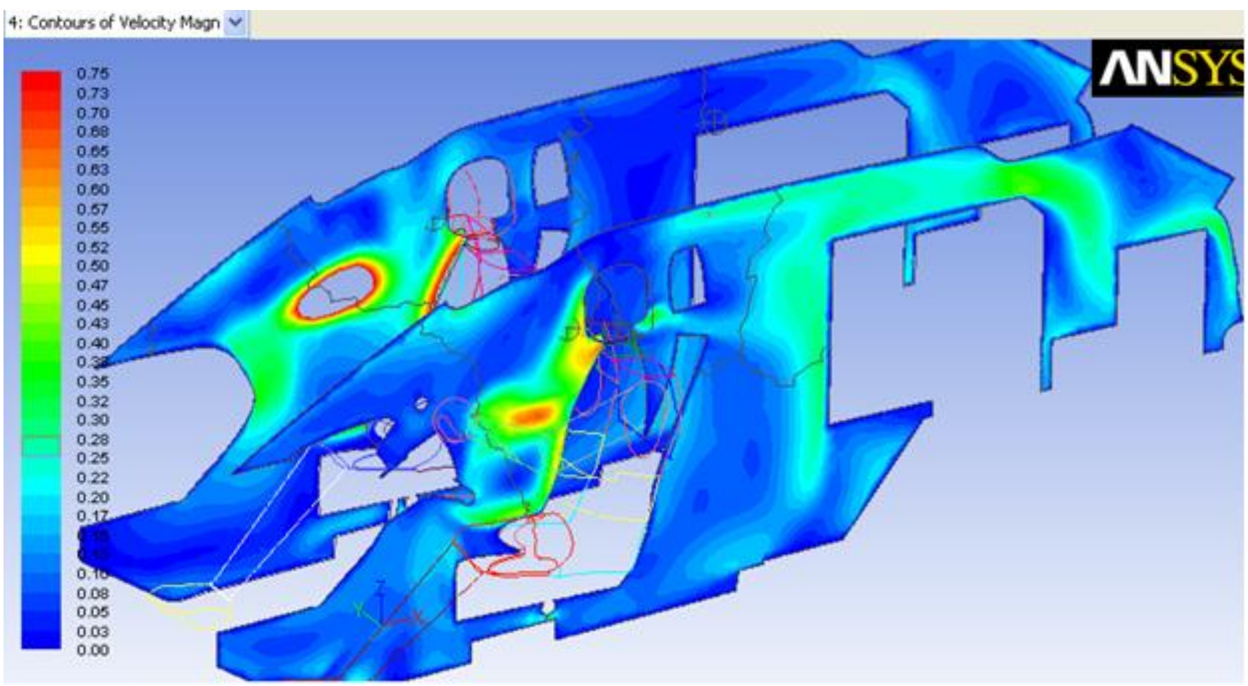

The CFD analysis showed the path-lines when spot cooling was turned on in conjunction with conventional HVAC air. The analysis also showed the temperature and velocity around the occupant when spot cooling was turned on. From this CFD run, it was observed that the front breath temperatures were lower by 1-3ºC than the baseline case when spot cooling was off. As expected, the air temperatures around the occupant were much closer to the nozzle air temperature of 24ºC.

The primary metric of significance that was used to compare the accuracy of the CFD model with test data was the front driver and passenger breath level temperatures. In the CFD model, the dummies were 50-percentile males. For the test data, thermocouples were hung a little higher and in front of the location specified for a 50-percentile male. The team performed a comparison of all the glass temperatures and the breath level temperatures from the CFD analysis with test data. Overall, the correlation was found to be quite good. The breath level temperature variations with test data were within < 2ºC. The correlation for all the windows, i.e., the glass and roof temperatures, were much better for the full cabin model.

There can be many factors contributing to variation between test data and CFD predictions. Uncertainty in HVAC airflow, directivity of the HVAC vents, uncertainty in material properties, and variance of the tunnel lights radiation intensity and spectra from the actual diffuse solar radiation found outside the car are thought to be the primary variables. For design purposes of multi-physics complex real life in-situ automotive HVAC systems with spot cooling, the accuracy of CFD prediction was quite good. Therefore, this approach was followed to rank order designs in AC and Heater mode in the later stages of the project.

G2.6.2 Spot Heating Test Results and Analysis

The team conducted spot heating tests in the climatic wind tunnel during the period of March 21 through April 11, 2011. Figure G42 shows the cabin EHT curve as a function of the in-car set temperature for the automatic climate control system. Different temperature scales are used for the vertical and horizontal axis in the chart as a matter of convenience. The temperature in the vehicle was set in degrees Fahrenheit for higher accuracy, while normal analysis was done in degrees Celsius.

Figure G42: Cabin EHT vs. HVAC Automatic Set Point

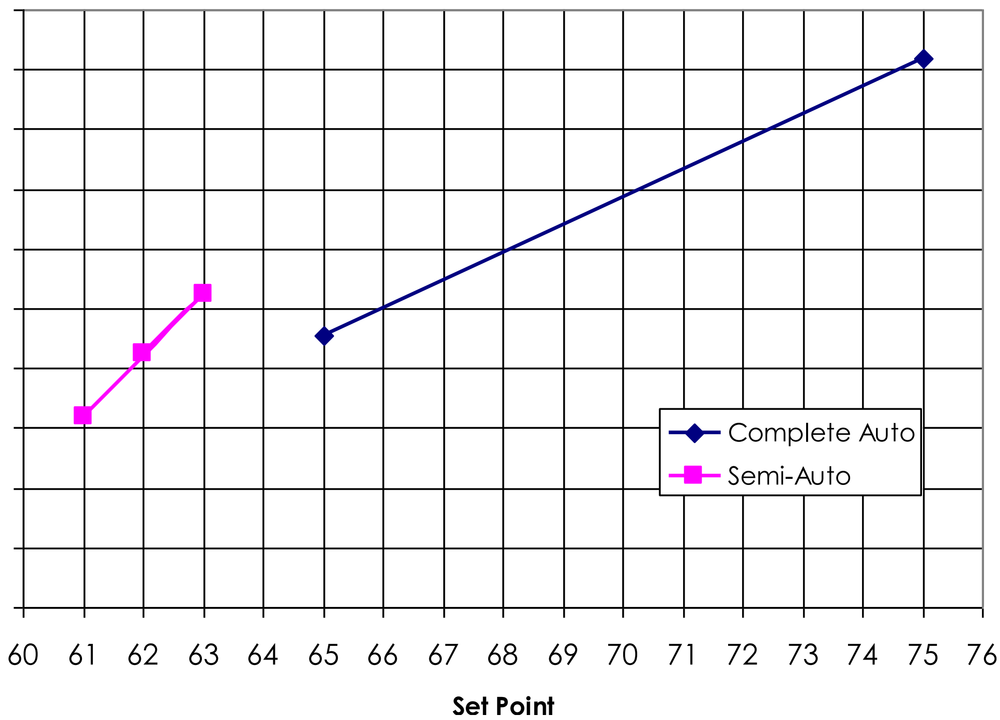

The manual HVAC settings were used to study the impact of the discharge temperature on body part EHT temperatures. In the manual settings, the blower voltage was overridden to 3 volts, and the discharge temperature was at the target level. The discharge mode was overridden to heater. These manual settings were determined to provide approximately the same amount of air discharge enthalpy from the HVAC system heater outlets as that when the HVAC system was in semi-auto mode. The subjective comfort rating from car riders was measured for the baseline EHT cabin. It was observed that most people indicated low thermal sensation and low thermal comfort.

G2.3.2.1 CFD Analysis of Spot Heating

A CFD model was developed to simulate the vehicle in winter conditions. The challenges involved in developing the Heater Mode CFD model were the following.

1. The model had to comprehend convective & radiation heat loss from warm cabin to ambient accurately.
2. Since the vehicle potentially operated at low HVAC heater flows with spot heating, the vehicle thus operated in a weak convection regime. In weak convection regimes, radiation flux from within the vehicle, especially from the warm occupants, become very important.
3. Body heat from the occupants and clothing effects needed to be modeled.

4. Unlike spot cooling where temperature differential was small, the temperature differential in spot heating was significantly large and had to be taken into account.
5. Overall energy budget heat loss from the cabin (radiation + convection), body heat into & lost from the cabin, and energy expended (thermoelectrically or otherwise) to heat up the spot heating air had to be accounted for accurately in the CFD simulation and spot heating design.

In order to capture the radiation effects, the more accurate but computationally expensive DO (Discrete Ordinates) Radiation model was used in CFD analysis. The fine flow aligned mesh was developed to capture the entrainment dynamics accurately. Body heat was modeled through heat-source terms in the CFD model. Natural convection effects in the cabin were captured through density dependent air properties.

Design of the spot heating system was done for simulations run at a vehicle speed of 30 mph with no-solar load ambient condition. Initially the baseline CFD ran with no spot heating; heater discharge temperatures and airflow were varied to maintain in-car cabin conditions from cool to warm with a range of outside temperatures.

G2.6.3 Milestone 5 – Identify final set of locations for distributed heating/cooling

The project's fifth major milestone, Build Mule Vehicle for thermal comfort Evaluation, was successfully completed as scheduled by April 29, 2011. After examining the heating/cooling performance (both modeled and measured) for various nozzle positions, the team identified the final set of optimal locations for use in further developing the distributed TE HVAC system.

CHAPTER G3:
GM Phase 2 – Exploratory Development

The focus of this phase was to develop the initial prototype distributed HVAC components and to evaluate them on both a test bench and a mule vehicle. At the beginning of this phase, the team changed the mainstream demonstration vehicle to an eAssist Buick LaCrosse. At the conclusion of this phase, a go / no-go decision was successfully passed based on expectations of achieving the primary project objective. For this phase, GM utilized Delphi to develop most initial prototype HVAC components with the addition of Faurecia to develop prototype seats and Marlow Industries to develop a prototype TE-based heater for the Volt. UCB supported control strategies and tunnel tests while continuing their primary Phase 1 activities in parallel.

G3.1 Task 7 – Project Management and Planning

The planning and coordination for this phase primarily utilized weekly team meetings. The addition of an alternative set of prototype seats plus delays in securing support for prototype controls development resulted in several months delay for this phase and the overall project.

G3.2 Task 8 – Define New Comfort Component Specifications

A key goal of the project was to demonstrate thermoelectric devices (TEDs) with COPs of 1.3 for cooling and 2.3 for heating. The project team originally estimated air-based TED designs in August 2011. In September, a coolant-based TE HVAC system was selected as the best overall, where coolant would be used for the thermoelectric exhaust. Accordingly, the team updated its detailed analysis and component specifications. In summary, COPs of 1.3 and 2.3 for cooling and heating were the design targets; however, this level of performance drove larger packaging sizes and significantly higher costs than those associated with slightly lower COPs.

G3.3 Task 9 – Define Control Strategies and Algorithms

A strategy for the controls of the supplemental thermoelectric HVAC system and the coordination with the OEM automatic climate control system were developed. The automatic climate control algorithm used in production for the Buick Lacrosse was very complex, and it was deemed impractical for the project team to modify this source code for the demonstration vehicle. Ultimately, the team selected a control set point temperature offset that was indexed in real-time by the calculated HVAC power. The real time HVAC power was calculated from the discharge temperature and discharge airflow rate. The stability of this calculation for controls was unproven, but filters were applied to help stabilize this value.

G3.3.1 Initial Control Strategy Development

Mechanization of this control scheme with a coolant-based TE exhaust system was developed. H-bridges were used to drive PWM output for the TEDs. The team identified off the shelf control hardware with custom software that was obtained from Intrepid. Delphi designed and built custom interfacing hardware. The Intrepid controllers can communicate with the existing

Campbell dataloggers to synchronize and record the system data. The system mechanization to implement the team's control strategy is shown below in Figure G43 through Figure G45.

Figure G43: Control system mechanization using Intrepid controllers

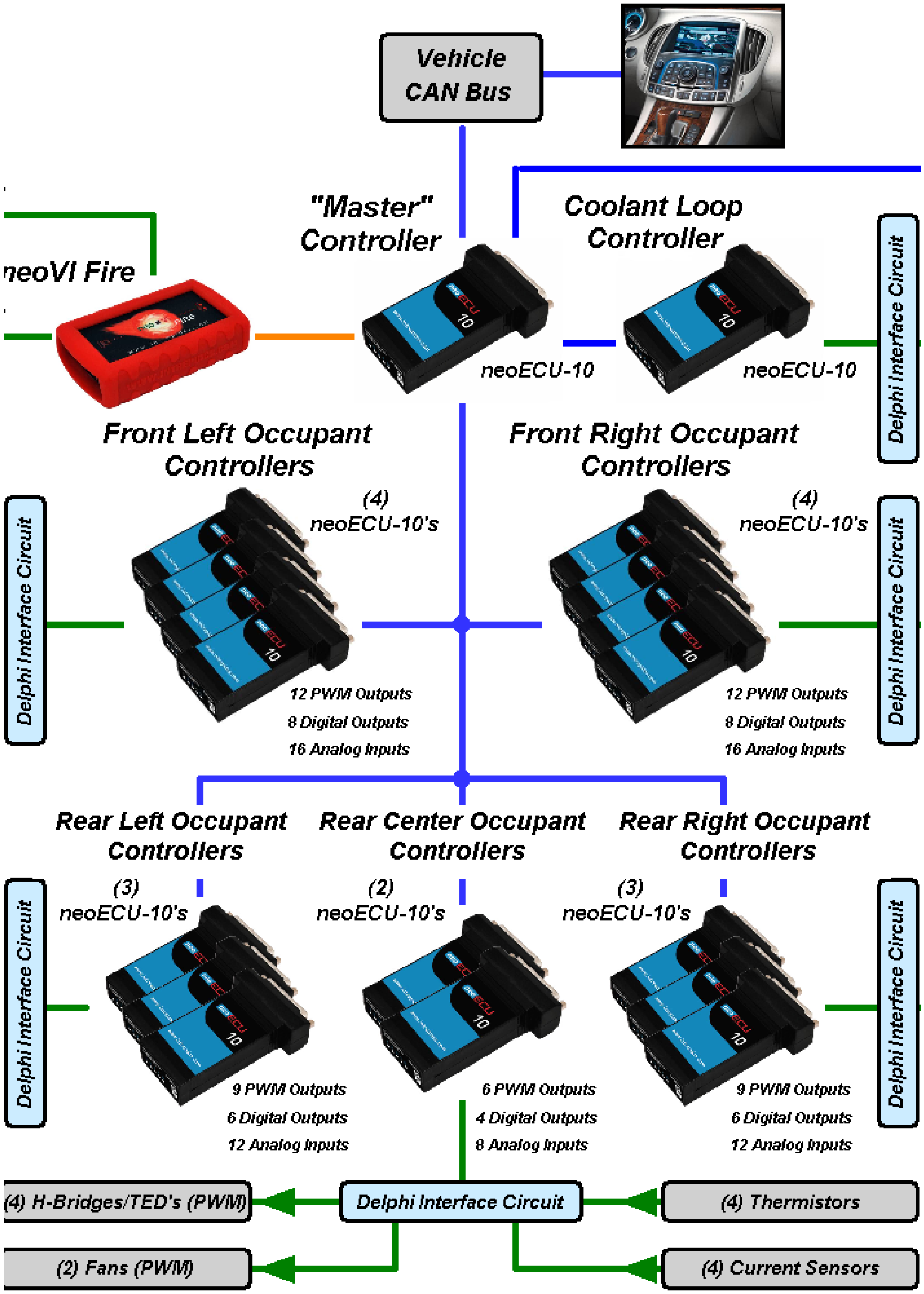

Figure G44: Control system mechanization using Intrepid controllers and remotes

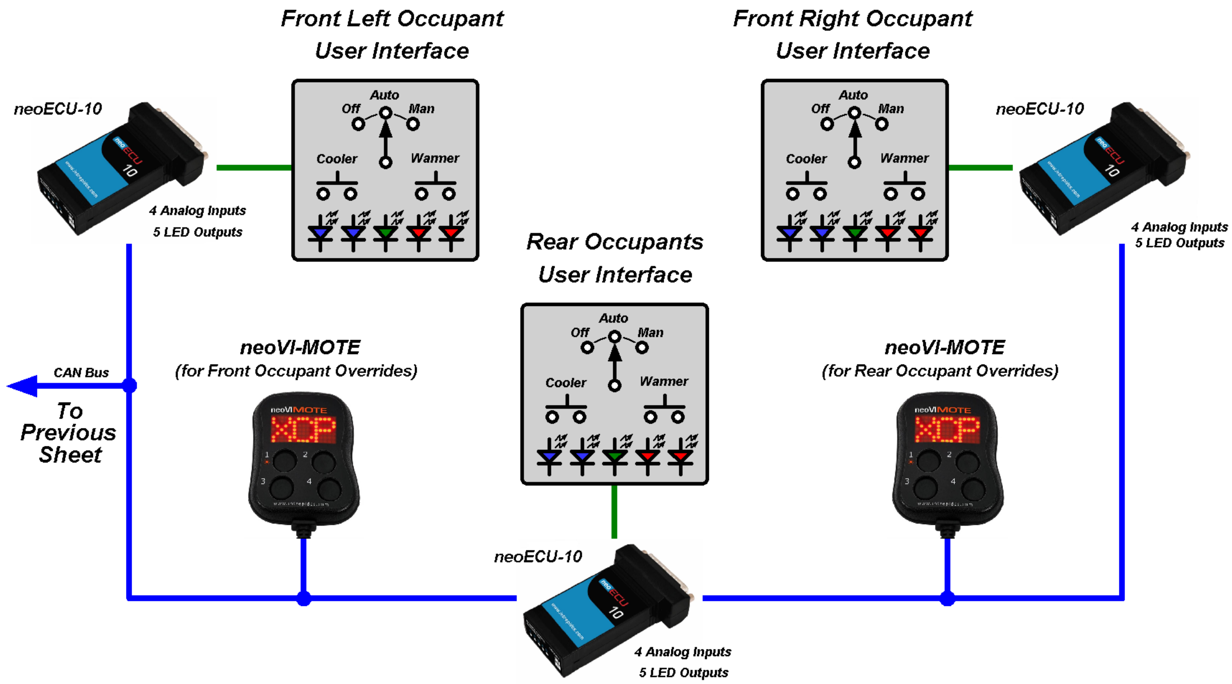

Figure G45: PWM H-Bridge, TED, and Fan Wiring Details

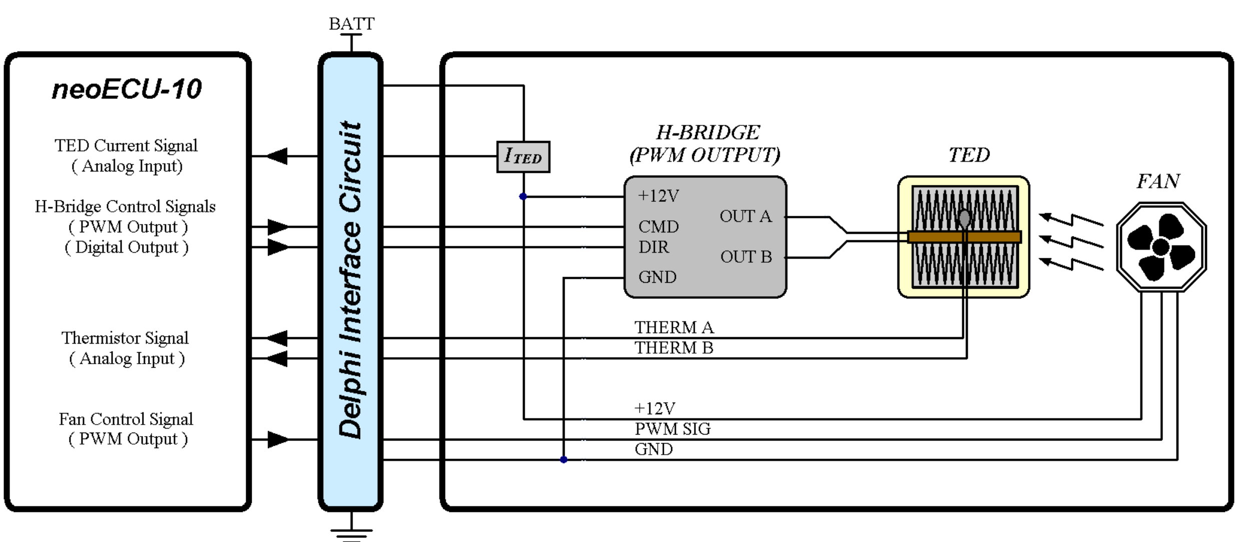

G3.3.2 Milestone 6 – Specify interface between GM & Delphi controllers completed

The project team completed the “Specify interface between GM & Delphi controllers” milestone on December 19, 2011. This milestone marked the project team’s agreement on a control strategy for the interface and integration of the central HVAC system with the prototype distributed HVAC system. The system mechanization to implement this control strategy is shown above in Figure G43 through Figure G45.

G3.3.3 Further Controls and Control Strategy Development

The control development activity spanned several fronts, each key to being able to test and develop the TED concept. These fronts included the development of control strategies, initial system calibrations, design & fabrication of support electronics, and configuration for data logging. The control strategy developed by the project team focused on the following areas:

- Partitioning control over a network of controllers.
- Providing the vehicle occupants with a method to bias or override the operation of their seat.
- Providing a control method for conditioning the coolant used with the TEDs.
- Providing a method to insure that the TEDs are operated within nominal conditions and only when sufficient cooling is being provided.
- Providing a "bypass" control method to allow individual control of each device to foster easier system checkout and development.
- Defining low level drivers for interfacing with various system sensors and control devices.

G3.3.3.1 Control Hardware

User control panels were developed and integrated into the vehicle. These can be seen in Figure G46 and Figure G47. These panels provided the occupants with a means to make adjustments to the TE HVAC system operation as desired. The front control panels were integrated into the center console of the Buick LaCrosse with labeling oriented for easy reading from the intended seating position. Each front seat had five inputs for setting automatic operation, manual operation, or to turn the system off. LEDs and switch ring lights provided user feedback on the state of operation. Similarly, the rear seat controls were mounted in the flip-down armrest located in the center of the rear seat. In addition to the functionality of the front control panel, the rear panel also was used to specify whether the rear seating positions were occupied by pressing the "Left On" or "Right On" switches.

Figure G46: Front seat system control panels

Figure G47: Rear seat system control panel close up

The software test bench consisted of several parts designed and built by Delphi. This resulted in a station that could simulate the entire coolant system, any seat of the system, and the control panels. Figure G48 shows the ECU10 mounting rack, bench wiring, and system simulator.

Figure G48: Software test / debug bench

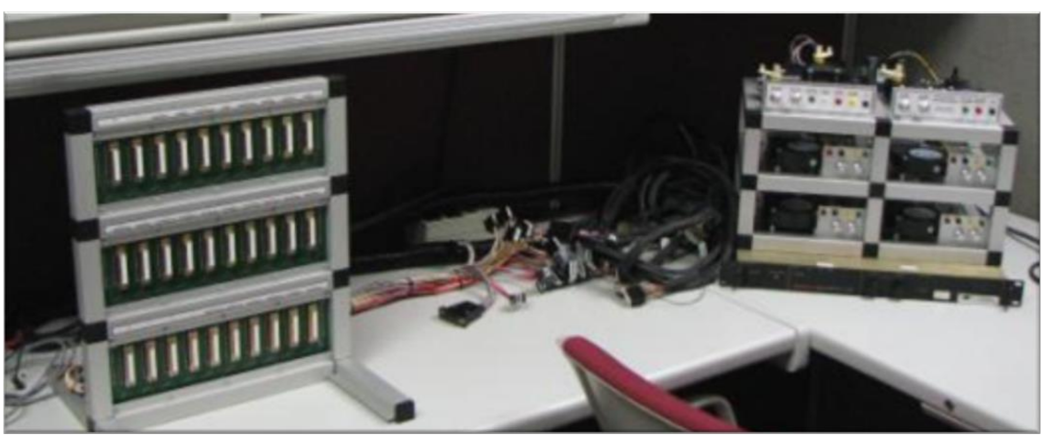

G3.3.3.2 Control Software

The effort required to program and debug the software for the Intrepid vehicle development control system was substantially more than originally planned. Considerable time was spent in the testing and refinement of the control software to meet prototype HVAC system requirements. The complexity of the control system development was due to the large number of controllers, the number of devices that needed management, and bugs within the firmware of the Intrepid controllers that were discovered by this project. The unexpectedly high complexity has delayed the completion of this task from the second quarter to the third quarter, and this has forced the delay of several key project activities including the climatic wind tunnel testing.

G3.3.3.3 Campbell Data Logging

The project team configured the Intrepid vehicle development control system and software to interface with two Campbell data loggers. Both physical units can be accessed and their information logged with the rest of the system data into a common data file. There are approximately two hundred data channels wired from the car to the data loggers.

G3.4 Task 10 – Build and Demonstrate Function-Intent Components

G3.4.1 Development of initial prototype thermoelectric devices

G3.4.1.1 TED Subassembly Packaging

Based on previous testing results, the plan were to have TED subassemblies in the seat bottom, seat back, knee bolster, and the roof. The available real estate in the roof area of any light-duty vehicle is generally quite limited. With sunroofs including oversized units being a reality for many vehicles, the packaging space for roof mounting of thermoelectrics is significantly constrained. The team focused on packaging in the roof with the expectation that packaging near the knee bolster and in the seat would not be so constrained. There was also a possibility to remote-mount the fan to gain packaging space. The team tentatively selected a dual fan design with one fan/motor assembly on each side of a person's head and located in the roof.

G3.4.1.2 TED System Options

The team made formal trade-off assessments for the initial prototype designs to ensure that all relevant aspects were considered. Engineering Value Analysis (Pugh Analysis) was used to allow weighting for each of the selected parameters. These weighting were then multiplied by a numerical rating for each parameter and then sum totaled. The project team considered four possible system options:

- Cabin air-based TEDs
- HVAC module air-based TEDs
- Coolant-based exhaust air TEDs
- Hybrid-system consisting of a combination of HVAC module air and coolant based TEDs

The coolant based exhaust air TED system ranks the highest overall, but less than 10% better than the HVAC-air based TED system. The engineering estimated costs of all systems are relatively high. The cost is driven primarily by the significant number of fans, TEDs, and PWM controllers needed. As such, the team is presently working on ways to change the design and thereby reduce cost.

G3.4.1.3 TED Development

The project team developed optimum solutions for cooling and heating with thermoelectrics based upon the initial requirements specified by the team for the distributed cooling and heating system. The initial design utilized air on the waste side to provide the heat rejection during cooling and heat utilization during heating. However, after several iterations, it was determined that air on the waste side was not satisfactory. Therefore, design concepts for air-to-water configurations were developed and completed. COP vs. cost plots were evaluated to understand the return on more couples. For seat heating in Figure G, ~400 couples were required to achieve the 2.3 COP target. However, a 25% reduction in couples resulted in only an 8.5% reduction in the COP, indicating a high relative cost for that last increment of efficiency.

Figure G49: Seat Heating COP vs. # of Couples

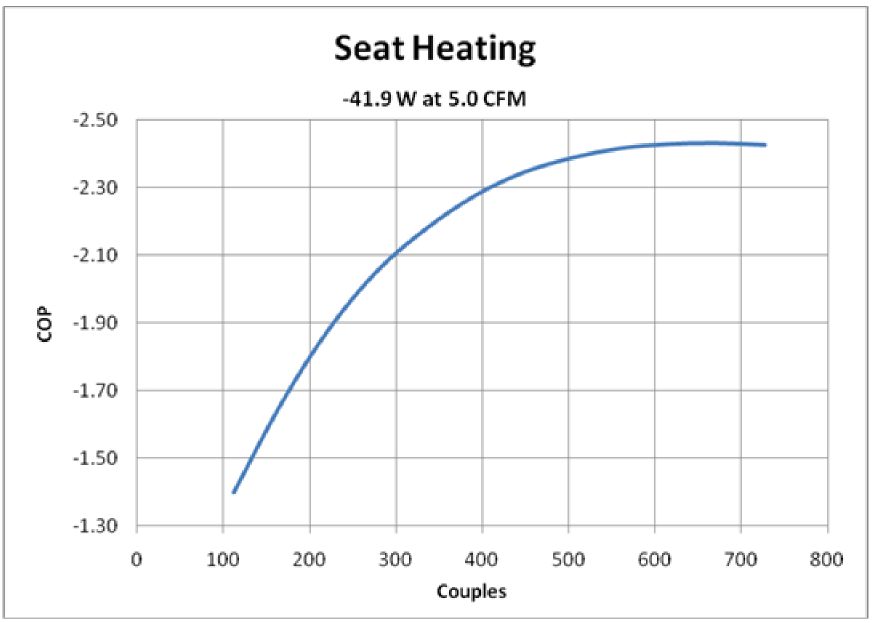

Based on these simulations, the team determined that the final set of recommended designs would feature two sizes, a small TED with 224 couples and a large TED with 336 couples. This approach gave the team flexibility to provide a wide range in the number of couples (from 224 with 1 small TED to 672 with 2 large TEDs). By using 1 or 2 TEDs at each position, these two TED sizes were able to supply an appropriate amount of TE material to meet the requirements of each location, e.g., seat, feet, lap, and chest. The TED designs required 20 large TEDs with 336 couples and 12 small TEDs with 224 couples to support the initial prototype components.

G3.4.1.4 *Fan & Blower Development*

An initial fan and blower selection from EBM-PAPST was evaluated. Each blower was operated via a PWM voltage frequency to vary the airflow rate. To determine the amount of flow delivered to the passenger, a calibrated orifice was used to supply the same airflow that was delivered by the fan, and the pressure was recorded to understand the fan's performance. The initial fan and blower selected showed adequate flow, but its size was large, measuring 120mm x 120mm x 25mm. It was subsequently decided that a higher flow blower might be required for the thermoelectric designs. A Delta Fan was then identified that provided slightly more flow (as shown inFigure G50) at a higher delta P. However, the main benefit was in the package size, which was reduced from 120mm x 120mm x 25mm to 95mm x 95mm x 25mm. The increase in flow and significant reduction in size provides an optimum solution.

Figure G50: Delta Fan Flow and Delta P versus Resistance

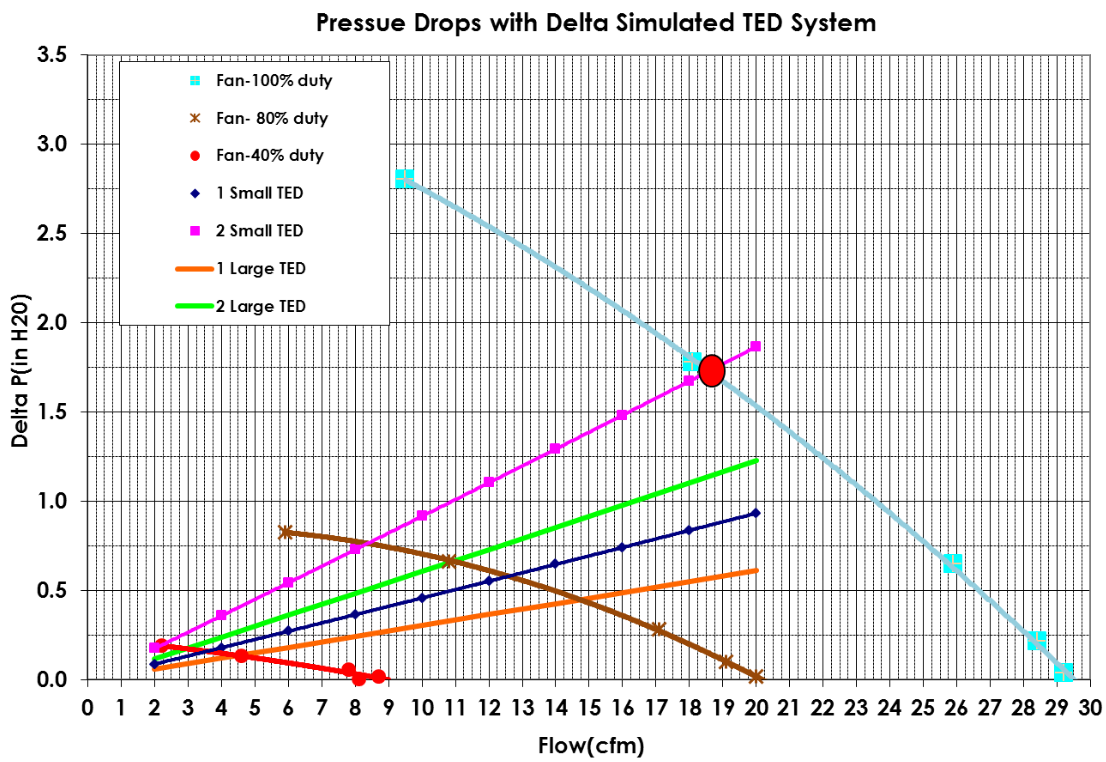

G3.4.2 Development of initial prototype TE-based cabin heater for Volt

The original project statement was amended to include the development of distributed HVAC components for electrified vehicles like the Chevrolet Volt. A key focus for this activity was to develop a TE-based alternative to the resistive cabin heater currently used in production for the Volt. During cold weather, electric vehicles must allocate a significant portion of the energy in their batteries to warm the cabin for the passengers, thereby reducing the effective electric-only range of the vehicle. This development effort used TE devices to provide improved heating efficiency beyond the existing electrical resistive heater. To accomplish this objective, a Plate and Frame heat exchanger concept was proposed that was designed specifically for use in conjunction with TE technology. This development activity is described below.

G3.4.2.1 Initial Design Concept for TE modules - Plate and Frame Exchanger System

The goal of the design concept was to achieve a thermal system that integrated multiple TE modules and exchanger plates into a compact package while improving heat transfer across the active surfaces. The final thermal system is to operate within the outlined specifications regarding electrical input power, performance, volumetric flow rates, pressure drops, available pump power, and other various attributes. The initial Plate and Frame Exchanger concept is shown in Figure G. This approach to the alternative heater design had the following characteristics:

- Segmented platform design that allows for expandability.
- Symmetrical design reduces number of parts.
- Parallel flow paths reduce pressure drop.
- TE modules are thermally in parallel. Can be electrically arranged is series, parallel or series/parallel circuit.
- Enhanced Plate and Frame exchanger design with improved heat transfer coefficient utilizing wire mesh screen.
- Compact size versus capacity.

Figure G51: Initial Plate and Frame Exchanger design concept

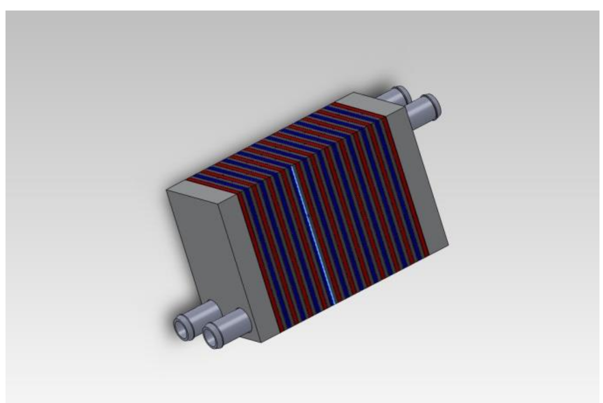

G3.4.2.2 Initial Prototype Configuration and Performance Testing

The initial prototype for validating the enhanced plate and frame exchanger concept was constructed using two rectangular plates of Lexan material, which functioned as end plates and formed the “frame” part of the exchanger. Placed in between the plates were two wire mesh screens separated by a single, thin metal plate to define the two independent flow paths along with the appropriate gaskets. This allowed multiple wire mesh sizes to be quickly evaluated with the least test variability. The prototype exchanger was instrumented to measure flow rates, pressure drops, and temperatures of both inlet and outlet sides along with power accepted into and rejected from each flow stream. The data was used to calculate the heat transfer and effective heat transfer coefficient for the different wire mesh screens tested. Based on the test data, the 8x8x063 wire screen mesh size was determined to provide the best overall performance for the given flow rate and pressure drop. Additional testing was performed using a single SP2297 TE module with the 8x8x063 wire mesh screen in the prototype system. This test yielded a total Q of 379 watts rejected into the hot side fluid stream with an input power of 257 watts to the TE module. 122 watts were transferred via the cold side.

To further improve the heating efficiency of the initial design, an enhanced Plate and Frame concept was proposed. The technical challenges addressed with the beta concept include:

- Thermal interface optimization
- Gasket optimization
- Plate material optimization
- Mesh orientation optimization
- High voltage experimental setup
- Beta prototype design

By increasing the thermal contact area, the COP of the alpha prototype was increased from 1.37 to 1.59. This represents a 14% decrease in necessary power to the TEC. These results were also verified using the alpha prototype with two TEG layers, showing heat flux to be additive with number of TECs while maintaining a constant COP.

Pressure paper tests were also performed on the Alpha prototype with 20 TEC layers to verify even pressure distribution throughout the system. However, there were several layers with “hot spots” indicating higher pressures (see Figure G52). These were the result of inconsistent mesh thickness. Proprietary methods were developed to overcome this “hot spot” issue.

Figure G52: Hot Spots on Grafoil and Pressure Paper

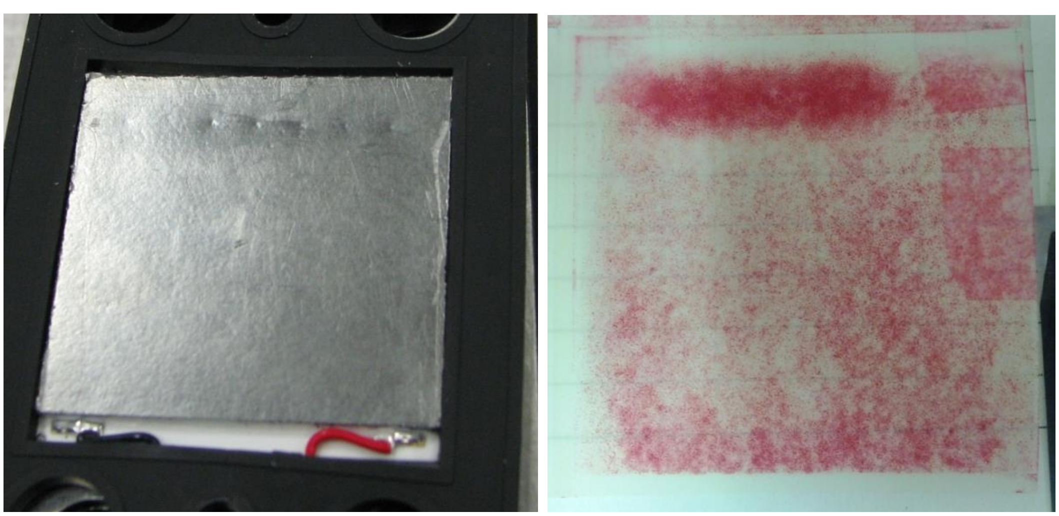

Prior to this point, the gaskets were in their original form. However, several design parameters were not believed to be optimized and, thus, changes were implemented. The new design accomplished two things: 1) increased U-value and 2) lowered pressure drop across the exchanger. The U-value increased approximately 26% using the new gasket design. The most obvious reason for this to occur would be due to a more efficient use of the heat transfer area. We hypothesized that the original design focused most of the water diagonally from one port to another. By opening up the entrance region, the water could more freely flow across the entire surface of the mesh. The ability to more freely flow across the entire mesh led to the second benefit: lower pressure drop. The water no longer had to fit through the small neck present in the original design, but could now spread out across the entire area. This led to a decrease in pressure drop of ~50% depending on the flow rate (see Figure G54).

Figure G53: Pressure Drop versus Flow Rate for the Two Gasket Designs

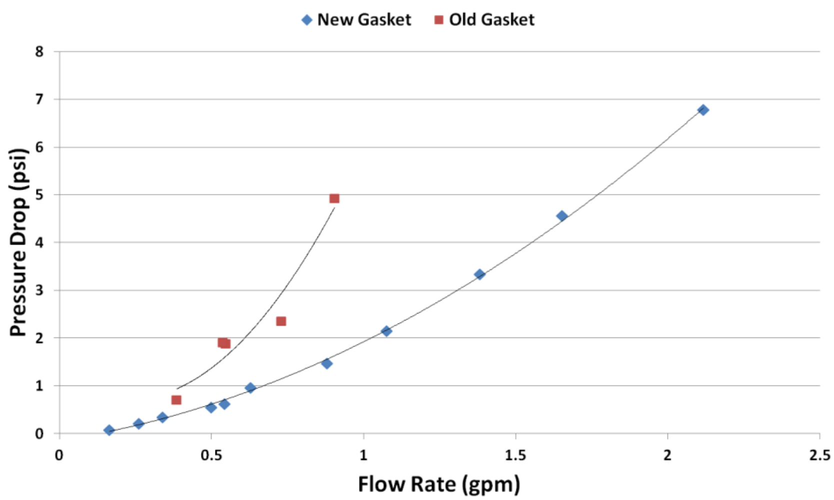

G3.4.2.3 Beta Prototype Construction

A newly designed heat exchanger concept involving more TECs was needed in order to accomplish the desired COP at the required heat load. Each TEC would be operating at a lower power and heat load. This beta prototype was designed and constructed as shown below (see Figure G54). The new prototype is 7.875"L x 7.45"H x 3.85"W.

Figure G54: Assembled Beta Prototype and Internal Components

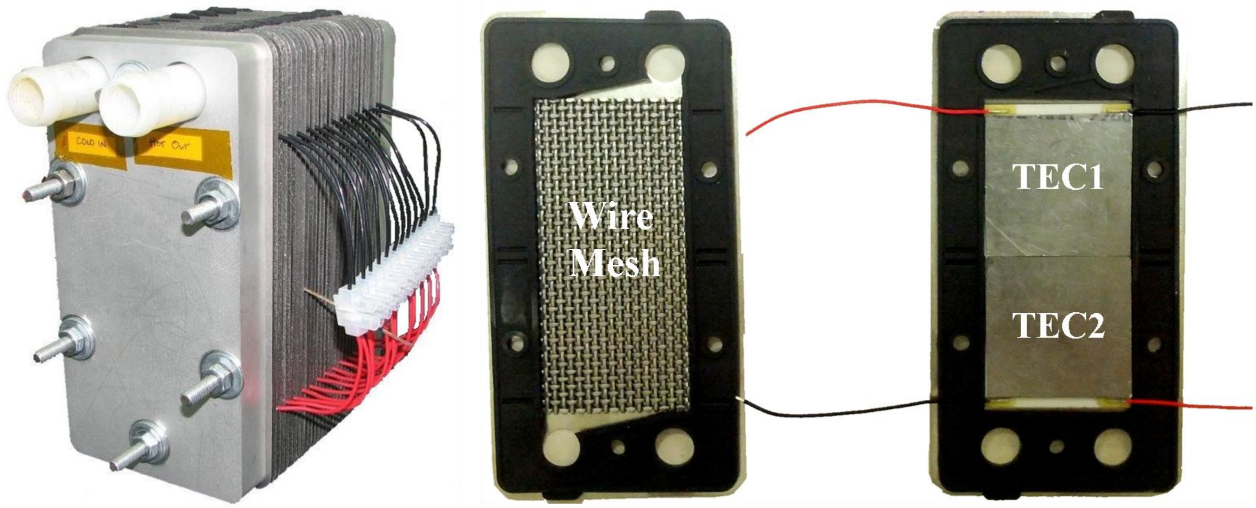

G3.4.2.4 Beta Prototype Testing

Several tests were performed to evaluate the performance of the Beta prototype heat exchanger over a range of inlet temperatures and temperature differentials. Key to understanding the performance graph shown in Figure G55 is the definition of ΔT on the x-axis. In this test configuration, ΔT is defined as

$$\Delta T = T_{engine} - T_{heater}$$

where T_{engine} is defined as the engine cooling fluid loop temperature and T_{heater} is defined as the heater fluid loop.

Using this nomenclature, a negative temperature differential indicates heat would naturally flow from the heater fluid loop into the engine cooling loop. For positive temperature differentials, heat would naturally flow from the engine cooling loop into the heater fluid loop. The Beta prototype performed well at start up, achieving a COP of ~2.9 when both fluid streams were at equal temperatures. Likewise, it achieved the target COP of >2.3 at all temperature differentials greater than -5°C. However, using a power supply capable of 405V, the necessary heat load (Qh) of 5kW was achieved only at temperature differences greater than -13°C. Beyond that point, the heat exchanger lacks the power to continue to drive 5kW of heat against the temperature gradient and into the fluid stream. The fluid temperatures will continue to diverge but at a slower rate. Once the temperature differential reaches -40°C, the COP is approximately unity and ceases to outperform a typical resistive heater. At temperature differentials less than -40°C the COP is less than unity as heat naturally flows from a much hotter liquid to a much cooler, despite the efforts of the thermoelectric heat exchanger.

Figure G55: COP and Qh Performance

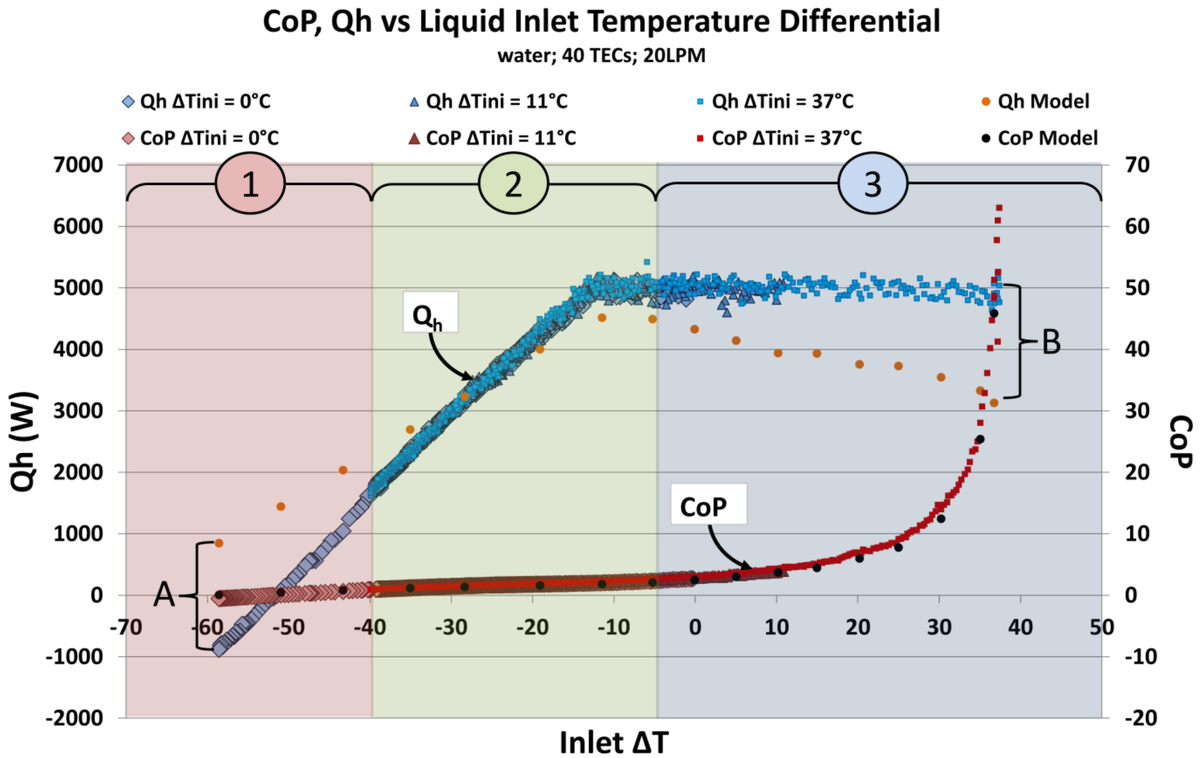

G3.5 Task 11 – Define Metrics for Efficiency and Comfort

The team's objective was to deliver equivalent comfort with the prototype distributed cooling and heating system while using significantly less energy than the production central HVAC system. The path for improving energy efficiency with distributed cooling and heating was through the reduction of AC compressor work or electrical energy consumption by resistive heating devices such as PTC heater in the vehicle. Within the scope of this project, the HVAC system power saving were achieved through elevation of the cabin temperature during cooling (or temperature reduction in the case of heating) to the threshold of discomfort, and then using the TE spot cooling or heating to regain the comfort. Under a constraint of equivalent comfort, a net energy reduction was expected after accounting for energy used by the TE HVAC system.

The team focused on the examination of the baseline comfort, which was expected to be maintained by the traditional HVAC system only, then reduced comfort when the ACC set point was lowered for cooling and raised for heating, and then restored comfort with the distributed TE HVAC system supplementing the reduced set point central HVAC system.

For spot cooling, the tunnel ambient condition of 85°Fx55%x500W/m^2 was the primary development condition, or standard ambient condition, for the TE HVAC system. Typically, steady state evaluation of the distributed cooling and heating system, including the corresponding passenger comfort, was carried out under this tunnel ambient condition. Once the TE HVAC system met the operational requirements under the standard ambient condition, a higher tunnel ambient condition of 100°Fx40%x1000W/m^2 was used as a secondary test condition to assess the system performance under a more severe thermal load. For spot heating development, the standard ambient condition was 0°CxXX%x0W/m^2.

The measurement scales for thermal sensation and thermal comfort were previously defined under Task 3, Perform Human Subject Testing. The key metrics was to achieve an equivalent comfort and an equivalent homogeneous temperature with the prototype distributed system as the standard centralized HVAC system. Other metrics compared the actual thermoelectric device COP in both heating and cooling modes to the established program targets. The COP measures the individual efficiency of each TE device.

G3.6 Task 12 – Integrate Initial Components into Mule Vehicle

G3.6.1.1 Vehicle Build & Instrumentation

The vehicle build began with instrumentation and the critical parts to be incorporated for the cooling loop. The overall vehicle build was divided into three parts, and these include basic instrumentation, coolant loop design, and thermoelectric/duct installation.

The overall basic cooling loop was designed to allow for cooling of each thermoelectric to provide the necessary heat rejection required by each thermoelectric. The basic concept was to distribute the coolant to three zones, these being driver seat, front passenger seat, and the rear three seats. Two flow pumps were utilized, one for the front seats and one for the rear seats. Variable resistance valves were placed at each zone to control the total flow to these areas. To further control the flow to each thermoelectric, a rotometer flow meter with control was plumbed into the cooling circuit. The rotometers were used to enable the proper flow to each thermoelectric, that being one l/min to each thermoelectric. After the flow was delivered to each thermoelectric, the flow was collected in a manifold that delivered it to a reservoir prior to going to the waste heat exchanger, which removed or added the waste heat delivered by the thermoelectric.

Figure G56: Waste Heat Exchanger and Blower (left) and Reservoir (right)

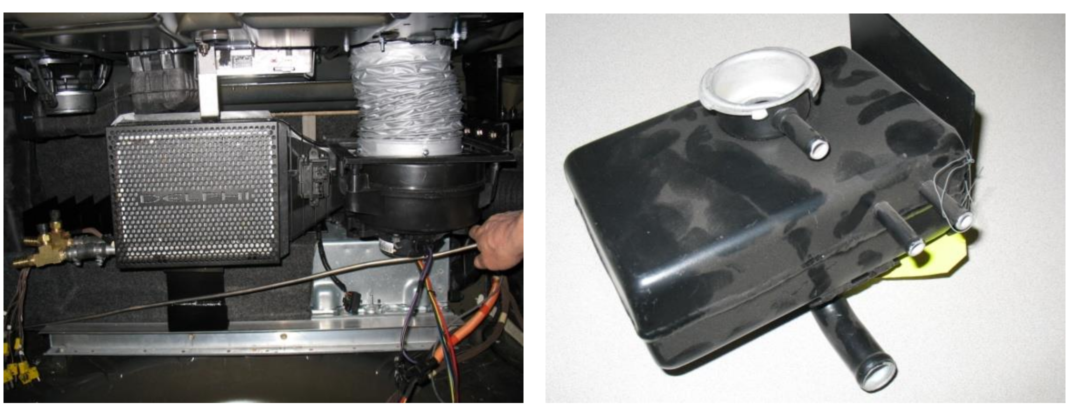

Figure G57: Rotometer Flow meter (left) and Liquid Pump (right)

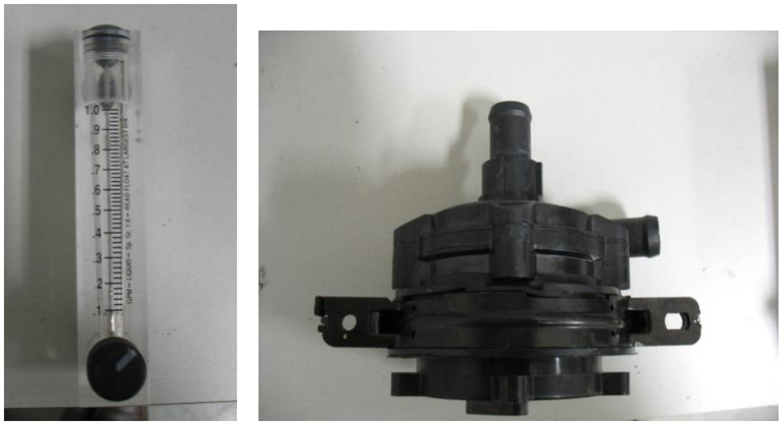

The vehicle instrumentation, coolant loop parts (see Figure G56 and Figure G57), thermoelectric devices, duct installation, and control system were installed in the Buick LaCrosse for testing.

G3.7 Task 13 – Evaluate Initial Comfort Components

G3.7.1 Perform testing and analysis of initial prototype HVAC components

G3.7.1.1 ACC System Baseline Comfort for Spot Cooling

The baseline cabin comfort of the vehicle is dependent on the set point of the Automatic Climate Control (ACC) system. The ACC system is typically calibrated by the OEM to maintain cabin comfort at the generic set point of 72°F. The final calibration of the ACC system occurs on the road to ensure accurate control of comfort. It is generally known, however, that ACC system performance in the environmental tunnel differs some from the on-the-road performance, and the ACC set point needs to be adjusted to achieve comfort. One factor is that the solar sensor reads differently in the tunnel vs. on the road. The solar lamps in general do not have the exact spectrum as that of the sun. Additionally, the discharge nozzle area of the tunnel air is limited in comparison with the cross-flow area of the car, causing some disparity of flow distribution around the body of the car.

Another complication for the present ACC system in the Buick LaCrosse is that the control head calibration has been modified to provide an elevated in-car temperature to 29°C by offsetting the control head set point input so as to save compressor power, with the TE system making up for the lost comfort by using spot cooling. Therefore, at the standard set point of 72°F, comfort cannot be achieved with the ACC system alone. A further modification to the control head was the configuration of the blower curve to operate on a lowered blower curve, approximately 75% of the standard blower curve.

In order to achieve comfort with the modified control head to provide a basis of assessment for compressor power consumption, passenger comfort rides were used to search for the proper ACC set point. After going through a stabilization process with an estimated control head set point, a crew of three comfort riders entered the vehicle to evaluate the in-car comfort. The front passenger seat was occupied by a thermal manikin for objective data recording. The driver made adjustment to the control point until an acceptable comfort was attained for the cabin. It was recognized that there is substantial front-to-rear breath level air temperature variations in the cabin. In addition to the normal front-to-rear temperature variation of the vehicle, the eAssist battery in the trunk generated enough heat to exacerbate the comfort deficit for the rear passengers. As a result, the ACC set point was determined to a large extent by driver comfort with the rear passenger comfort serving as secondary input.

For the ambient of 85°Fx55%RHx500W/m^2, the final set point for the modified control head to achieve comfort was determined to be 66°F. The comfort rating and the compressor power consumption at this set point formed the basis of comparison for the TE-assisted HVAC system.

Figure G58: Baseline Thermal Sensation Rating at 66°F ACC Set Point

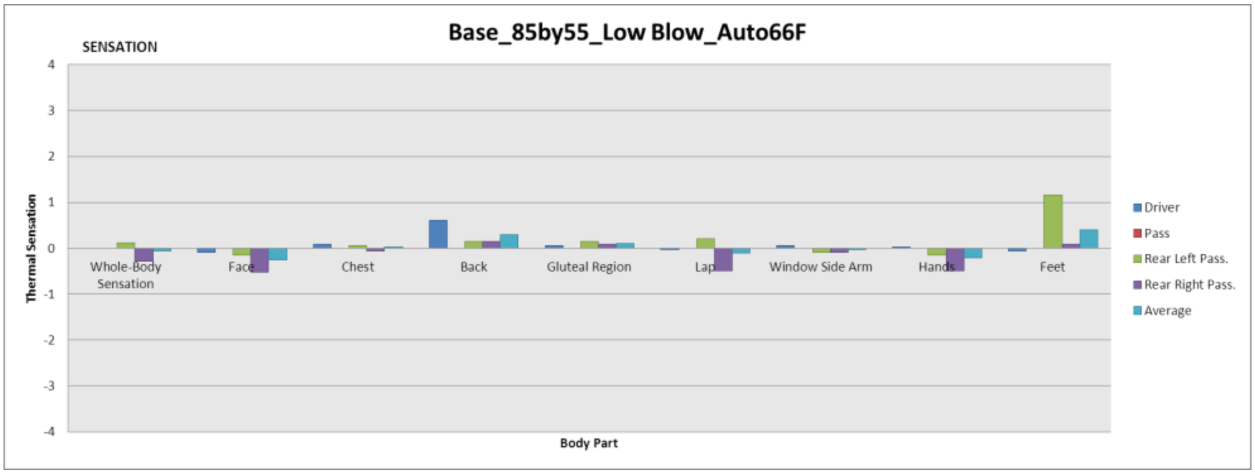

Figure G58 and Figure G59 show the baseline thermal sensation and baseline thermal comfort, respectively, for the Buick LaCrosse passenger compartment. It was seen that the cabin generally achieved thermal neutrality for the front and rear passengers. Thermal comfort ratings indicated that the driver and rear right passenger achieved better comfort than the rear left passenger. The average whole body thermal comfort was rated near the value of 1. It was recognized that, in additional to the normal temperature rise over the front passenger breath temperatures, there was also vertical temperature stratification for the rear seat. Toward the roof liner of the rear cabin, the temperature rose to a higher temperature. A tall passenger in the rear seat would be impacted by the temperature stratification and perceive the associated discomfort while a shorter passenger in the rear seat would be less impacted.

Figure G59: Baseline Thermal Comfort at 66°F ACC Set Point

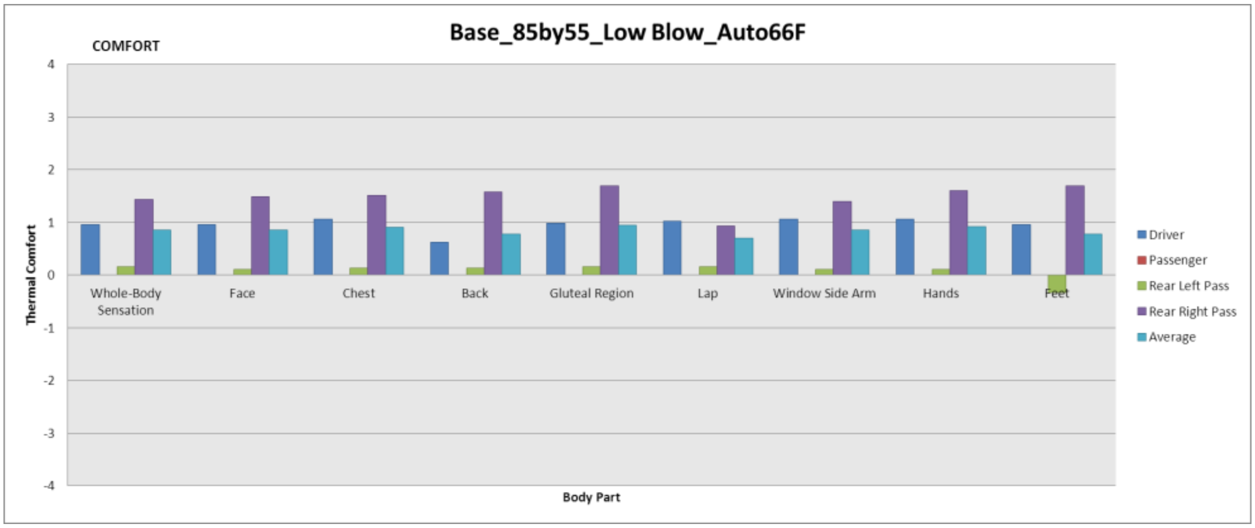

G3.7.1.2 Distributed TE HVAC System Cooling Comfort

The TE HVAC System was composed of all the TE modules in proprietary locations for each seating position. The TE modules were calibrated and operated to provide comfort to the cabin occupants under an elevated cabin temperature. The standard elevated temperature planned for the cabin was 29°C EHT, as was recommended from the Phase I studies. The elevated in-car temperature was to be maintained by the ACC system with a higher set point than the baseline comfort set point. Vehicle testing showed that an ACC set point of 74°F provided the 29°C EHT cabin temperature. It was subsequently found that the 74°F set point introduced heating via the coolant heater in the HVAC module into the cabin, instead of the expected, elevated EvaporatorOut Air Temperature (EOAT) setting for compressor power reduction, as is practiced in the Series Reheat Reduction technology for energy efficiency. At this set point, the EOAT set point for compressor reached it maximum temperature imposed for humidity control, and the mixed door (or temperature door) in the HVAC module opened up to introduce heater heat into the cabin. The portion of heat from the heater simply warmed up the cabin without allowing any compressor power reduction. In fact, additional electrical energy to the TE modules was required to reject the heat outside the cabin, leading to a deterioration of the overall energy efficiency.

It was therefore determined that the optimal set point when using the ACC system was 72°F. This control head set point allowed the in-car temperature to be raised to about 27°C EHT without any significant amount of coolant heat bleed. One does expect, however, that a more intelligent Series Reheat Reduction algorithm may be implemented with the support of an in-car humidity sensor to allow higher EOAT set point limit for the compressor when ambient conditions permitting. Such a smarter algorithm would allow higher energy efficiency to be achieved by the TE HVAC system.

Figure G shows the thermal sensation rating from comfort ride evaluation of the TE-assisted HVAC system under the ambient condition of 85°Fx55%RHx500W/m^2. Compared with the baseline thermal sensation rating of Figure G, it can be seen that the TE HVAC system provided a comfort environment that is cooler than the baseline run. The whole body thermal sensation rating average is near zero for the baseline, whereas the whole body rating average for the TE HVAC system is -0.8, a fairly significant improvement over the baseline.

Figure G60: Passenger Thermal Sensation Rating with the TE HVAC System

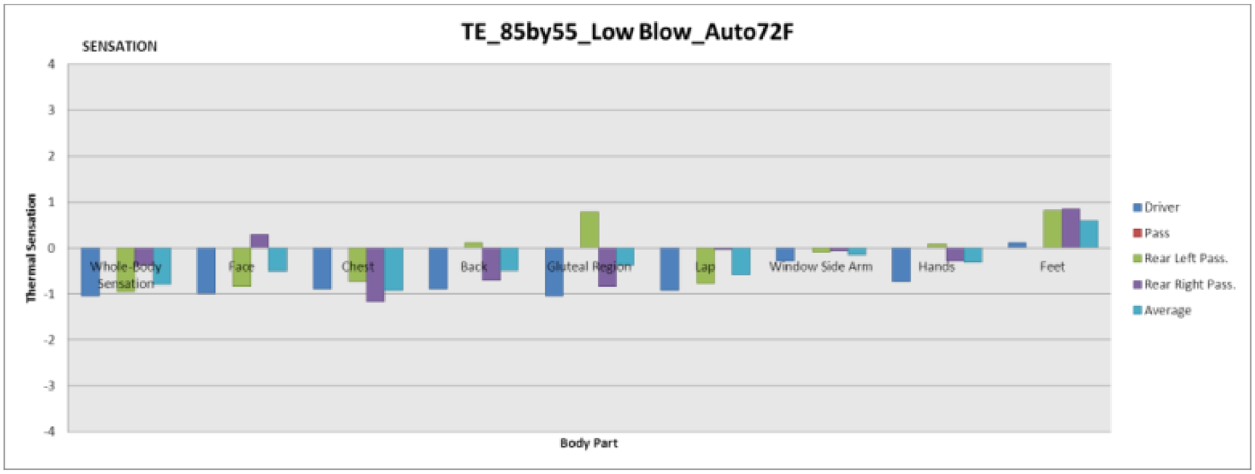

Figure G611 shows the thermal comfort rating from the same ride. Similarly, it can be seen that the thermal comfort rating for the TE HVAC system was more uniform across all the body parts and among the three riders. The whole body thermal comfort rating for the baseline system was about +0.9. For the TE-assisted HVAC System, the riders' whole body thermal comfort rating average was close to +1.5, confirming an improved riding comfort environment for the passengers.

Figure G61: Passenger Thermal Comfort Rating with TE HVAC System

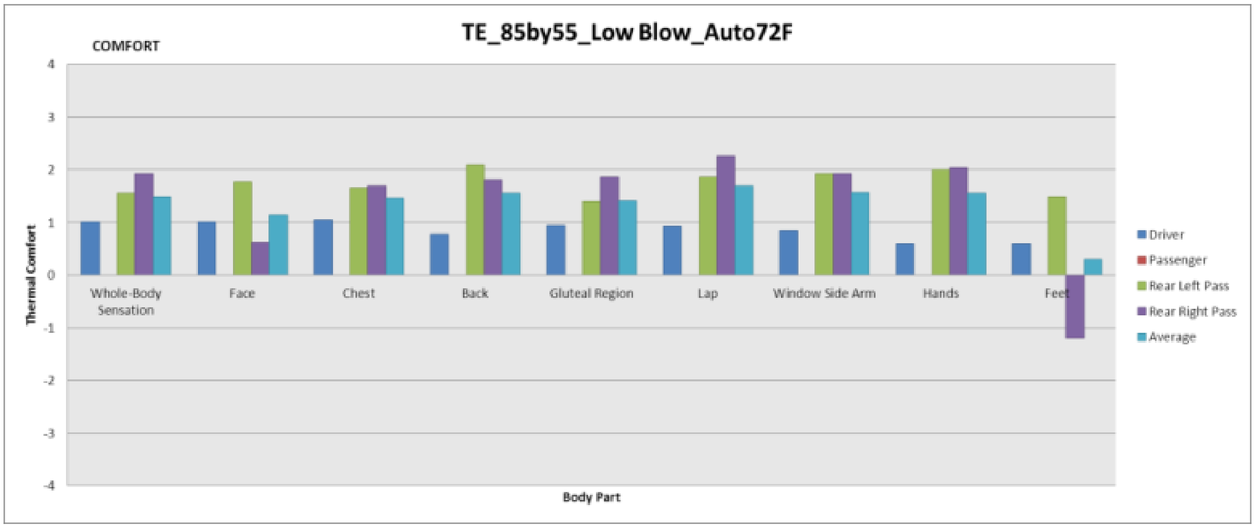

The slight edge for the TE HVAC system in maintaining comfort does not indicate that the TE HVAC system was more capable of maintaining comfort. In fact, the baseline system set point can be slightly reduced or the TE HVAC system operating point can be changed to bring about exactly equivalent comfort. However, it may still be concluded that comfort is achievable under a more elevated in-car temperature of 27°C EHT with the assistance of the TE HVAC system. And it may also be noted that any energy saving estimate for the TE HVAC system over that of the baseline system might be on the conservative side, since it is possible to further reduce the TE operating power to achieve a bit more energy efficiency.

Figure G62 shows the calculated EHT data as perceived by the different body parts and the whole body of the manikin for three different comfort evaluation runs: the baseline, TE HVAC system at a 72°F set point and at a 74°F set point with the manikin placed on the passenger seat during the comfort evaluations. The EHT curves indicate a general equivalency of comfort in the cabin for the three cases with slight variation for some body parts. The whole body EHT is within close proximity of each other.

Figure G62: Manikin Objective Comfort Comparison

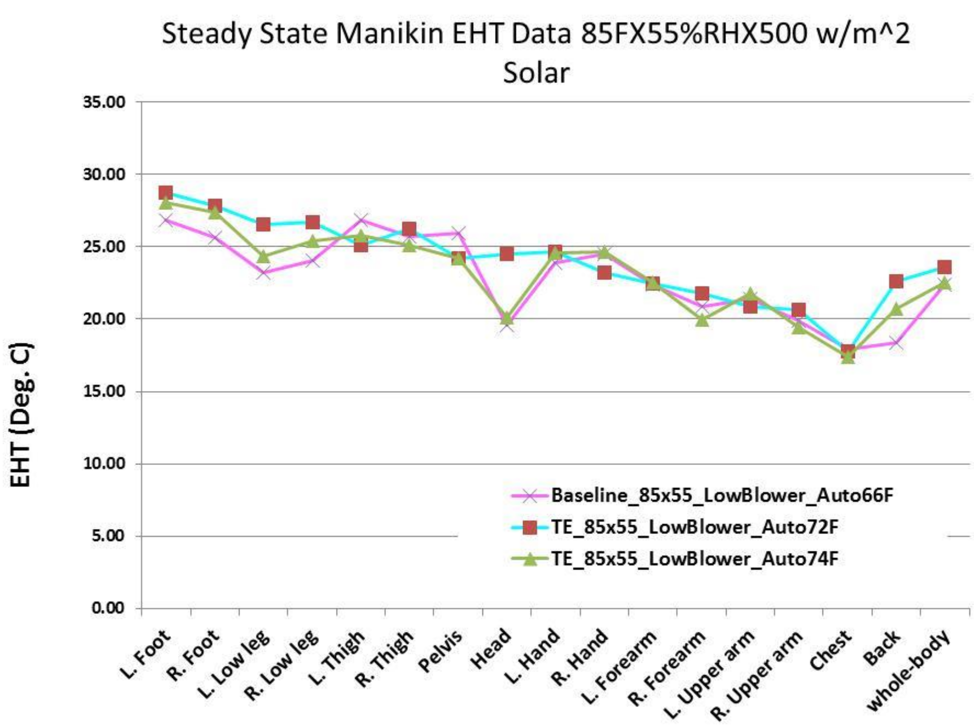

G3.7.1.3 ACC System Baseline Comfort for Transient Cooling at High Ambient

As a starting point to evaluate the TE HVAC system for the higher ambient condition of 100°Fx40%x1000W/m^2, the baseline ACC system was evaluated for comfort using the 66°F as set point. The blower curve was still the 75% down-scaled curve. Figure G3 shows the thermal sensation ratings for the baseline ACC system. The rear left passenger reported warm ratings, while the driver and the right rear passenger reported neutral to cool sensation. It appeared that the driver was slightly overcooled and rear passengers perceived non-uniform thermal sensation ratings due to rider variation and in-car thermal stratifications.

Figure G63: Thermal Sensation for Baseline ACC System with Low Blower Curve and 66°F Set Point for 100°Fx40%x1000Watts Ambient Condition

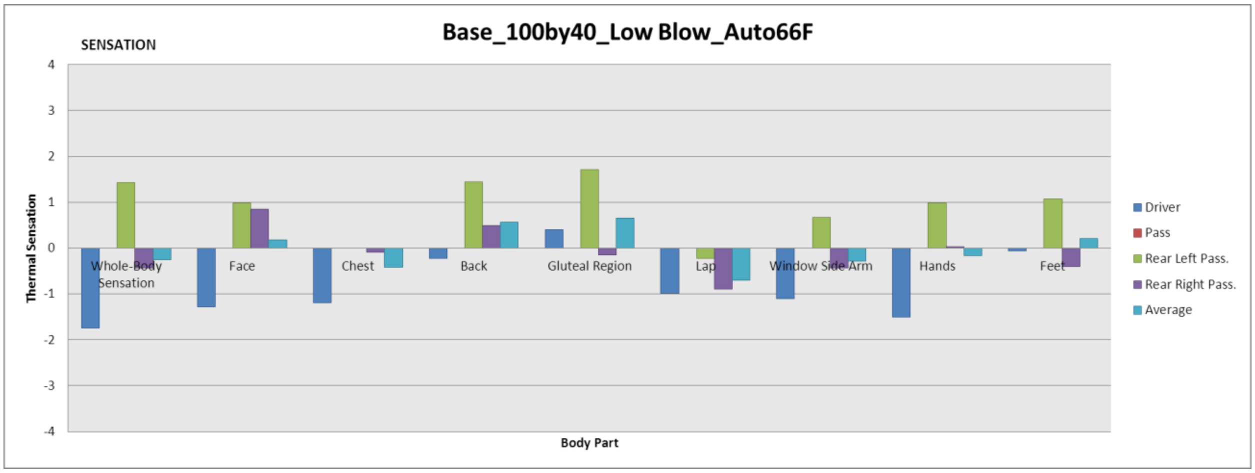

Figure G64 shows the thermal comfort ratings for the high ambient condition. The seating contact surface was marginal in comfort for the rear left passenger, but otherwise the riders were mostly comfortable. The average whole body thermal comfort rating for the riders was about +1.1. This evaluation basically established that the 66°F ACC set point was acceptable for the 100°Fx40%x1000W/m^2.

Figure G64: Thermal Comfort for Baseline ACC System with Low Blower Curve and 66°F Set Point for 100°Fx40%x1000Watts Ambient Condition

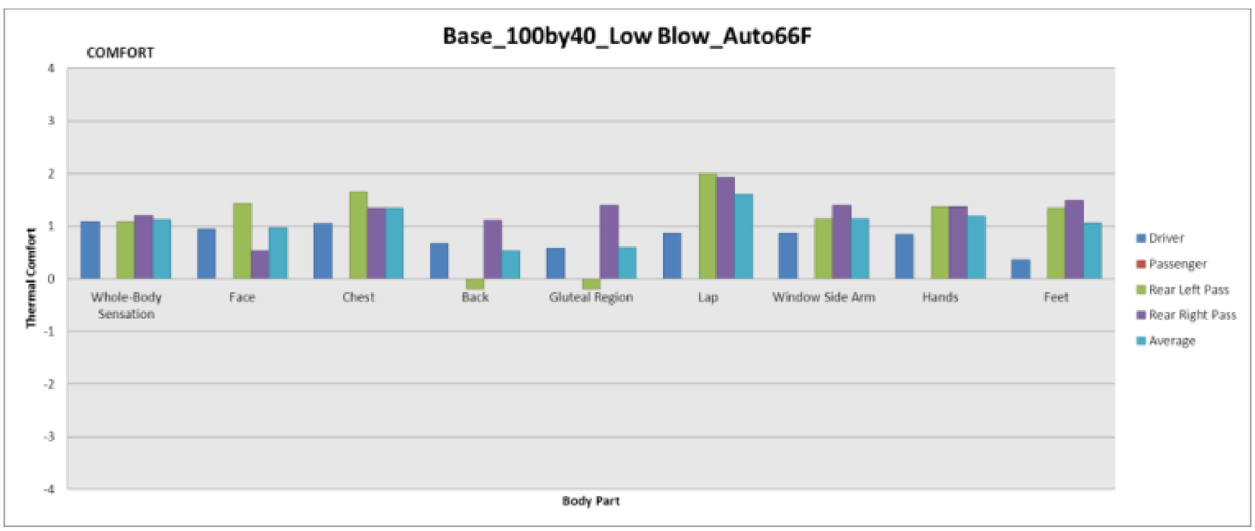

G3.7.1.4 Distributed TE HVAC System Cooling Comfort for High Ambient

The TE HVAC system was first tested with the lower HVAC blower curve and an ACC set point of 72°F, similar settings used in the 85°Fx55%x500W/m^2 condition. Although the driver regarded the seating environment to be close to comfort, the rear passengers deemed it unacceptable even when the TE modules operated at high settings. The main complaint was that there was insufficient airflow in the rear cabin from the HVAC rear console outlets.

To regain comfort, the ACC system was reset to run with the standard blower curve. Further, the operating point for the ACC system was lowered to a set point of 70°F. Under these new ACC operating settings, the TE HVAC system was able to provide in-car comfort when calibrated and optimized to run at near maximum settings. Figure G65 shows the improvement from the new ACC settings. The whole body EHT temperature decreased from about 26°C to about 24°C.

Figure G65: In-car EHT Improvement under Enhanced ACC Settings

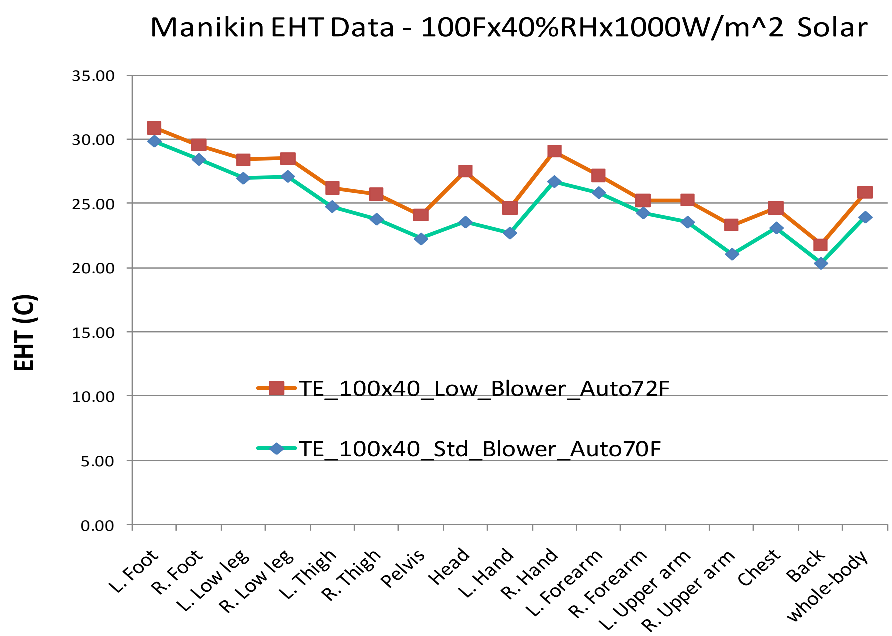

The thermal sensation ratings for the TE HVAC system under the new settings indicated that all riders gained neutral or cool thermal sensation ratings, except one or two body parts. Based on their thermal comfort ratings, the rear passengers achieved high comfort. It appears that the rear passengers were more comfortable than the driver. This might be due to the sharp contrast in the improvement of the rear passenger thermal environment from the increased delivery of HVAC console airflow.

G3.7.1.5 Spot Heating Comfort under Standard Ambient Condition

Spot heating evaluation was done under the ambient condition of 0°C without regard for humidity and with no solar. Spot heating was designed primarily for hybrid and electric vehicle applications where electric energy was used to provide heating under low ambient conditions. By reducing the cabin temperature maintained by the traditional HVAC system and using the

TE HVAC system to provide localized heating, it is expected that overall energy saving may be achieved without sacrificing comfort.

On the LaCrosse test vehicle, due to the primary focus being on spot cooling and the obstacles of estimating energy saving on a vehicle with available engine waste heat, the spot heating development was focused mainly on functional development, i.e., to answer the question whether the TE HVAC system can be operated to provide spot heating and calibrated to supplement a down-powered HVAC system so as to provide equivalent comfort to the occupants.

Figure G shows the comfort ride thermal sensation evaluation under the 66°F ACC set point with the lower blower curve. The thermal sensation ratings are centered around neutral with the driver being on the cooler side. The average whole body thermal sensation rating from all riders was effectively zero. With the comfort ride evaluation, the 66°F ACC set point under the lower blower curve was established as the baseline condition for TE HVAC system development.

Figure G66: Baseline Thermal Sensation Ratings under 66F ACC Set Point

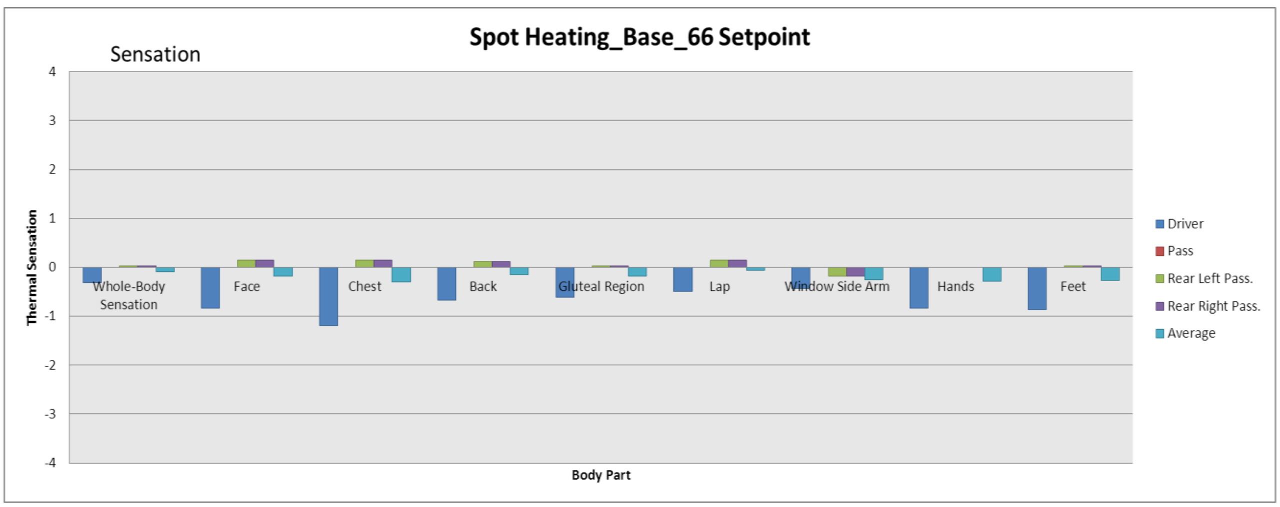

Figure G67 provides the thermal comfort ratings for the baseline ACC operation. The rear passengers indicated a high degree of thermal comfort satisfaction, whereas the driver gave a relatively low thermal comfort rating. The average whole body thermal comfort rating is at about +1.5, an acceptable level of comfort.

Figure G67: Baseline Thermal Comfort Ratings under 66F ACC Set Point

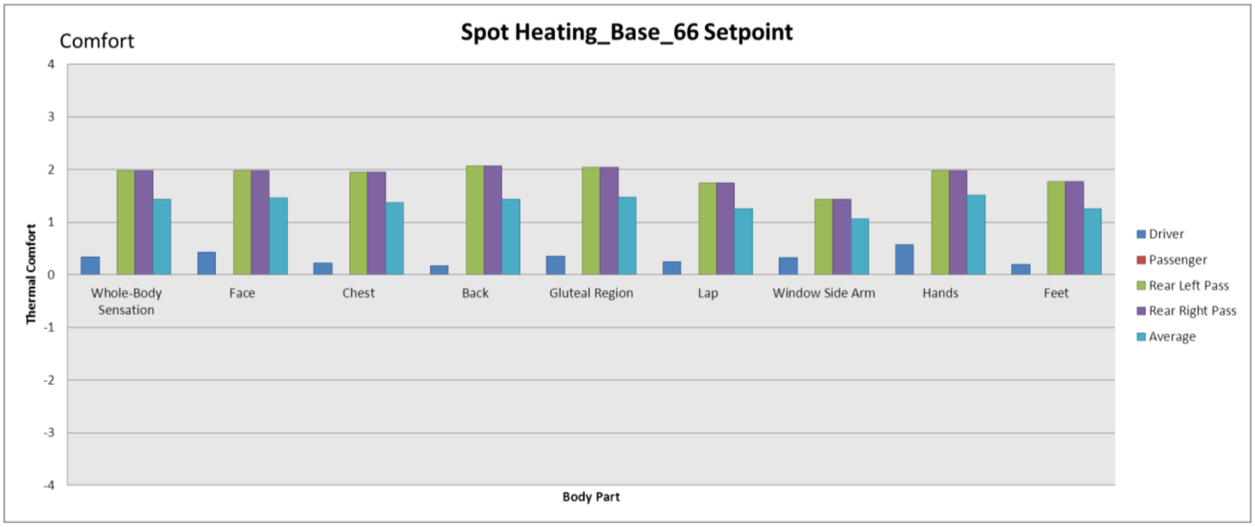

Figure G68 shows the deterioration of in-car condition when the ACC set point was reduced to 64°C while still under the lower blower curve. Under this operating condition, it was seen that all the comfort riders indicated discomfort. All the thermal sensation ratings were between "Cool" and "Cold".

Figure G68: Thermal Sensation Ratings for Reduced Set Point

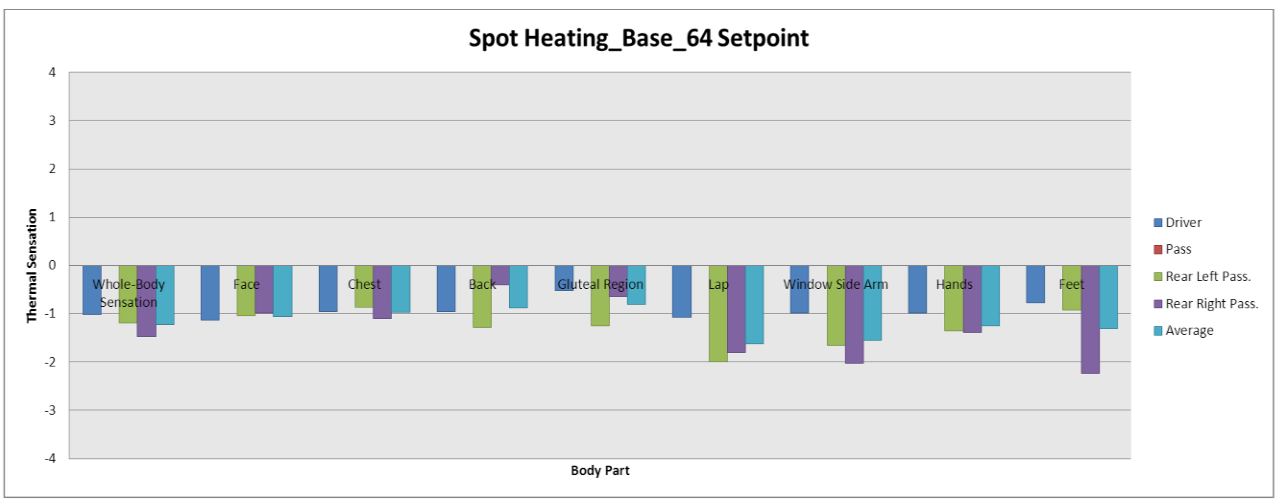

This was validated by the thermal comfort ratings in Figure G69. In general, the thermal comfort ratings were below zero, in the region of discomfort. As reminder, a thermal comfort rating in the range between +1 and +2 are required for comfort, preferable near +2.

Figure G69: Thermal Comfort Ratings for Reduced Set Point

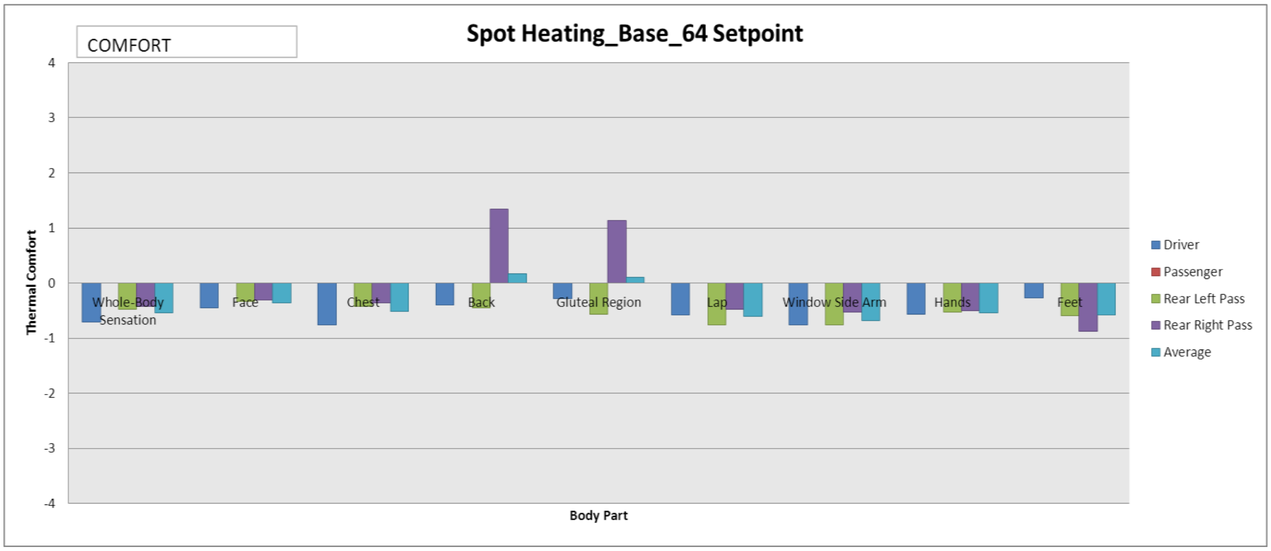

Subsequent to the establishment of the baseline operating point and comfort ratings, the TE HVAC system was turned on with the ACC system operating at 64°F set point to restore the thermal comfort deficit. In comparison with Figure G68, where the ratings were "Cool' or "Cold", Figure G70 shows that the thermal sensation ratings were restored to a range between "Neutral" and "Warm", making the in-car environment acceptable.

Figure G70: Thermal Sensation for TE HVAC System in Spot Heating

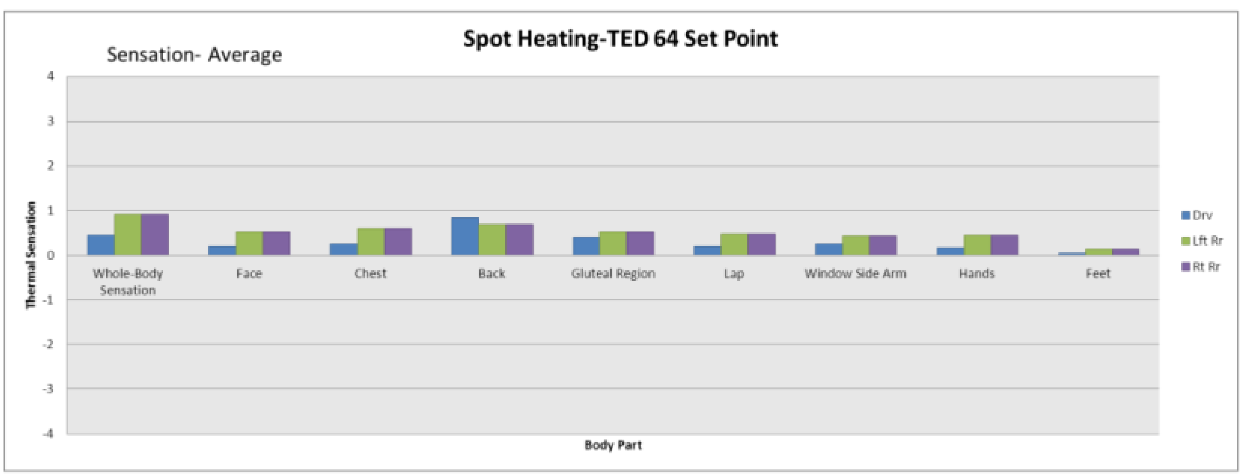

Figure G71 shows the corresponding thermal comfort ratings for the same car ride. It was seen that the thermal comfort ratings were comparable or better than that of the baseline ride in Figure G50. The driver's ratings were still relatively low compared with the rear passengers, but they showed a degree of improvement over the baseline case.

Figure G71: Thermal Comfort for TE HVAC System in Spot Heating

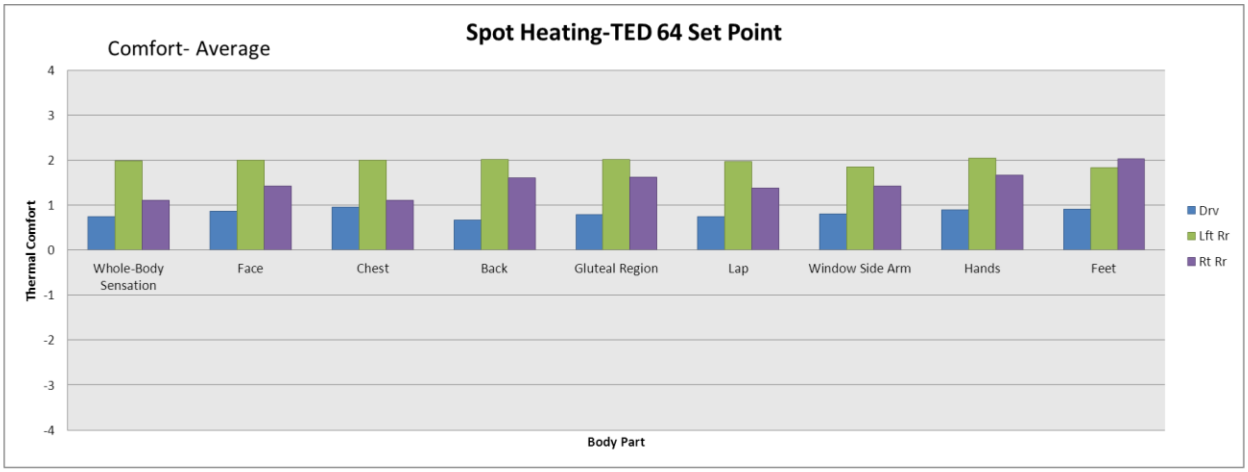

Figure G72 is the comparison of front passenger seat manikin EHT temperatures for the baseline ACC operating condition with 66°F set point and the reduced set point operation at 64°F supplemented by the TE HVAC system. The objective data demonstrates that better comfort was achieved with the TE HVAC system. In fact, the whole body EHT was at 24.3°C, while the baseline whole body EHT was at 21.4°C.

Figure G72: Manikin Objective Evaluation of Comfort

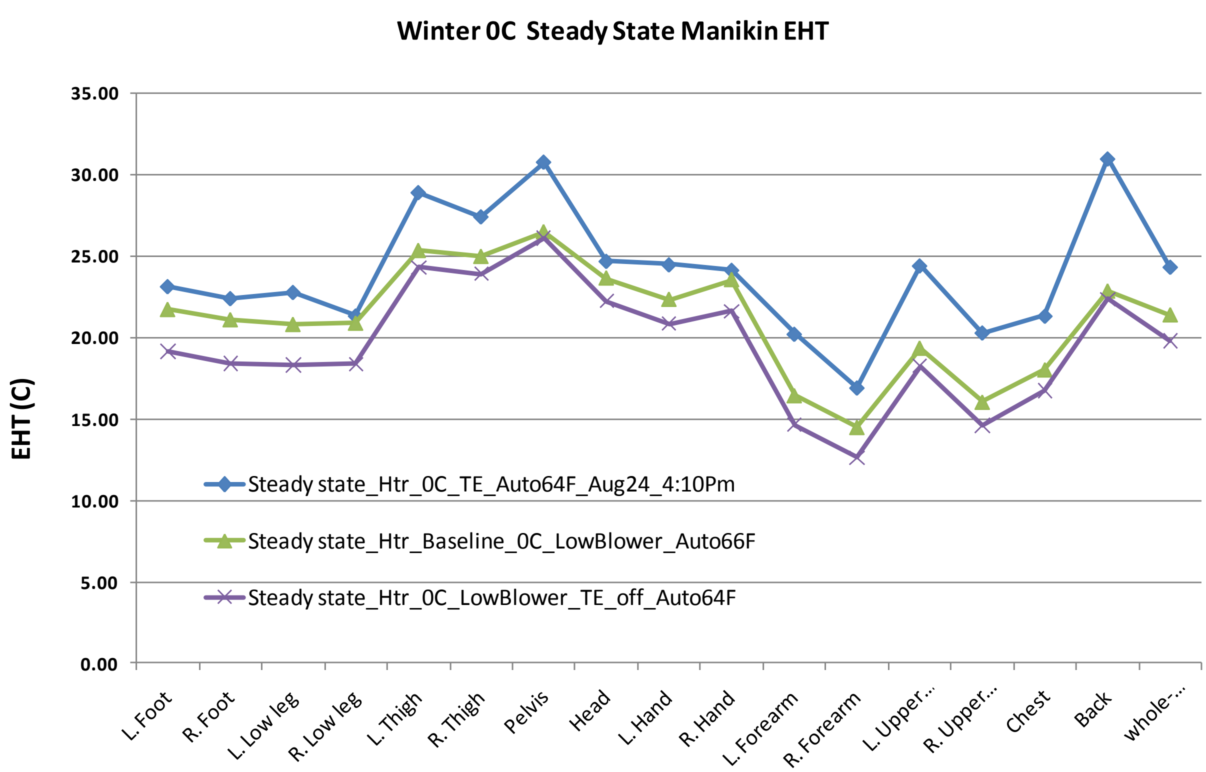

Due to the modified control head internal offset, the baseline comfort was established through comfort ride evaluation and not through manikin EHT mapping. It appeared that the baseline set point of 66°F might be on the lower side in consideration of the driver ratings. On the other hand, the 64°F set point appeared to have established enough discomfort for the TE HVAC system to compensate and worked reasonably well. For future spot heating energy saving estimates, the baseline operating point needs to be increased, perhaps to 68°F with the modified control head, or to whatever setting that provides a baseline comfort close to 24°C EHT.

G3.7.1.6 TE HVAC System Power Consumption Test and Analysis

A focused effort was made to provide the initial energy efficiency assessment of the TE HVAC system in comparison with the baseline eAssist Buick LaCrosse vehicle. The primary energy efficiency assessment of interest was in the area of compressor power saving.

Generally speaking, the energy efficiency assessment was based on the steady state tunnel test data. It was understood that energy savings were available during the transient operations of the vehicle; however, due to the complexity of test protocols and concerns about repeatability, presently only the steady state energy savings were examined. For the baseline vehicle steady state energy consumption under each of the test ambient conditions, the compressor and HVAC blower power use were conglomerated to represent the HVAC system power use. For both the baseline and the TE HVAC system, miscellaneous power use by the Campbell data logger and the TE HVAC controller were not included.

The electrical power consumed by each passenger was then combined with the compressor and HVAC blower power to form three different occupancy scenarios: driver only, driver and passenger, and four passengers. There was no effort made to differentiate between one or two rear passengers. Even though the control mechanism may be designed into the vehicle's TE HVAC control system, the occupancy weighting for the rear passengers was very low when compared with the front passengers; therefore, four-passenger occupancy was considered an adequate representation of the power consumption by the rear passengers.

From the test point of view, no repeated tests were performed for each of the occupancy scenarios. For a given ambient condition, the vehicle was tested with all four TE seats switched on. The power consumption scenarios for one, two, and three/four occupants were based on the power allocated to each occupant. For the driver only case, the power allocated to the driver was added to the compressor and HVAC blower power used to achieve the total TE HVAC system power, while the power allocated to the other seats was ignored.

The Ambient Sweep test procedure was used to establish the power use for the baseline and the TE HVAC equipped Buick LaCrosse. Some complicating factors impacted the final test procedure. Typically, the Automatic Climate Control (ACC) system was road tested and calibrated before being launched into production. There was some difference in ACC performance when a vehicle was tested in the tunnel. The ACC system may not be able to maintain 100% comfort across the entire ambient sweep temperature range. The factors causing the performance variation from the road mainly are the air flow distribution around the vehicle and the solar sensor response to the actual sun versus the heating lamps in the climatic wind tunnel. The second complicating factor was that the control head for the LaCrosse was not a standard production control box. Modifications to the software were made in the effort to automate the coordination of the TE module operation and the HVAC ACC system. The ACC set point was offset by certain amount according to the ambient temperature and solar sensor reading. Thus, there was a considerable uncertainty as to what comfort level the ACC system would offer at a particular set point.

The Ambient Sweep test procedure compensated for these ACC uncertainties by using actual passenger comfort rides. At any given ambient condition, the vehicle was run and stabilized with a preliminary control point. Once stabilized to a steady state, engineers were invited to sit in the car and make adjustment to the control point based on their comfort perception. This was done with a panel of three or four engineers based on consensus of the group. The same approach was followed for both the baseline vehicle and the TE HVAC equipped vehicle. Thus the power usage data was collected on equivalent comfort basis for the two HVAC systems. Compressor power was calculated using the measured refrigerant flow rate plus the suction and discharge enthalpy with an estimated mechanical efficiency.

G3.7.1.7 Power Savings Projection

Comparison of the baseline and the TE HVAC system power consumptions allowed the team to estimate the expected power savings with this technology. The methodology used to calculate the expected savings and the proprietary results were used to support the completion of two Phase 2 milestones, the evaluation of initial comfort components and the estimation of the final COP for thermoelectric devices. These results indicated that the project should successfully accomplish the stated objectives for energy savings of 30% improvement (current status is 29%) and for COP of the TE devices (nearly all initial prototype components exceeded the cooling mode COP target of 1.3 and the heating mode COP target of 2.3).

G3.7.2 Milestone 7 – Evaluate Initial Comfort Components Completed

To complete this milestone, the project team tested the initial set of prototype distributed HVAC components on the Buick LaCrosse in a climatic wind tunnel. For spot cooling, the tunnel ambient condition of 85°F x 55% relative humidity (R.H.) x 500W/m^2 solar load (S.L.) was the primary development condition for the TE-assisted HVAC System. Typically, steady state evaluation of the distributed cooling and heating system, including the corresponding passenger comfort, was performed under this tunnel ambient condition. Once the TE-assisted HVAC system met the operational requirements under the standard ambient condition, a higher tunnel ambient condition of 100°F x 40% R.H. x1000W/m^2 S.L. was used as a secondary test condition to assess the system performance under a more severe thermal load. For spot heating, the ambient condition was 0°C with tunnel humidity uncontrolled and with no solar load applied. The proprietary results from these tests were used to guide the team’s efforts in Phase 3. The project team’s analysis of these test results and overall evaluation of the initial comfort components was completed on November 27, 2012.

G3.7.3 Milestone 8 – Estimate Final COP for Thermoelectric Components

A key portion of the team’s analysis was to evaluate the energy efficiency of this distributed thermoelectric HVAC system. This evaluation had two primary constituents: assessing the initial energy efficiency of the prototype HVAC system in comparison with the production HVAC system on the Buick LaCrosse test vehicle and estimating the final coefficients of performance for the prototype thermoelectric components. The primary energy efficiency assessment of interest is in the area of potential AC compressor power savings.

Generally speaking, the energy efficiency assessment is based on the steady state tunnel test data. It is understood that energy saving is available during the transient operations of the vehicle, however, due to the complexity of test protocols and concerns about repeatability, presently only the steady state energy saving is examined.

The TE system power consumptions are allocated to each passenger in the vehicle. Due to the capability to turn off components by location, unoccupied seats do not consume any power. For example, with the rear seats turned off, all the TE devices, TE cooling fans, and the associated coolant pump are turned off. For the front seats, which share the same coolant pump, power consumption by the pump is divided between the two front seats. It is expected that when there is only the driver in the seat, coolant pump flow rate may be halved to reduce pump power consumption.

The electrical power consumed by each passenger is then combined with the compressor and HVAC blower power to form three different occupancy scenarios: driver only, driver and passenger, and four passengers. There is no effort made to differentiate between one or two rear passengers. Even though the control mechanism may be designed into the vehicle TE control system, due to that the occupancy weighting for the rear passengers are very low as compared with the front passengers, four-passenger occupancy is considered an adequate representation of the power consumption by the rear passengers. The proprietary details of this analysis were used to guide the team's efforts in Phase 3.

In summary, the results of the estimate completed on November 27, 2012, indicate that the project should successfully accomplish the stated objective for AC energy savings of at least 30% and also achieve the thermoelectric COP targets of at least 1.3 in cooling mode and 2.3 in heating mode.

CHAPTER G4:
GM Phase 3 – Advanced Development

The focus of this phase was to develop the final prototype distributed HVAC components while considering production-intent requirements such as noise and packaging. For this phase of the project, GM will continue to utilize Delphi to develop most final prototype HVAC components with Faurecia developing final prototype seats and Marlow Industries developing a final prototype TE-based heater for the Volt. UCB will continue their primary Phase 1 activities in parallel with this phase.

G4.1 Task 14 – Project Management and Planning

The planning and coordination for this phase primarily utilized weekly team meetings. Delays in reaching contractual agreements with key team partners for their support of both Phase 3 and Phase 4 activities resulted in several months delay for the overall project. However, project spending remains on budget, so the delays resulted in a no-cost time extension for the project.

G4.2 Task 15 – Commercialize Design of New Comfort Components

The main activity for this task was to develop the final prototype distributed HVAC components while considering production-intent requirements such as noise and packaging.

G4.2.1 Develop final prototype distributed HVAC components

G4.2.1.1 TED Subassembly Packaging

A major challenge for the project team during Phase 3 was to reduce the blower noise in the thermoelectric device (TED) modules. The objective was to reduce the noise level produced by the final set of prototype distributed HVAC components to create a more production-intent environment for occupants of the demonstration vehicle. The fans in the initial set of prototype components developed during Phase 2 were oversized to support a broad range of airflow values during testing. For Phase 3, the requirements for the final prototypes were reduced to a narrower range of effective airflow values. As Figure G73 demonstrates, the project team undertook extensive investigations to identify and evaluate alternative fans for the final prototype components that both lowered noise levels and required less power. Fan size was also a consideration as the team tried to improve the packaging of the final prototype components and their associated ductwork.

Figure G73: Comparing two fans – new NIDEC fan in purple and old Delta fan in cyan

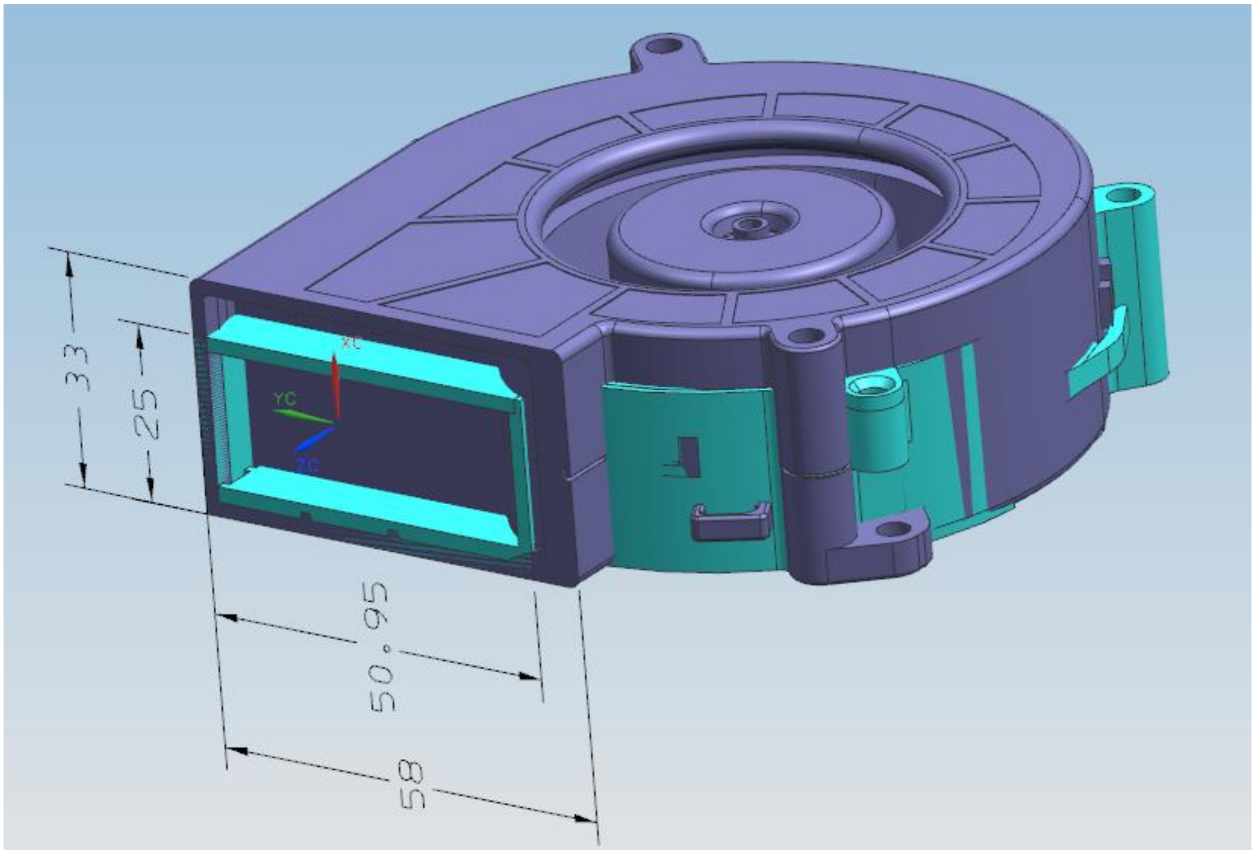

G4.2.1.2 Design of the Plume Seating System

During Phase 2, the team developed, installed, tested, and evaluated two sets of front seats, a conventional seating configuration plus an innovative "plume" system concept that delivered air from near the occupant's neck in an attempt to create a blanket of conditioned air around the front seat occupants. While the initial plume development did not result in power savings for this project, the plume system was designated as an HVAC comfort feature with the potential for future energy savings from further refinement. Based on this potential, the team decided to include the plume system in the Phase 3 front seats, because the plume system feature can be disabled if it detracts from the project's energy savings objective. A revised plume system has been included in the final front seat prototypes for the Buick LaCrosse demonstration vehicle, and this feature will continue to be evaluated for potential improvements in comfort and energy savings. However, the team is confident that it can achieve the project's energy savings objective without using the plume system, so the plume is currently considered an HVAC system comfort feature instead of an energy-saving feature. As shown in Figure G74, air can be diverted from the rear passenger air to feed the plumes for the front seats. A duct switching mechanism featuring an isolator valve has been designed to allow the air to proceed to the rear seats when there are rear occupants or to feed the front plumes when there are no rear seat occupants. The airflow exiting the plumes can be controlled by changing the fan speed.

Figure G74: Isolator valve directing the flow to the front plume system or to the rear vents

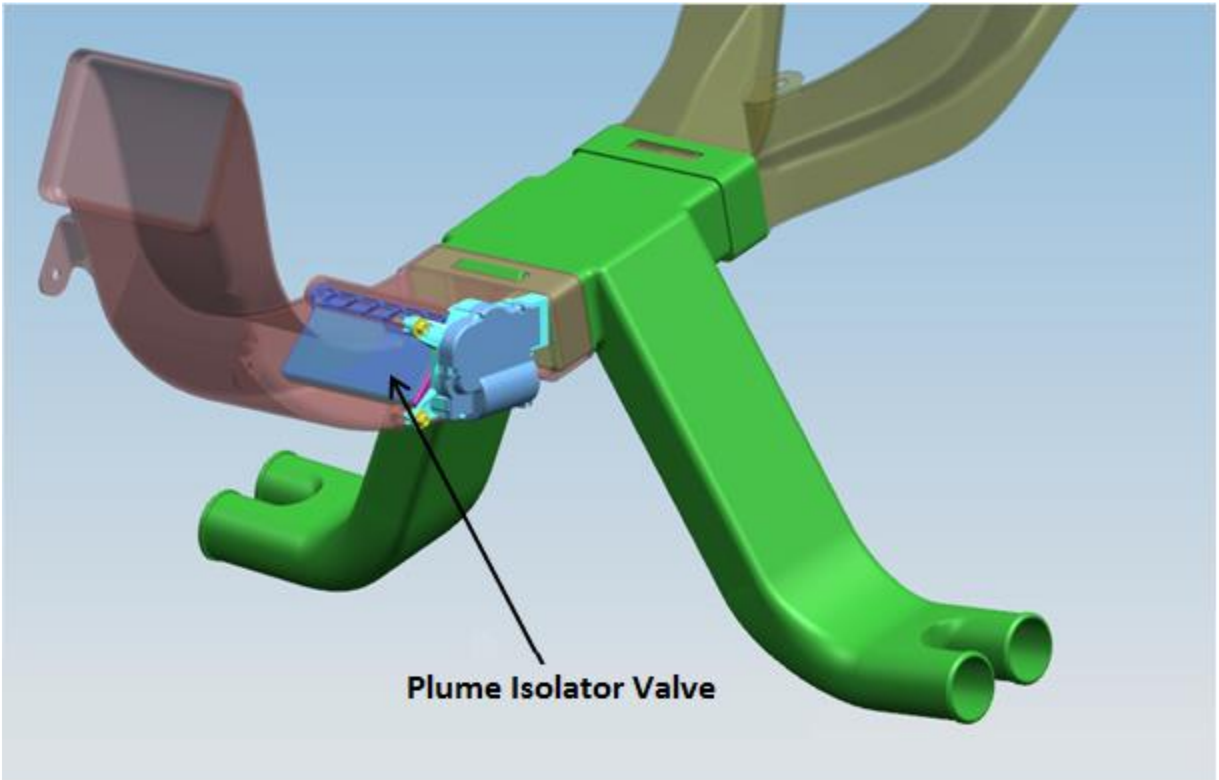

Other refinements to the final prototype components are ongoing.

G4.2.2 Develop final prototype TE-based cabin heater for Volt

G42.2.1 Final Design Concept for Plate and Frame Heater System

After testing the beta design prototype, some key issues and potential solutions that could enhance performance of the final prototype heater were quickly identified. Most of the changes would focus on the gasket design, but the changes would also influence other components of the heat exchanger. It was understood that some heat (30% of Qh in some cases) was being transferred from one fluid to another through peripheral parts of the heat exchanger (plates and gaskets) rather than through the TE modules. When there was a negative ΔT across the exchanger, this became problematic as the heat has an alternative path against the desired direction of heat flow. In order to lessen this effect, a smaller gasket design was conceived. Figure G75 shows the original gasket in red and a redesigned, smaller gasket overlaid in black with a plate behind.

Figure G75: Original and Revised Gasket Comparison

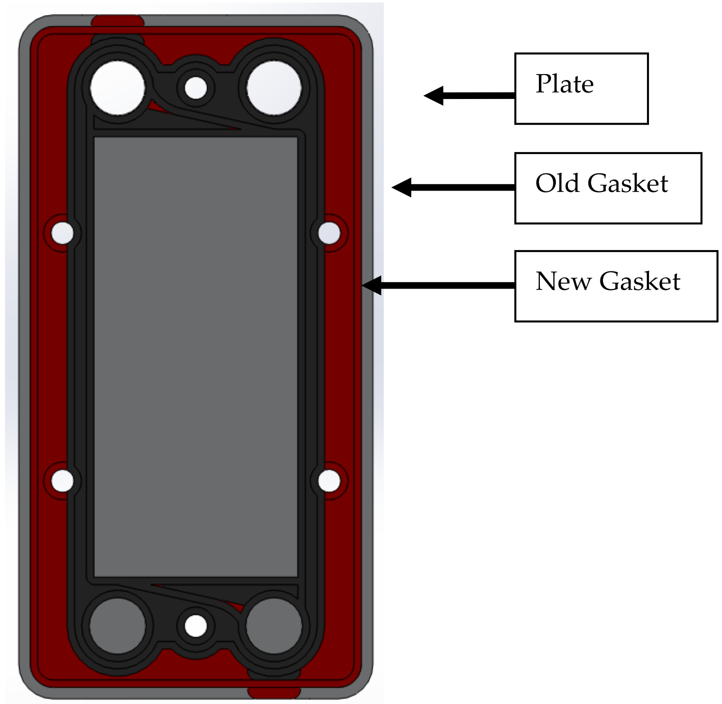

The new gasket maintains a double-sealed design while decreasing total gasket surface area by 49.7% and total gasket weight by 45.9%. The main weight advantage, however, comes not in the gaskets but in the decreased size of the plates: with a smaller gasket, the plates can also shrink accordingly. Using a smaller plate made of 316SS, the overall weight of the unit would be reduced by approximately 18%, a difference of over 3 pounds. The final design is shown in Figure G76 with an optional cover design and electronics interface included on the right.

Figure G76: Final Gamma Prototype Design

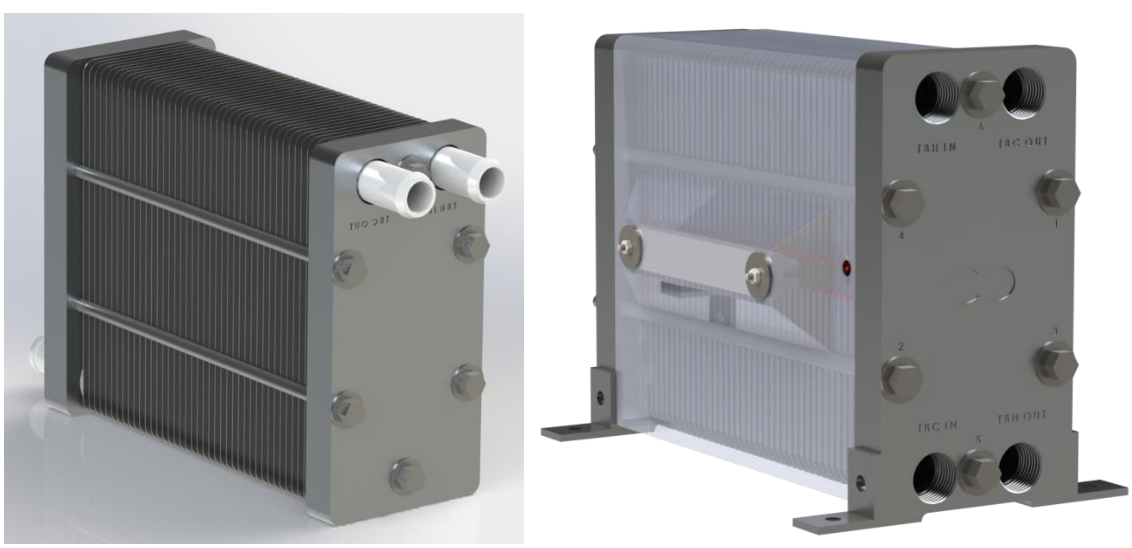

There are several distinct changes to the final gamma prototype design. First, it relocates all four liquid access ports to the front frame. This should allow for the heat exchanger to occupy a smaller volume within the vehicle and simplify the construction process. The ports have also been modified to be ½" NPT pipe thread rather than the previous barbed hose fittings. This allows greater versatility in the design as well as shortens the overall assembly. Second, the gasket and plate designs have been optimized to include as little material as possible while still maintaining a strong static seal. One additional safety feature which is now included is the bent edges of the plates. The plates now wrap around the gasket (see Figure G), reducing the possibility of gasket movement under high pressure situations as was previously seen. Third, the materials have also been updated. The frames are now made of 6061 Aluminum rather than 7075 Aluminum to save cost. Additionally, the gaskets are now made of hydrogenated nitrile butadiene rubber (HNBR), which allows the unit to handle liquid temperatures up to 150°C.

Figure G77: Gasket Containment Walls

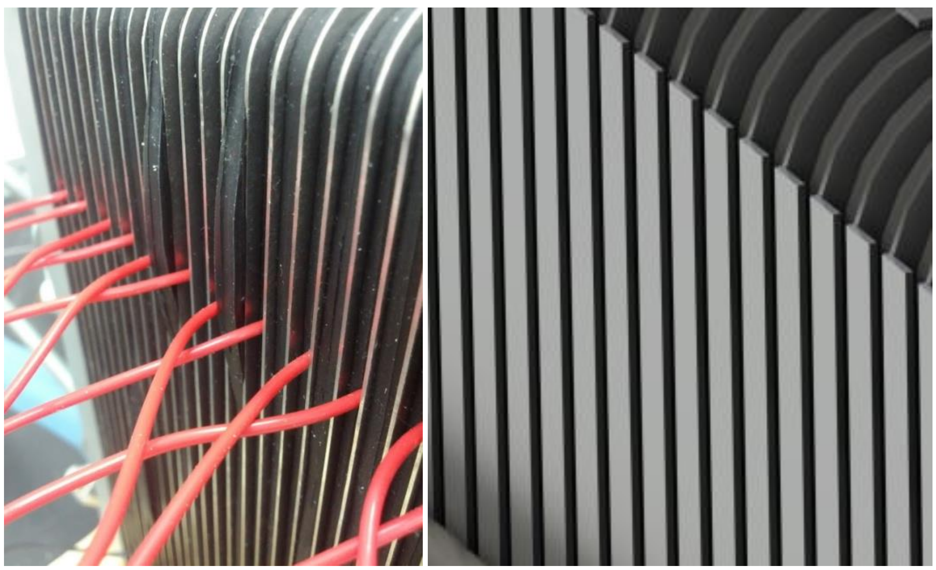

Compared to the Beta prototype, the Gamma prototype will be safer, lighter, more versatile, and capable of handling much higher temperatures.

G4.2.2.2 Limited operating range at 5kW heat load

As was discovered during testing of the beta prototype, the TE-based heater design had limited capability to drive a 5kW heat load, and its COP continues to decrease as it operates for an extended period. To prevent its COP from dropping below that of a resistive heater, the team developed a concept for temporarily connecting the inlet and outlet coolant loops of the TE-based heater. It was determined that by shorting the fluid loops thru the exchanger at the point that COP equals unity, the COP curve would plateau, allowing the thermoelectric heat exchanger to perform similarly to the current resistive heater. To prove such a concept, a simple experiment was carried out in which only one fluid loop was used. That fluid loop was then split between the two exchanger loops before being reunited on the other side and recirculated (see Figure G78).

Figure G78: Shared Liquid Loop Experimental Setup

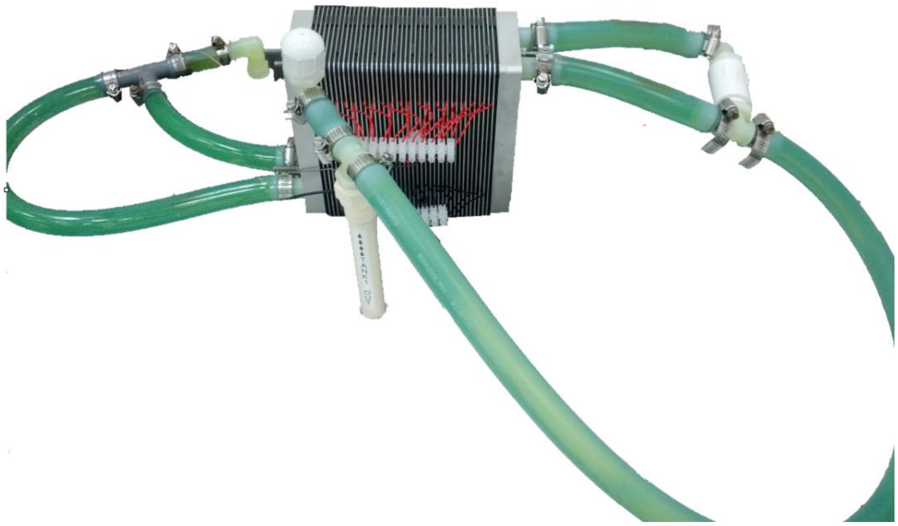

The results from the experiment are shown in Figure G79, indicating that the COP plateaus at 0.9 (there are some thermal losses to ambient) regardless of the inlet liquid temperature. The power to the device decreases with increasing liquid temperature as expected due to the increase in electrical resistivity of the thermoelectric material. The Q_h, thus, also decreases in proportion resulting in a constant COP.

Figure G79: Shared Liquid Loop Results

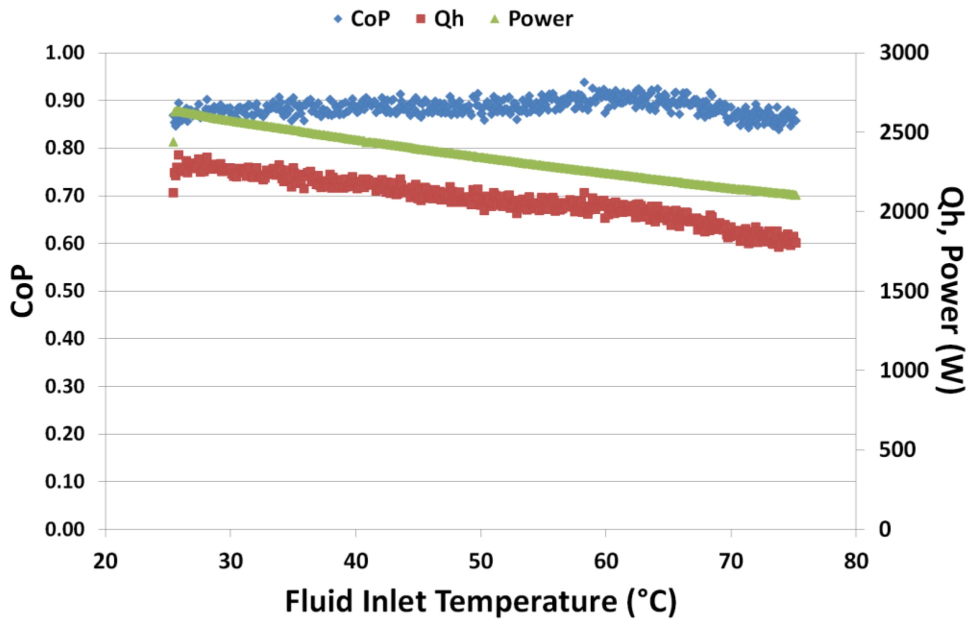

Based on these results, we believe the heat exchanger could be designed in such a way to always perform *at least as well* as a conventional resistive heater. However, to do so would require additional plumbing components capable of redirecting the various liquid loops at the appropriate time based on the temperature difference between the loops.

G4.3 Task 16 – Produce Packaging- and Function-Intent Final Components

Production of the final prototype HVAC components is currently in-process.

G4.4 Task 17 – Test and Evaluate Final Comfort Components

Testing and evaluation of the final prototype components will occur in 2013 and 2014.

G4.4.1 Milestone 10 – Evaluate Final Comfort Components Completed

Evaluation of the final prototype components for the Buick LaCrosse is scheduled to be completed by August 31, 2013.

G4.5 Task 18 – Estimate Efficiency Improvements

The estimation of TED and TE HVAC system efficiencies will occur in 2013 and 2014.

CHAPTER G5: GM Phase 4 – Engineering Development

The focus of this phase was to integrate the final prototype distributed HVAC components with the production central HVAC system and to optimize the performance of the demonstration vehicles. A final analysis will be made to compare the expected efficiency and fuel economy improvements to the program targets. For this phase of the project, GM will continue to utilize Delphi to integrate most final prototype HVAC components into the demonstration vehicle with Faurecia installing their final prototype seats into the Volt. UCB will support control strategies and tunnel tests while completing their primary Phase 1 activities in parallel with this phase.

G5.1 Task 19 – Project Management and Planning

The planning and coordination for this phase will primarily utilize weekly team meetings. Based on a no-cost time extension, the key deliverables of a Buick LaCrosse demo vehicle will be completed by September 30, 2013, and a Chevrolet Volt demo vehicle by March 31, 2014.

G5.2 Task 20 – Integrate Final Components into Demonstration Vehicles

This activity includes the integration and build of two demonstration vehicles, a Buick LaCrosse and a Chevrolet Volt. This activity also includes the final modifications to the control system in order to deliver a well-integrated solution for distributed heating and cooling.

G5.2.1 Integration and build of mainstream demonstration vehicle (Buick LaCrosse)

G5.2.1.1 Redesign of Waste Energy Coolant Loop

The coolant system for Phases 3 and 4 has been redesigned to have the system under hood as compared its' previous location in the trunk of the vehicle in Phase 2. The system will rely on a front end heat exchanger to provide cooling to the TED when spot cooling is requested. The system will utilize the same front end heat exchanger evaluated in Phase 2, but all plumbing will be located in the front end of the vehicle. Additionally, to provide a heat source for spot heating requirements, the system has been valved into the Belt Alternator Starter (BAS) loop. Initial testing showed the loop could provide up to 1 kW of heat over time. Below are some initial test results of the heat provided by the BAS loop.

As seen in Figure G0, the q or heat transfer does not occur until 12-15 minutes where we get about 1kW of heat. However, this is due to the fact that the BAS system's pump does not come on until the alternator pump reaches 65deg C. Therefore, an additional pump was added to the BAS system to allow the TED loop to receive heat all the time. To not affect the loop, a liquid to liquid heat exchanger was added with a valve to allow the liquid to flow through this when spot heating is requested. An additional valve is located on the front end heat exchanger to bypass the front end heat exchanger when spot heating is requested, so as not to cool the TED loop.

Figure G80: BAS Heat Transfer

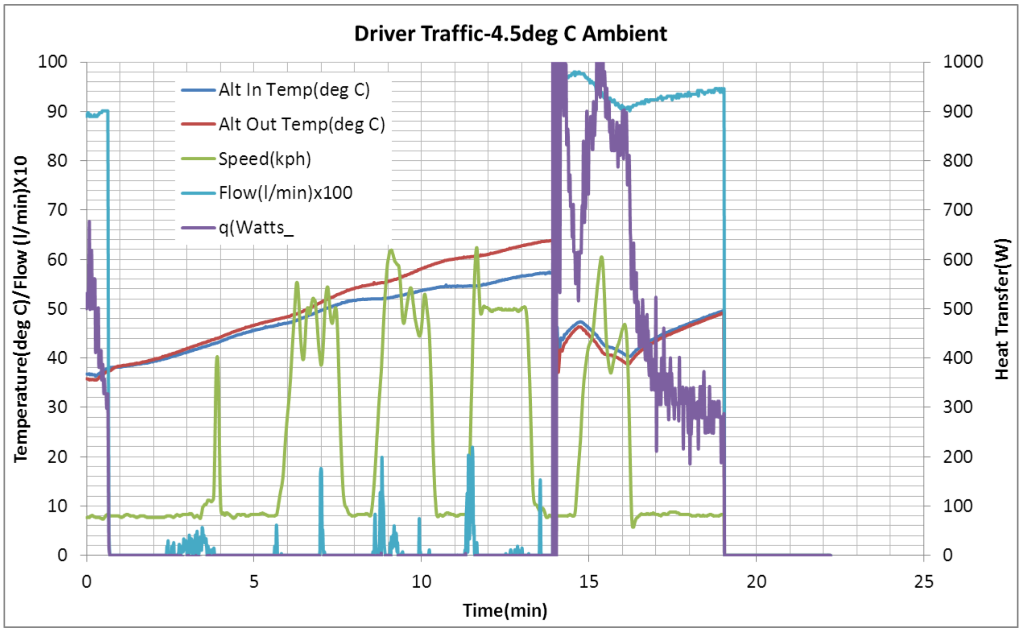

G5.2.1.2 Final Controls Modifications

Due to changes in the intended hardware implementation of the system, the controls and wiring were modified to meet the system needs. Specifications for the Human Machine Interface (HMI), TED locations, addition of plume seats, and coolant system implementations were updated for Phase 3 requirements.

The Human Machine Interface (HMI) designs for the various seating positions were simplified. The control input panels no longer have the option to select offsets to automatic control or direct manual control. The resultant panel offers a hybrid of the two control methods depending on which “level” of control is chosen.

As can be seen from the front panel, there are new controls for controlling the plume seat feature which is unique to the front seats. When enabled, the speed of the plume fan can be varied from its minimum to maximum allowed speeds via the “Plume Speed” knob.

The remaining set of controls is common for each seat location where comfort can be adjusted from “Max Cool” to “Max Warm”. The reduction in complexity from the elimination of the Manual and Automatic inputs is reflected in the front seat control state diagram shown in Figure G81: The resultant logic for the rear seat control state is similar except one chart controls the whole rear seat.

Figure G81: Control State Diagram for Front Seats

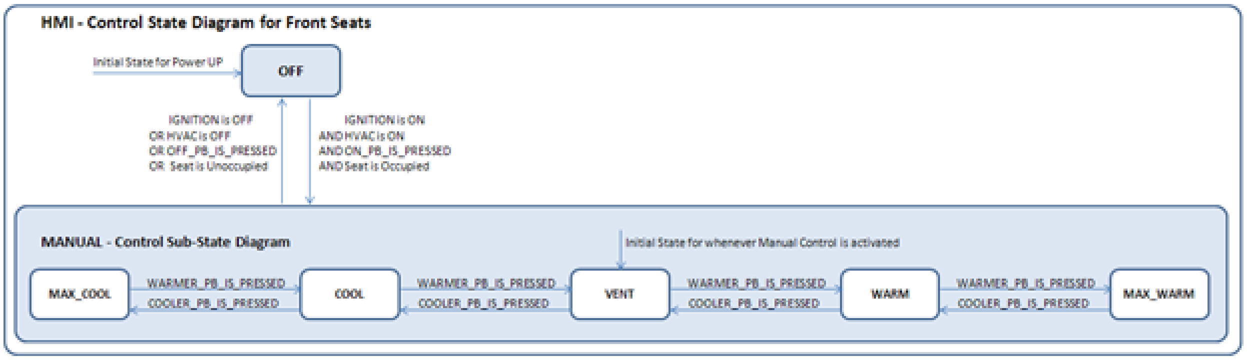

The operation of the front plume seats interacts with the airflow to the rear seats since both have a common airflow source. To insure comfort for the rear passengers a decision was made to place a higher priority on providing rear airflow over the plume seat operation.

The coolant system underwent a drastic reconfiguration which resulted in a simplification of the control logic. The cooling fan for the system was eliminated with the movement of the system's waste heat exchanger being moved to the front of the vehicle. As was described above for the "Redesign of Waste Energy Coolant Loop", the BAS coolant loop was integrated with the TED coolant system.

A good measure of the reduction of complexity of the system is the number of the ECU10 control units used to implement it. For Phase 2, twenty four units were used. After the changes were made for Phase 3, seven units were removed and two were reconfigured for new functionality.

The previously mentioned changes and redesign of TED packaging led to a significant effort in rewiring the software test bench and vehicle. The movement of the coolant pumps, temperature sensors and coolant control valves to be under hood from the trunk lead to rewiring the whole vehicle coolant system. Changes to the HMI panels forced changes for both the software test bench and vehicle. A test panel was developed and built to test the vehicle wiring changes to insure correct operation in preparation to vehicle software debugging.

Final Build of Buick LaCrosse Demonstration Vehicle

At the end of Q1 2013, the Buick LaCrosse had been rebuilt to 80% of the Phase 3 design and instrumentation. The vehicle has new TED modules and ducts installed. The liquid system build was completed with flow meters, pumps, valves, heat exchangers in place. Figure G82, Figure G83, and Figure G84 show the build progress.

Figure G82: Buick LaCrosse Trunk with TED Controllers

Figure G83: Adafruit Flow Meters Installation

Figure G84: TED Pump Installation

The remaining items to complete the build are as follows:

- Install the seats
- Install the headliner
- Fill and test the coolant system
- Complete minor instrumentation

The TED module and system redesigns were performed to fill some design gaps and improve overall performance. These redesigns dictated new or updated parts to be purchased. Below is a list of items that were purchased and received:

- 4 Front Seat Back Covers
- 1 Rear package shelf
- 1 Headliner
- 8 High Power PWM Fans
- 8 Mid Power PWM fans
- 5 Low Power PWM fans
- Purge valve actuator
- High temp/high pressure hose
- Coolant flow meters
- Water pump for BAS & connector

G5.2.2 Integration and build of Chevrolet Volt demonstration vehicle

Unlike the mainstream Buick LaCrosse application, a Chevrolet Volt "mule" vehicle was not built during Phase 2. For Phase 2, the only unique component for the Volt was the TE-based passenger compartment heater, and the initial TE-based heater (alpha and beta) prototypes were only bench-tested. Integration activities for the Volt are just beginning, and the vehicle build with instrumentation and the final prototype components will occur during the fourth quarter of 2013.

G5.3 Task 21 – Test and Evaluate Distributed HVAC System in Vehicle

The testing of evaluation of the Buick LaCrosse will begin shortly. It will occur for the Chevrolet Volt in the first quarter of 2014.

G5.3.1 Test and Evaluate mainstream demonstration vehicle (Buick LaCrosse)

The testing and evaluation of the Buick LaCrosse will be completed by September 30, 2013.

G5.3.2 Milestone 12 – Make mainstream demonstration vehicle available to U.S. DOE

The Buick LaCrosse will be made available to the Energy Commission and the US Department of Energy for their evaluations following the completion of the project team's testing and evaluation by September 30, 2013.

G5.3.3 Test and Evaluate Chevrolet Volt demonstration vehicle

The testing and evaluation of the Chevrolet Volt will be completed by March 31, 2014.

G5.3.4 Milestone 14 – Make Chevrolet Volt demonstration vehicle available to U.S. DOE

The Chevrolet Volt will be made available to the Energy Commission and the US Department of Energy for their evaluations following the completion of the project team's testing and evaluation by March 31, 2014.

G5.4 Task 22 – Calculate Efficiency Improvements of Distributed HVAC System

This task has not yet begun, and the analysis of efficiency improvements for the final prototype distributed HVAC systems on both the Buick LaCrosse and the Chevrolet Volt will be completed by March 31, 2014.

G5.4.1 Milestone 13 – Calculate Efficiency Improvements of Distributed HVAC System

The efficiency improvements for the Buick LaCrosse will be calculated at the completion of the project team's testing and evaluation by September 30, 2013.

CHAPTER G6:
GM Phase 5 – Thermoelectric Generator Development

The focus of this phase was to develop improvements in the TE materials for thermoelectric generators that could be used to produce electrical power for TE HVAC system loads. For this phase of the project, GM utilized first principle calculations by UNLV to identify underlying mechanisms that guided the research into new TE materials. Oak Ridge National Laboratory advised on potential composition improvements and measured material samples. Marlow Industries developed new module processes to incorporate these optimized TE materials.

G6.1 Task 23 – Develop Thermoelectric Materials / Modules for Waste Heat Recovery

The project team made significant progress under the waste heat recovery objectives of Phase 5. Much of these efforts focused on high-temperature TE materials research, including the evaluation of melt-spun skutterudite materials, low-cost skutterudite TE materials, and defect diamond-like materials. An evaluation of thermal interface materials was also performed.

G6.1.1 Evaluation of Melt Spun Skutterudite Materials

In the past quarter, Magnequench has delivered several different formulations of n- and p-type skutterudite that were prepared by melt spinning of pre-melted charges. Further for the n-type materials, three different quench rates were investigated (those being slow, fast and very fast that corresponds to the quench wheel's speed). A comparative study was undertaken comparing the thermoelectric properties of materials which were first annealed then consolidated by spark plasma sintering and those which were direct sintered without annealing. For the n-type materials a formulation using dual elemental fillers was chosen for 100 g scale up, for the p-type materials formulations of the type $M_xFe_{4-y}Ni_ySb_{12}$ were selected. Figure G85 below is an SEM micrograph of an as spun skutterudite ribbon showing the contact and free surface.

Figure G85: Back-scattered electron images of as-spun ribbons

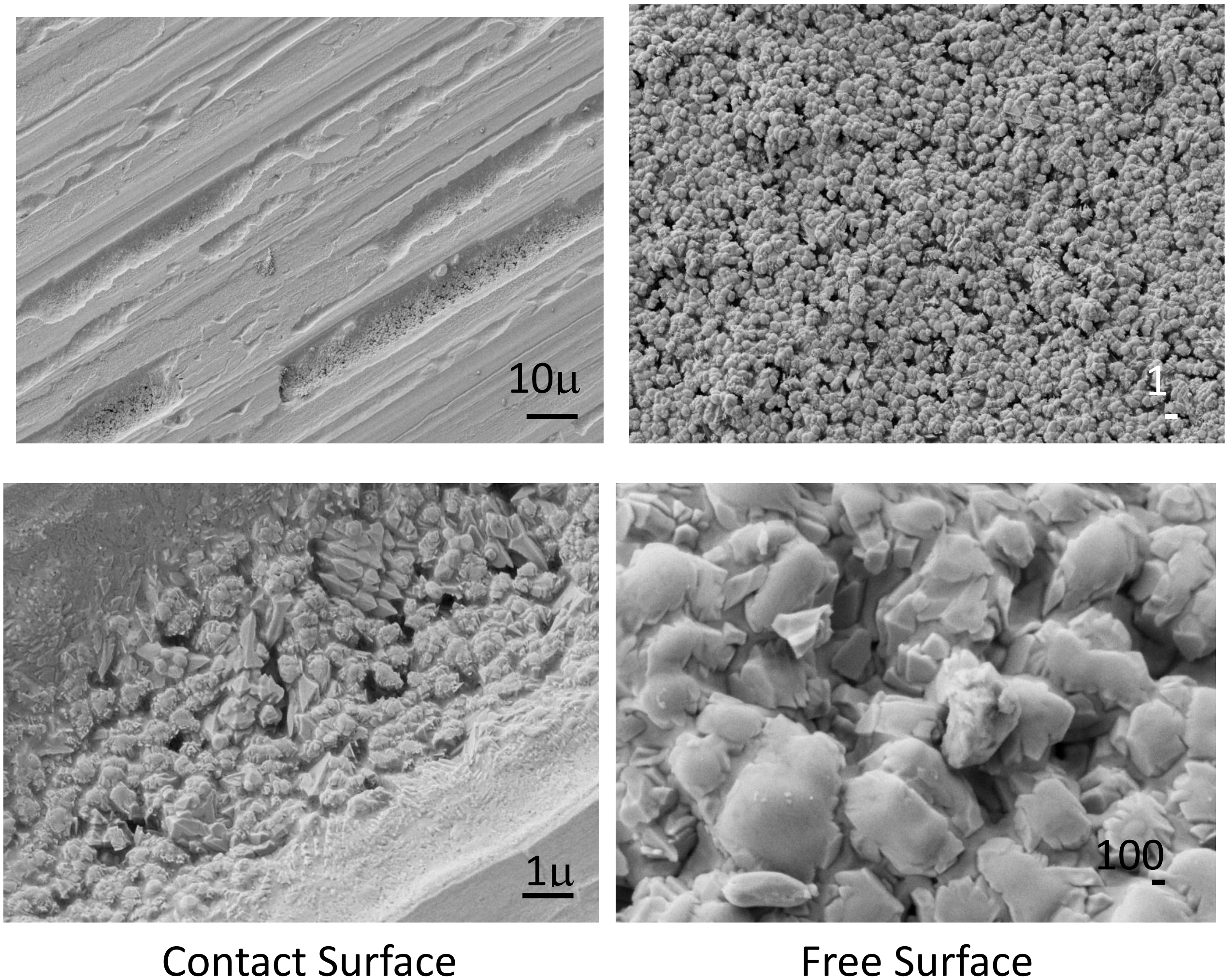

The ribbons pictured in Figure G85are of the fast quench variety. The images on the left are the contact surface and the gashes observed are due to Ar gas entrainment during quenching. The images on the right are the free surface which is considerably more textured due to the fact that crystal growth was allowed to take place.

The as-received n-type materials were a complex mixture of binary antimonides and skutterudites. This is a result of the fact that temperatures above the peritectic decomposition are required for processing, however despite this and the rapid quench rates skutterudite phase is still observed in the ribbons by powder x-ray diffraction. Similar multi-phasic materials were observed in the as-received p-type samples with an even wider variety of phases present due the fact that p-type are quinary phases as compared to n-type which are quaternary. We have determined that these materials can be transformed into single phase materials simply consolidation by spark plasma sintering (SPS). From Powder x-ray diffraction and electron probe microanalysis there is no significant difference in phase purity, composition as far as the extent of homogeneity as it applies to the distribution of fillers from grain to grain. We do however see a significant difference in the grain size distribution between the very fast quench materials and those produced with slower quench rates with the former having a finer grain size. Figure G86 shows the backscattered electron images of polished melt-spun and SPS's billets with the EPMA-determined compositions listed in the bottom of the images.

Figure G86: Backscattered electron images of, from left to right, slow quench and very fast quench n-type skutterudites

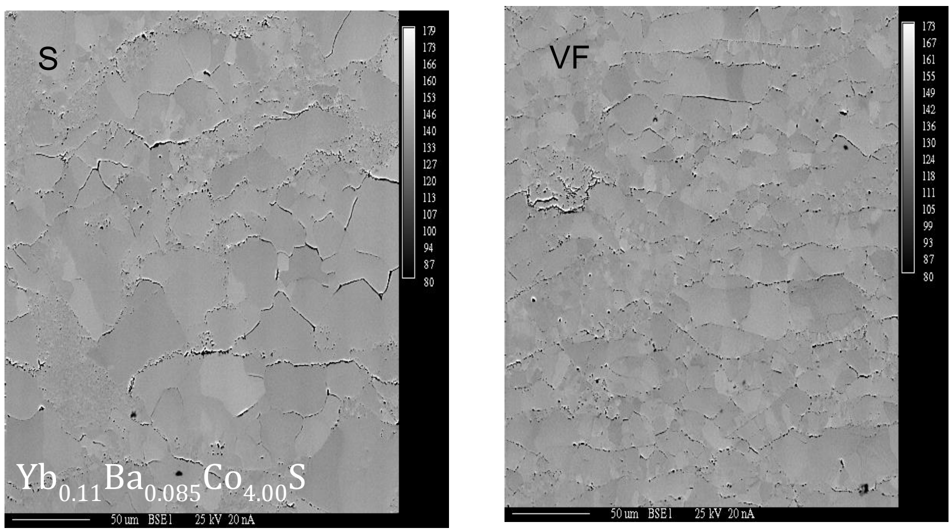

We conclude that melt spinning combined with spark plasma sintering results in materials with properties comparable to those where annealing was performed, therefore this step can be eliminated, thereby increasing materials throughput and reducing cost and energy inputs for production. This was true of both n- and p-type materials and was independent of quench rate. Further the direct SPS processing of melt spun materials is scalable. We have produced 5 gram billets of n- and p- type materials for the purposes of transport property evaluation and 80+ g billets of n- and p-type materials for residual stress analysis and for the fabrication of tensile stress bars. In all cases, the as-spun ribbons can be completely converted to pure phase skutterudites in the matter of 20 minutes of processing, including the heating ramps. The results of the residual stress analysis will be presented next quarter.

Figure G shows the transport properties of n-type materials, with the three different quench rates. As can be seen all samples have virtually identical thermal and electrical transport properties consistent with their similar compositions. An 80 g billet of fast quench n-type material (3.0 cm in diameter and 1.5 cm in thickness) was delivered to Marlow industries for sectioning into tensile fracture bars. These bars were delivered to Oak Ridge National Laboratory for room and high temperature 3-point bend testing using their test fixture. The results of these tests are presented in Figure G88 below. As can be seen in the figures below there is a decrease in the characteristic strength as the temperature increases. Fractography is currently underway to understand the failure modes of the test bars and will be reported during the next quarter. Comparable p-type fracture strength testing is currently underway and the results of these measurements will also be reported in the following quarter.

Several n-type fracture test bars were kept for transport, thermal expansion measurements, and resonant ultrasound spectroscopy to determine Young's modulus and Poisson's ratio. The CTE was found to vary from 10 to 14 PPM and the Young's modulus and Poisson's ratio were 139 Gpa and 0.2, respectively at room temperature. These values compare well to those found for n-type materials prepared in the traditional manner. Transport properties from a bar cut from the 80 g billet were also measured to ensure that the properties are retained even when processing at larger batch sizes. Further, the transport properties for the bar cut from the 80 billet were performed along the axis of the billet, while transport properties for 5 g billets are performed perpendicular to the axis. As shown in Figure G, the transport properties between the 5 g billet and the 80 g billet agree well indicating the quality of material is still high even at larger batch sizes for SPS.

Figure G87: Temperature dependence of the Seebeck coefficient (S), electrical resistivity (ρ), Thermal conductivity (k) and ZT

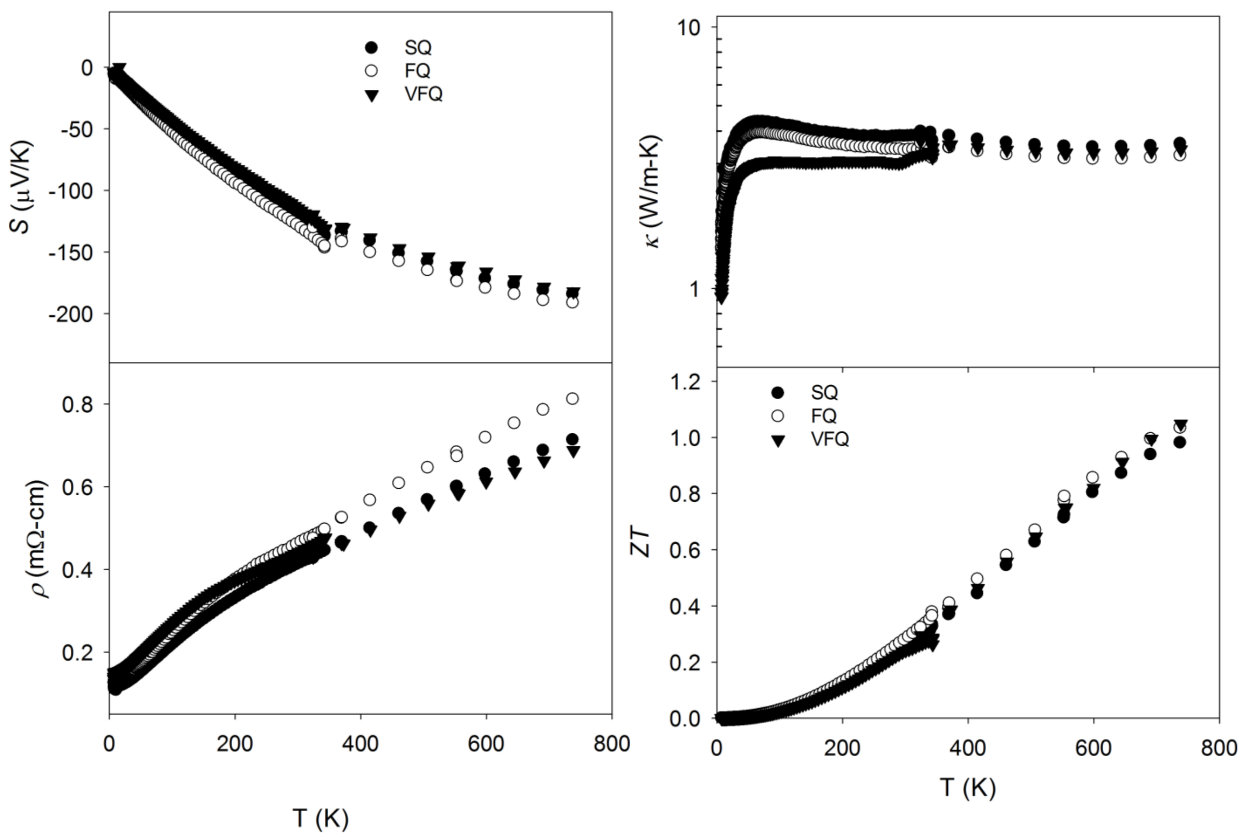

Figure G88: Characteristic tensile strength as a function of temperature for n-type skutterudite materials made by melt spinning and SPS

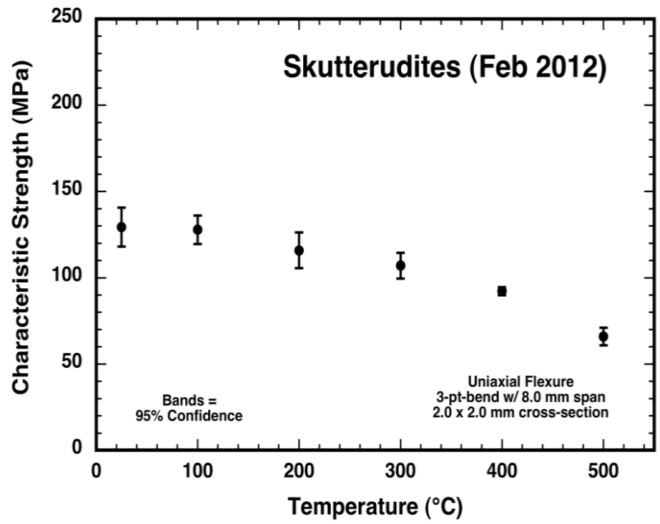

Figure G89: Comparative high temperature transport properties of n-type skutterudite with samples cut from a 5 g and 2 from an 80 g billet

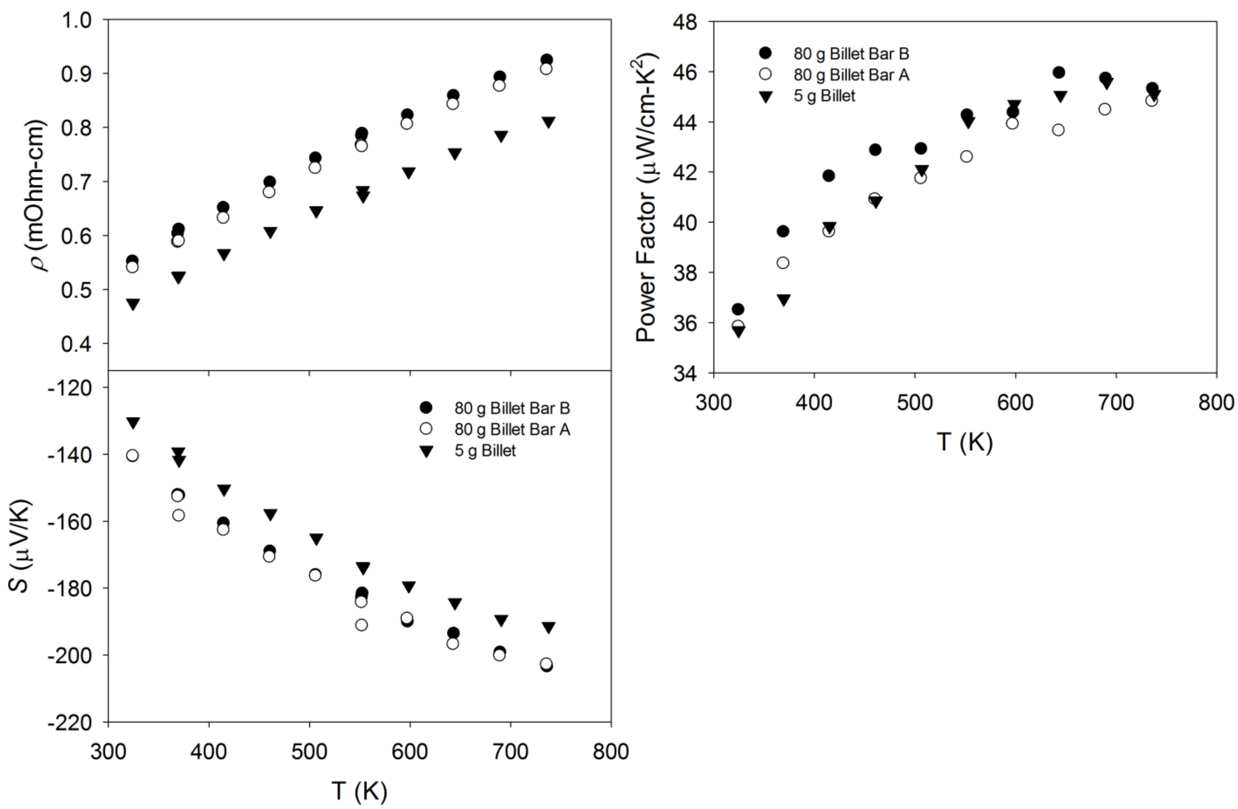

Several formulations of p-type melt spun skutterudite were investigated andthe transition metal ratios (Fe and Ni) were altered. In the case for one of the formulations, both slow and fast quench samples were investigated. As was found the for the n-type materials, the fast quench condition led to a finer grain structure but no significant differences were observed in the transport properties. Based on these finding, only fast quench materials were investigated for the later 2 composition. As discussed in the following sections, we have found that the best way to affect the carrier concentration is by adjusting the Fe to Ni ratio. Figure 4.6 shows the transport properties of the three different formulations. High temperature measurements will be performed for the two latter materials in the following quarter. A ZT of ~1 at 750 K was found for $DD_{0.72}Fe_{3.4}Ni_{0.6}Sb_{12}$.

Figure G90: Temperature dependence for three different formulations of p-type skutterudite.As the Fe to Ni ratio is increased, the carrier concentration increases and results in lower ρ

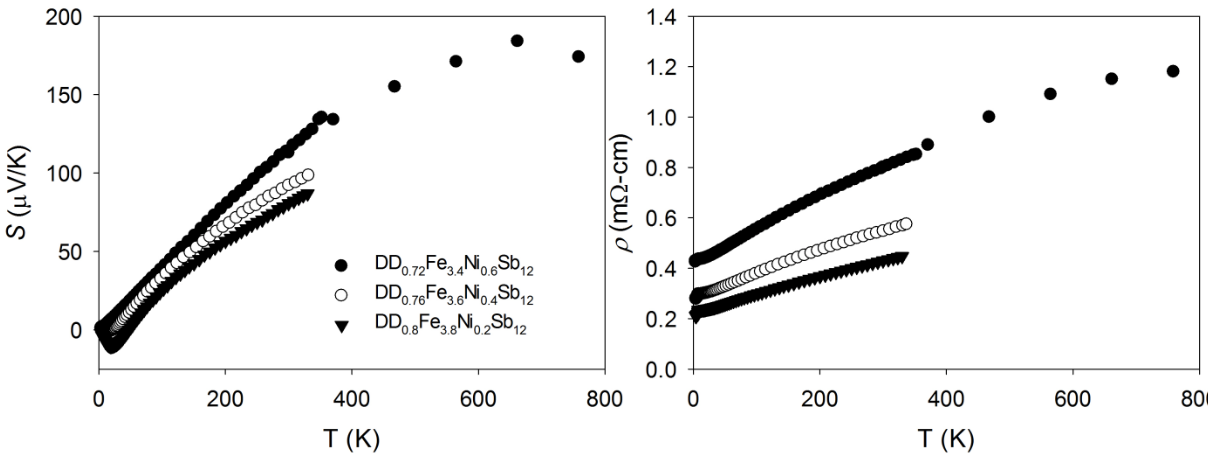

Instrumentation Installation: In the first quarter of 2012, two pieces of new instrumentation were installed at GM R&D that will facilitate the rapid screening of high temperature transport properties of both new and developmental thermoelectric materials. A Linseis LSR-3 high temperature Seebeck and Electrical resistivity measurement system was installed in January and an Anter Flashline diffusivity measurement system was installed in March. This instrumentation along with those currently operating at GM R&D will allow for the evaluation of thermopower, electrical resistivity, and thermal conductivity from 3 K to 1000 K.

G6.1.2 Low-Cost p-type Skutterudite Thermoelectric Materials

With the emphasis on the reduction of rare earth materials due to supply concerns, we feel that the current p-type formulations being considered for skutterudites, which are rich in rare earth, are not a long-term sustainable solution for automotive thermoelectric applications. With this in mind, we have begun to explore the thermoelectric properties of $Ca_xFe_{4-y}Ni_ySb_{12}$. These materials were prepared using the traditional melt-quench-anneal technique. Several different formulations were investigated. The first was to hold the Fe and Ni ratio fixed at 3:1 and adjust the filling fraction of Ca resulting in nominal compositions of the type $Ca_xFe_{4-y}Ni_ySb_{12}$ (y is fixed). The second was to fix the nominal composition of Ca and vary the ratio of Fe to Ni resulting in nominal compositions of the type $CaFe_{4-Y}Ni_ySb_{12}$ (Ca content is fixed y varies). From the evaluation of transport measurements we find that the approach of altering the Fe to Ni ratio is a more effective approach for controlling the carrier concentration as compared to changing the filling fraction. Figure G shows the low and high temperature transport properties of $Ca_xFe_{4-y}Ni_ySb_{12}$ (fixed y). There is little to no variation in the magnitude and temperature dependence of the Seebeck coefficient, and with the exception of one sample, the resistances are quite similar as well. The fact that there is a down turn in the magnitude of *S* above ~600 K and that there is a significant increase in κ at around the same temperature result in lower ZT above this temperature. Both phenomena are likely associated with the onset of bipolar conduction. There is a peak in the ZT curve at 600 K with a magnitude on the order of 0.55. This is similar to the behavior we observed for Yb-filled p-type materials and indicate that the Yb and Ca atoms have a similar effect on the band structure of the $Fe_{4-y}Ni_ySb_{12}$ network, which seems to be that of 2+ ions for the balancing of charge.

Figure G91: Thermal transport properties of $Ca_xFe_{4-y}Ni_ySb_{12}$

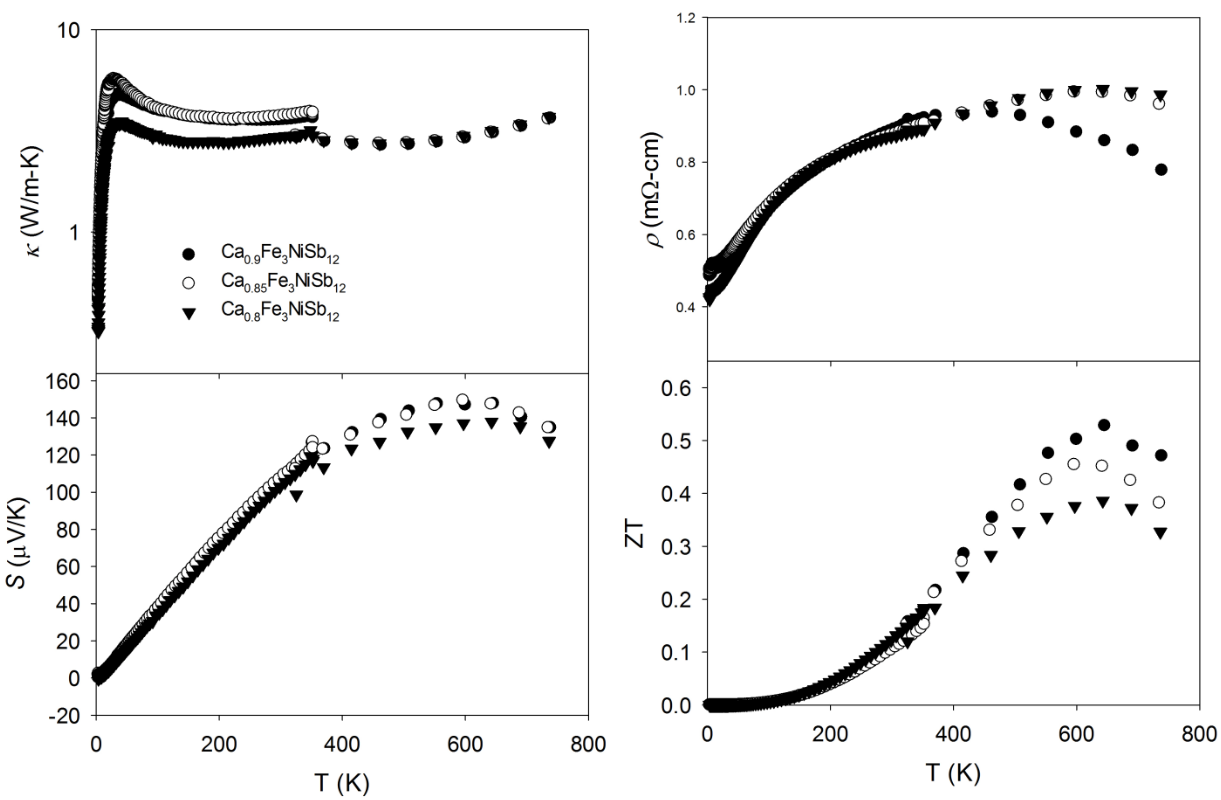

Figure G shows the low and high temperature *S* and ρ for the $CaFe_{4-y}Ni_ySb_{12}$ samples. As seen there is a significant difference in the magnitude and temperature dependence of these parameters for the three samples, which suggests that the hole doping level is increasing with increasing Fe content. Also evident is for the higher Fe ratios the onset of bipolar conduction is suppressed as we would expect for higher hole carrier concentrations, which would tend to cancel out the effects of the minority electron carriers. Power factors approaching 30 μW/cmK^2

were found for these samples. High temperature thermal conductivity measurements are currently underway, and we will report those and resultant ZT values of these samples in the next quarter.

Figure G92: Thermoelectric properties of $CaFe_{4-y}Ni_ySb_{12}$

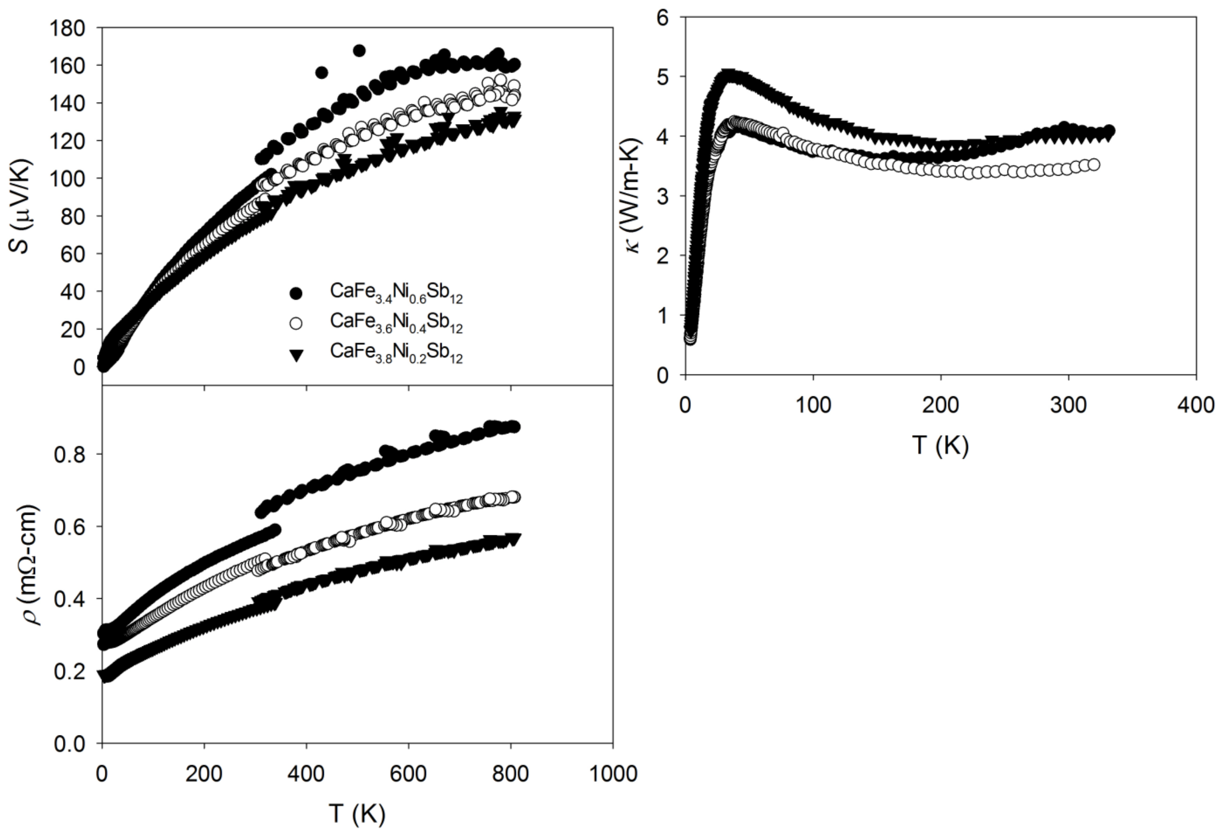

G6.1.3 Defect Diamond-Like Materials

Various zincblende or chalcopyrite compounds with a wide range of transition metal and tri-al ratios may contain structural vacancies, the amount of which increases with the increasing trial content. Although structural vacancies scatter heat carrying phonons, hence reduce the lattice thermal conductivity, they may also scatter the charge carriers and reduce the electrical conductivity. We have studied $(Cu_2Te)_{1-x}(Ga_2Te_3)_x$ to find out how the overall thermoelectric properties of this material system are affected by the vacancy content. Polycrystalline samples were synthesized by melting, annealing, and hot-pressing. Pure phase materials were obtained for all the compositions. All the samples show *p*-type semiconducting behavior in the temperature dependence of the Seebeck and Hall coefficients. The structural vacancies were found to scatter both phonons and charge carriers. The room temperature charge carrier mobility drops from 91 $cm^2V^{-1}s^{-1}$ 4.6 $cm^2V^{-1}s^{-1}$ depending on vacancy level. The total thermal conductivity decreases significantly as the Ga content increases at low temperatures where the vacancies act as the point defects which dominate the phonon scattering. At high temperatures, the dependence of thermal conductivity on the Ga content is much less significant. The highest *ZT* ~ 1.4 among the samples in this study was found at 840 K. The temperature dependence of the thermoelectric properties is shown in Figure G93. The thermoelectric properties can be further tuned by doping. Mn has been found to be an effective dopant. A series of Mn doped samples are being prepared to optimize the thermoelectric properties.

Figure G93: Temperature dependence of the thermal conductivity, resistivity, Seebeck coefficient, and ZT

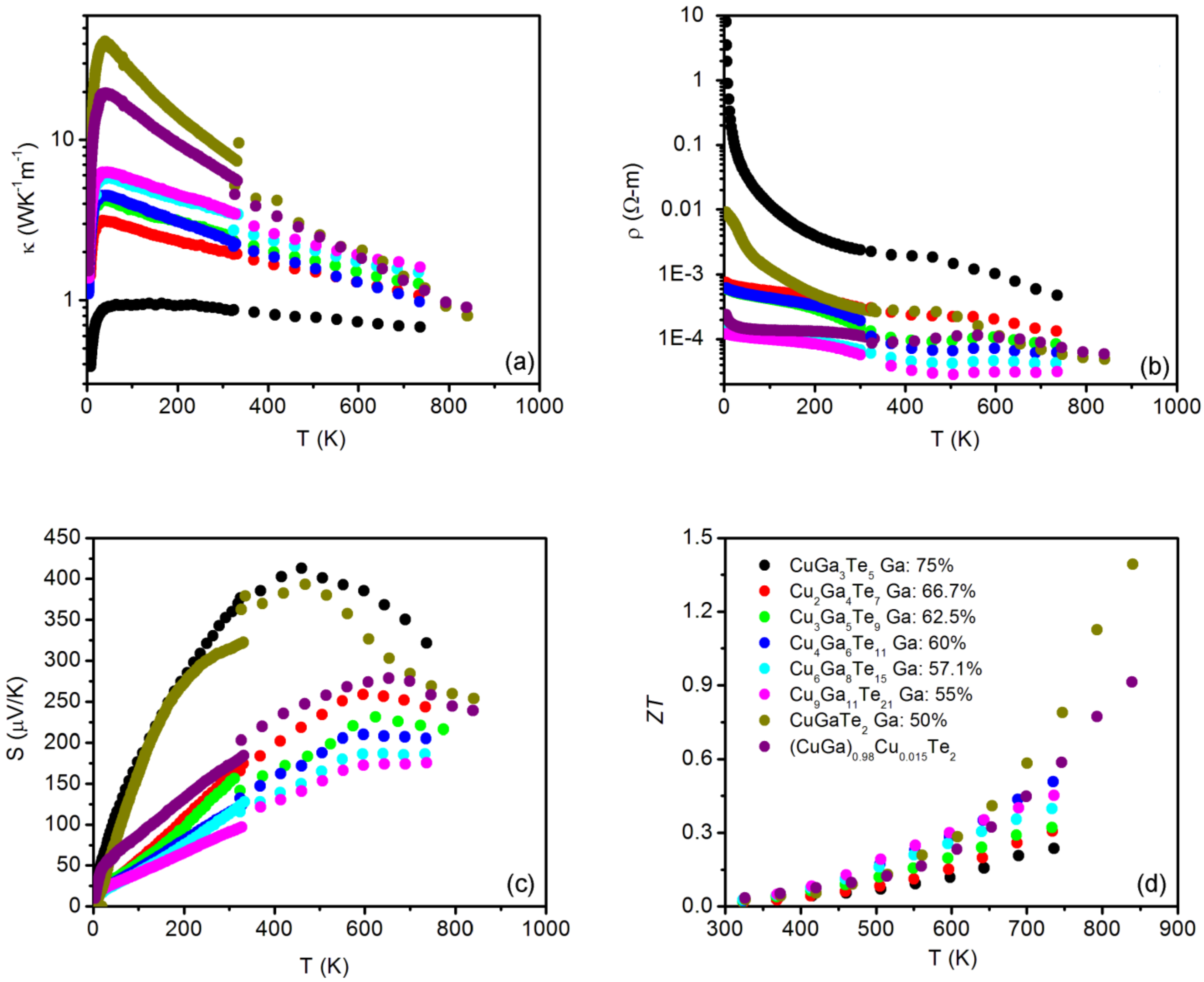

G6.1.4 Evaluation of Thermal Interface Materials

In conjunction with Purdue University, GM R&D has been investigating the effects of carbon nanotube (CNT) based thermal interface materials on the performance of an off-the-shelf Bi_2Te_3 module.

Figure G4 shows an SEM micrograph of the carbon nanotube arrays as deposited on a copper foil substrate.

Figure G94: SEM micrograph of CNT arrays deposited on copper foil

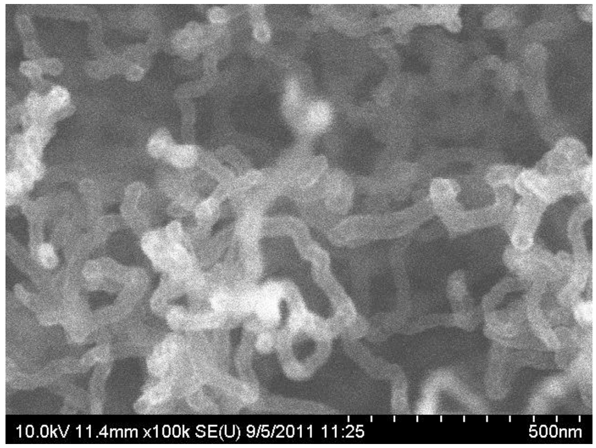

The measurements were performed using an Ulvac PEM module performance test system at GM R&D. The experiment is set up to measure the steady state electrical power output of a module under a virtually constant thermal gradient. Heat is delivered to the hot side of the module though a Ni bar with a cross sectional area of 4 cm^2 three thermocouples are placed along the length, two to monitor the temperature drop along the length to assess heat flow into the module and one at the bottom of the block near the contact with the module header to transducer the hot side of the thermoelectric module. On the cold side is a symmetrically identical arrangement with a copper block that is cooled to 20 ^{o}C by a programmable chiller. Thermal contact resistance exists between the hot and cold side block and the module's ceramic header, in addition there is a small but finite thermal resistance associated with the ceramic headers. Under the conditions of steady state heat flow both the interface contact resistance and the ceramic header will result in the temperatures of the he TE legs being lower and higher at the hot side and cold side respectively. That is lower (hot side) and higher (cold side) than the temperatures measured by the thermocouples embedded in the hot and cold sinks. This series of thermal resistances is shown schematically in Figure G95.

Figure G95: Thermal equivalent circuit superimposed on an image of Bi_2Te_3 module in the PEM test stand

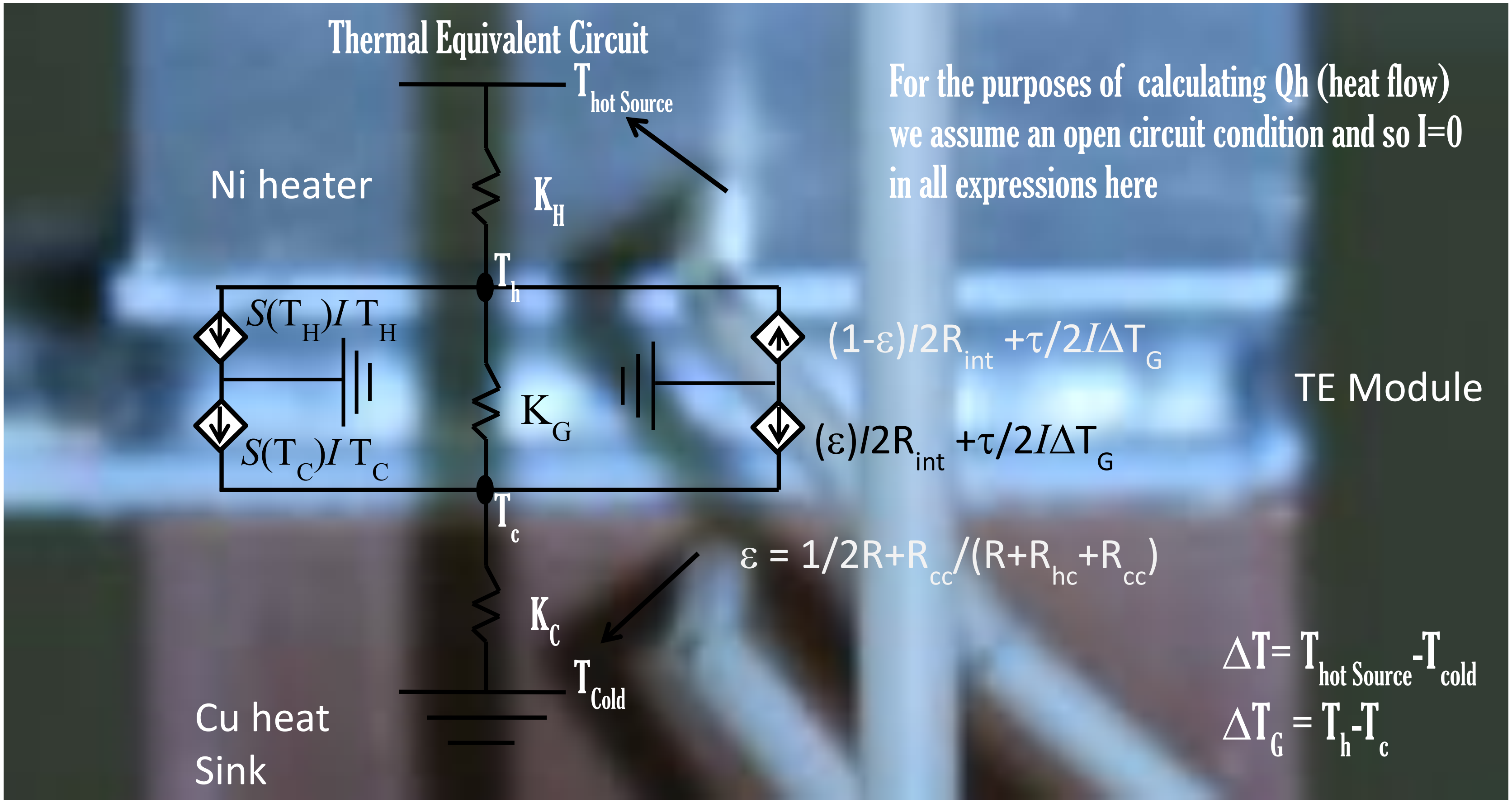

From the last program, we found that thermal interface contact resistance was a major source of parasitic efficiency loss, and was particularly under conditions of high heat flux. To assess the effect of using CNT based arrays as thermal interface materials, a series of experiments were run where the cold side thermal interface material was kept constant with grafoil and the hot side interface materials were altered, varying from no interface materials (bare interface between the Ni heat source and the ceramic header) to grafoil, copper foil, single sided CNT arrays on copper foil with the CNT arrays facing the ceramic header, and a double sided CNT array on copper foil where the CNT arrays were in contact with both the hot source and ceramic header.

Initial findings indicate that there is a gradual increase in the module open-circuit voltage with changing the interface materials from nothing to grafoil to copper to single-sided CNT, and finally, the double-sided CNT array that showed the largest open-circuit voltage. Figure G96 shows this result in a series of I-V curves for the same module and same temperature gradient, but with different interface materials at the hot side. This corresponds to a lower thermal contact resistance between the hot source and the module. Not shown are the results for the bare interface as they are virtually identical to the grafoil interface case. The open-circuit voltage of the module is a sensitive function of the temperature gradient along the length of the legs. Heat flowing through the moudle including the interface between the heater and the ceramic will lead to a temperature drop between the heater and the hot side of the legs. Likewise, thermal contact resistance at the cold side will result in an increase in the cold side tempertaure and depending on the nature of the construction of the module and the thermal contact resistance on the two sides this temperature drop may be symmetric. In any case, the increase in the open circuite voltage that we observed with a change in the measured delta T is indicative of a larger delta T across the TE materials and corresponds to a decreased thermal contact resistance at the hot side. The larger open-circuit voltage leads to a higher maximum power output and higher effeiciency as shown in Figure G7. The increased efficiency is a result of a higher electrical power output (resulting from the increased Voc) for the same nominal heat flow. Quantification of the thermal interface contact resistance is currently underway and will be reported next quarter.

Figure G96: V vs I curve for a module test the Voc (Y intercept of the curve) changes as a function of differing interface materials

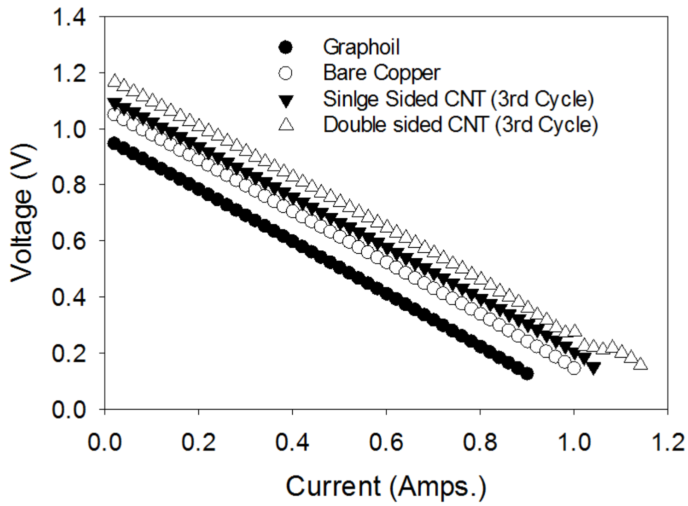

Figure G97: Percent conversion efficiency (P_{out}/Q_H) ($Q_H$is the heat flow)

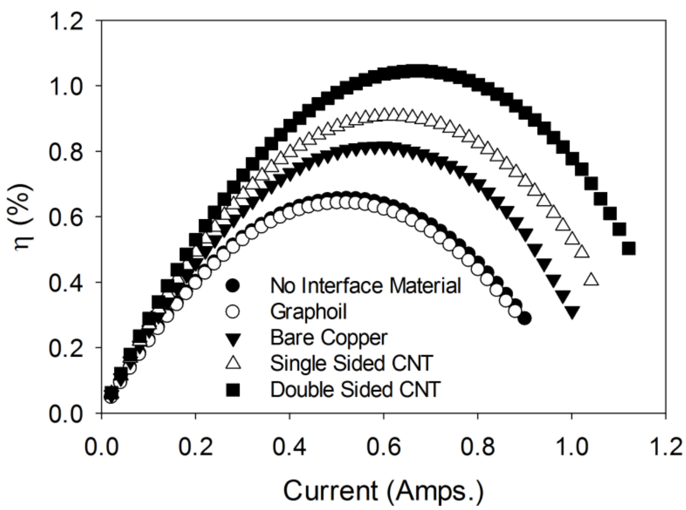

G6.1.5 Diffusion Barrier Evaluation

Thermally arc-sprayed (TAS) diffusion barriers have the potential to provide superior barriers in terms of low cost and performance. During this reporting period, we have continued to focus a substantial effort on the development of these barriers. Based on discussions with TAS experts from Praxair, the manufacturer of our TAS equipment, and observations of the results achieved using 60T-SS, a greater than 13% Cr TAS wire was evaluated. We sprayed ALCRO, a 23% Cr, Fe-based TAS wire. The adhesion of the ALCRO wire was not satisfactory.

60T-SS was applied to the p-type skutterudite material used in the β-TEG prototype build, as reported last quarter. ZT as a function temperature was measured on the 40mm^2, β-TEG prototype device. The device underperformed when compared to expected model results. These results will be presented later in our report. The reason for the poor performance was high device ACR. A cross-sectional failure analysis provided evidence of delaminating 60T-SS TAS diffusion barrier from the p-type skutterudite in the second row of elements from the negative lead wire. Figure G98 is an optical image of one of the failed interfaces.

Figure G98: Failed diffusion barrier on p-type skutterudite element from the prototype β-TEG

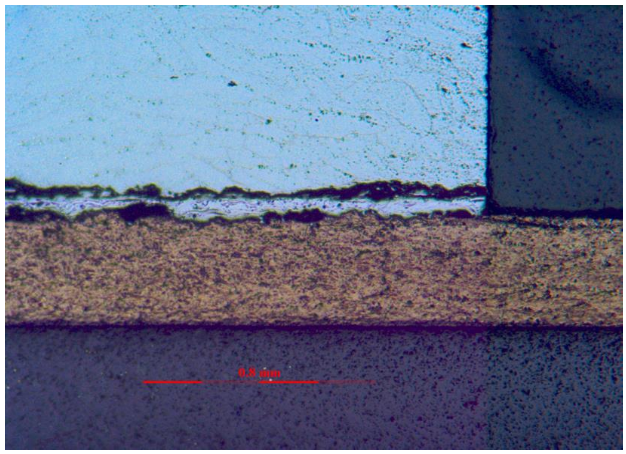

In addition to the observed interface failure in the device, we began to experience unexpected TAS 60T-SS / p-type skutterudite failures. We conducted 23, Fe alloy containing 13% Cr, stainless steel (60T-SS) TAS experiments during this reporting period. After many TAS experiments that concluded with microscopic observations of the TAS / p-type skutterudite interface, we suspect a process change related to the stability of power supply used on the TAS equipment. We will continue to carefully and methodically evaluate eight key processing variables related to the TAS process in order to develop an understanding of the cause for these failures. Table G4 provides a list of 60T-SS experiments conducted with selected processing conditions and a barrier-bond evaluation. A pass (P) or fail (F) in the as-TAS bond state is also included for a quick review of progress.

Table G4: TAS experiment conditions

SAMPLE	PASSES	PSI	FEEDRATE	TRAVERSE RATE	ROTATION SPEED	Pass/Fail	V/A
60T001-N	1.5	25	1.5	152	44	+	
60T002-P	0.5	25	1.35	152	44	+	
60T003-P	1.5	25	1.5			P	
60T006-N	1.5	25	1.5			+	
60T007-P	1.5	25				P	
60T008-P	1.5	25				P	
60T009-P	1.5	25				P	
60T011-N	1.5	25	1.25	152	44	P	
60T013-P	1.5	25	1.5			P/F	
60T014-P*	1.5	25				P	
60T015-P	1.5/2	25	1.3	152			
60T016-P	2	35	1.3	152			
60T018-P*	1.5	25				P	
60T020-P	1.5	25	1.3	154	44	P	
60T021-P	1.5	25	1.25	154	44	P/F	
60T022-N	2/2.5	50	1.25	154	44	P/F	
60T023-N	1.5/2	50	1.25	154	44	F	
60T024-P*	1.5	25	1.25	154	44	P	
60T025-P*	1.5	25	1.25	154	44	P	
60T026-P	1.5	25	1.25	154	44	P	
60T027-P	1.5	25	1.25	154	44	P	
60T028-N	1.5	50	1.25	154	44	P	
60T029-N	1.5	50	1.25	154	44	F	
60T030-N	1.5	50	1.25	154	44	F	
60T031-P	1.5	25	1.6	152	44	F	
60T032-N	1.5	50	1.6	152	44	F	
60T033-N	1	50	1.6	152	44		
	1.5	50	1.25	152	44		
60T034-P1	1.5	25	1.6	152	44	F	
60T034-P2	1.5	25	1.25	152	44	F	
60T034-P3	1	25	1.25	152	44		
60T035-N	1	50	1.6	152	44		
60T036-P	1	25	1.3	152	44		
60T036-P	1	25	1.25	132	44		
60T037-P	1.5	25	1.3	152	44	F	36/130
60T037-P	1	25	1.35	152	44	P	36/130
60T038-P	1	25	1.5	152	44		34/120
60T038-P	1	25	1.7	152	44		34/180
60T039-P	1	25	1.6	152	44		34/180
60T039-P	1.5	25	1.25	152	44		42/100
60T040-P	1.5	25	1.6	152	44		34/180
60T041-P	1	25	1.7	152	44	f	40/200
60T041-P	1	25	2	152	44	f	36/280
60T042-P	2	25	1.25	152	44		42/100

The thermal stability testing started in the last quarter on an Fe alloy containing 13% Cr, stainless steel (60T-SS) has been completed in this quarter. The results were mixed; the n- and p-type specimens that were heat-treated for 30 days and 60 days showed limited success. Complete evaluation of the Fe-coated skutterudite samples proved to be unsatisfactory. Delaminating occurs when the TAS layer is applied in thicknesses required for a continuous protective barrier.

CHAPTER G7: GM Conclusions

After the project has been completed in 2014, the overall Conclusions for the project will be written in a revision to this final report planned for June 30, 2014.

G7.1 Summary of Major Findings

Based on the Phase 2 testing and analysis, the team achieved the primary project objective to develop a distributed automotive HVAC system that provides thermal comfort equivalent to current state-of-the-art systems while using significantly less energy. In achieving this primary objective, the team met the following specific goals:

- Reduced fuel consumption used to maintain occupant comfort in cooling mode by ~30% through the use of TE technology for localized spot cooling (and spot heating).
- Developed TE-based components with a COP greater than 1.3 for cooling and greater than 2.3 for heating. These prototype components were integrated and tested in an eAssist Buick LaCrosse and an extended range electric Chevrolet Volt.
- Updated the UCB Thermal Comfort model for localized heating and cooling, and developed CAE tools to integrate distributed HVAC components into future vehicles.

G7.2 Conclusions and Recommendations

Based on the interim results and analysis from Phase 2, the team expects to achieve the primary objective and the associated goals for the project.

GM GLOSSARY

Term	Definition
AC	air conditioning
ACC	automatic climate control; the controls for a vehicle's standard central HVAC system
CAE	computer-aided engineering (tools)
CFD	Computational Fluid Dynamics (Analysis)
COP	coefficient of performance; ratio of the useful output to the amount of energy input
DoE	Design of Experiments
U.S. DOE	U.S. Department of Energy
EHT	equivalent homogeneous temperature
EOAT	evaporator out air temperature
OEM	original equipment manufacturer; typically refers to production vehicle features
HVAC	heating, ventilation, and air conditioning (system)
PTC	Positive Temperature Coefficient; a PTC heater provides heat in electrified vehicles
RH	relative humidity
TE	thermoelectric; a material that can convert electricity into a temperature differential
TEC	thermoelectric cooler; standard term for a TE module, but it can also function as a heater
TED	thermoelectric device; a collection of TE modules packaged to provide heating or cooling
TE HVAC system	TE-based system using distributed and localized spot heating and cooling
UCB	University of California at Berkeley, recognized experts in thermal comfort modeling

GM REFERENCES

Huizenga, C., S. Abbaszadeh, L. Zagreus and E. Arens, 2006. “Air Quality and Thermal Comfort in Office Buildings. Results of a Large Indoor Environmental Quality Survey.” *Proceedings, Healthy Buildings 2006*, Vol. III, 393-397, Lisbon, Portugal, June.

de Dear, R.J. (1998) "A global database of thermal comfort field experiments," *ASHRAE Transactions*., V.104(1b), pp.1141-1152. Reprinted in Schiller Brager, G (ed.) (1998) Field Studies of Thermal Comfort and Adaptation - ASHRAE Technical Data Bulletin, V.14(1). pp. 15-26.

Kuno Y (1956), Human perspiration. Charles C. Thomas Publ., Springfield.

Cotter JD, Patterson MJ, Taylor NA (1995), The topography of eccrine sweating in humans during exercise. Eur J Appl Physiol Occup Physiol 71: 549 – 554

Soon Ja Park and Teruko Tamura (1992) ,Distribution of evaporation rate on human body surface. Ann. Physiology Anthropology, 11 (6): 593 – 609.

Caroline J. Smith, George Havenith (2010), Body mapping of sweating patterns in male athletes in mild exercise-induced hyperthermia. European Journal of Applied Physiology.

J. Werner, T. Reents, A contribution to the topography of temperature regulation in man (1980). European Journal of Applied Physiology, 45, 87 – 94.

C. Uher (2010), Journal of Electronic Materials, 39, 2122.

APPENDIX A:
Ford Publications

C.W. Maranville, et al., "Development of a High-Efficiency Zonal Thermoelectric HVAC System for Automotive Applications", Proceedings of the 2009 DEER Conference, Dearborn, MI, August 5, 2009.

C.W. Maranville, "Thermoelectric Opportunities in Light-Duty Vehicles", Proceedings of the 2009 Thermoelectric Applications Workshop, San Diego, CA, October 1, 2009.

C.W. Maranville, et al., "Progress towards Development of a High-Efficiency Zonal Thermoelectric HVAC System for Automotive Applications", Proceedings of the 2010 DEER Conference, Detroit, MI, September 29, 2010.

C.W. Maranville, et al., "Towards the Development of a Distributed Thermoelectric HVAC System for Light-Duty Vehicles", Proceedings of the 2010 Global Powertrain Congress, Troy, MI, November 4, 2010.

C.W. Maranville and Peter Schmitz, "Thermoelectrics for Waste Heat Recovery and Climate Control in Light-Duty Vehicles", Proceedings of the 2nd IAV Thermoelectrics goes Automotive Congress, Berlin, Germany, December 2, 2010.

C. W. Maranville, "Overview of Ford-U.S. DOE Thermoelectric Programs: Waste Heat Recovery and Climate Control", Proceedings of the 2nd U.S. DOE Thermoelectric Applications Workshop, Coronado, CA, January 3, 2011.

C.W. Maranville, et al., "Improving the Efficiency of Light-Duty Vehicle HVAC Systems using Zonal Thermoelectric Devices and Comfort Modeling", Proceedings of the 2011 DEER Conference, Detroit, MI, October 5, 2011.

J.G. Gebbie & C.W. Maranville, “Zonal Climate System Test Conditions for Passenger Vehicles”, Paper #12TMSS-0051, presented at the 2012 SAE TMSS Conference, Scottsdale, AZ, October 31, 2012.

C.W. Maranville, et al., "Improving the Efficiency of a Vehicle HVAC System with Comfort Modeling, Zonal Design, and Thermoelectric Devices ", Proceedings of the 2012 DEER Conference, Dearborn, MI, October 18, 2012.

GM Publications

Meisner, G. P.; “Improving Energy Efficiency by Developing Components for Distributed Cooling and Heating Based on Thermal Comfort Modeling,” Vehicle Technologies Program Annual Merit Review Meeting, U.S. Department of Energy, Washington, DC, June 2010.

Meisner, G. P.; “Develop Thermoelectric Technology for Automotive Waste Heat Recovery,” Vehicle Technologies Program Annual Merit Review Meeting, U.S. Department of Energy, Washington, DC, June 2010.

Meisner, G. P.; “Thermoelectric Generator Development for Automotive Waste Heat Recovery,” 16th Directions in Engine Efficiency & Emissions Research (DEER) Conference, Detroit, MI, September 2010.

Yang, J.; “Advanced Materials for Future Propulsion”. 2010 Frontiers of Renewable Energy Sciences & Technologies Conference, Harvard University, Cambridge, MA, September 2010 (Invited).

Shailendra Kaushik, Kuo-Huey Chen, Taeyoung Han, and Bahram Khalighi, "Micro-Cooling/Heating Strategy for Energy Efficient HVAC System", SAE paper #2011-01-0644, 2011.

Shailendra Kaushik, Kuo-Huey Chen, Taeyoung Han, and Bahram Khalighi, “Micro-Cooling/Heating Strategy for Energy Efficient HVAC System”, SAE-2011-01-0644, presented at 2011 SAE World Congress, Detroit, MI, April 12, 2011.

Jeffrey Bozeman, Kuo-Huey Chen, and Shailendra Kaushik, “Distributed Climate System Impact on Human Comfort and MAC Efficiency”, 11AAR-0029, presented at SAE Alternative Refrigerant and System Efficiency Symposium, Scottsdale, AZ, Sep. 29, 2011.

GM R&D internal report #VDR-282, Shailendra Kaushik, Kuo-Huey Chen, Taeyoung Han, and Bahram Khalighi, “Micro-Cooling/Heating Strategy for Energy Efficient HVAC System”, May 17, 2011.

GM R&D internal report #VDR-289, Shailendra Kaushik, Taeyoung Han, and Kuo-Huey Chen, “Development of A Virtual Thermal Manikin to Predict Thermal Comfort in Automobiles”, Sep. 20, 2011.

Kaushik S., Han, T and Chen, K-H, “Development of a Virtual Thermal Manikin to Predict Thermal Sensation in Automobiles”, SAE 2012-01-0315, April, 2012 SAE World Congress, Detroit, MI.

Chen, K-H, Kaushik, S, Han T, Ghosh, D and Wang, M, “Thermal Comfort Prediction and Validation in a Realistic Vehicle Thermal Environment”, SAE 2012-01-0645, April, 2012 SAE World Congress, Detroit, MI.

A. Thompson, J. Sharp, J. Moczygemba, H. Wang, D. Brown, "Implementation and Performance of Skutterudite based Thermoelectric Generators", Presentation, International Conference on Thermoelectrics (Aalborg, Denmark; August 2012).

D. Ghosh, Mingyu Wang, E. Wolfe, K. Chen, S. Kaushik, and T. Han, Energy Efficient HVAC System with Spot Cooling in an Automobile – Design and CFD Analysis, SAE Int. J. Passenger. Cars – Mech. Syst., Vol. 5, pp.885-903, June 2012.

Yi Zhang, Xuezhi Ke, Paul R. C. Kent, Jihui Yang and Changfeng Chen "Anomalous Lattice Dynamics near the Ferroelectric Instability in PbTe,", Physical Review Letters 107, 175503 (2011) [appeared in October 21 issue].

Thermal to Electrical Energy Conversion of Skutterudite-Based Thermoelectric Modules. James R. Salvador, Jung Y. Cho, Zuxin Ye, Gregory P. Meisner, Joshua E. Moczygemba, Alan J. Thompson, Jeffrey W. Sharp, Jan D. König, Ryan Maloney, Travis Thompson, Jeffery Sakamoto, Hsin Wang, Andrew A Wereszczak, and Gregory P. Meisner. Journal of Electronic Materials, DOI: 10.1007/s11664-012-2261-9.

Electrical and thermal properties of Fe substituted double-filled BaxYbyFezCo4−zSb12 skutterudites. Sedat Ballikaya, Neslihan Uzar, Saffettin Yildirim, James R. Salvador. Solid State Chemistry. http://dx.doi.org/10.1016/j.jssc.2012.08.025.